Aus dem Institut für Medizinische Psychologie und dem Institut für Molekularbiologie im Biomedizinischen Centrum München (BMC) der Ludwig-Maximilians-Universität München

Vorstand: Prof. Martha Merrow, PhD und Prof. Dr. Peter Becker

in Kooperation mit TranslaTUM - Zentralinstitut für Translationale Krebsforschung im Klinikum Rechts der Isar der Technischen Universität München

Proteomic profiling and circadian dynamics in pancreatic ductal adenocarcinoma

Dissertation

zum Erwerb des Doktorgrades der Naturwissenschaften an der Medizinischen Fakultät der Ludwig-Maximilians-Universität München

vorgelegt von
Styliani Koutsouli

aus
Athen, Griechenland

Jahr
2022

Mit Genehmigung der Medizinischen Fakultät

der Universität München

Betreuerin:	Prof. Maria Robles Martínez, PhD
Zweitgutachter(in):	Prof. Dr. rer. nat. Axel Imhof
Dekan:	Prof. Dr. med. Thomas Gudermann
Tag der mündlichen Prüfung:	14. März 2023

Declaration

I hereby declare that the thesis submitted is a presentation of my original research work. All direct or indirect sources used are acknowledged as references. Wherever contributions of others are involved, every effort is made to indicate this clearly, and acknowledgement of collaborative research and discussions.

I am aware that the thesis in digital form can be examined for the use of unauthorized aid and in order to determine whether the thesis as a whole or parts incorporated in it may be deemed as plagiarism. For the comparison of my work with existing sources I agree that it shall be entered in a database where it shall also remain after examination, to enable comparison with future theses submitted. Further rights of reproduction and usage, however, are not granted here.

This thesis was not previously presented to another examination board and has not been published.

Munich, June 30th, 2022

Styliani Koutsouli

To all those
who never give up

Summary

Pancreatic ductal adenocarcinoma (PDAC) is an aggressive malignancy with poor prognosis, due to genetic heterogeneity, complex tumor microenvironment, increased chemoresistance, invasiveness and lack of reliable biomarkers for an effective diagnosis or treatment response. The circadian clock is a pacemaker mechanism that imposes daily control in physiology and behavior, and is critical for organismal homeostasis. In recent years, several epidemiological studies have suggested that circadian rhythm disruption is linked to increased cancer risk in humans under chronic light exposure at night.

Despite recent advances in other cancer types, the role of the circadian clock in PDAC development and progression has been largely unexplored. For this, I aimed to elucidate whether primary murine PDAC cells with distinct oncogenic mutations retain circadian functionality by performing a medium-scale, bioluminescence-based screening after generating circadian reporter (*Bmal1::Luc*) PDAC cell lines. Subsequently, the molecular mechanism of the clock in selected rhythmic PDAC cell lines was genetically disrupted using the CRISPR-Cas9 editing system, and the potential role of the tumor- endogenous circadian clock *in vivo* was assessed using a PDAC implantation mouse model system. For this, wild-type mice were orthotopically implanted with two different *Bmal1::Luc* KRAS-mutant subtype-specific PDAC cell lines, each harboring either a functional or a partially disrupted cell-intrinsic circadian clock. The tumor size, survival time and metastasis formation were determined at the end of the study, along with immunophenotypic characterization. In addition, circadian oscillations were recorded from tumor organotypic slices with either a functional or partially ablated tumor-endogenous circadian clock before and after phase synchronization.

Collectively, the results showed that the circadian clock is largely functional in primary cancerous cells of PDAC independently of the oncogenic mutation driver, and the circadian rhythm is maintained in the tumor *in vivo*. Furthermore, the tumor-endogenous circadian clock in PDAC did not affect tumor growth, survival nor immune cell composition in the tumor microenvironment considering though that the tumor-intrinsic circadian rhythm was not fully ablated at the population level.

An additional objective of this thesis work was to molecularly characterize primary murine PDAC cell lines derived from different oncogenic pools by employing mass spectrometry (MS)-based label-free quantitative proteomics. Statistical and functional enrichment analyses showed that 1) PDAC cells from distinct functional clusters irrespective of the oncogenic driver mutation(s) are enriched in common metabolic pathways, 2) KRAS-driven PDAC tumor cell lines differentiate on the proteome level based on molecular subtype and 3) KRAS-driven PDAC epithelial tumors functionally diverge on the proteome level, highlighting a rewiring of cellular processes downstream of transcription. Ultimately, integration of circadian clock functionality and proteome profiling identified potential time-dependent functional vulnerabilities in KRAS-driven tumors in PDAC. These data together with future functional studies may pave the way to optimize timed drug administration as part of multimodal therapeutic strategies for patients that do not respond to standard chemotherapeutics.

Zusammenfassung

Das duktale Adenokarzinom der Bauchspeicheldrüse (PDAC) ist eine aggressive Malignität mit schlechter Prognose wegen genetischer Heterogenität, komplexer Mikroumgebung des Tumors, erhöhter Chemoresistenz, Invasivität, und es fehlt an zuverlässigen Biomarkern für eine wirksame Diagnose oder Behandlung Ansprechen. Die zirkadiane Uhr ist ein Schrittmacher-Mechanismus, der die tägliche Koordinierung und Kontrolle in der Physiologie und im Verhalten sicherstellt, und der ist für die Homoostase des Organismus entscheidend. In den letzten Jahren haben mehrere epidemiologische Studien darauf hingewiesen, dass eine Störung des zirkadianen Rhythmus mit einem erhöhten Krebsrisiko bei Menschen mit chronischer nächtlicher Lichtexposition verbunden ist.

Trotz der jüngsten Fortschritte bei anderen Krebsarten ist die Rolle der zirkadianen Uhr bei der Entwicklung und Progression von PDAC noch weitgehend unerforscht. Aus diesem Grund wollte ich herausfinden, ob primäre murine PDAC-Zellen mit verschiedenen onkogenen Mutationen die zirkadiane Funktionalität beibehalten. Hierzu habe ich PDAC Zelllinien mit zirkadianem Rhythmus Reporter (*Bmal1::Luc*) erzeugt und ein Biolumineszenz -basiertes Screening im mittleren Maßtab durchführt. Anschließend wurde der molekulare Mechanismus der Uhr in ausgewählten PDAC-Zelllinien mit dem CRISPR-Cas9-Editiersystem genetisch unterbrochen, und die potenzielle Rolle der tumorendogenen zirkadianen Uhr *in vivo* mit einem PDAC-Implantationsmausmodellsystem untersucht. Dafür wurden Wildtyp-Mäusen orthotopisch mit zwei verschiedenen *Bmal1::Luc* KRAS-Mutanten-Subtyp-spezifisch PDAC-Zelllinien implantiert, jede von ihnen entweder eine funktionelle oder eine unterbrochene zirkadiane Uhr besitzt. Am Ende der Studie wurden die in den Mäusen gewach-

senen Tumore, die Überlebenszeit und die Metastasenbildung bestimmt sowie die Immunphaenotypisierung vorgenommen. Des weiteren, wurden die zirkadianen Oszillationen von organotypischen Tumorschnitten von Mäusen mit funktionierender oder unterbrochener Uhr zum ersten Mal *ex vivo* aufgezeichnet.

Insgesamt hat die Studie gezeigt, dass die zirkadiane Uhr in primären Krebszellen von PDAC unabhängig vom onkogenen Mutationstreiber weitgehend funktionsfähig ist und der zirkadiane Rhythmus im Tumor *in vivo* erhalten bleibt. Darüber hinaus hat die tumorendogene zirkadiane Uhr in PDAC begrenzten Einfluss auf das Tumorwachstum, das Überleben oder die Zusammensetzung der Immunzellen in der Mikroumgebung des Tumors, da der tumorendogene zirkadiane Rhythmus auf Zellpopulationsebene nicht vollständig unterbrochen wurde.

Ein weiteres Ziel dieser Doktorarbeit war die molekulare Charakterisierung primären muriner PDAC-Zelllinien, die aus verschiedenen onkogenen Pools stammen, mit Hilfe der Massenspektrometrie (MS) und markierungsfreier quantitative Proteomik. Statistische und funktionelle Anreicherungsanalysen zeigten, dass 1) PDAC-Tumore unabhängig von der/den onkogenen Treibermutation(en) verschiedene funktionelle Cluster bilden, die in stoffwechselbezogenen Signalwegen angereichert sind, 2) KRAS-getriebene PDAC-Tumorzelllinien sich auf Proteomebene je nach molekularem Subtyp unterscheiden und 3) KRAS-getriebene PDAC epitheliale Tumore funktionell in drei Proteinclustern unterschiedlich divergieren, was hervor hebt, dass es Neuverdrahtung zellulärer Prozesse nach der Transkription gibt. Schließlich wurden durch die Integration der Funktionalitätsstudie der murinen Primärzellen in Bezug auf ihre zirkadiane Uhr und der Proteom-Profile potentielle zeitabhängige funktionelle Schwachstellen in KRAS-getriebenen PDAC Tumoren identifiziert. Diese Daten zusammen mit zukünftigen funktionellen Studien könnten den Weg für eine zirkadiane Modulation der medikamentösen Behandlung als Teil multimodaler therapeutischer Strategien für Patienten ebnen, die

nicht auf Standard Chemotherapeutika ansprechen.

List of Figures

List of Tables

Contents

Abbreviations

ACF	Autocorrelation function
ACN	Acetonitril
ADM	Acinar-to-ductal metaplasia
ANOVA	Analysis of variance
BCA	Bicinchoninic acid assay
BMAL1	Brain and Muscle ARNT-Like 1
cAMP	Cyclic adenosine 5'-monophosphate
CCG	Clock-controlled gene(s)
CDK	Cyclin-dependent kinase
CFA	Colony formation assay
CLOCK	Circadian Locomotor Output Cycles Kaput
CREB	cAMP response element-binding protein
CRISPR	Clustered regularly interspaced short palindromic repeats
DEX	Dexamethasone
ECM	Extracellular matrix
ELISA	Enzyme-linked immunosorbent assay
EMT	Epithelial-to-mesenchymal transition
FACS	Flow-assisted cell sorting
FDR	False discovery rate
FFT	Fast fourier transform
FFT-NLLS	Fast fourier transform - Non-linear least squares
FSK	Forskolin
GDP	Guanosine 5'-diphosphate

GFP	Green fluorescent protein
GR	Glucocorticoid receptor
GTP	Guanosine 5'-triphosphate
GWAS	Genome-wide associated studies
HPLC	High pressure liquid chromatography
iTRAQ	Isobaric tags for relative and absolute quantitation
KRAS	Kirsten rat sarcoma virus
LFQ	Label-free quantification
LSP	Lomb-Scargle periodogram
Luc	Luciferase
m/z	mass-to-charge ratio
MAPK	Mitogen-activated protein kinase
MS	Mass spectrometry
mTOR	mammalian Target of Rapamycin
MTT	3-(4,5-dimethylthiazol-2-yl)-2,5-diphenyl-tetrazolium
NADH	Nicotinamide adenine dinucleotide
NADPH	Nicotinamide adenine dinucleotide phosphate
NGS	Next-generation sequencing
P_{fa}	False-alarm probability
PanIN	Pancreatic intraepithelial neoplasia
PCR	Polymerase chain reaction
PDAC	Pancreatic ductal adenocarcinoma
PDX1	Pancreatic and duodenal homeobox 1
PKA	Protein kinase A
PKC	Protein kinase C
PTF1a	Pancreas associated transcription factor 1a

RLU	Relative light units
ROS	Reactive oxygen species
RTK	Receptor tyrosine kinase
SCN	Suprachiasmatic nucleus
SDB-RPS	Styrenedivinylbenzene-reverse phase sulfonate
SDC	Sodium deoxycholate
SDS-PAGE	Sodium-dodecyl-sulfate polyacrylamide gel electrophoresis
sgRNA	signle guide RNA
T_c	Cytotoxic T cells
T_h	Helper T cells
TAM	Tumor-associated macrophages
TCA	Tricarboxylic acid
TEO	Tumor-endogenous oscillator
TFA	Trifluoroacetic acid
TGF-β	Transforming growth factor beta
TME	Tumor microenvironment
TMT	Tandem mass tags
TTFL	Transcriptional-translational feedback loop

CHAPTER 1

Introduction

Abstract | In this chapter, the general structure of the thesis is described and current knowledge and understanding about circadian rhythms and pancreatic ductal adenocarcinoma (PDAC) is comprehensively presented. In addition, an overview about signal analysis of molecular circadian rhythms is given. At the end of the chapter, the research aims of this doctoral thesis are specified.

Contents

1.1 Motivation and state of the art

This thesis work is a result of an interdisciplinary research effort that investigated the role of circadian clock's function in the development and progression of an aggressive malignancy as PDAC. In addition, given the genetic heterogeneity in PDAC progression, quantitative mass spectrometry (MS)-based proteomic profiling was employed to functionally characterize a large cohort of primary murine PDAC cell lines with distinct oncogenic mutations aiming to identify potential vulnerabilities that could serve as novel therapeutic targets.

1.2 Document organization

The document is structured in five chapters. The first chapter "Introduction" contains theoretical background about circadian rhythms, mechanism of function and outputs of the circadian clock. In addition, the biology and current standings in PDAC research are described. The second chapter "Materials and Methods" includes an extensive description of all experimental designs and methods implemented for data collection and analysis. In the third chapter "Results" the experimental and analytical results are demonstrated, and the forth chapter "Discussion" discusses thoroughly those results. In the last chapter "Conclusions and Outlook", a number of scientific conclusions are made as the result of this thesis accompanied by future perspectives.

1.3 Biological rhythms

In nature, there are several rhythmic processes that repeat over a certain amount of time. The origin of those rhythms can be physical forces (e.g., the lunar and tidal rhythms or the seasons) as well as of biological etiology with periods ranging from milliseconds to years. Biological rhythms are considered as special temporal niches that organisms have developed to be in synchrony with the environment's physical rhythms [1].

Biological rhythms with a (very) short period of time are called ultradian rhythms, and examples include neuronal activity in vertebrate species that range from milliseconds to seconds, and circumnutation (the spinning movement of elongating organs) in plant species, that takes place every 2-3 hours [2]. On the other hand, biological rhythms can be in the scale of months or years, such as reproductive activity in mammals, migration in bird species and whole population fluctuations that are based on predator-prey oscillations [3]. Reproductive and migration rhythms represent examples of circannual rhythms, i.e., endogenous rhythms that are favourable in specific seasons and therefore their period approximates one year [4].

In between of the aforementioned biological rhythms are those with a period of about 24 hours, that is a period of the Earth rotation around its axis, therefore referred to as "circadian" rhythms (from the Latin word *circa diem* meaning "about a day"). For instance, circadian oscillations are observed in body temperature and hormonal release in animal species [5], while leaf and stomatal movements in plants follow a 24-hour cycle [6].

The circadian clock is in essence an intrinsic time-tracking system regulating the timing, across 24 hours, of certain biological, physiological and molecular processes. Such a timekeeping system enables organisms to anticipate environmental changes such as food availability or predatory pressure. In evolutionary terms, circadian clocks provided an advantage resulting in increased fitness, by allowing animals to adapt their physiology

and behavior in an appropriate and most effective time of day [7]. The function of the circadian clock and its outputs is explained in detail in section 1.4.

One of the best characterized examples showing the importance of the circadian clock system in predicting and therefore coping with changing ambient conditions is the unicellular alga *Lingulodinium polyedra* (previously *Gonyaulax polyedra*) [8]. It is found in the ocean in southern California and exhibits a circadian migration behavior moving from shallow to deep waters over the course of the day. In essence, during the day, the algae cells are primarily on the surface, where light and nutrients essential for photosynthesis (carbon dioxide, nitrogen, phosphate) are abundant. During the night, the alga travels into deeper waters where nutrients coming from dead organisms are denser, hence heavier, and therefore move towards the bottom. This allows for the alga to sustain its high proliferation rate and survival throughout the whole day. Interestingly, towards the night, given the generation of carbon molecules inside the cell, a bioluminescence reaction take place that is believed to serve a protective mechanism against predators [8]. In addition, carbon dioxide is generated as by-product of the bioluminescent (biochemical) reaction, that leads to a decrease in cell density, facilitating the movement of the cells towards the surface.

The example of *Lingulodinium polyedra* shows how dynamically circadian clocks are controlling daily rhythms of the living organisms, from cyanobacteria to fungi, plants and animals [9]. This is possible due to fundamental characteristics and outputs of circadian clocks which are described in the next section 1.4.

1.4 The circadian clock

As evolutionary conserved, circadian clocks are present in all organisms, and regulate physiological and behavioral processes in a time-of-day-dependent manner [9]. In the

section 1.4.1, the unique properties of circadian rhythms are described, underlining the importance of circadian clocks' function. In section 1.4.2 the hierarchical organization and outputs of the circadian clock are presented in detail.

1.4.1 Main properties of the circadian clock

In 1960, the chronobiologist Colin Pittendrigh defined the first generalizations about circadian clocks, making him one of the fathers of biological rhythms [10]. The list of sixteen so-called formalisms can be summarized in three unique characteristics [11]:

1. Circadian rhythms are endogenously generated and self-sustained oscillations with a period of approximately 24 hours under constant environmental conditions.

In the absence of light-dark cycles, or other external stimuli, the circadian clock can continue running; they can be at *free-run*. The very first observation that circadian rhythms are self-sustained came in 1792, when the French astronomer De Mairan noticed that the daily leaf movements of the plant *Mimosa pudica* persisted in constant darkness [12]. A human study that involved individuals who spent four months in a cave without exposure to sunlight or information about the external time, found that their free-running period was 25.1 hours [13]. This highlights that in the absence of external cues the free-running period can persist to be around 24 hours. Like humans, monkeys also exhibit precise circadian oscillations in the behavior as shown by Richter [14]. He recorded the free-running activity of a squirrel monkey (*Saimiri sciureus*) for over three yeas that found to be persistent and regular.

2. Circadian clocks are dynamic and can respond or *entrain* to environmental changes.

The property of circadian clocks to respond to an external stimulus provides a mechanism to synchronize to the cycling environment. The alignment to the external cue, that is called *Zeitgeber* (from German meaning "time giver" or "synchronizer") is called entrainment. The work of Jürgen Aschoff, who is considered as co-founder of the Chronobiology field, has been instrumental in understanding how light-dark cycles affect the *phase of entrainment*. He worked with both birds and mammals, and showed that in constant light conditions (LL) the activity phase of nocturnal animals shortens, while in diurnal animals it lengthens [15]. This principle was named after him and known as Aschoff's Rule.

Other than the light-dark cycle, circadian clocks can be entrained to temperature cycles, feeding and hormones. This is of particular importance for multicellular organisms in which circadian coordination within different tissues is required for organismal homeostasis, and is further described in section 1.4.2.

3. Circadian rhythms show temperature compensation; their period remains nearly unchanged within a range of physiological temperatures.

As is the case for biochemical reactions governing the life of a cell, temperature could affect the period of circadian rhythms. In lower temperatures circadian clocks would run slower and in higher temperatures would run faster. However, such a response to environmental changes would not reliably anticipate the time of day. On the contrary, the capability of circadian clocks to compensate changes in ambient temperature makes them robust in adapting to the cycling environment, especially in poikilotherm animals. In mammals, in which the internal temperature does not vary depending on ambient temperature, temperature cycles are considered weak external cues, although temperature

acts as *Zeitgeber* for circadian rhythms in unicellular organisms [16] and tissues [17].

1.4.2 Organization and outputs of the circadian clock in mammals

In mammals, circadian clocks are present in nearly all tissues and cells. The master pacemaker or central clock is located in the brain, in the suprachiasmatic nucleus (SCN) of the hypothalamus which get synchronized to external conditions primarily by the light-dark cycles. Light is detected by specialized photoreceptors in the retina that relay the information via neuronal communication to the SCN. Subsequently, this signal generates electrical and endocrine signals that are sent to organs and tissues in the periphery via the autonomic nervous and endocrine systems, respectively, leading to circadian alignment between the master clock and the periphery (Fig. 1.1). This is exerted by interconnected physiological and behavioral processes that take place at specific times of day. For example, it has been shown that cognitive performance and muscular training in humans can be more effective at certain time windows throughout the day, both linked to oscillations in cardiovascular function and body temperature [9].

Peripheral clocks are thought to be synchronized by the central clock to ensure temporal control of coordinated physiological outputs that is essential for organismal homeostasis. In parallel, all mammalian tissues, such as the liver, heart, lungs and kidneys, have their own internal oscillator, that can be synchronized by other stimuli, such as temperature, feeding and glucocorticoids [19], [20], [21]. Peripheral clocks generate circadian rhythms that facilitate the function of the given tissue, thus one can speculate that tissue-specific co-regulators of the core clock mechanism may enhance the temporal control of the specialized tissue physiology. For example, time-restricted feeding of mice during their inactive phase (day) has been shown to modulate circadian gene expression in the liver separately from the SCN [22].

The understanding that circadian rhythms are endogenously generated in cells and

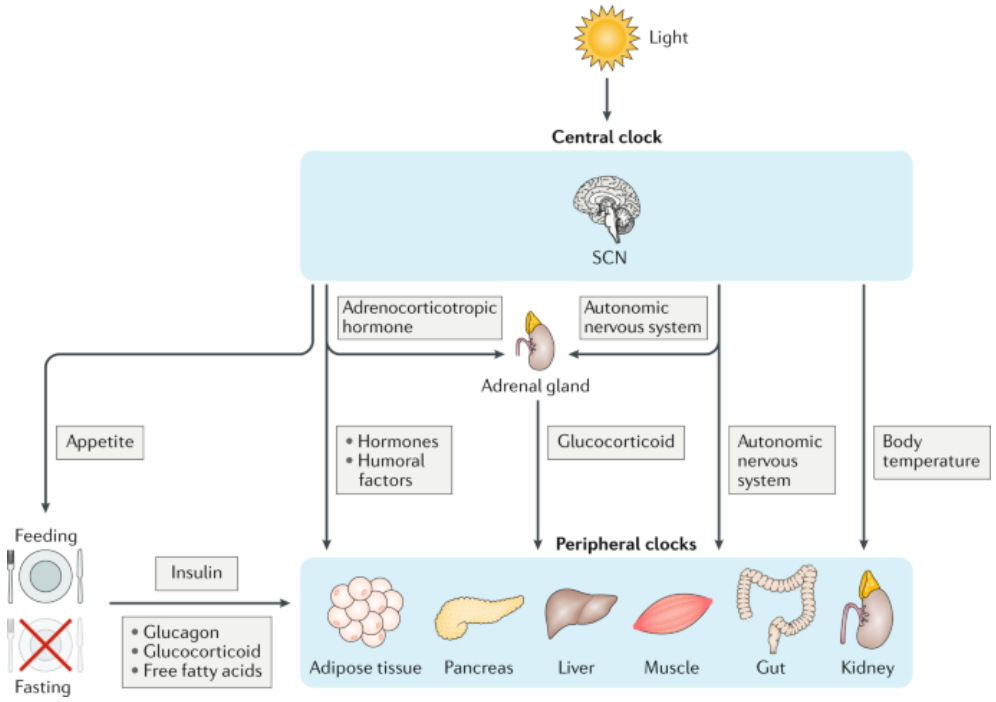

Figure 1.1: Organization of the circadian internal clock in mammals and its outputs. The central clock located in the suprachiasmatic nucleus (SCN) of the hypothalamus is synchronized by the light-dark cycles, that generates signals to ultimately synchronize peripheral clocks present in different organs and tissues. Peripheral clocks can be entrained to other cues, such as temperature, feeding and hormones. For more details, see text. Figure reproduced from [18].

tissues without the presence of the SCN became possible by recording the activity over time of the luciferase gene (*Luc*) that is under the control of a core clock promoter (e.g., *Bmal1* or *Per2*). Thus, both cultured cells and peripheral tissue explants sustain circadian oscillations [23], [24]. Nevertheless, without any external cue the cells in cultured conditions lose synchronization to one another, their phases become randomly distributed and show different intrinsic periods [24]. This indicates that a phenomenon called *coupling* is important for phase coherence among a cell population and sustaining the amplitude of the circadian rhythm. A more detailed description on how circadian synchrony can be monitored and measured is given in section 1.5.

1.4.3 The molecular mechanism of the circadian clock

The elucidation of the molecular clock mechanism across different domains of life has been achieved by using model organisms that allow genetic manipulation and laboratory housing. The non mammalian model systems that have been extensively used in circadian biology research are the non-photosynthetic bacterium (*Synechococcus elongatus* is the most studied model), the fungus *Neurospora crassa* and the fruit fly *Drosophila melanogaster*. Albeit involving different molecular components, the concept of how circadian rhythms are endogenously generated is conserved in different model organisms. For the rest of this thesis, any reference to circadian clock is about the mammalian circadian clock machinery, which is illustrated in Figure 1.2.

The molecular mechanism of the circadian clock can be described as a main Transcriptional - Translational Feedback Loop (TTFL). The core clock machinery is comprised of Brain and Muscle ARNT-Like 1 (BMAL1) and Circadian Locomotor Output Cycles Kaput (CLOCK) that act on the positive "arm" of the feedback loop (Fig. 1.2). BMAL1 and CLOCK proteins form heterodimer complexes (BMAL1:CLOCK) in the cytosol, that translocate into the nucleus and act as transcription factors. They induce the expression of target genes by binding to consensus motifs on their promoter region that are called E-boxes. The target genes are collectively called clock-controlled genes (CCGs). Among them are the *Cry1, Cry2* and *Per1, Per2* and *Per3*, which encode for CRYPTOCHROME and PERIOD proteins, respectively. These proteins constitute the negative "arm" of the molecular mechanism, which, together with common and other tissue-specific protein regulators, form a multi-subunit protein complex that binds to the BMAL1:CLOCK heterodimer, thereby inhibiting their own trascription and allowing for the loop to close. The time delay between gene expression activation and suppression is about 24 hours and is also achieved via post-translational modifications, such as phosphorylation, acetylation

and ubiquitination. For example, the casein kinases CKIδ and CKIϵ phosphorylate PER proteins that leads to ubiquitin-mediatated degradation [25]. Also, CRY protein turnover is regulated by a FBXL3 ubiquitin ligase-dependent manner [26]. The degradation of both PERs and CRYs is crucial for the repression state to hault and a new transcription cycle to commence.

Furthermore, the molecular mechanism contains an "accessory" or secondary feedback loop, that regulates the expression of *Bmal1* in a circadian manner (Fig. 1.2). *Bmal1* expression is activated by the nuclear receptors retinoid-related orphan receptor alpha (RORα) and receptor subfamily 1 group D member 1 (REV-ERBα). Both receptors bind to ROR elements in the promoter region of *Bmal1* inducing or suppressing the expression of *Bmal1*, respectively.

As molecular outputs of the circadian clock, it has been shown that the CCGs are involved in a variety of cellular processes, such as cell cycle regulation, apoptosis regulation, DNA damage response (DDR) and metabolism [27]. Genomic studies have shown that they account for up to 10-20 % of a given healthy tissue [28], although more recent studies have attributed up to 40 % of cycling genes (i.e., their expression oscillates in a 24-hour manner) of the protein coding genes in at least one organ [29]. Despite that the number of cycling genes can vary between different studies, the timed gene expression is of particular importance, because it can be speculated that there is a fundamental relationship between circadian rhythms and health [5]. In fact, in 2007 the International Agency for Research on Cancer (IARC) classified "shift work that involves circadian disruption" as a "probable human carcinogen" (Group 2A in the IARC classification system) [30]. Whether and how aberrant circadian rhythms may be connected to one of the most detrimental human diseases such as cancer is discussed in section 1.7.

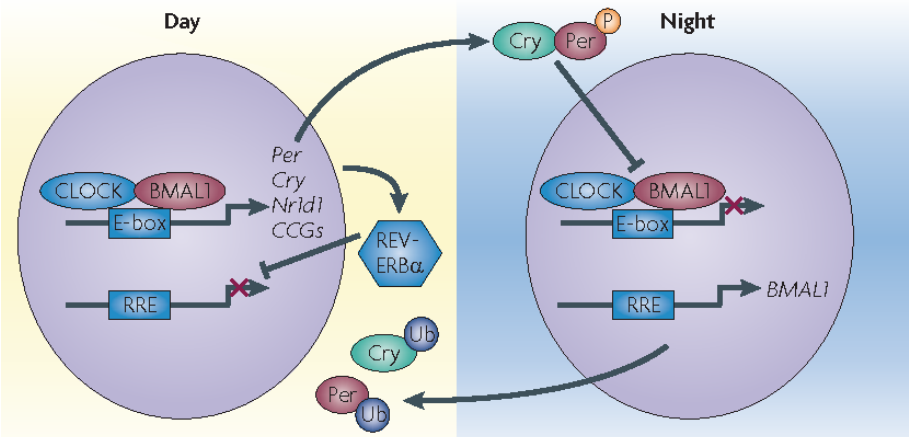

Figure 1.2: The molecular mechanism of the circadian clock in mammals. A core transcriptional-translational feedback loop (TTFL) in every tissue and cell takes places between the cytoplasm and the nucleus (purple). The TTFL consists of an activating arm that drives the expression of clock-controlled genes (CCGs), and a suppressing arm that inhibits their own transcription thereby closing the loop with a 24-hour delay. A secondary TTFL regulates the expression of BMAL1 in a circadian manner. For more details, see text. Figure reproduced from [31].

1.5 Signal analysis of molecular cycles

As described in section 1.4, circadian clocks are oscillatory systems that regulate molecular, physiological and behavioral rhythms in all phyla. While behavioral cycles, such as locomotor activity rhythms, require longer periods of observation to understand and describe their patterns, monitoring of molecular cycles in real-time has become possible using transgenic reporters [32]. Before explaining the different steps for the numerical analysis of circadian rhythms, the characteristics that describe circadian oscillations are first given in the section 1.5.1.

1.5.1 Parameters that describe circadian rhythms

Circadian rhythms describe an oscillatory process that repeats over the course of about 24 hours. Mathematically, this description is commonly represented as a sine wave curve depicted in Figure 1.3. One full oscillation -or one cycle- occurs around a baseline and

consists of a peak and a trough, that is the highest and the lowest point of the oscillation from the baseline, respectively. The distance of either a peak or trough from the baseline gives the Amplitude of the oscillation, and the distance between two consecutive peaks (or troughs) constitutes the Period of one cycle. The Phase of the rhythm within a cycle represents the time when a certain reference point (such as the peak) occurs given that the commencement of the oscillation takes place after or in response to a previous rhythm or stimulus [32].

When studying molecular circadian rhythms within a cell population (homogeneous or not), it is crucial to define and measure synchrony, a property that is exerted when the intrinsic circadian rhythms synchronize to the environment. To elucidate the degree of this synchrony, it is essential to record the circadian rhythm for as many cycles as possible [33]. When in synchrony, cells share the same period and maintain a constant *phase relationship*, that is when the rhythms of two different oscillators peak in relation either to a third oscillator or to each other [5]. For example, a group of rhythmic subjects (e.g., cells within a tissue) might share the same period after analysis of the circadian signal (the raw data collected over time), but this does not predict whether the circadian rhythm peaks at the same time for every single cell in the population.

Circadian synchrony (i.e., synchrony with a 24-hour periodicity) is for unicellular organisms a strategy to synchronize to the cycling environment and anticipate daily changes (see the example of *Lingulodinium polyedra* described in section 1.3). For cells in a multicellular organism, synchrony to the external cycles is less evident, and rather they synchronize to each other as being part of a larger cell population group, as is a tissue or an organ [33]. Intriguingly, cellular clocks within different local niches of a multicellular organism are not synchronized (or not "coupled") [34], indicating that each peripheral oscillator maintains a phase relationship with other clocks in the periphery as wells as with the central clock. This leads to interesting research questions, such as how

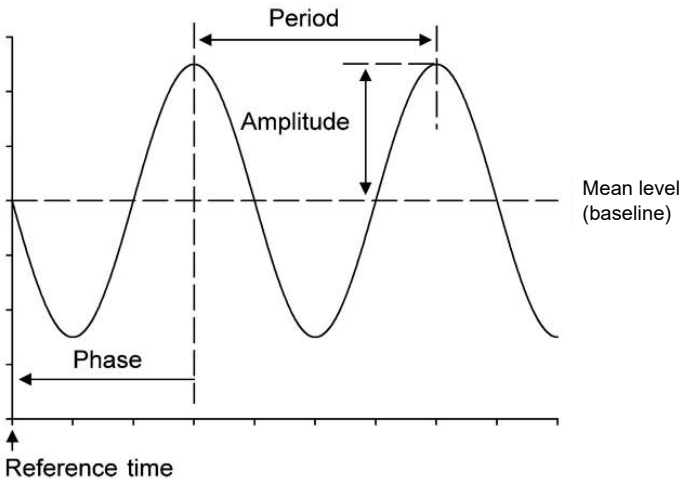

Figure 1.3: Circadian rhythms can be described with three parameters: the Period, the Amplitude and the Phase. For details, see text. Figure adapted from [35].

the rhythmic properties of cellular oscillators that are essential for synchrony within a defined cell population can sustain an indirect misalignment with the rest of the periphery, but resulting overall in organismal homeostasis and circadian alignment.

1.5.2 Signal acquisition

The monitoring of cellular rhythmicity involves measurement of a physiological or chemical reaction over time. Examples include recording of gene expression-driven bioluminescence (or fluorescence) and cAMP activity. In essence, a gene encoding for luciferase (LUC) or destabilized green fluorescent protein (GFP) is driven by a clock gene promoter [36], [37], [38]. The luciferase assay has been since its conception employed in a variety of model systems in circadian biology, from cyanobacteria [39], to plants [40] and mammals [41].

The bioluminescent or fluorescent signal is recorded at evenly spaced time intervals (usually every 15 up to 60 minutes), thereby circadian function can be elucidated by capturing gene expression dynamics. In essence, luciferase assay data represent the intensity of bioluminescence that was generated and acquired during the measurement. Before

the measurement begins, it is essential to stimulate the cells with external agents in order to synchronize their phases and, thereby, a reference time point can be set for the recording. Synchronization strategies include treatment with dexamethasone (DEX) [42] or forskolin [43], serum shock after starvation [44] and entrainment via temperature cycles with subsequent release in free-running conditions [45].

DEX is a glucocorticoid analogue that is potent to bind, and thereby, activate the cytosolic glucocorticoid receptor (GR), which in turn translocates into the nucleus and binds to GR elements on the promoters of core clock genes leading to the activation of the clock cycle [42]. Forskolin treatment leads to CREB activation, and thereby, to cAMP synthesis activating protein kinase A (PKA) [43]. PKA is further involved in phosphorylation of CREB, which binds to cAMP response elements in promoters of clock genes, such as *Per1* and *Per2* [46], thereby resetting the clock. In the same context, serum shock induces phosphorylation of the CLOCK protein via the Ca^{2+}-dependent PKC pathway [47], which leads to clock activation. Regarding the response to ambient temperature cycles, it has been shown that peripheral tissues and cells can be synchronized by temperature fluctuations [17], [45] that simulate the physiological body temperature changes [45].

The necessity to use synchronization agents suggests that the circadian rhythm - when aimed to be evaluated from the real-time recording- is a collective output of cellular circadian rhythms that are not inter-distinguishable. Such phenomenon is illustrated in Figure 1.4, where the response (in terms of the intensity of the bioluminescent or fluorescent signal produced or the power of the period estimate) of a cell population that is in synchrony or not can substantially differ. The ability to infer circadian function and synchrony in a cell population is achieved through signal conditioning methods, rhythmicity and period estimation. In order to elucidate the population dynamics within cellular oscillators, single-cell bioluminescence imaging could be employed [36], which is a matter of the research questions that are to be answered.

It is important to note that the frequency of the signal acquisition is required to be at least twice that of the highest frequency to be analysed. This is known as the *Nyquist* frequency [32], [48]. It indicates that if the sampling rate is once per hour, then the shortest periodicity that could be estimated would be two hours. Regarding the resolution of the period estimate, which defines whether a period of 24.5 hours can be distinguished from a period of 25.0 or 24.0 hours, depends on the number of total cycles that are recorded [32], [48]. Similarly, a long acquisition, thereby more available cycles are included in the data, proportionally correlates with the accuracy of the period estimation. Importantly, the sampling rate itself (e.g., whether the signal is measured every five, ten or 20 minutes) over a given duration of time does not increase the accuracy of a period estimate [32], [48].

What is more, it is often the case that in the recorded signal there are periodicities present other than 24 hours [32]. This might be due to ultradian rhythms, which include periodicities between 5 to 18 hours [49], that could interfere with the signal analysis evaluating 24-hour periodic components. For this, it is common to filter out both short and long periodicities as discussed in section 1.5.3.

1.5.3 Signal conditioning

After the measurement is completed, the signal is subject to preprocessing that is essential for further analysis. The first step is to assure that the acquired time series are non-stationary, which means that the period and amplitude do not change throughout the recording [48] -an example of a stationary and non-stationary signal is shown in Figure 1.5. This can be elucidated by plotting the raw data series, which is also crucial for determining the presence of any missing data points or outliers (that could be assigned to technical issues during the measurement). In that case, by averaging the intensity of consecutive time points (e.g., five or six), a so-called smoothed time series is produced,

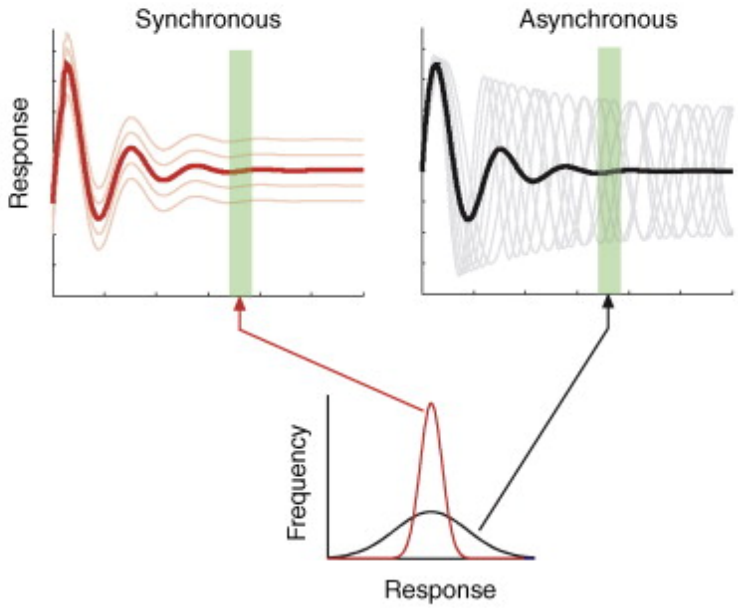

Figure 1.4: Responses in molecular cycles underlying circadian synchrony within a cell population vary depending on the phase relationship between the individual cells. For details, see text. Figure adapted from [50].

in which high frequency spikes are removed without eliminating any further frequencies that are likely present in the signal [32].

A common feature of luciferase recordings is that the intensity of bioluminescence decreases at a constant rate during the measurement generating a linear trend in the data (Fig. 1.6 middle panel). It is of particular importance that this trend is removed, because it can mask any underlying periodicity in the data [32]. The aim is therefore to produce a steady baseline around which the signal oscillates (Fig. 1.3). There are multiple methods for detrending, including i) subtracting a running average, ii) subtracting a linear or polynomial fit from the entire dataset, iii) applying a wavelet transform [51], or iv) applying a convolution filter [32].

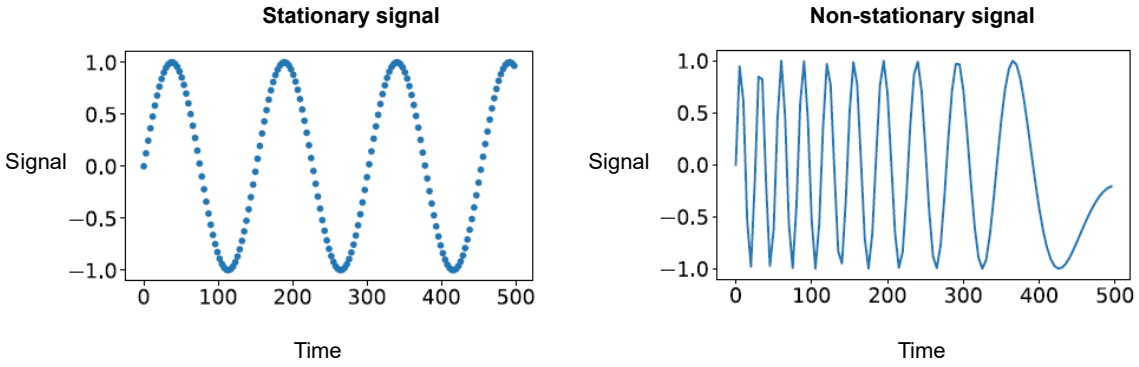

Figure 1.5: Stationary and non-stationary signals. Parameters of a time series signal, such as the period and amplitude, can remain constant (stationary signal) or change (non-stationary signal) throughout the measurement. Plots were reproduced from the Biological Oscillations Analysis Toolkit pyBoat from the GitHub repository (https://github.com/pyBOAT). Time scale in seconds.

1.5.4 Estimation of rhythmicity

The smoothed and detrended bioluminescent signal is subsequently used for rhythmicity testing that aims to identify whether there are any rhythmic components in the signal or whether the recording constitutes only by random frequencies (i.e., noise; Fig. 1.6 lower panel). Common tests for rhythmicity include: i) the autocorrelation function (ACF), ii) the Fisher's test and iii) the Lomb-Scargle periodogram (LSP) [48]. Statistical tests such as Analysis of Variance (ANOVA) cannot be implemented to determine rhythmicity, because it can only test if time is a significant variable in the analyzed dataset, not whether the data change over time [33].

The simplest test for rhythmicity is the ACF, which determines whether and to which extend a delayed (or lagged) copy signal correlates with the conditioned signal. The degree of autocorrelation is given by the autocorrelation coefficient, that ranges from 0 to 1. When the lag between the two time series is 0, then the autocorrelation coefficient is 1 and the signal is "perfectly" rhythmic, while an autocorrelation coefficient equal to 0 indicates a non-rhythmic signal. If the series is random, then the autocorrelation coefficient is close to 0 without increase. In a rhythmic signal, the autocorrelation coefficient is

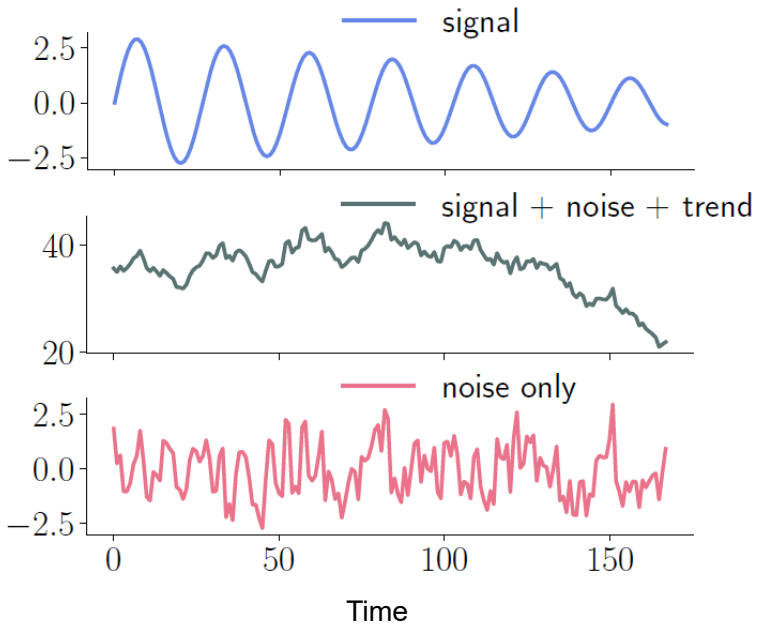

Figure 1.6: Components of a time series signal. For details, see text. Plots were reproduced from the Biological Oscillations Analysis Toolkit pyBoat from the GitHub repository (https://github.com/pyBOAT).

1 or close to 1 when the lag approximates the periodicity, revealing the presence of a periodic component. To elucidate whether this constitutes a real periodic component or it is due to a stochastic process, the ACF implements an ihnerit statistic test which computes the probability of a rhythmic componenent at 95 % conficence interval [32].

Regarding the ACF, two important aspects are worth highlighting. First, it is possible that the ACF does not determine significant rhythmicity, yet the time series appear to be rhythmic by visually inspecting the raw and detrended data. Reasons for such an inconsistency include a weak signal, noise in the signal or a short recording (less than 5 cycles). The confidence limit can thus be unrealistically high [32]. Second, it is possible that the ACF does determine significant rhythmicity, albeit there is no real rhythmic process in the data. In that case, two alternatives can be implemented: a) test for rhythmicity after data randomization and b) test for rhythmicity with an additional method (e.g., LSP).

1.5.5 Estimation of period

Once the signal has been evaluated and determined to contain a real rhythmic component, the period estimate and the certainty of the estimate can be calculated. Methods of period estimation are based on either fitting a periodic function on the detrended data or spectral analysis.

The cosine fit (or cosinor) method was first introduced by Franz Halberg [52]. The method assumes that circadian rhythms resemble sine wave-like rhythms with added noise, therefore they can be represented mathematically as cosine curves with known (or approximately known) period. The fit can be then obtained by linear regression using the method of least squares [35], therefore providing the parameters of the cosine curve that best describes the time series signal.

A set of methods for period estimation are based on spectral or *Fourier* analysis. The basis of those methods is the revolutionary idea of Joseph Fourier that any type of signal sampled over time at equal intervals -independently of its shape- can be represented as an infinite sum of sine and cosine curves of various frequencies [53]. This modulation is known as the Fourier Transform (FT) and its concept is depicted in Figure 1.7. FT constitutes a powerful tool for period estimation, because if a major spectral component is identified in the circadian range after spectral analysis, it can be inferred that the time series signal elicits circadian rhythmicity [35], [32]. Taken together, spectral analysis can detect and characterize the periodic components in a time series dataset, and the period length can be directly calculated by the inverse of the frequency (f = 1 / T).

Fourier-based methods used in chronobiology for period estimation are the LSP, the Chi-squared (X^2) periodogram and the Fast Fourier Transform - Non-Linear Least Squares (FFT-NLLS). Although no method is impeccable for period estimation, there are few points that are crucial for deciding which method to use when estimating period

length, one of the most important characteristics of the circadian rhythms [54].

First, a major advantage of the LSP is that it can accommodate time series data with missing time points or unevenly-sampled data. In principle, it assumes a sinusoidal pattern for a rhythmic component in the time series, but it is not a prerequisite [35]. On the other hand, LSP is considered to be prone to artifacts given that spurious peaks may appear in the spectrum in case of periodic harmonics present in the signal [35], [33]. However, the associated statistic test determines whether a peak is random or reveals significant rhythmicity [48]. Whether a peak is spurious or not is evaluated by computing statistical levels that correspond to false-alarm probabilities (P_{fa}) [55]. For example, usually P_{fa} of 10 %, 0.1 % or 0.01 % are used, which indicate the probability of a frequency peak to be false-positive corresponding to the chosen percentage threshold. By this inspection a spectral component at the circadian range can be further evaluated for its certainty. What is more, the presence of noise in the time series results in low-frequency estimates in the periodogram (Fig. 1.7 lower panel), albeit the major -when present- spectral component in the signal can still be detected with high accuracy (Fig. 1.7 lower panel).

The X^2 periodogram is a widely used method for estimating circadian period. The periodogram includes all frequencies that exceed a 95 % significance level and the peak with the highest power is given as the circadian period. Several studies have raised serious considerations about its accuracy when employed in short time series [35], [54]. A more recent study characterized a major source of bias in the X^2 periodogram resulting from the interaction between the true period and the length of the time course [56]. The X^2 periodogram is supported by numerous software packages for circadian data analysis, such as LumiCycle Analysis (Actimetrics) and BioDare (https://biodare2.ed.ac.uk/).

The FFT-NLLS method, as the name implies, estimates the period using FFT and then fits a sinusoid to the data giving the estimated period as starting point [32]. This approach has been considered weakened by cycle-to-cycle period and amplitude variation result-

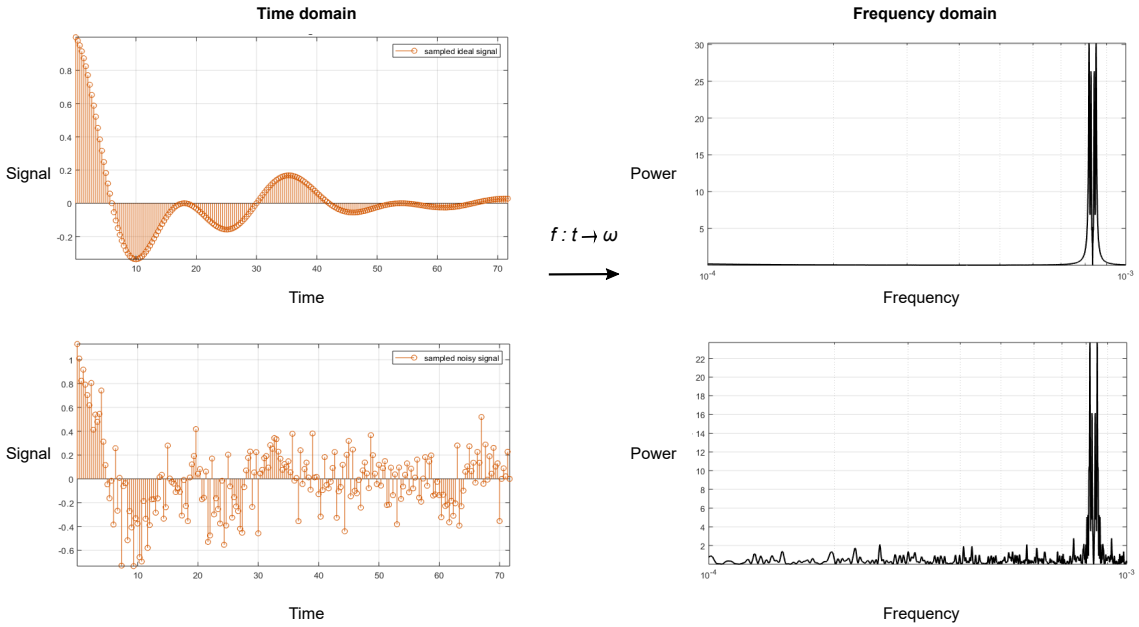

Figure 1.7: Fourier transform (FT) for time series signal analysis. Fourier analysis converts a signal from the original (time; t) domain to a representation in the frequency (ω) domain and vice versa. Various period estimation methods implement the FT (for details, see text). In case of noisy time series, low-frequency period estimates are present in the periodogram, albeit without exceeding the statistical threshold (not shown).

ing in spurious periodicities [33]. It can be computationally slow, and is supported by the Biodare platform (https://biodare2.ed.ac.uk/).

1.6 Pancreatic Ductal Adenocarcinoma

Pancreatic ductal adenocarcinoma (PDAC) is a deadly cancer type characterized by a number of biological hallmarks which are described in section 1.6.3, while current advances in PDAC research based on systems biology approaches are summarized in section 1.6.4. The molecular developmental program of the exocrine pancreas (section 1.6.1) combined with the most prevalent genetic mutations that have been identified in PDAC (section 1.6.2) are crucial for highlighting the importance of genetically engineered mouse models (section 1.6.2.2) as research tool for understanding the development and

progression of human PDAC as well as for pre-clinical testing.

1.6.1 Development of the exocrine pancreas

Given that PDAC is an exocrine type of pancreatic cancer, and the study of PDAC using animal models (see section 1.6.2.2) is based on utilizing pancreas- and exocrine pancreas-specific transcription factors, it is considered important to give a short overview of pancreatic cell fate determination (Fig. 1.8 A). The development of the pancreas arises from the foregut endoderm after inhibition of the Hedgehog signaling and the expression of two homeodomain transcription factors, HLXB9 and PDX1 [57]. PDX1 is also critical for the development of the stomach, duodenum and the bile duct, while *Pdx1* homozygous deletion results in failure of pancreatic development [57].

At an early stage of embryonic development, PDX1-positive multipotent precursor cells further differentiate in endocrine (islet), acinar and ductal cell lineages [57]. To note, islet cell types are involved in the regulation of systemic glucose metabolism by secreting hormones as insulin (β cells) and glucagon (α cells). The exocrine pancreas is responsible for production and secretion of digestive enzymes, such as proteases (chymotrypsinogen and trypsinogen), lipases (pancreatic lipase) and carboxylases (amylase) as well as bicarbonate for optimal pH regulation [58]. The secretion of the pancreatic juice in the common bile duct is facilitated via the pancreatic duct (Fig. 1.8 B), which ultimately drains into the intestine [58].

The transcription factor PTF1a-p48 (p48) is required for the fate determination of all three pancreatic cell lineages. Exocrine cells maintain p48 and lose PDX1 expression, while islet precursor cells maintain PDX1 and lose p48 expression. Interestingly, no ductal cell-specific have been identified as regulators of ductal differentiation [58]. Relatively recent studies have shown that differentiated exocrine cell types can effectively act as sources for β cell neogenesis [59], illustrating unexpected plasticity between pancreatic

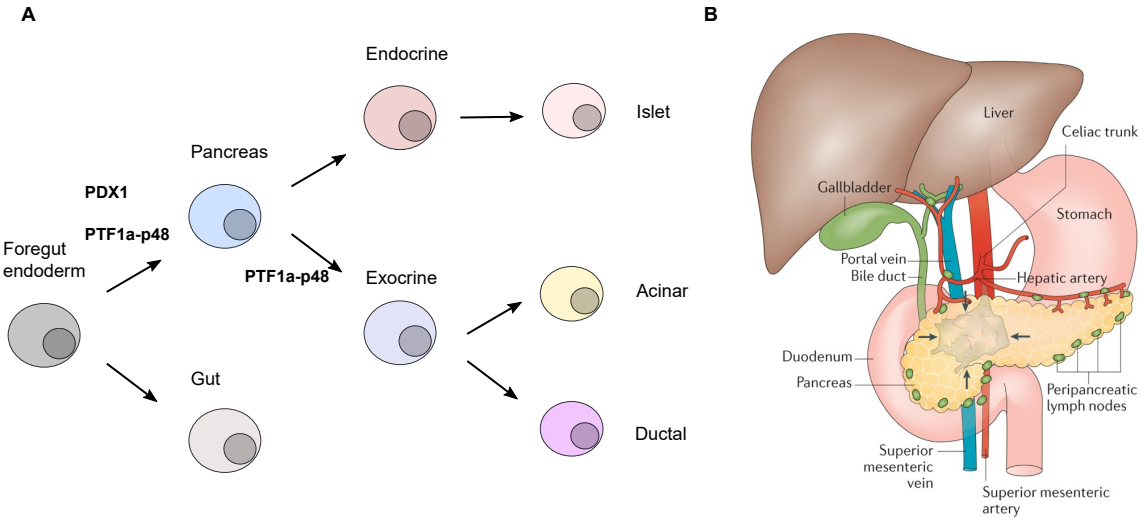

Figure 1.8: A) Development of the exocrine pancreas follows strict transcriptional programs. Figure adapted from [57]. B) The pancreas is located in close proximity to liver, spleen and stomach. The pancreatic juice essential for digestion is secreted in the bile duct via the pancreatic duct. The development of a solid tumor mass in the pancreas is supported by the portal vein circulation system. Figure reproduced from [61].

lineages. Importantly, acinar plasticity is highly evident in acinar-to-ductal metaplasia (ADM), an early crucial event for PDAC tumorigenesis [60].

The transcriptional cascades determining the pancreatic cell fate have been the basis for genetic engineering approaches to generate mouse models that could recapitulate pancreatic development and offer the tools for understanding PDAC development and progression. More details are given in section 1.6.2.2.

1.6.2 Progression model of PDAC development

Histological and genetic analyses have identified that PDAC results from accumulation of genetic alterations that is usually a lengthy yet dormant process without apparent physiological symptoms.

In human PDAC, the most prevalent hypothesis for PDAC development is that genetic mutations give rise to ductal neoplasms designated pancreatic intraepithelial neo-

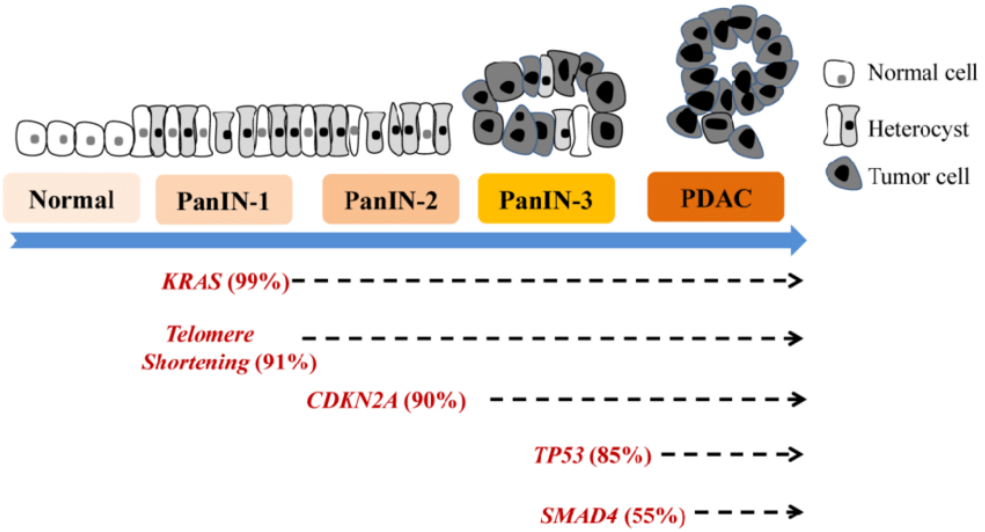

Figure 1.9: Genetic model for PDAC development and progression. For details, see text. Figure reproduced from [65].

plasias (PanINs), which result in a stepwise manner to carcinoma (Fig. 1.9), accompanied by accumulation of specific genetic mutations [62]. PanINs have been characterized in three different morphological architectures: PanIN-1 and PanIN-2 include transformed, elongated epithelium, while PanIN-3 display increased neoplastic cellular atypia [63] (Fig. 1.9). Activating mutations in *Kras* gene (see section 1.6.2.1) are present in PanIN-1 precursor lesions, while PanIN-2 and PanIN-3 are commonly characterized by genomic structural alterations and inactivation of tumor suppressor genes, such as *Cdkn2a*, respectively. Therefore, it is believed that the initial oncogenic mutation of *Kras* is necessary but not sufficient for PDAC progression [64]. Genomic instability events, such as telomere shortening, and further mutations in tumor suppressor genes as tumor protein p53 (*Tp53*), cyclin-dependent kinase inhibitor 2A (*Cdkn2a*), and SMAD family member 4 (*Smad4*), arise during PanINs progression as depicted in Figure 1.9.

1.6.2.1 Signaling cascades of oncogenic KRAS in PDAC

The most prevalent genetic mutation found in 75-100 % of pancreatic cancers [63], [66] is the gain-of-function point mutation of the *Kirsten rat sarcoma virus (Kras)* gene resulting in substitution of a single amino acid in the KRAS protein; mostly in codon 12, in which the point mutation results in exchange of Glycine (G) for Aspartic acid (D) [66]. As a result, the mutated KRAS protein ($KRAS^{G12D}$) is constitutively active which is detrimental for the regulation of cell proliferation due to its involvement in multiple downstream signaling cascades [63] as depicted in Figure 1.10.

Under normal conditions, KRAS, the effector protein of the mitogen-activated protein kinase (MAPK) signaling pathway, exchanges GDP with GTP as a response to activation of membrane-bound protein receptors by growth factors, cytokines or hormones [63]. The signaling cascade consisting of subsequent phosphorylation events leads to activation of transcription factors that induce the expression of genes associated with cell survival, proliferation and/or inhibition of apoptosis (Fig. 1.10).

In oncogenic KRAS signaling, GTP hydrolysis is inhibited after activation of receptor tyrosine kinases (RTKs) and GDP-bound exchange for GTP in KRAS, which would allow the inactivation of the signaling cascade as a feedback loop and ultimately return to homeostasis. In contrast, the continuous activation of KRAS leads to constant expression of protooncogenes even in the absence of mitogenic stimuli leading to uncontrolled cell proliferation. Interestingly, amplification and/or overexpression of RTKs [67] as well as simultaneous activation of multiple RTKs [68] has been reported, thereby further hindering the inactivation of oncogenic KRAS signaling cascades.

Importantly, additional activating mutations downstream of KRAS signaling have been reported in PDAC, such as PI3K/mTOR and BRAF/MAPK, albeit less frequent [69]. For example, oncogenic mutations in *Pik3c2a* results in constitutive activation of

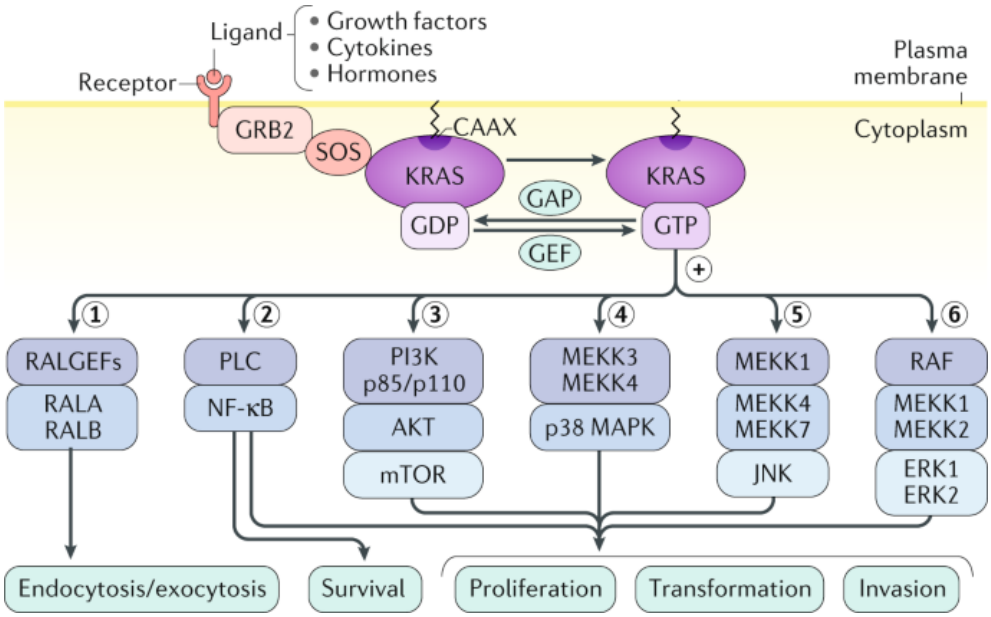

Figure 1.10: Signaling pathways of effector KRAS. Oncogenic KRAS signaling cascades impact a plethora of biological pathways related to cell proliferation and survival. Figure reproduced from [71].

PI3K/AKT/mTOR pathway singaling, which leads to high fatty acid biogenesis [70].

1.6.2.2 Genetically engineered mouse models of PDAC

The elucidation in the development of the molecular architecture of normal pancreas in the mouse has provided the framework for genetic manipulations to generate genetically engineered mouse models (GEMM) of PDAC. These models have been crucial for the study and understanding of PDAC early development and progression with the goal to facilitate the discovery of novel genetic and phenotypic markers that could explain, and possibly predict treatment outcome or serve as diagnostic markers.

The most prevalent of genetic mutations in *Kras* and *Tp53* as seen in section 1.6.2 have been used for generating conditional gene "knock-in" mouse models using the Cre-loxP system [57]. Breeding between transgenic mice harboring pancreatic progenitor cells, such as *Pdx1-Cre*, with mice expressing a "lox-$Kras^{G12D}$-lox" cassette results in off-

spring mice that express endogenous $Kras^{G12D}$ in a tissue-specific manner. This model was introduced in 2005 by Horigami, who few years later reported an additional GEMM model that combines endogenous Kras activation with tumor suppressor $Tp53^{R172H}$ inactivation [57]. GEMMs recapitulate very closely the morphological and molecular events that characterize PDAC phenotype in humans. However, there are pathologic features of mouse PDAC that differ from human PDAC, such as multilineage differentiation, little to no desmoplasia and development of metastasis [57].

Lastly, transplantation models that involve the transplantation of human or mouse PDAC cells into recipient wild-type mice (xenograft and allograft models, respectively) also mimic PDAC development and progression, albeit they serve as more time- and cost-efficient models [72]. The transplantation can be either in the pancreas (orthotopic injection) or in distal sites (heterotopic injection), such as in spleen or skin. Allograft models have been shown to develop up to 90 % liver metastases [73], which is considered to closer resemble sporadic mutations in KRAS as found in human PDAC.

1.6.3 Biological hallmarks

PDAC is an aggressive malignancy arising from the exocrine glands of the pancreas. About 90 % of pancreatic cancers are exocrine [62], while the remaining 10 % accounts for neuroendocrine cancers (also called islet tumors that will not be discussed). PDAC is the 7th leading cause of cancer-related deaths worldwide [74] and the 5-year survival rate does not exceed 9 % of diagnosed PDAC patients preceding the poorest prognosis among all cancer types [74]. In addition, 80 % of PDAC patients are diagnosed at an advanced stage or with present metastases restricting treatment options such as surgical resection [75]. The ultimate therapeutic regimen consists of chemo- and radiotherapy sessions that have detrimental side effects for the patients.

A number of risk factors for pancreatic cancer have been identified. Apart from

chronic pancreatitis and aging [76], a prevalent risk factor constitute metabolic-related disorders such as type II diabetes and obesity [77], [78]. Importantly, life style habits as tobacco and alcohol abuse have also been reported as risk factors [79]. Lastly, genetic predisposition due to germline mutations account for approximately 6 % of PDAC cases [80].

Thanks to the advancement of next-generation sequencing (NGS) technologies, genome-wide associated studies (GWAS) in human patients have identified that numerous distinct genetic mutations account for the PDAC phenotype [81]. In addition, chromosomal rearrangements, copy number variations, gene expression alterations and epigenetic modifications have shown to underpin the genetic instability that governs PDAC development and progression [82]. Thus, PDAC is considered a highly heterogeneous malignancy characterized further by a dense stromal reaction, immunosuppressive tumor microenvironment (TME), metabolic reprogrammning, metastasis formation and treatment limitations. In the following paragraphs each one of those characteristics is discussed.

The TME in PDAC consits of pancreatic cancer cells, pancreatic stellate cells (PSCs), diverse immune cell populations, blood vessels and extracellular matrix (ECM) [83]. An illustration of TME is depicted in Figure 1.11. Apart from tumor cell-intrinsic pathways that largely attribute to an escape from immune response, TME fosters a niche of immunomodulation via cytokine secretion. In essence, pancreatic cancer cells secrete cytokines that chemically attract immunosuppressive cells, such as regulatory T cells (T_{reg}), neutrophils and tumor-associated macrophages (TAMs). This results in inhibition of cytotoxic T cells ($CD8^+$). Immune cell infiltration also promotes angiogenesis by cytokine and growth factor release. This enhances the nutrient supply and supports the invasive capacity of mesenchymal cancer cells undergone epithelial-to-mesenchymal transition (EMT). Furthermore, as a response to cytokines, activated PSCs (also known as cancer-

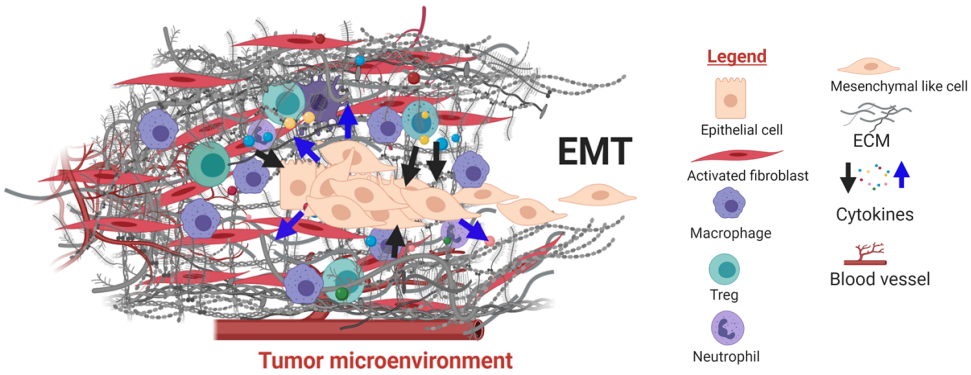

Figure 1.11: Tumor microenvironment (TME) composition and desmoplasmic reaction are indispensable components for PDAC development and progression. For details, see text. EMT: Epithelial-to-mesenchymal transition. Figure reproduced from [83].

associated fibroblasts) produce ECM proteins, including fibronectin and type I collagen [84], underpinning a dense desmoplastic reaction that can account for up to 90 % of the total tumor volume [75]. Overall, TME in PDAC can be described as an immunosuppressive niche that fosters tumor growth, metastasis and ultimately resistance to chemotherapy, thus constituting an essential component in PDAC progression.

Another important hallmark of PDAC biology is the metabolic rewiring required for meeting the extensively high energy demands of PDAC cells to maintain aberrant cell proliferation and growth. In essence, metabolic rewiring derives from the ability of cancer cells to "steer" nutrients, such as glucose and tricarboxylic acid (TCA) cycle intermediates, and maintain redox homeostasis. This is instrumental for sustaining anabolic processes for energy production at a high rate as well as for balancing oxidative stress byproducts of those anabolic reactions. PDAC cells depend heavily on glucose and anaerobic metabolism despite the presence of oxygen (known as Warburg effect) [85]. This has been shown to be mediated by upregulation of the glucose transporter GLUT1 and of rate-limiting enzymes in the glycolytic pathway, such as Hexokinase 1 and 2 (HK1, HK2) [85], [86].

Constitutive KRAS activation is also linked to increased production of precursors for DNA and RNA synthesis via the pentose phosphate pathway (PPP) [86], which additionally results in production of reducing power that is necessary for anabolic processes. Furthermore, KRAS-driven PDAC tumors have been found to rewire glutamine (Gln) metabolism for obtaining nitrogen and carbon precursors to support the anabolic demands [87]. This is achieved by oncogenic KRAS signaling-mediated upregulation of glutamate dehydrogenase (GLUD1) and aspartate transaminase (GOT1). In mitochondria, GLUD1 catalyzes the conversion of glutamate (Glu) to aspartate (Asp), which is further converted in the cytosol to oxaloacetate and malate, ultimately resulting in NADPH production [87]. It is known that NADPH serves as coenzyme of redox agents, such as glutathione and, thereby, facilitates scavenging of reactive oxygen species (ROS). ROS are by-products of high cell proliferation, and antioxidant molecules, sush as glutathione and thioredoxin, are constantly recycled to outweigh oxidative stress. At the same time, NAD(P)H oxidation results in $NAD(P)^+$ production, which supports enhanced glycolysis.

An alternative pathway that may be enhanced in PDAC to maintain high proliferative rates is autophagy [88]. In healthy cells, autophagy-mediated nutrient scavenging takes place in presence of a stressful stimulus, such as hypoxia, starvation, radiation or due to a cytotoxic agent [89]. In cancer cells, this mechanism can be activated with pro-proliferative effects, thereby supporting tumor growth and may be linked to tumor cell survival and resistance therapy in PDAC [90].

Lastly, a detrimental characteristic of PDAC is its invasiveness due to metastasis. To metastasize, tumor cells detach from their primary niche and migrate through the circulation or the lymphatic system to finally extravasate and form a secondary tumor niche [91] (Fig. 1.12). The transition of epithelial tumor cells residing in the primary tumor site into motile mesenchymal cells takes place through a process called epithelial-to-mesenchymal transition (EMT) [92]. EMT is an important developmental process during

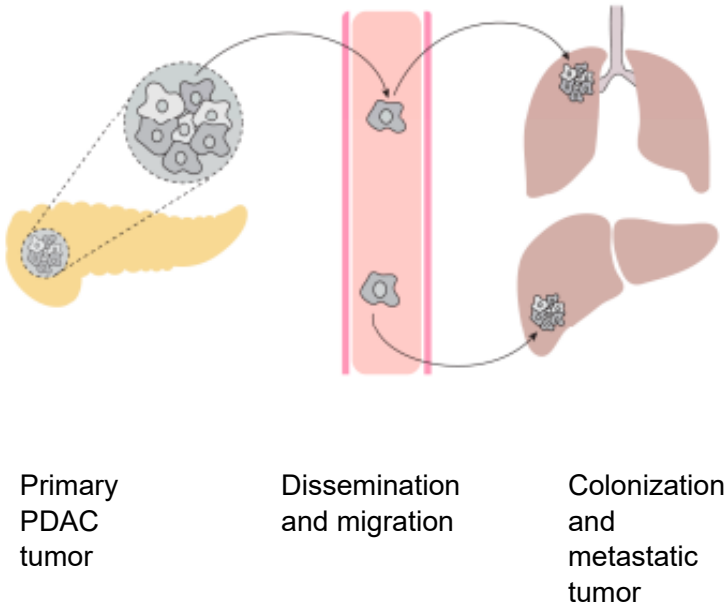

Figure 1.12: Metastasis formation in PDAC require dissemination of the primary tumor and establishment of a secondary tumor niche after migration through the circulation. Major metastatic sites are the liver and the lungs. Figure adapted from [72].

embryogenesis [93], and essential for cancer metastasis. On the molecular level, it has been extensively studied and it has been shown that TGF-β signaling is the most prominent pathway associated with EMT [92]. It involves activation of TGF-β receptor and subsequent activation of proteins SMAD1 and SMAD3 that collectively activate SMAD4. The latter translocates to the nucleus and induces the activity of transcription factors, such as SNAIL and TWIST [94], that ultimately lead to repression of E-cadherin expression, necessary for the adherence of the epithelial cells at cell junctions [94].

It is important to note that metastasis can occur at early stages of PDAC development and research efforts have been performed to identify potential pre-metastatic genes or markers [72]. However, the results have been unfruitful so far, although it was shown that additional genetic mutations are indispensable for dissemination of the tumor cells [95].

1.6.4 Systems biology approaches in PDAC research

Over the last two decades, high-throughput sequencing technologies and phenotypic quantitative methods, such as proteomics and metabolomics, have been introduced in cancer research. Systematic studies aim to functionally characterize cancer cells and tissues, and to integrate the generated knowledge for elucidating the complexity of a pathological condition as cancer. Ultimately, the aim is to translate the available information into clinical applications by discovering novel diagnostic markers, designing customized treatment strategies and predict treatment outcomes.

In the context of PDAC, the vast majority of systematic efforts have focused on sequencing technologies (genomics and transcriptomics) in order to define molecular subtypes of PDAC that could lead to novel biomarker discovery and assist the design of subtype-specific therapies. So far, there is a substantial overlap in classification from different transcriptomics studies, albeit no identical, as depicted in Figure 1.13 Collisson and colleagues identified three subtypes (exocrine-like, classical and quasimesenchymal) [96]. Moffitt and colleagues classified PDAC tumors in two subtypes (basal-like and classical) [97], while Bailey and colleagues stratified PDAC tumor samples in four subtypes, that included squamous, ADEX, immunogenic and pancreatic progenitor subtype [98].

To date, PDAC molecular subtyping is based on global gene expression utilizing RNA sequencing technologies (RNA-seq). Functional characterization of PDAC subtypes may prove to add invaluable information given that gene expression is far from proportional to protein function due to post-transcriptional and post-translational mechanisms [99]. In essence, phenotypic profiling of PDAC tumors via proteomics could identify additional features that may facilitate the identification of subtype-specific protein markers in an unbiased manner. Proteomic profiling of PDAC tissue would also facilitate the stratifica-

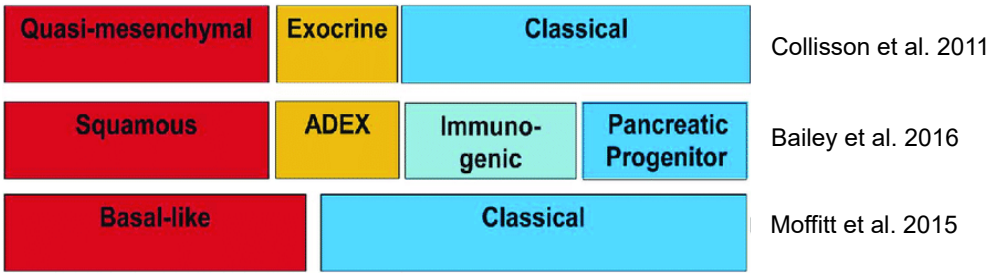

Figure 1.13: Molecular subtypes in PDAC based on transcriptomic profiling as established from different studies. Figure adapted from [100].

tion of patients and potentially predict the response to treatment.

1.7 Links between circadian rhythms and cancer

In this section, the interplay between circadian clock outputs and carcinogenesis will be discussed. The application of circadian biology in cancer research has been intensified in the last few years, albeit the first studies about potential circadian timing in cancer treatments as well as studies linking circadian misalignment to cancer biology have been performed about two decades ago [101], [102]. In the following sections, an overview of accumulated evidence supporting the reciprocity between circadian clock function and tumor development is given (Fig. 1.15). Overall, understanding the role of circadian rhythms in tumor development and progression is crucial for better understanding causes of cancer and how to treat them.

1.7.1 Environmental disruption of circadian rhythms and cancer

As described in section 1.4.2, circadian rhythms temporally regulate many physiological and behavioral processes. Environmental disruption of circadian rhythms is evident when there is a desynchronization between the internal free-running clock and the external conditions, that can result from shift work, jet lag or aberrant meal timing [5]. For effects as detrimental as carcinogenesis, such desynchronization relies on chronic expo-

sure under the aforementioned conditions.

Several lines of evidence have shown that environmental circadian disruption is associated with carcinogenesis. For example, a prospective cohort study on nurses working night shifts, found that women chronically working at night had 36 % higher risk in developing breast cancer [103]. A more recent study showed that night shift work increases the risk of breast cancer in pre-menopausal women, especially in those with long light exposure at night [104]. Kubo and colleagues conducted a prospective cohort study with male night shift-workers and found a higher risk for prostate cancer in rotating shift-workers [105]. Furthermore, aberrant or antiphase sleeping schedule was correlated both with higher risk for breast and prostate cancer in individuals that had never worked at night [106].

In addition to epidemiological data, experimental studies have shown association between physiologic circadian disruption and increased cancer risk. For example, disruption of the central clock in an engineered mouse model of lung cancer resulted in increased tumor growth and progression [107]. Van Dycke and colleagues exposed breast cancer-prone mice in alternating light-dark cycles and found increased breast cancer development, linking internal desynchrony with tumorigenesis [108]. What is more, mice kept under constant light conditions developed hepatocarcinoma, lung carcinoma and leukemia at higher frequency compared to mice kept under normal light/dark schedule (12 hours light : 12 hours night) conditions [109].

Furthermore, restoration of circadian rhythms in melanoma and colon cancer cells was found to inhibit tumor growth [110]. Filipski and Lévi showed that timed food intake in mice with a disrupted systemic clock due to chronic experimental jet-lag conditions decreased tumor growth in the liver. This study showed that meal timing outweighed the accelerating tumor growth due to physiologic circadian disruption, highlighting the impact of circadian rhythms on tumor development and their potential in preventing

and/or treatment of circadian malfunctions that can lead to tumorigenesis [111].

1.7.2 Genetic disruption of circadian rhythms and cancer

The link between circadian disruption and carcinogenesis is further supported by studies that have identified genetic mutations and/or altered gene expression of core clock genes among different types of cancer. For example, using data from The Cancer Genome Atlas (TCGA), Ye and colleagues analyzed multi-dimensional omics data from 32 different cancer types and reported that clock genes exhibit global alterations at genetic (i.e., mutations), transcriptional (i.e., up- or downregulation of gene expression) and epigenetic (i.e., methylation) level [112]. Importantly, these global modifications were linked to dysfuntion of the circadian clock in patient tumor samples. Moreover, alterations in clock gene expression was found to be correlated with patient survival and clinical features, such as tumor stage and subtype. Finally, the study suggested that the core clock genes *Nr1d1, Npas2 and Arntl2* may function as oncogenes, while *Pers, Crys* and *Ror* may act as tumor suppressors [112].

In addition, the expression of *Per1, Per2* and *Per3* was found deregulated in several breast cancer cell lines [113], while decreased expression of *Per1* and *Per2* has been found in breast tumor samples [114]. In a recent study, Jiang and colleagues showed that clock protein levels were downregulated in tumor samples from pancreatic cancer patients [115]. Moreover, the expression of *Per* genes and *Clock* was found significantly lower in ovarian cancer tissues compared to health ovarian tissues [116]. In this study, the authors suggested the combination of *Cry1* and *Bmal1* expression as prognostic factor for ovarian cancer. In addition, in untreated colorectal cancer tissue was found that the expression of *Clock* was significantly lower compared to the adjacent mucosa, while high expression of *Bmal1* and low expression of *Per1* was correlated with liver metastasis [117].

It is also important to note that several studies have investigated whether genetic

deletion of clock genes predisposes mouse models to carcinogenesis. In particular, Fu and colleagues were the first to report that *Per2*-mutant mice developed tumors at a higher rate after irradiation compared to the wild-type counterparts [118]. The authors attributed the phenotype to increased *c-Myc* expression and lower p53 protein expression, leading to increased cell proliferation and inhibition of apoptosis. However, Yu and Weaver have summarised in an extensive review article the effects of total deletion of clock genes on a variety of factors related to circadian behavior, response to irradiation and aging [119]. It can be concluded that null mutant mice for clock genes do not show higher cancer incidence, albeit clock gene deletion accounts for aging phenotypes. This is also supported by another study that showed BMAL1-dependent mechanisms correlate with lifespan through mammalian Target of Rapamycin Complex 1 (mTORC1) activity [120].

Overall, dysfunction of the circadian clock in tumors appears to be a common characteristic. Experimental data show that these genetic disturbances are linked to increased cancer incidence and progression. In the next two sections, possible mechanistic connections between circadian clock and "hallmarks" of cancer are presented.

1.7.3 Hallmarks of cancer and connection to the circadian clock

It is worth mentioning that several biological processes that are deregulated in cancer have been found to be linked in circadian rhythms, such as cell division cycle, metabolism, apoptosis and DNA damage response [121], [122]. In the frame of this thesis work, the first two are discussed further and illustrated in Figure 1.15.

1.7.3.1 Cell cycle

The cell cycle is a well-defined and tight-regulated sequence of cellular processes that ascribe to the lifetime of the cell. The cell cycle progression has been described more

than 70 years ago [123] and aims to control cell division, an important element for cell and tissue homeostasis. The cell cycle consists primarily of two phases, the pre-mitotic and the mitotic (M) phase. The former comprises further by three phases, that are G_1, where signaling processes that are important for upcoming cell division take place. S phase, in which DNA replication occurs, and G_2 phase, where growth of cell components essential for subsequent division takes place (Fig. 1.14). In the latter phase, the actual cell division takes place and the duration is substantially shorter than the pre-mitotic phase [124]. Lastly, somatic, non-dividing cells are considered to have "exited" the cell cycle and be in the quiescent G_0 phase, and can "enter" upon stimulation by growth factors (mitogens).

The transition from each phase of the cell cycle to the next (also referred to as "checkpoints") is tightly controlled by specific protein complexes consisting of cyclins and cyclin-dependent kinases (CDKs) that are activated in a sequential manner [125]. In essence, entry to G_1 is regulated by cyclinD-CDK4/6 complex, G_1/S transition is controlled by cyclinE/CDK2; S phase is regulated by cyclinA/CDK2 complex and the transition S/G_2 is activated by cyclinA/CDK1; G_2 checkpoint depends on cyclinB/CDK1 (Fig. 1.14).

The deregulated cell cycle resulting in aberrant cell proliferation is a hallmark of cancer [126]. Recent studies have shown that circadian regulated genes may act as upstream regulators of the cell cycle checkpoints, providing a time window where the corresponding process may take place. For example, the protein kinase WEE1, a clock-controlled gene, was found to inhibit the cyclinB/CDK1 complex activity by phosphorylating the CDK1 [127]. Furthermore, cyclins B1 (*Ccnb1*) and D1 (*Ccnd1*), as well as cell cycle-related genes, such as *p21*, *p16* and *c-Myc* are considered to be under circadian control in normal tissues [128]. In a study by Altman and colleagues, it was suggested that in human osteosarcoma (U2-OS) cells, c-MYC recognizes and binds to the same DNA binding re-

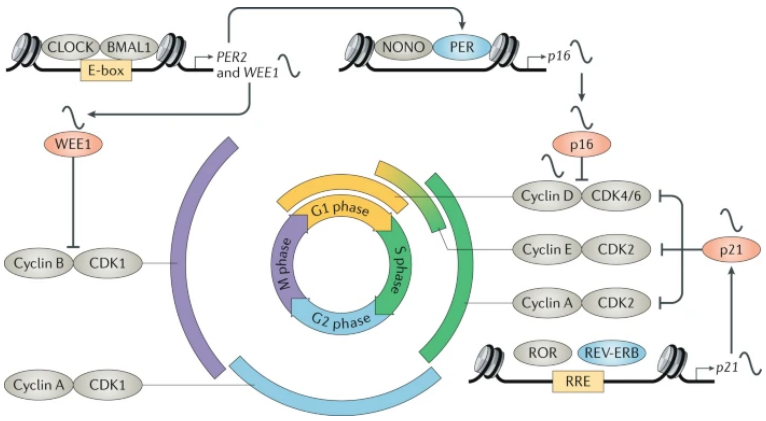

Figure 1.14: Molecular links between the circadian clock and cell cycle. The two cellular oscillatory systems are interconnected via protein regulators, such as WEE1, p21 and p16. For details, see text. Figure reproduced from [18].

gions as the BMAL1:CLOCK heterodimer [129]. Thus, the molecular mechanism of the clock is disrupted without the core clock components to be altered. The possible implication of c-MYC in the circadian clock function is also supported by the finding that c-MYC is a target of CRY2-dependent protein turnover [130], suggesting that degradation of c-Myc at specific times of day is essential for normal function of the molecular clock.

Given that functional interplays between the circadian clock machinery and the cell cycle have been identified, it has been speculated that circadian rhythms may play a role in temporally gating the cell division. It is challenging to elucidate such a "cause-consequence" relationship in a cancer cell, since there are multiple interconnections between the two systems that could disrupt their coupling [131]. This suggests, that whether circadian clock disruption is a prerequisite or a result of cell transformation still remains unclear. Taken together, a comprehensive understanding of the molecular links between circadian clock and cell cycle is crucial when studying circadian rhythms in carcinogenesis.

1.7.3.2 Metabolism

Another important hallmark of cancer is the altered state of cellular metabolism [126]. There are several lines of evidence showing a close relationship between circadian clock function and metabolic processes. Therefore, it is tempting to speculate that metabolic abnormalities seen in cancer cells might be a result of circadian dysfunction [18].

In a study by Kettner and colleagues, it was found that chronic jet lag in wild-type mice induced formation of hepatocellular carcinoma (HCC), while gene expression analysis showed global metabolic deregulation in the liver [132]. In addition, exposure of wild-type rats to constant light conditions facilitated glioma tumor growth compared to rats kept under normal night/dark conditions [133]. The authors demonstrated that systemic circadian disruption promoted a global anabolic upregulation exhibited by elevated glucose and triglycerides levels that supported tumor growth. Interestingly, genetic disruption of circadian rhythms impacts systemic metabolic regulation, since *Clock* null mutant mice show signs of metabolic syndrome [134].

A further indirect connection between cancer, metabolism and circadian regulation is supported by the finding of a recent study using a mouse model for lung adenocarcinoma [135]. The authors showed that lung cancer does not impact core clock components of the hepatic clock rather the overall rewiring of hepatic metabolism. Lung cancer was interpreted as an endogenous circadian modulator producing cytokines that have the potential to distally act as metabolic regulators [135].

On the molecular level, it still remains unclear how clock proteins modulate metabolic processes, and in which degree this is further impacted by a cancerous cell state. One intriguing mechanism involving chromatin remodelling via the Sirtuin 1 (SIRT1) has been suggested [136]. In particular, SIRT1 is a NAD^+-dependent histone deacetylase that plays an important role in epigenetic control of metabolism regulating

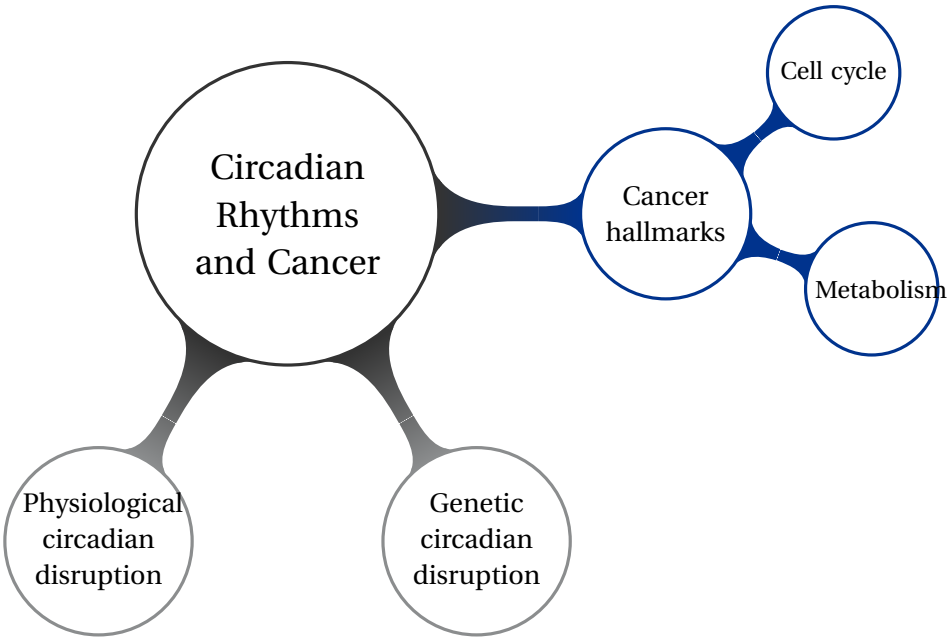

Figure 1.15: Links between circadian rhythms and carcinogenesis. For details, see text.

glucose homeostasis [137] and fatty acid metabolism [138]. SIRT1 (as the rest of Sirtuins, and in contrast with other classes of histone deacetylases) has a variety of non-histone substrates, such as p53 and forkhead box class O (FOXO [139]. Interestingly, SIRT1 was found to directly interact with CLOCK, and deacetylate BMAL1 [136]. It has been proposed that SIRT1 imposes metabolic imbalance in cancer cells supporting aberrant and high energetic cell proliferation by modulating the circadian clock [136].

Taken together, the indirect exertion of circadian clock output in cancer cells has been characterized via cross-talk with the cell cycle, that ultimately regulates cell proliferation and survival, as well as via metabolic regulators. These lines of evidence are crucial for identifying potential novel targets for therapeutic purposes integrating their time-of-day-dependent regulation (*chronotherapy*).

1.8 Aims of the thesis

My thesis work aimed :

1. To characterize circadian clock functionality in primary pancreatic tumor cell lines harboring distinct oncogenic driver mutations.

2. To functionally characterize primary pancreatic tumor cell lines from different oncogenic mutation pools based on their global proteome profiling.

3. To investigate the role of the tumor-intrinsic circadian clock in pancreatic cancer development and progression.

Each of the three aims is presented as a separate section in Results (Chapter 3) and Discussion (Chapter 4). The conclusions derived from each research objective and future perspectives are collectively given in Chapter 5.

CHAPTER 2

Materials And Methods

Abstract | In this chapter, all experimental procedures and protocols that were performed are described in detail, including cell culture techniques, sample preparation for mass spectrometry-based proteomics, animal tissue processing and data analyses. The animal studies were conducted in collaboration between the laboratories of Prof. Dr. Robles Martinez and Prof. Dr. Saur. The animal experiments were carried out in accordance to the European Guidelines for the care and use of laboratory animals and were approved prior to the start of experimental work by the Government of Upper Bavaria.

Contents

2.1 Cell culture

2.1.1 Generation and availability of primary murine PDAC cell lines

All primary murine PDAC cell lines used in the experimental procedures were kindly provided by the group of Prof. Dr. Saur (TranslaTUM, Munich). All PDAC cell lines were isolated from endogenous mouse models of PDAC and cultured for less than 30 passages. All were tested for mycoplasma contamination by PCR before commencement of the experiments. Cells were maintained in standard tissue culture flasks or dishes and cultured in Dulbecco's Modified Eagle's Medium (DMEM) medium with 10 % fetal bovine serum (FBS) and 1 % penicillin (100 U/ml)/streptomycin (100 μg/ml) (P/S). All cell lines were kept in humidified incubators (37 °C with 5 % CO_2).

For the remaining part of this thesis all primary murine PDAC cell lines used may referred to as PDAC cells.

2.1.2 Circadian rhythm reporter PDAC cell line generation

The firefly luciferase gene under the control of a mouse *Bmal1* promoter (*Bmal1::Luc*) was part of the plasmid construct that was kindly provided by Dr. Achim Kramer (Charité, Berlin), and used for the generation of circadian rhythm reporter PDAC cells (Fig. 2.2).

First, HEK293T cells were used for lentivirus (LV) production. HEK293T cells were seeded at a density of 4 x 10^5 cells in three different 15 cm dishes, each with 20 mL medium (Day 1). The following day, a plasmid mix consisting of the expression plas-

mid DNA (Bmal1-Luc-Hygro; 2 μg) and packaging plasmids pSpax (1.25 μg) and pMD2 (0.75 μg) was prepared. A master mix of TransIT (18 μL per 15cm plate) and OptiMEM medium (270 μL per 15cm plate; without FBS or P/S) was also prepared and incubated for five minutes in room temperature (RT). Then, the plasmid mix was added to the master mix and left at RT for 30 minutes. Subsequently, the transfection mix was carefully added (drop-wise) to the medium of HEK293T cells, which were kept at 37 °C overnight (Day 2). The next day, the medium of the transfected HEK293T cells was exchanged with 8 mL DMEM medium with 30 % FBS (Day 3), and after 24 hours the viral supernatant was taken and stored at 4 °C (Day 4). Fresh medium (8 mL DMEM with 30 % FBS) was added and 24 four hours later (Day 5) the viral supernatant (in total 16 mL) was filtered through a 0.45 μm sterile filter using a syringe, aliquoted in 15 mL falcons (5 mL each) and stored in -80 °C until usage.

For the transduction, PDAC cells were seeded in duplicates in a 6-well plate at a density of 1-1.5 x 10^5 cells per well. The following day, cells at 60 to 70 % confluency were transduced with LV particles. For this, a 5 mL LV aliquot was mixed with 5 mL DMEM medium (10 % FBS, 1 % P/S) and Polybrene (Merck) at a final concentration of 8 μg/mL. 2 mL of LV master mix was added to each well (after removing the medium) and incubated overnight at 37 °C. The following day, the medium was exchanged and 48 hours post-tranduction, the transduced PDAC cells were maintained in medium with hygromycin at a starting concentration 250 μg/mL, which increased sequentially until the control cells ("mock") for each cell line, which did not receive the antibiotic, died. The selection lasted three to seven days and the final antibiotic concentration ranged from 300 to 800 μL/mL depending on the PDAC cell line.

The transduction of the PDAC cells was performed in two different time points throughout the thesis work, therefore two different batches of LV were prepared. All experimental procedures and handling of LV were performed in the specialized humidified

hood of biosafety level 2 (S2) after obtaining the necessary legal-bound introduction.

2.1.3 *Bmal1* knockout KRAS-mutant cell line generation

For generating control (Bmal1-proficient) and Bmal1-deficient *Bmal1::Luc* KRAS-mutant cell lines the CRISPR all-in-one editing system [Cas9 nuclease and single-guide RNA (sgRNA)] was used. First, two different sgRNA sequences were designed *in silico* by the PhD student Mr. Sebastian Widholz, MSc. targeting the first exon of the *Bmal1* gene. The sgRNA sequences were:

1. Arntl_284_64590 GAGAGTAGGTCGGTGGGGCC
2. Arntl_26_75355 GTTACTAGGTACCTTCCATG.

A sgRNA targeting the *LacZ* gene (sglacZ) was used as control. Then, each sgRNA sequence was cloned into the expression LV vector pLV-CRISPR-puro Three different plasmid vectors for each *Bmal1::Luc* PDAC cell line were used for LV production following the same procedure as described in section 2.1.2. For the transfection of the HEK293T cells the protocol was adjusted for 10 cm plates (instead of 15cm) and the generated LV was aliquoted in 1.5 mL cryotubes (instead of 15 mL falcons). The selection of the successfully transduced *Bmal1::Luc* PDAC cell lines was based on puromycin resistance ($puro^R$) that was included in each expression LV vector. The selection lasted three to seven days and the final antibiotic concentration ranged from 2.5 to 6 μL/mL depending on the cell line.

Upon selection, genomic DNA was extracted from *Bmal1::Luc* KRAS-mutant cell lines using the Mammalian Genomic DNA Miniprep kit (Sigma-Aldrich) following the manufacturer's instructions. The DNA sequence flanking of the respective sgRNA binding site at the *Bmal1* locus was amplified via PCR and subsequently sequenced by Sanger se-

quencing. The CRISPR data analysis webtool Inference of CRISPR Edits (ICE) (Synthego; https://ice.synthego.com) was used to determine the percentage of insertions and/or deletions (indels) in the *Bmal1* gene. For this, the quide sequences of sglacZ and targeted-to-Bmal1 sgRNA for each *Bmal1::Luc* PDAC cell line were uploaded to the corresponding online section. Ultimately, by selecting "add sample to analysis" the software proceeded with the deconvolution process and provided the result as percentage of indels relatively to the control. The overview of the experimental procedure is given in Figure 2.1 and the obtained traces are presented in the Appendix C.

The validation of the *Bmal1* editing in all KRAS-mutant cell lines was performed by measuring BMAL1 total protein levels by Western blot and assessment of circadian rhythmicity (see section 3.3.2).

2.1.4 Cell viability and proliferation assays

2.1.4.1 MTT assay

The 3-(4,5-dimethylthiazol-2-yl)-2,5-diphenyl-tetrazolium (MTT) assay was performed to assess cell viability as a function of redox potential. The cells were seeded into five different 96-well plates at a density of 0.25, 0.5 or 1 x 10^3 cells per well. The first measurement was performed 16 to 20 hours post-seeding, and the following four plates were measured at roughly the same time (+/- 30 minutes). Each day, 10 μL of MTT reagent were added to each well and the plate was incubated for four hours at 37 °C in 5 % CO_2. Subsequently, the medium was discarded and the oxidized formazan crystals were solubilized with 50 % (vol/vol) ethanol in dimethyl sulfoxide (DMSO) solution after incubation at room temperature for ten to 20 minutes under slight agitation.

The absorbance was subsequently measured at 590 nm in a microplate reader (BMG Labtech). For the analysis, the absorbance values of a given day were normalized to Day 0 (first day of the assay). The experimental procedure was performed independently at

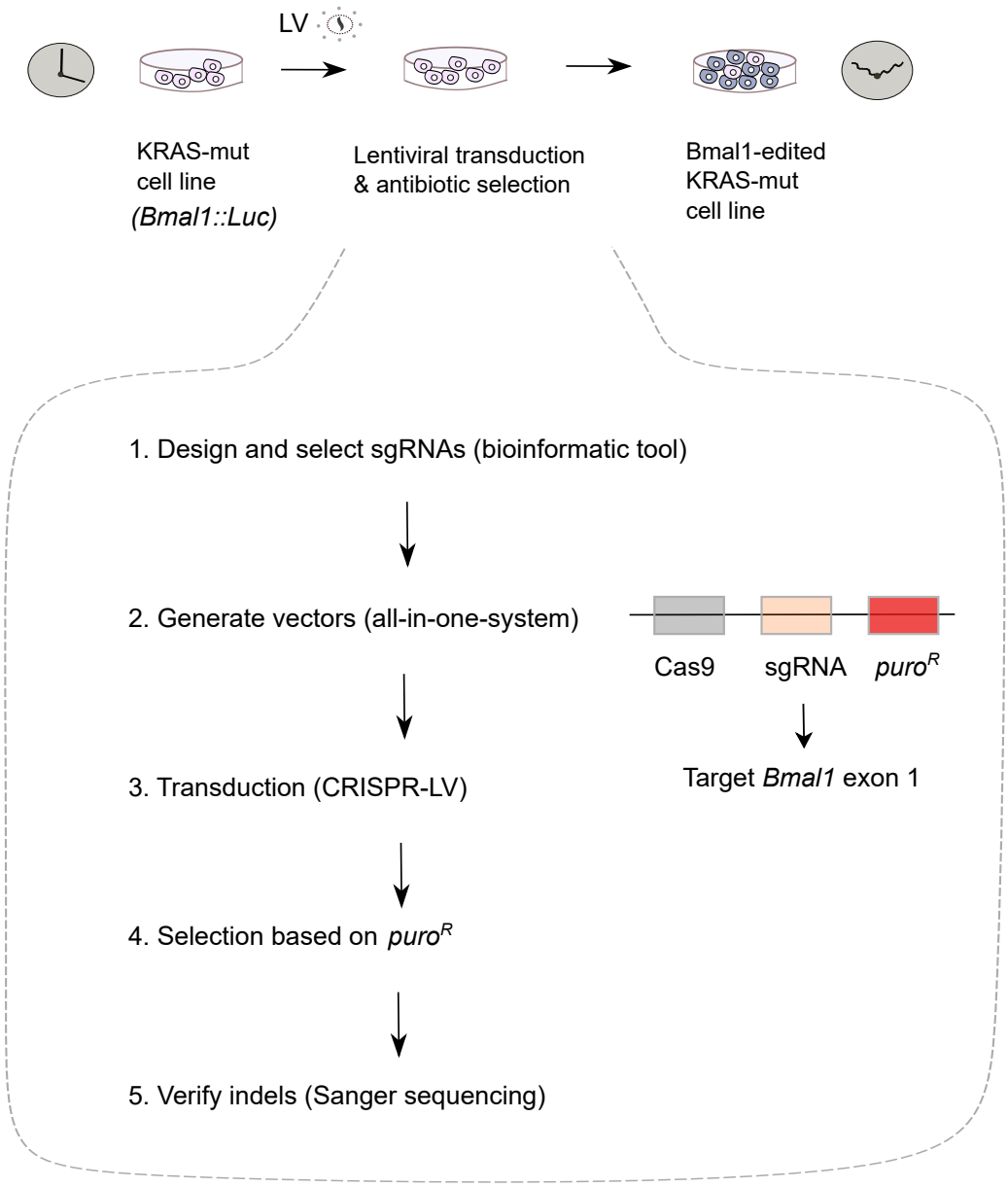

Figure 2.1: CRISPR-Cas9-mediated *Bmal1* editing in *Bmal1::Luc* KRAS-mutant PDAC cell lines with a functional cell-intrinsic clock resulted in circadian clock disruption. For details, see text.

least three times.

2.1.4.2 Clonogenic assay

The cells were seeded into 24- or 12- well plates at a density of 1.2 x 10^3 cell per well based on the optimal growth rate, and kept at 37 °C in 5 % CO_2. After of at least seven days, according to the confluence reached by one of the two *Bmal1::Luc* cell lines under examination in a single well plate, the supernatant was discarded and the cells were fixed and stained with 0.2 % (wt/vol) Crystal violet in 2 % ethanol aqueous solution.

Crystal violet was solubilized with 10 % (vol/vol) acetic acid after incubation at room temperature for one hour under slight agitation. The absorbance was subsequently measured at 570 nm in a microplate reader (BMG Labtech). The assay was performed independently at least three times.

2.1.5 Whole cell extracts and Western blotting

Cells at 80 to 90 % confluency were lysed on ice with cold RIPA buffer (50 mM sodium chloride, 1.0 % (vol/vol) IPEGAL, 0.1 % (vol/vol) sodium dodecylsulfate (SDS), 50 mM Tris, pH 8.0) prepared freshly with proteinase inhibitors (Roche) for protein extraction. Cell extracts were were transferred into a 1.5 mL tube and were left on ice for 20 minutes. After centrifugation (20,000 *g*, 20 minutes at 4 °C), the supernatant was transferred into a new 1.5 mL tube and used for estimation of protein concentration based on the Bicinchoninic acid (BCA) assay (Pierce) following the manufacturer's instructions. SDS-PAGE and Western blotting was performed using in house-made 10 % polyacrylamide gels and subsequent protein detection recognized by the antibodies was conducted using the SuperSignal West Pico PLUS Chemiluminescent kit (Pierce). Signal development was performed in the ChemiDoc MP Imaging System (Biorad). The following antibodies were used: BMAL1 rabbit mAb (1:1000, Cat #14020, Cell Signaling), actin mouse mAb

(1:3000, Cat #sc-47778, Santa Cruz Biotechnology), GAPDH mouse mAb (1:3000, #MAS-15738, Invitrogen) diluted in 5 % milk in Tris-buffered saline (TBS) buffer containing 0.05 % (vol/vol) Tween-20 (Sigma).

2.2 Circadian clock function in PDAC cell lines

2.2.1 Preparation for bioluminescence recodring

Upon successful transduction and antibiotic selection, the generated circadian rhythm reporter PDAC cell lines (see section 2.1.2) were used for bioluminescence recordings (Fig. 2.2). Briefly, each *Bmal1::Luc* PDAC cell line was seeded in a white 96-well plate format at a density of 4 x 10^3 cells per well. The following day, the cells were 90% - 100% confluent (confluence was assessed in a transparent 96-well plate that was complementary seeded with the same amount of cells) and received a dexamethasone pulse (DEX, 1 μM) for phase synchronization for two hours at 37°C. Then, the medium was exchanged with 200 μL luminometry assay medium (phenol red free; 10 % FBS, 1 % P/S and 250 μM D-Luciferin) after washing the cells with phosphate buffered saline (PBS, Sigma-Aldrich) (Fig. 2.2).

In darkness -to protect from light-induced degradation of D-Luciferin- the 96-well plate was covered by a plastic membrane to prevent evaporation of the medium during the measurement, and placed in a microplate luminometer (Centro XS3, Berthold Technologies) after removing the plate lid. The luminometer device was contained in an incubator and the bioluminescent recordings were conducted at 37°C. During the entire measurement care was taken to avoid any technical disturbances that could interfere with data acquisition (e.g., no external light in the luminometer room, no door opening of the incubator). Lastly, to ensure that the temperature was constant during the recording a temperature data logging device (HOBO Pendant) was placed in the incubator on

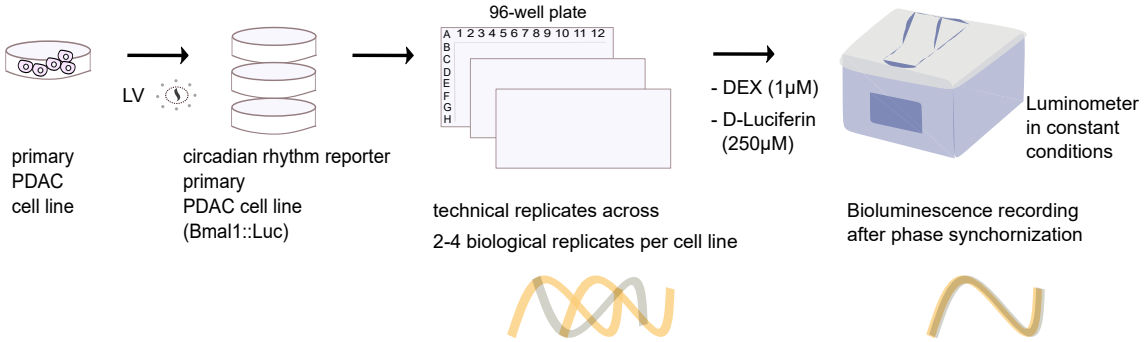

Figure 2.2: Luminometry-based screening for characterizing circadian clock functionality in primary PDAC cell lines. Circadian rhythm reporter PDAC cell lines were transduced with LV that was generated to express *Bmal1::Luc* construct. After antibiotic selection *Bmal1::Luc* PDAC cell lines were used for the functional screening after phase synchronization with DEX. For details, see text. LV: lentivirus, DEX: dexamethasone

top of the luminometer. Throughout the data collection included in this thesis work two different luminometer devices were used.

Each experimental plate contained up to 11 different *Bmal1::Luc* PDAC cell lines along with *Bmal1::Luc* human osteosarcoma U2-OS cells that served as positive control, because this cell line is used widely as model system in circadian research. Each *Bmal1::Luc* PDAC cell line was seeded in at least two different experimental plates, and the number of total replicates from each *Bmal1::Luc* PDAC cell line is summarized in Table A.1.

2.2.2 Bioluminescent signal acquisition and analysis

The addition of D-Luciferin in the luminometry assay medium allowed for the biochemical reaction to take place in the cells (bioluminescence). The generated bioluminescent signal consisting of photons was captured by the photomultiplier tube (PMT) integrated in the luminometer and expressed as relative light units (RLU) -relative to the background values recorded by an empty or medium-containing well- after the signal's analog-to-digital conversion. The signal was measured every ten minutes with integration time of

one second for at least five consecutive days.

At the end of the recording, the time series data were exported from the luminometer software in a spreadsheet that included the RLU values at each time point (rows) from each well (columns). The time series data were preprocessed and analyzed using custom Matlab-based scripts (version 9.6.0, Mathworks) for trend removal (detrending), detection of rhythmicity, subsequent period estimation and visualization. The Matlab scripts included integrated functions from the "Signal Processing" Toolbox and were combined in a software tool (ChronoTool). The ChronoTool facilitated the overall organization of each experimental 96-well plate in a database structure, controlled the assignment of the *Bmal1::Luc* PDAC cell lines from each experiment, and allowed the continuous review of the data. A comprehensive representation of the ChronoTool can be found in the Appendix B.

2.2.2.1 Preprocessing of the bioluminescent signal

Each well in every 96-well plate was considered an individual time series dataset and, therefore, was preprocessed separately. First, the raw RLU values of each time series were plotted over time to identify potential outlier data points (Fig. 2.3). In case that a RLU value of a time point differed more than 10^5 from its pre- or subsequent time points was excluded, thereby reducing the probability of "spikes" in the signal that could negatively impact the data analysis. In addition, a moving average was applied at the RLU values of every six time points (i.e., every hour) of the time series for removing random variation (i.e., "noise") from the signal, resulting in a "smoothed" signal. Furthermore, the first 24 hours from each time series were excluded to remove "transient" RLU values. This is because it was observed that a very high RLU peak was generated immediately after the commencement of the recording. By removing an entire cycle ensured that the measurement was performed under "steady-state" conditions.

The plotting of the smoothed time series enabled the identification of a trend, which was eliminated by applying an additional moving average with a window of 24 hours, resulting in a baseline with zero-mean about which the time series oscillated (Fig. 2.3). For all experiments, after data preprocessing, the number of cycles remained in the time series was at least four and up to six.

2.2.2.2 Assessment of rhythmicity in the bioluminescent signal

As the next step in bioluminescent signal analysis, the detrended signal from each time series was assessed for circadian rhythmicity. The autocorrelation function (ACF) was applied for detection of a rhythmic signal, i.e., that contained a periodic component. For more details, see section 1.5.3. The threshold that defines whether the correlation is significantly different from zero is given by the grey dashed line shown in Fig 2.3.

To systematically, comprehensively and in an unbiased fashion analyze the time series data of all luciferase reporter PDAC cell lines, all replicates of each individual *Bmal1::Luc* PDAC cell line across the experimental 96-well plates were used for the calculation of an average ACF (annoated as Average ACF in Fig 2.3). If the autocorrelation coefficients exceeded the significance level, it was ensured that a rhythmic periodic component was present in the detrended time series.

2.2.2.3 Period estimation via Lomb-Scargle Periodogram

The detrended time series of each *Bmal1::Luc* PDAC cell line comprised all replicates from all experimental plates were used for period estimation using the Lomb-Scargle Periodogram (LSP).

The implementation of the LSP is accompanied by a statistic test that assess the false alarm probability (P_{fa}), that is the likelihood for a peak in the LSP to be random (for more details, see section 1.5.5). The most stringent threshold (P_{fa} 0.01%) was selected, suggest-

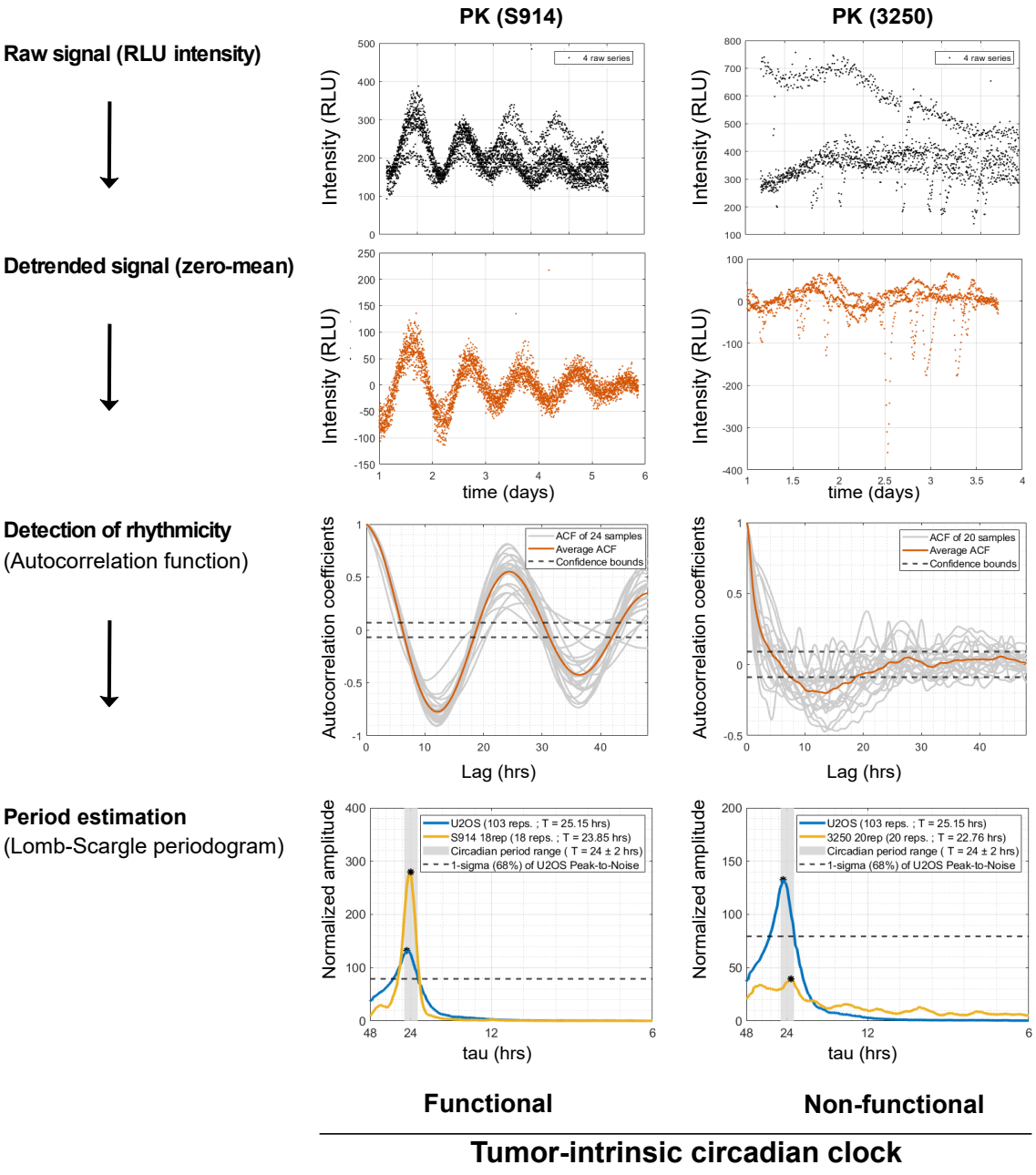

Figure 2.3: Signal conditioning and period estimation of the bioluminescence time series. After excluding the first 24 hours of recording, the raw time series data were detrended by subtracting a 24 hour-running average generating a time series with zero mean. Assessment of rhythmicity in the detrended signal was performed by applying the ACF. The LSP was implemented for period estimation resulting in characterization of the tumor-intrinsic circadian clock as functional or non-functional. For details, see text. ACF: autocorrelation function; LSP: Lomb-Scargle periodogram.

ing that only those peaks with 0.01% probability to be false were detected as "true" peaks, that additionally indicated significant rhythmicity at the detrended signal.

Importantly, the collective LSP estimates for each *Bmal1::Luc* PDAC cell line are normalized to the noise level of the U2-OS cell line that used as a positive control, thus giving a relative robustness of the circadian rhythm between different *Bmal1::Luc* PDAC cell lines (Fig. 2.3).

2.3 Mass spectrometry-based proteomic profiling of primary PDAC cell lines

2.3.1 Sample preparation

PDAC cells were grown in 15 cm cell culture dishes in quadruplicates and at 80 %-90 % confluency were lysed on ice by adding 1 mL 2 % (wt/vol) sodium deoxycholate (SDC) buffer in 100 mM Tris(hydroxymethyl)aminomethane hydrochloride (Tris-HCl), pH = 8.0. Cell lysates were then collected using a cell scraper, transferred to 2 mL low-bind eppendorf tubes, boiled for five minutes at 95°C and stored at -80°C until further processing (Fig. 2.4 A).

For each sample, protein concentration was determined using the colorimetric Bicinchoninic acid (BCA) assay kit (Pierce) following the manufacturer's instructions. Then, 200 μg of protein from each sample were used as starting material for enzymatic digestion. First, protein alkylation and reduction was performed by adding 30 μL of freshly prepared alkylation buffer [10X; 100 mM Tris(2-carboxyethyl)phosphine hydrochloride (TCEP-HCl), 400 mM Chloroacetamide (CAA), pH = 7] and incubation at 45°C with agitation (1,500 rpm) for five minutes. The protein content of each sample was then digested overnight at 37°C with agitation (1,500 rpm) with the exopeptidase trypsin (ratio enzyme:protein 1:100) and endopeptidase Lys-C (ratio enzyme:protein 1:100).

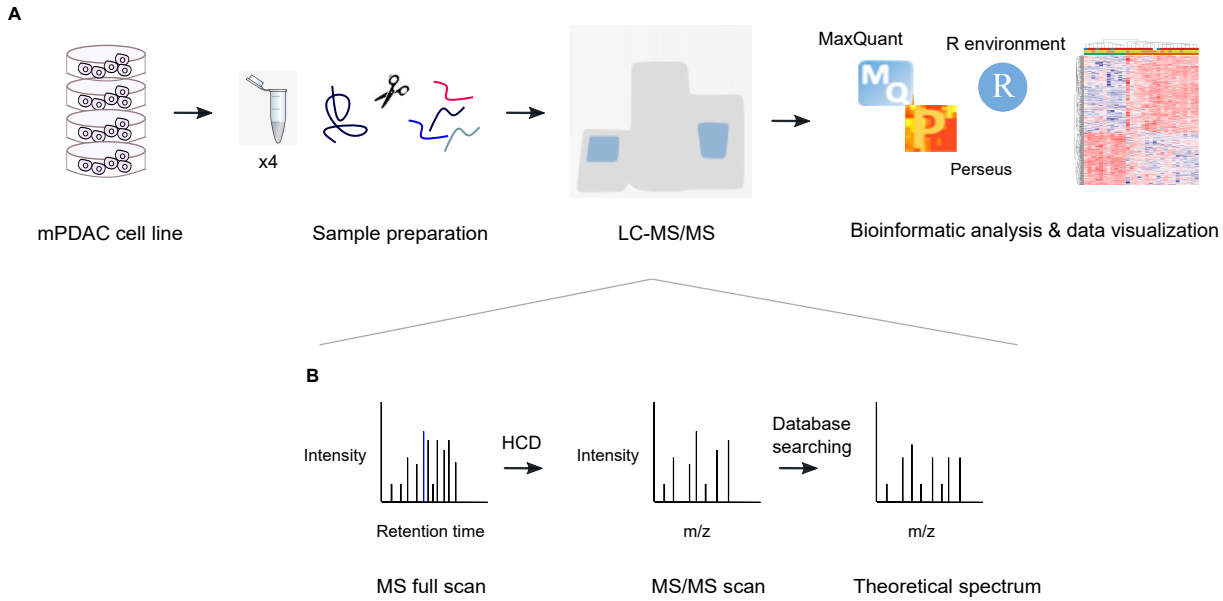

Figure 2.4: A) Sample preparation and B) data-dependent acquisition for mass spectrometry-based proteomics. For details, see text. LC-MS/MS: High pressure Liquid Chromatography coupled to Mass Spectroscopy; HCD: High energy collisional dissociation.

The following day, in 10 μL (equivalent to 5 μg) of the digested peptides, 100 μL Loading buffer (1 % (vol/vol) Trifluoroacetic acid (TFA) in isopropanol) was added to stop the tryptic activity. Then, the peptides were desalted and cleaned-up using the in-house-made three-layer Styrenedivinylbenzene-reverse phase sulfonate (SDB-RPS) stage-tips. Briefly, after binding to the SDB-RPS material, the peptides were washed with the SDB-RPS wash buffer 1 (1 % (vol/vol) TFA in isopropanol) and wash buffer 2 [0.2 % (vol/vol) TFA, 5% (vol/vol) acetonitril (ACN)]. Subsequently, the peptides were eluted [32 (vol/vol) % ACN, 0.125 % (vol/vol) NH_4OH] via centrifugation at 1,500 g for five minutes and concentrated by a SpeedVac Vacuum Concentrator (Eppendorf) for 20-25 minutes until dryness. The cleaned peptides were resupsended at mass spectrometry (MS) compatible buffer [2 % (vol/vol) ACN, 0.1 % (vol/vol) TFA] and stored in -20°C until MS measurement (Fig. 2.4 A).

2.3.2 High Pressure Liquid Chromatography coupled to Mass Spectrometry

400 ng of cleaned-up peptides were analyzed by High Pressure Liquid Chromatography coupled to Mass Spectroscopy (LC-MS/MS). In detail, the analytes were separated via a 50 cm reversed-phase column (in-house packed with 0.75 μ m ReproSil-Pur C18-AQ 1.9 mm resin), which was mounted onto the EASY-nLC 1200 System (Thermo Fisher Scientific), over a 120-minutes gradient of 5 %-60 % buffer B (0.1 % formic acid and 80 % ACN) with a flow rate of 300 nL/min.

The tip of the column was coupled to an electrospray ion source via which the separated peptide ions were analysed at a single-shot manner in a Q Exactive HF-X Hybrid Quadrupole Orbitrap mass spectrometer (Thermo Fisher Scientific) on a data-dependent acquisition (DDA) manner (Fig. 2.4 B). The MS was operated in the MS-MS/MS mode alternating an MS survey scan with 15 MS/MS scans. After every full MS scan, the fifteen most intense ions (Top15) were isolated and fragmented in the higher-energy collisional dissociation (HCD) cell (target value 1e5 ions, maximum injection time 28 ms, isolation window 1.4 m/z, underfill ratio 1 %). Full scans were acquired from 300 to 1650 m/z with a target value of 3e6 ions at a resolution of 60,000 at 200 m/z. Ion fragments were finally detected in the Orbitrap mass analyzer at a resolution of 15,000 at 200 m/z.

2.3.3 Proteomics raw data analysis

For the processing of the raw MS data files, the MaxQuant software [140] was used (version 1.6.13) to calculate label-free intensities with the integrated Andromeda search engine. Each raw file corresponding to one biological replicate of each PDAC cell line was treated as one independent experiment. False discovery rate (FDR) for both peptide and protein levels was set at 0.01. Oxidised methionine (M) and acetylation (protein N-terminus) were set as variable modifications, and carbamidomethyl (C) as fixed mod-

ification. The minimal length of the peptides considered for identification was seven amino acids, and the option "match between runs" was included with a matching time window of 0.7 minutes. This corresponded in matching missing peptide intensities between biological replicates of *Bmal1::Luc* PDAC cell lines. The UniProt database from mouse (September 2014) including 51,210 entries was used for peptide and protein identification.

2.3.4 Bioinformatic analysis of the proteomics data

For bioinformatic analyses, the Perseus platform [141] (version 1.6.10.50) was used. Complementary to Perseus, the R environment (version 4.0.2) was used for data visualization. The label-free proteomics data were filtered for the following peptide sequences: i) reverse identified, ii) identified only by site and iii) potential contaminants. Then, the dataset was transformed in the log2 scale and proteins without quantified LFQ intensities in less than 50 % of the total number of the samples were filtered out. Before statistical analysis, data were inspected for outliers (based on number of quantified proteins) and the sampleID "LFQ intensity 123" was excluded from the dataset.

2.4 *In vivo* studies

The *in vivo* studies were conducted in female mice (8 to 12 weeks old) based on the gender of the endogenous tumor mouse that the primary PDAC cell line originated from. Two different mouse experiments were performed.

The first study was a time point experiment that included both immunodepleted ($Rag2^{-}/^{-}$) and immunocompetent (C57BL/6J;129S6/SvEv; F1 hybrid) mice. In both cohorts, the mice were orthotopically implanted with 20 μL cell suspension containing 2,5 x 10^3 cells. The mice were randomly assigned into two different groups and injected in the pancreas with the KRAS-mutant *Bmal1::Luc* 4706 cell line -either with Bmal1-proficiency

Table 2.1: Characteristics of the female mice used in the time point experiment.

Bmal1::Luc Cell line	Immune system	Age when implanted	Group size
4706 sglacZ	Competent	8-10 weeks	7
4706 sg284	Competent	9 weeks	7
4706 sglacZ	Deficient	28 weeks	3
4706 sg284	Deficient	28 weeks	3

(sglacZ) or Bmal1-deficiency (sg284). The group size was three for the RagII-KO groups, and seven for the F1 cohort (2.1). After the transplatation, the mice were followed until the tumor size reached 100mm^3 in at least one animal independent of the group in each cohort. At this point, all the mice were sacrificed with cervical translocation. The tumor size and macroscopic metastasis formation were assessed. In addition, from each group of F1 mice, a piece of tumor was obtained for immunophenotyping by flow cytometry (section 2.4.3) and tissue sectioning for *ex vivo* bioluminescence recording (section 2.4.2).

The second *in vivo* study was an endpoint experiment that included only immunocompetent F1 mice. The study included two different *Bmal1::Luc* KRAS-mutant cell line pairs (each with Bmal1-edited or non-edited cells). In total, there were four groups of mice, each consisted of seven animals. All mice were injected in the pancreas of 20 μL cell suspension containing 10^4 cells. In this experiment, the *Bmal1::Luc* 4706 (epithelial KRAS subtype) and S914 (mesenchymal KRAS subtype) were used.

After the implantation, all mice were followed until the tumor reached a size of 100mm^3. At the endpoint, the tumor size and macroscopic metastatic lesions were assessed. From each tumor mouse, a piece of tumor was obtained for subsequent immunophenotypic analysis with flow cytometry (section 2.4.3). The experimental design and readout of the animal work is collectively depicted in Fig. 2.5, and any relevant characteristics of each mouse study are summarized in Tables 2.1 and 2.2.

Table 2.2: Characteristics of the female mice used in the endpoint experiment.

Bmal1::Luc Cell line	Subtype	Age when implanted	Group size
4706 sglacZ	Epithelial	12-14 weeks	7
4706 sg284	Epithelial	12-14 weeks	7
S914 sglacZ	Mesenchymal	12-14 weeks	7
S914 sg284	Mesenchymal	12-14 weeks	7

2.4.1 Orthotopic implantations

The mice were first anaesthetized by intraperitoneal (i.p) injection of MMF [Midazolam (5.0 mg/kg), Medetomidin (0.5 mg/kg), Fentanyl (0.05 mg/kg)] and the fur was locally removed using an electric shaver. The animals were kept at controlled temperature during the implantation procedure. The cell suspension was injected with the help of a sterile needle in the head of the pancreas and subsequently the wound was closed with stitching. After the implantation, the mice received a subcutaneous (s.c) injection of AFN [Atipamezol (2.5 mg/kg), Flumazenil (0.5 mg/kg), Naloxon (1.2 mg/kg)] that antagonized the analgosedation by MMF, along with s.c injection of Meloxicam (Metacam; 5 mg/kg) as analgesic. For the first three days after the surgery, all mice were examined twice a day and further analgesic was provided if necessary.

The transplatations were performed by the PhD students of Prof. Saur's lab, Ms. Stefanie Bärthel, MSc. and Ms. Chiara Falcomatá , MSc. The rest of the animal work (scoring of the mice, animal tissue processing) was performed by myself.

2.4.2 *Ex vivo* bioluminescence recordings

Fresh tumor samples were mounted in 4 % low melting agarose (Sigma) using plastic histology embedding molds. The blocks were left on ice until agarose polymerization and subsequently were placed on the vibratome filled with ice-cold Hank's balanced salt solution (HBSS) using super-glue. The sectioning was performed with the following param-

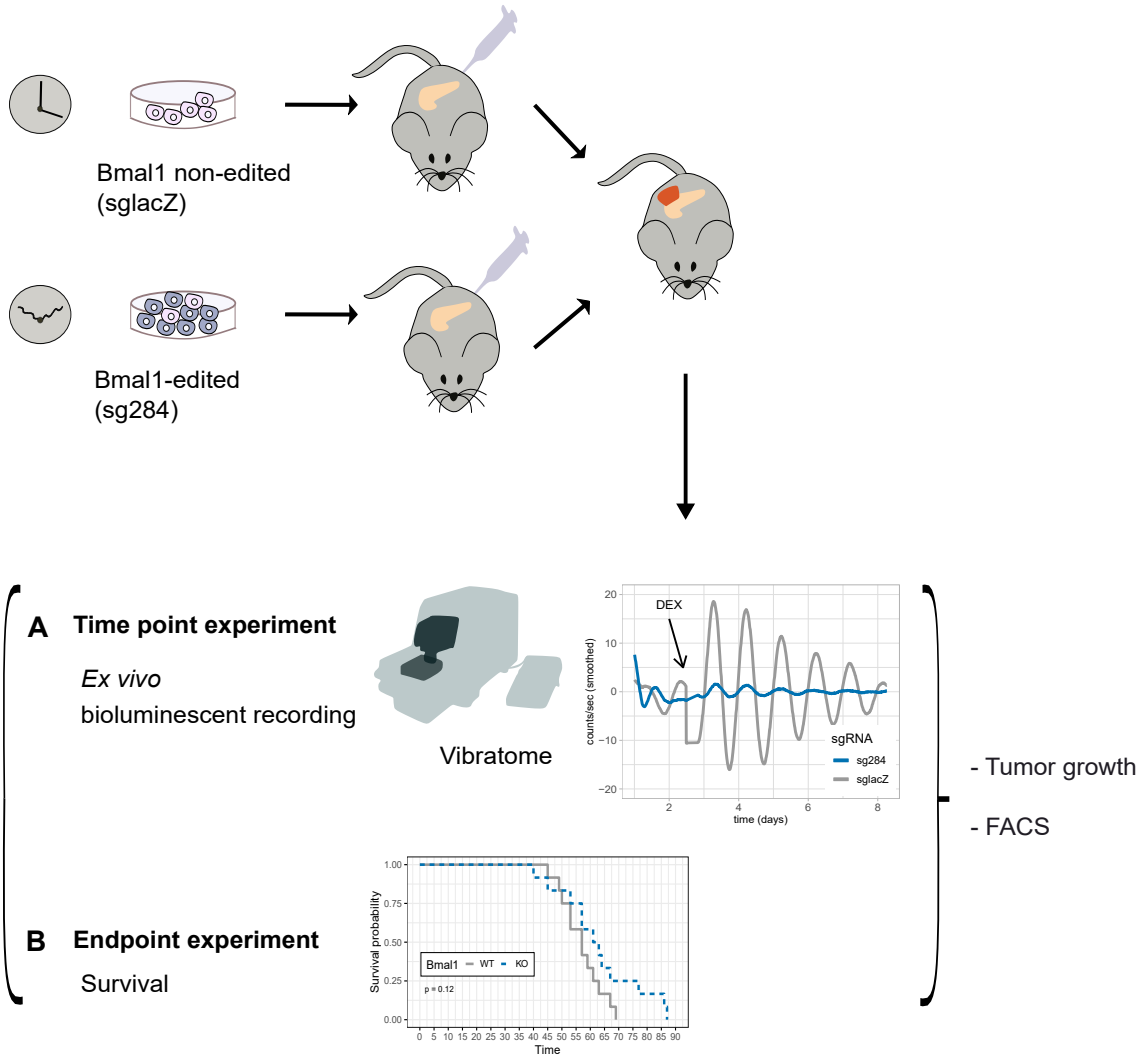

Figure 2.5: Overview of the *in vivo* studies. Each experimental group of mice was orthotopically injected with a *Bmal1::Luc* PDAC cell line with either Bmal1-edited (sg284) or Bmal1 non-edited cells (sglacZ). A) At the end of the time point experiment *ex vivo* bioluminescence recording of organotypic tumor slices was performed after tissue sectioning in the vibratome. B) Survival of tumor-bearing mice was assessed in the endpoint experiment. In both A) and B) experiments, tumor size was assessed and immunophenotyping by FACS was performed. For details, see text. FACS: Flow-assisted cell sorting.

eters: Object speed 0.15 mm/second, Vibration relatively high and thickness of slices 300 μM. The intact slices were transferred from the basin onto a petri dish filled with ice-cold HBSS. Then, each tumor slice was transferred on a 35 mm dish filled with 1 mL DMEM medium (phenol-free; supplemented with 3 mM sodium carbonate, 10 mM HEPES, 2 mL L-glutamine, 2 % B-27 supplement and 25 U/mL P/S) containing D-Luciferin (Sigma) at a final concentration of 0.1 mM. Each slice was placed on a plate insert (Millipore), that separated it from the bottom of the petri dish, and a glass cover slip sealed the petri dish using silicon fat. Subsequently, each petri dish was placed into a LumiCycle (Actimetrics) kept inside a cell culture incubator (37 °C). After about 36 hours the slices were treated with 1 μ M DEX for two hours at 37 °C. Then, the medium was replaced and the recordings continued for another six cycles. In total, the measurement lasted for more than eight days. The integration time was one minute and the measurement interval ten minutes. The data analysis was performed with the LumiCycle analysis software, both before and after DEX treatment.

The PhD student Ms. Muriel-Katja Frisch assisted me in the execution of the experimental procedure for the *ex vivo* bioluminescence recordings as well as for the data analysis. In particular, the LumiCycle software (Actimetrics) was used to determine rhythmicity and to extract the cycling parameters. Rhythmicity was determined based on three different criteria: the goodness of fit, the statistic of the X^2 periodogram and the detection of at least two clear peaks in the signal (Sin fit option). Subsequently, the cycling parameters (period, phase and amplitude) were extracted from the software only for those slices with a rhythmic bioluminescent signal. The amplitude was further normalized to the average brightness of the signal recorded for the total duration of the recording.

2.4.3 Immunophenotyping by flow cytometry

Fresh tumor samples were placed at 10 cm Petri dishes and minced on ice with a sterile scalpel. The minced tissue was enzymatically digested using a tumor dissociation kit (Miltenyi) in DMEM medium at 37 °C for 40 minutes with agitation. All further steps were performed at 4°C. After digestion, samples were centrifuged (1,500 rpm, five minutes) and the pellet was resuspended in 5 mL PBS containing 2 % FBS (PBS/FBS). The cell suspension was then strained through a 70 μM strainer and after centrigufation (1,500 rpm, five minutes) the pellet was resupsended in 1 mL PBS/FBS, and subsequently transferred into a 1.5 mL eppendorf tube. The cell suspension was further centrifuged (1,500 rpm, five minutes) and the pellet was resuspended in 200 μL PBS/FBS. After counting the cells using a hemocytometer, 2,5 x 10^6 cells were transferred in a V-shaped-bottom 96-well plate in 200 μL. The cells were then blocked with anti-mouse FC block (Biolegend, 1:100) and stained with Zombie Aqcua (Biolegend, 1:500). After 1.5 washes with PBS/FBS, the cell suspension was divided in two parts for the acquisition of the innate and adaptive immune cell populations. The antibody mix for the innate part (or "panel") was the following: CD11c (1:30, BD), NK1.1 (1:25, BD), Ly6c (Biologend), CD11b (1:100, Biologend), F4/80 (1:30, Biologend), CD45 (1:100, Biologend), Single-F (1:100, BD), Ly6G (1:200, Biologend), CD68 (1:20, Biolegend) and EpCAM (1:200, Biologend). The mix for the adaptive panel consisted of the following antibodies: CD4 (1:100, BD), CD3e (1:20, BD), CD8a (1:100, Biologend), CD25 (1:50, Biologend), TCRγ/δ (1:50, Biologend), CD45 (1:100, Biologend), CD19 (1:100, Biologend), CD62L (1:500, Biologend), CD44 (1:30, Biologend) and EpCAM (1:200, Biologend).

Per panel, 1,000,000 events were acquired on a BD LSR Fortessa Cell analyser. Flow cytometry data were analyzed with the FlowJo software (version 10.7.2).

2.5 Additional statistical methods and data analysis

Statistical analyses of the clonogenic assay, MTT assay, FACS data and cycling parameters of the *ex vivo* recordings were performed with the GraphPad Prism software (version 8.4.3) and the R environment (packages plotrix and ggsignif) and presented as mean ± standard error of the mean (SEM). The significance levels was set to 0.05. For the analysis of cycling parameters, rhythmicity was tested using the Actimetrics software and outliers were removed based on the ROUT test (q value = 1 %) implemented on Graphpad Prism (version 8.4.3).

Statistical analysis of the RNA-seq data was based on the non-parametric Mann-Whitney (Mann-Whitney-Wilcoxon) U test for independent samples using the R environment (package ggpubr). The significance level was set to 0.05.

CHAPTER 3

Results

Abstract | In this chapter, the results of the functional screening for elucidating circadian clock functionality in primary PDAC cell lines are comprehensively presented in section 3.1, and whether the tumor cell-intrinsic circadian clock impacts tumor development and progression *in vivo* is shown in section 3.3. The proteomic profiling results from a large PDAC cell cohort are described in section 3.2.

Contents

3.1 Circadian clock function in primary PDAC cell lines

In order to assess the functionality of the circadian clock in primary PDAC cell lines with distinct oncogenic mutations, a luminometry-based medium-scale screening was performed. For this purpose, I generated 44 different luciferase reporter (*Bmal1::Luc*) PDAC cell lines (section 2.1.2) originating from three oncogenic pools. The *Bmal1::Luc* cell lines from each PDAC cohort as well as the number of biological replicates are depicted in Figure 3.1 and in detail in Table A.1.

Conceptually, the ability to record over a period of time a biochemical reaction that is controlled by a circadian gene promoter enabled to elucidate the presence of an endogenous circadian oscillator in the *Bmal1::Luc* PDAC cells. The bioluminescence generated by the luciferase enzymatic activity was an indirect output of the circadian clock function, because the *Bmal1* promoter was the driver of luciferase expression.

3.1.1 Assessment of circadian functionality in primary PDAC cell lines

Signal conditioning and period estimation based on the bioluminescence time series (sections 2.2.2.1-2.2.2.3) allowed the characterization of the circadian clock functionality in 44 *Bmal1::Luc* PDAC cell lines. The majority of them (65.9 %) originated from KRAS-driven tumors (PK), 22.7 % from PI3K-driven tumors and 11.4 % of the screened cell lines had both *Kras* and *p53* oncogenic mutation drivers (PKP). Collectively, the numbers and relative percentages of the total cell lines from each PDAC cohort are shown in Figure 3.2 A.

Based on the autocorrelation function (ACF) that was applied on the detrended time series of each PDAC cell line (section 2.2.2.2), it was tested whether the recorded bioluminescent signal was rhythmic or not after trend removal (section 2.2.2.1). The ACF considered all replicates in each *Bmal1::Luc* PDAC cell line and in case of a significant

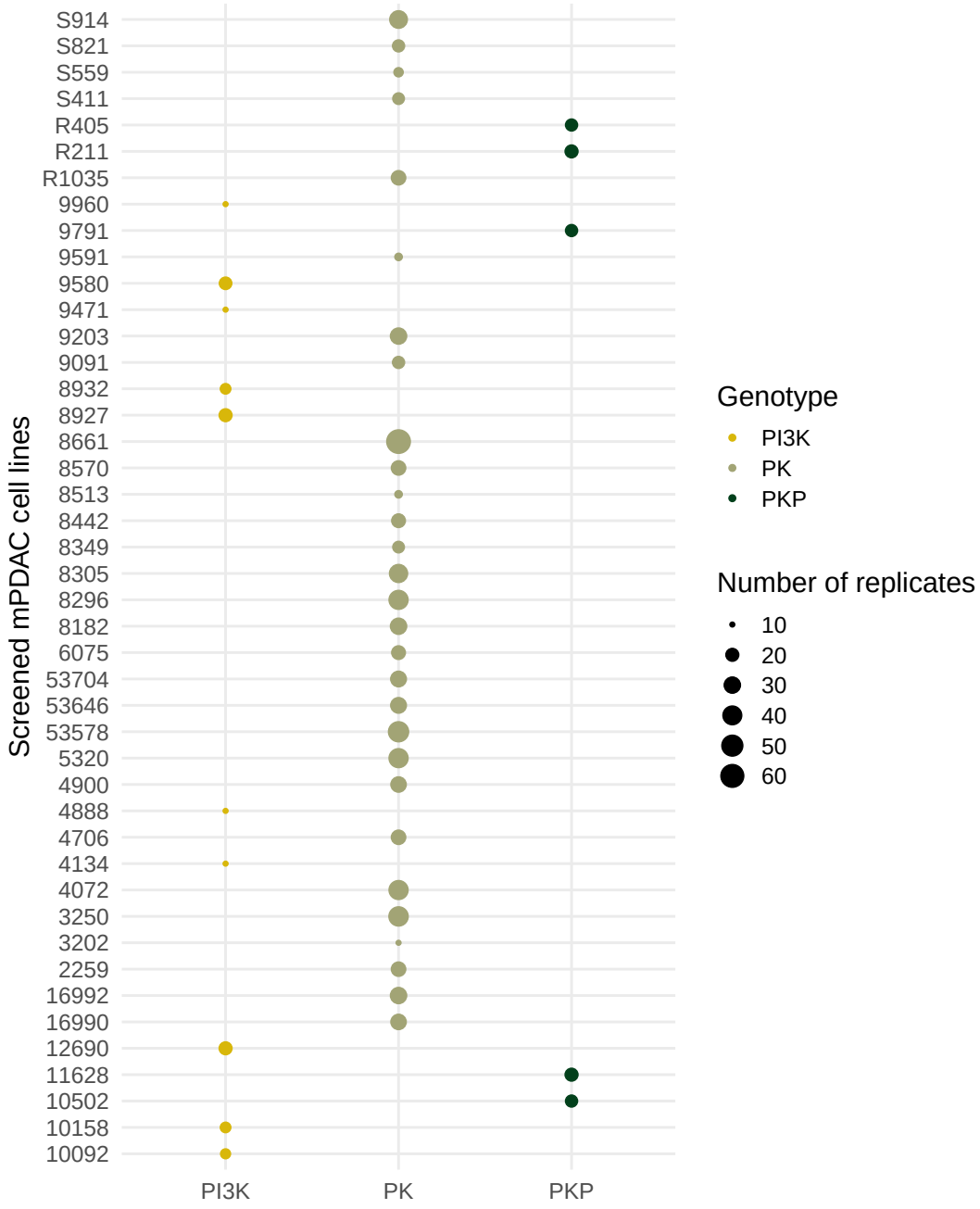

Figure 3.1: The *Bmal1::Luc* PDAC cell lines included in the luminometry-based functional screening. The dot size is proportional to the number of biological replicates of each cell line. The screened PDAC cell lines originated from three different oncogenic pools (genotypes) of PI3K-driven (yellow), KRAS-driven (PK; olive green), and KRAS;p53-driven (PKP; dark green) PDAC primary tumors. mPDAC: murine PDAC

autocorrelation (for details see also section 1.5.4), the cell line was characterized as Functional oscillator. Based on this, it was found that 75 % of the total *Bmal1::Luc* PDAC cell lines that were analyzed retain circadian functionality, and 25 % do not (Fig. 3.2 B). Furthermore, it was elucidated that the functionality of the circadian clock is not attributed to any specific oncogenic pool that were included in the functional screening. In essence, the majority (86.2 %) of the PK cell lines are characterized as functional oscillators, while in the PI3K and PKP cohorts the corresponding percentages are 60 % and 40 %, respectively (Fig. 3.2 C).

Representative examples of both the detrended bioluminescent time series and their ACF result plots are given in Figures 3.3 and 3.4, 3.5 and 3.6, 3.7 and 3.8 for PK, PKP and PI3K cohorts, respectively. In the detrended plot of a *Bmal1::Luc* PDAC cell line, the detrended time series of all replicates that were recorded from a given experimental 96-well plate after phase synchronization with dexamethasone (DEX) are shown as individual lines. It may be hard to distinguish the replicates in case they show similar oscillation patterns (e.g., compare iv and viii in Fig.3.3). The *Bmal1::Luc* PDAC cell line number is depicted on the top of each plot and the number of the replicates in each individual Figure legend. For the PK cell lines, the transcriptomics cluster is also shown on each individual Figure title, which facilitated the analysis in section 3.1.3 (programming reasons).

Ultimately, the detrended time series of each *Bmal1::Luc* PDAC cell line were used for period estimation by implementing the Lomb-Scargle periodogram (LSP; see sections 2.2.2.3 and 1.5.5). Moreover, the LSP was used as a complementary test for rhythmicity and for characterizing the robustness of the underlying circadian component. Given the absence of a comprehensive characterization of circadian rhythm in primary PDAC cells so far, the circadian oscillations in U2-OS cell line was used as a comparative system. Collectively, the LSP estimates for the PK cell lines are shown in Figure 3.9, for the PKP cohort

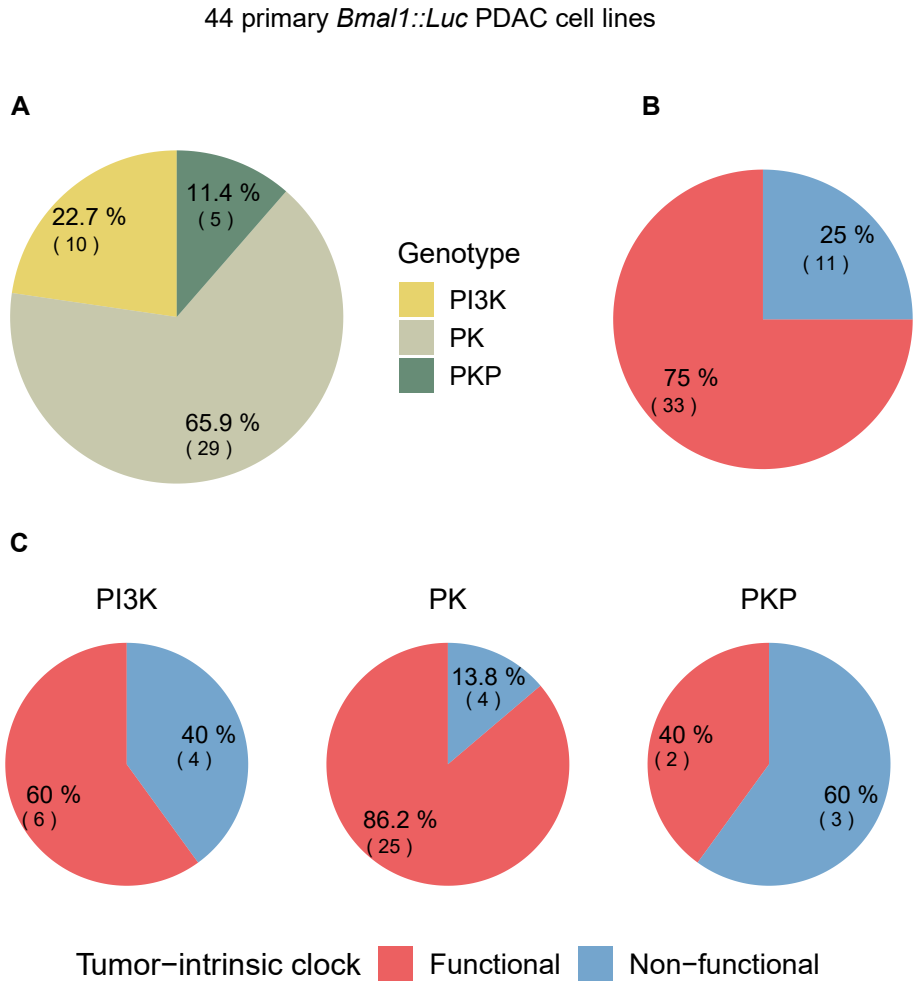

Figure 3.2: Results of the functional screening in three *Bmal1::Luc* PDAC cell cohorts. A) The relative proportions of the PDAC oncogenic pools included in the screening for circadian functionality. The relative percentages of Functional (red) and Non-functional (red) circadian oscillators in all three (B) and in each PDAC cohort (C). PI3K: PI3K-driven; PK: KRAS-driven; PKP: KRAS;p53-driven.

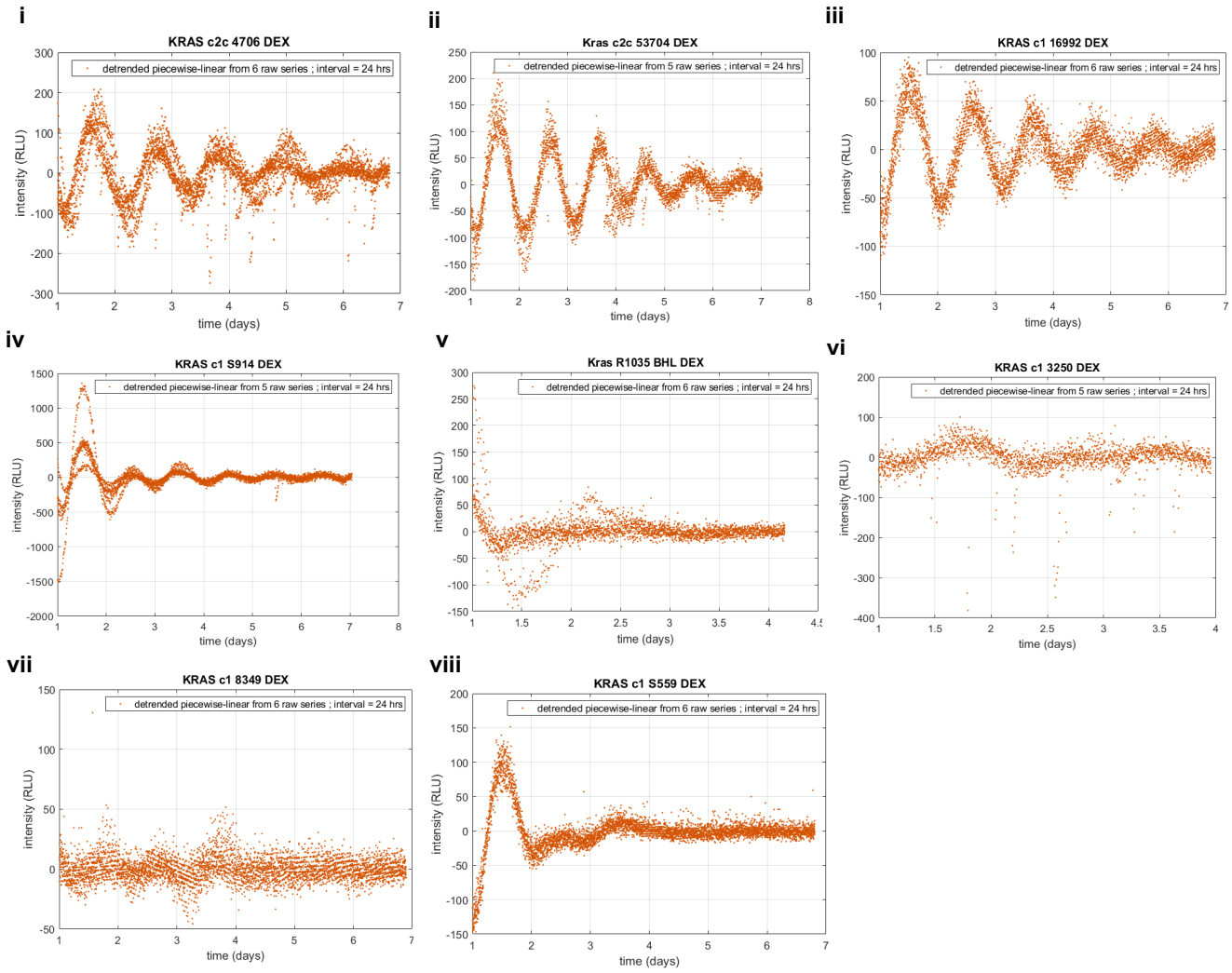

Figure 3.3: Representative results of detrended bioluminescence time series in KRAS-driven (PK) cohort. In the inlet of each plot the number of replicates from a single experiment is given. For details, see text. c1: mesenchymal subtype; c2c: epithelial subtype; DEX: dexamethasone.

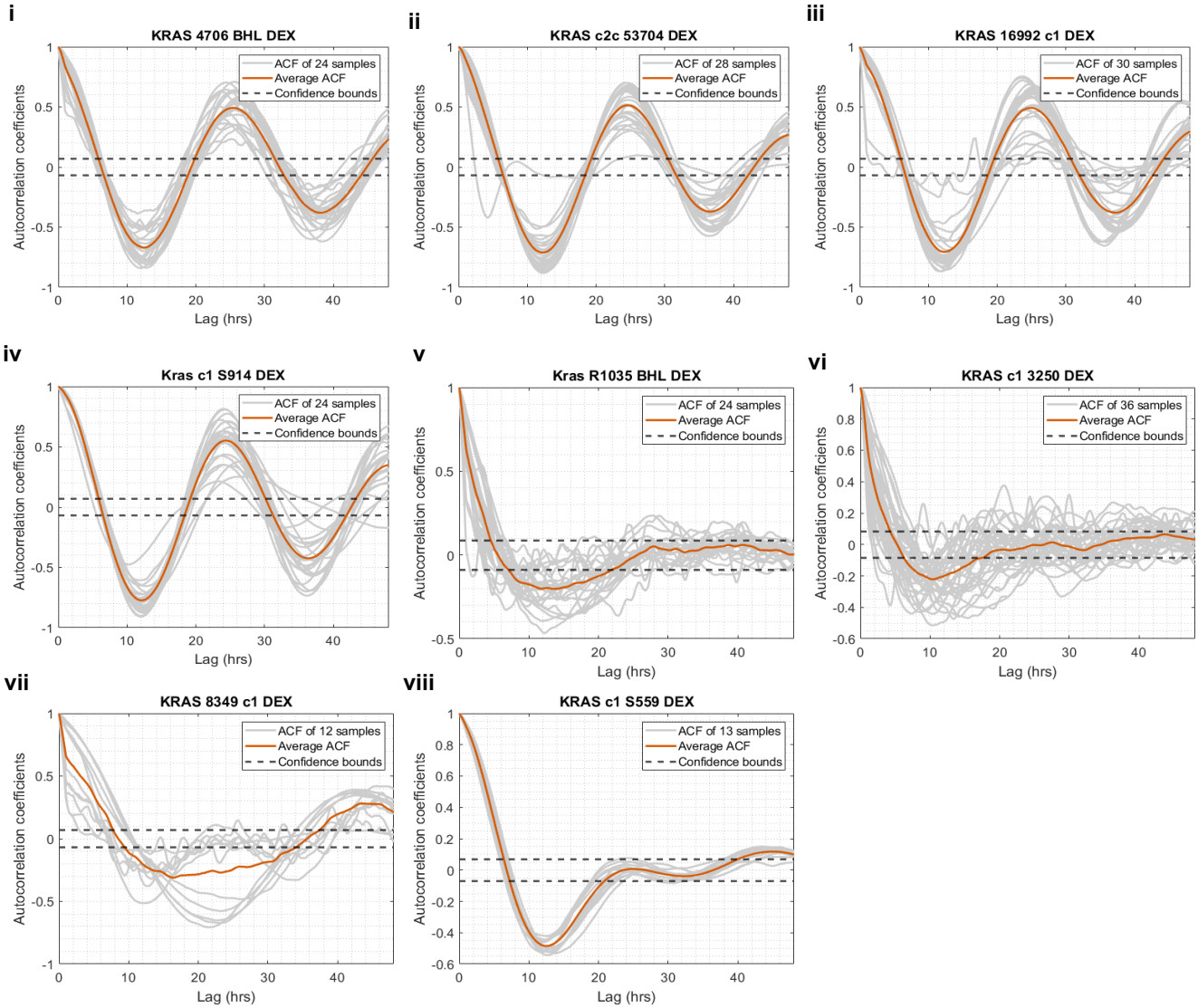

Figure 3.4: Representative results of autocorrelation function in KRAS-driven PDAC (PK) cohort elucidating rhythmicity from the bioluminescence time series. In the inlet of each plot the number of replicates is given. For details, see text. c1: mesenchymal subtype; c2c: epithelial subtype; DEX: dexamethasone.

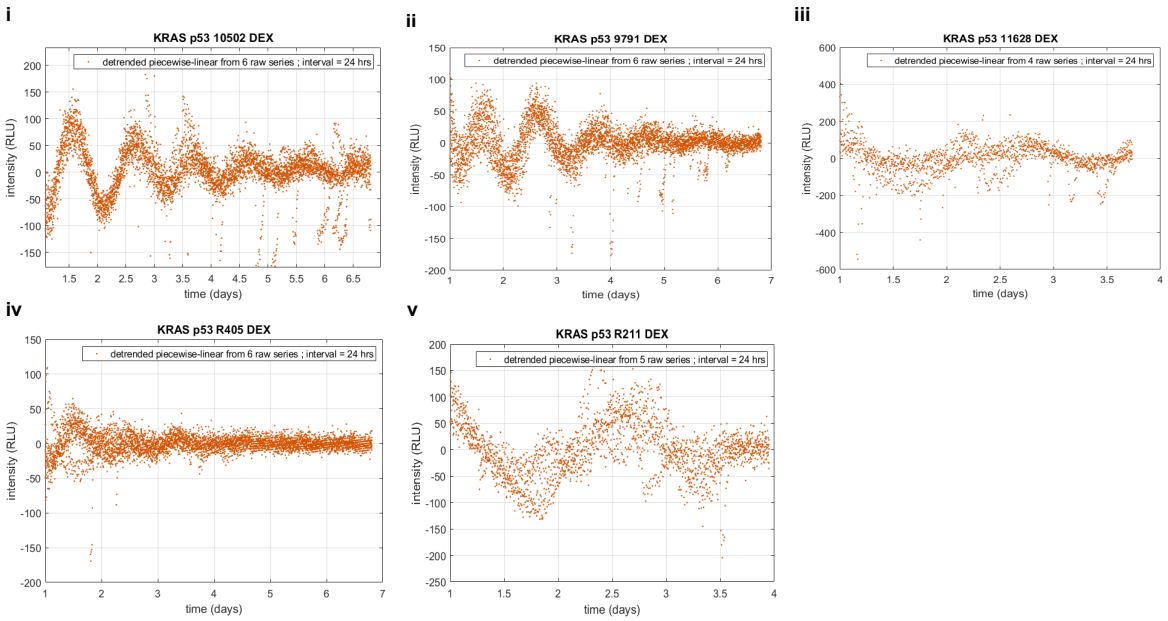

Figure 3.5: Representative results of detrended bioluminescence time series KRAS;p53-driven PDAC (PKP) cohort. In the inlet of each plot the number of replicates from a single experiment is given. For details, see text. DEX: dexamethasone.

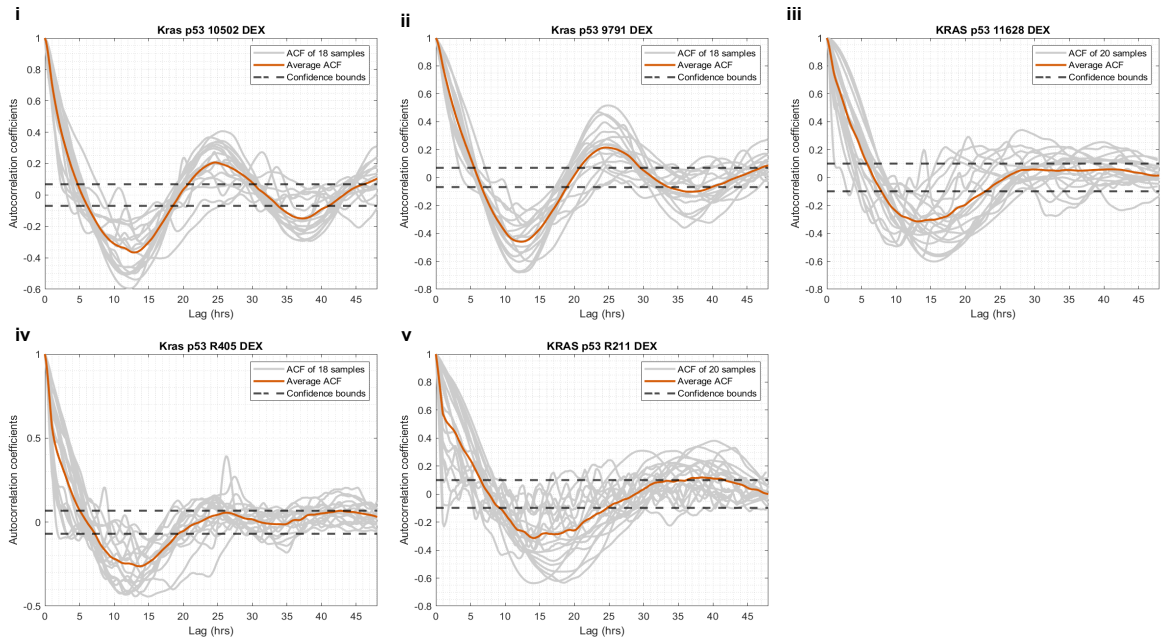

Figure 3.6: Representative results of autocorrelation function in KRAS;p53-driven PDAC (PKP) cohort elucidating rhythmicity from the bioluminescence time series. In the inlet of each plot the number of replicates is given. For details, see text. DEX: dexamethasone.

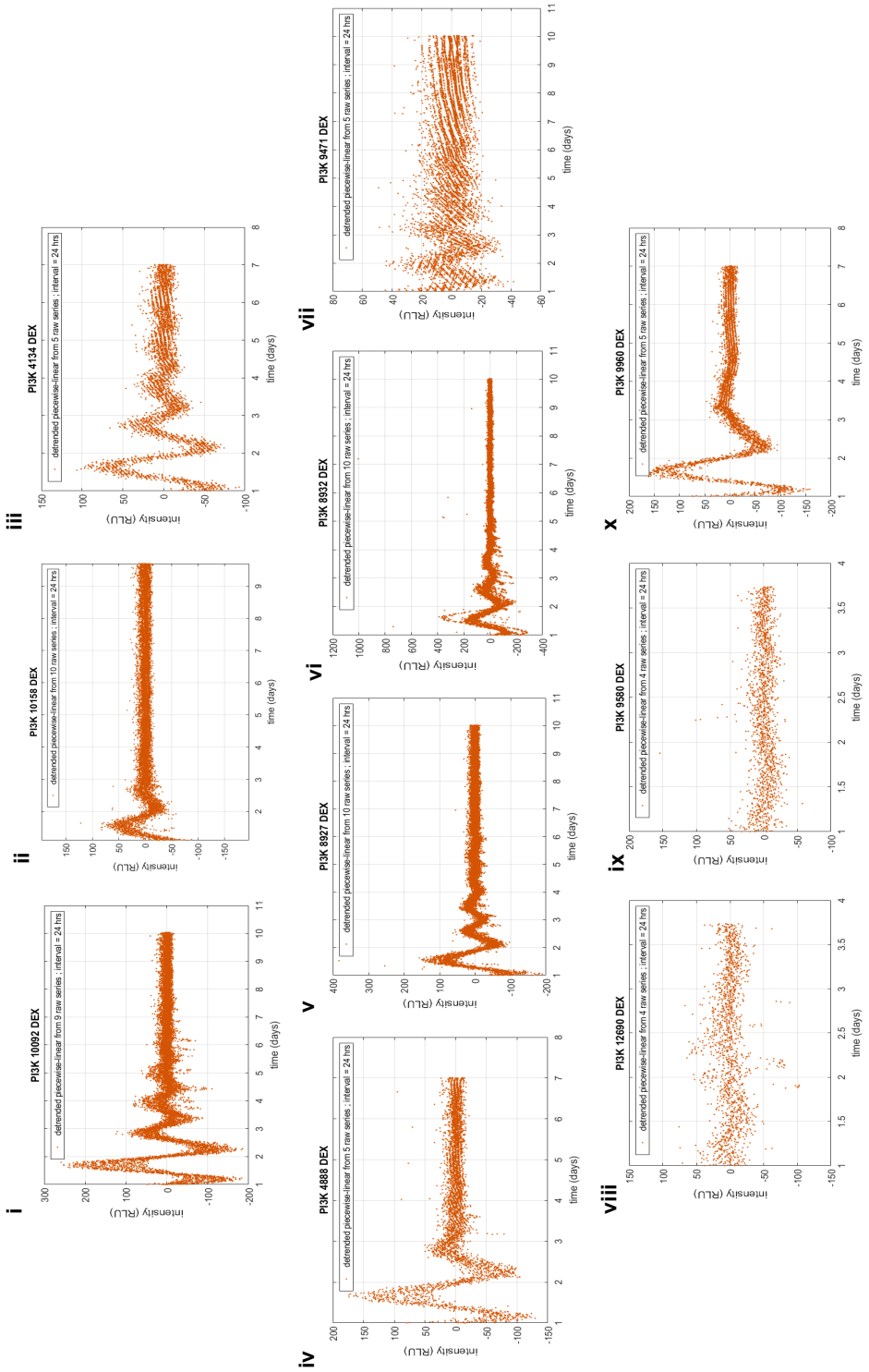

Figure 3.7: Representative results of detrended bioluminescence time series PI3K-driven PDAC (PI3K) cohort. In the inlet of each plot the number of replicates from a single experiment is given. For details, see text. DEX: dexamethasone.

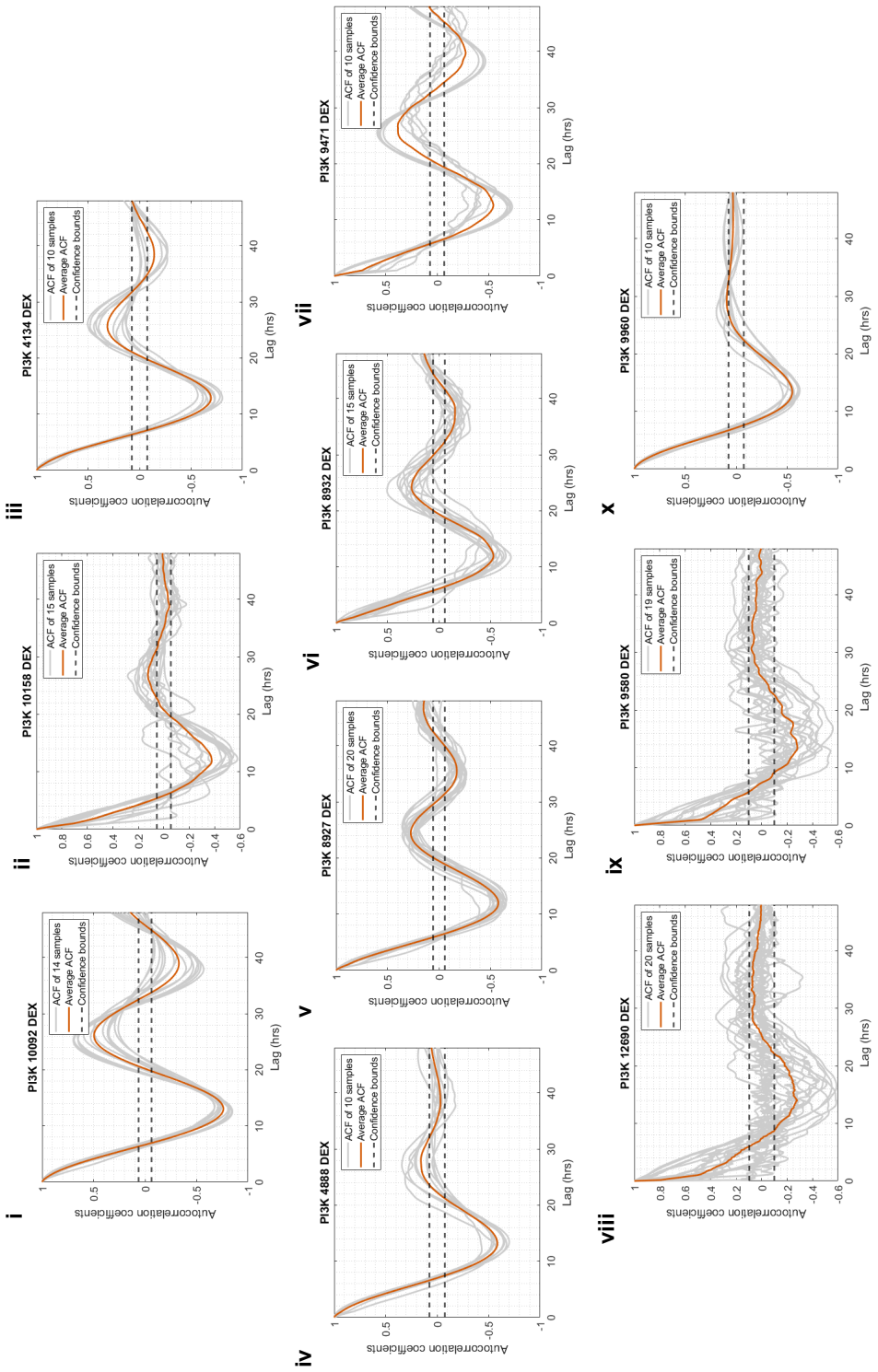

Figure 3.8: Representative results of autocorrelation function in PI3K-driven PDAC (PI3K) cohort elucidating rhythmicity from the bioluminescence time series. In the inlet of each plot the number of replicates is given. For details, see text. DEX: dexamethasone.

in Figure 3.11 and for the PI3K in Figure 3.10. The period of the highly probable rhythmic component identified via the LSP was defined as circadian when its estimate was within a limited range of 24 ± 2 hours. Based on this, there are time series of PDAC cell lines with a significant rhythm, however the LSP failed to identify a circadian periodicity (e.g., compare ACF plot of 8349 cell line in Fig. 3.4 and LSP plot in Fig. 3.9 i).

Regarding the PK cohort, to elucidate which cell lines could be characterized as Non-functional oscillators, both ACF and LSP results were considered. Thereby, the *Bmal1::Luc* cell lines 3250, 8349, R1035 and S559 were included in the Non-functional group for further comparative analysis with the Functional oscillators. In the latter, the group size is 25, which ultimately included four cell lines with the highest normalized amplitude based on the LSP estimate and were the following: 4706, 53704, 16992 and S914 (Fig. 3.9 i, ii, iv and vi).

Furthermore, in the large cohort of the *Bmal1::Luc* KRAS-driven PDAC cell lines it was possible to observe that the robustness of the circadian rhythm varies within the cohort despite the presence of the same oncogenic mutation (Fig. 3.9). This was not seen in the PKP cohort (3.11), while the PI3K-driven PDAC cell lines showed lower variability regarding the power of the period estimate (Fig. 3.10).

Taken together, the functional screening results show that primary PDAC cell lines retain a functional cell-intrinsic circadian clock independently of the oncogenic driver mutation(s). Additionally, the heterogeneity in the strength of the circadian rhythm within the Functional oscillators in PK and PI3K cohorts indicated that the parameters of circadian rhythms are probably tumor cell line-specific in PDAC.

3.1.1.1 Assessment of circadian functionality with different synchronization agents

An important aspect for the functional screening of the luciferase-reporter PDAC cell lines was the phase synchronization with dexamethasone (DEX) before the commence-

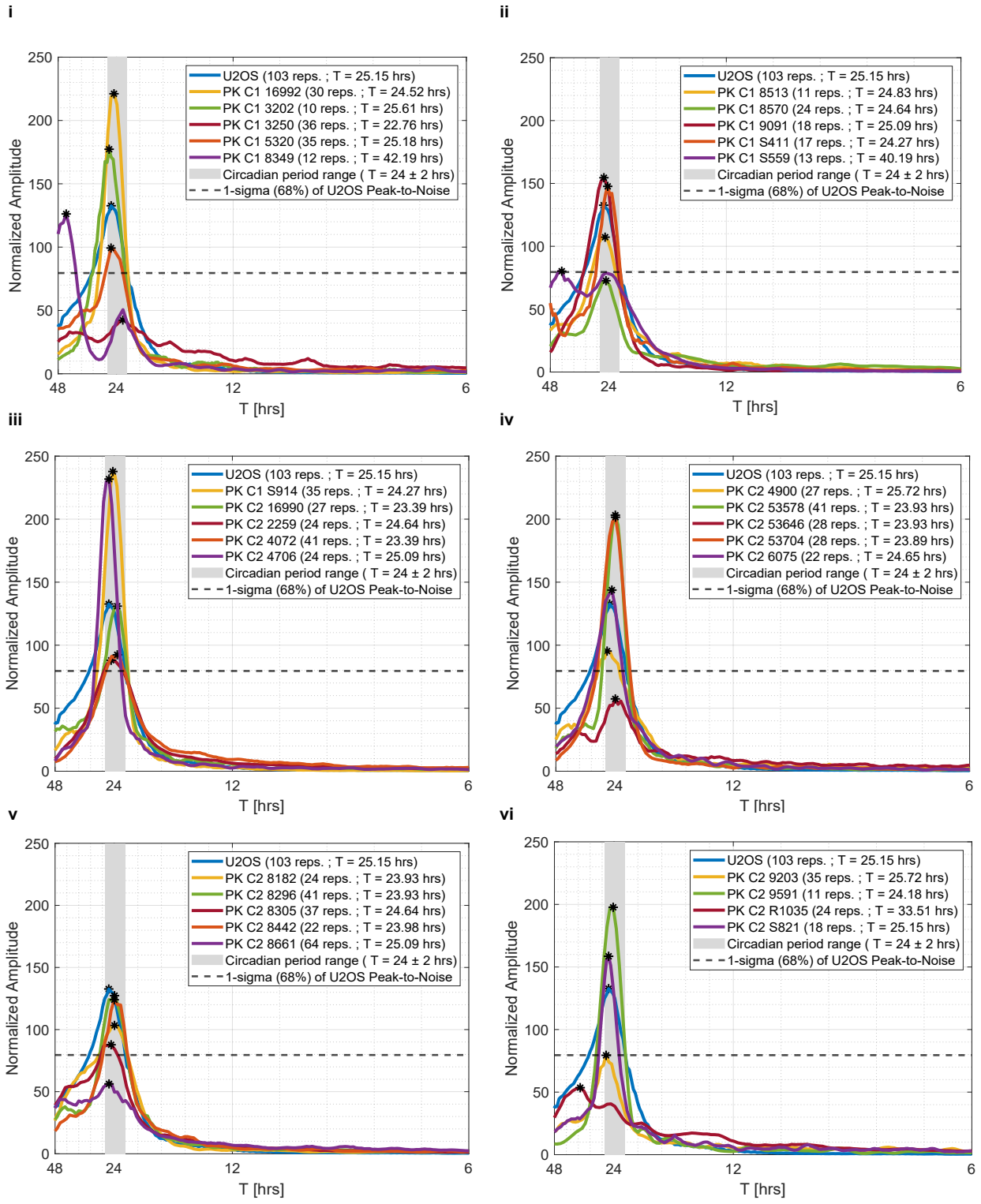

Figure 3.9: Period estimates (T; in hours) of *Bmal1::Luc* KRAS-driven PDAC (PK) cell lines based on the Lomb-Scargle periodogram. C1: Mesenchymal subtype; C2: Epithelial subtype; reps: replicates.

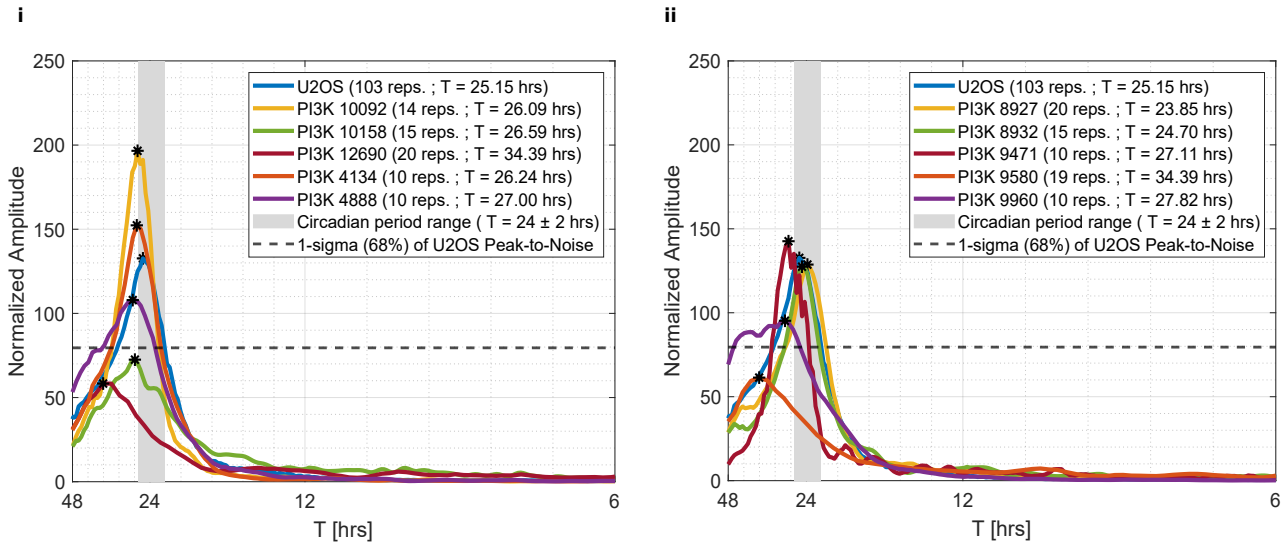

Figure 3.10: Period estimates (T; in hours) of *Bmal1::Luc* PI3K-driven PDAC (PI3K) cell lines based on the Lomb-Scargle periodogram. reps: replicates.

ment of the bioluminescence recording (see sections 1.5.2 and 2.2.1).

Given the characterization of the *Bmal1::Luc* PDAC cell lines as Functional or Non-functional oscillators (see section 3.1.1), I reasoned that the expression of the glucocorticoid receptor (GR), which is necessary for DEX signaling [110], in the Non-functional oscillators might be the limiting factor for phase synchronization, and thereby absence of circadian rhythmicity. For this, the expression of the GR on the protein level for all the corresponding *Bmal1::Luc* PDAC cell lines was extracted from the proteome dataset (see section 3.2) and compared between the established groups of Functional and Non-functional oscillators in PK, PKP and PI3K cohorts. As depicted in Figure 3.12, GR protein levels (expressed as protein LFQ intensity) was not found significantly different between the two compared groups in any of the three PDAC cohorts.

Next, to rule out a plausible effect of the synchronization agent rather than lack of a functional circadian clock for characterizing circadian clock functionality in PDAC, it was investigated whether other synchronization agents, such as forskolin (1 μ M; FSK), serum

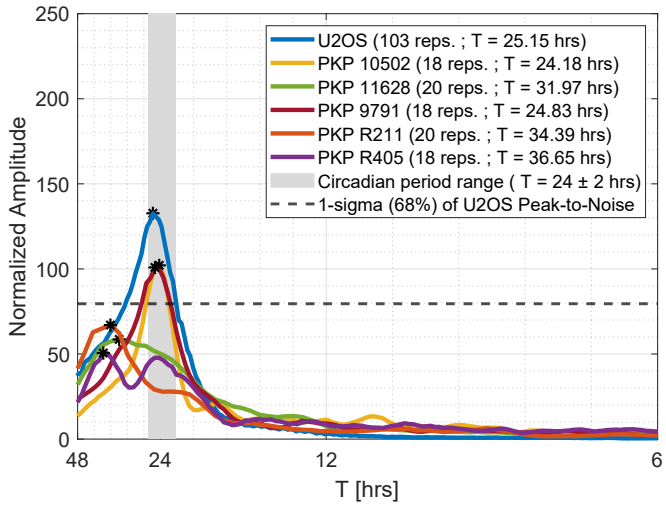

Figure 3.11: Period estimates (T; in hours) of *Bmal1::Luc* KRAS;p53-driven PDAC (PKP) cell lines based on the Lomb-Scargle periodogram. reps: replicates.

shock (DMEM medium with 50 % FCS after starvation for 24 hours; SS) and release in free-run conditions after entrainment with temperature cycles (FR) might elicit circadian rhythmicity in the *Bmal1::Luc* PDAC cell lines characterized as Non-functional oscillators in all three PDAC cohorts. In each experiment, both U2-OS and Functional oscillators from the corresponding cohort were used as positive controls.

For the FSK and SS treatments, it was found that the *Bmal1::Luc* PDAC positive controls could be not synchronized with those two synchronization agents in all three PDAC cell cohorts. Regarding the FR results, the bioluminescent signal in free-running conditions was not found rhythmic for all of the Non-functional oscillators in the PK (Figs. 3.13 iii-vi and 3.14) compared to the positive controls (Figs. 3.13 i-ii and 3.14). For both PI3K and PKP cohorts, FR conditions did not synchronize the Functional oscillators.

Taken together, phase synchronization agents other than DEX did not elicit rhythmicity in characterized Functional oscillators in *Bmal1::Luc* PDAC cell lines. Particularly, in the PK cohort, the Non-functional oscillators were not found rhythmic compared to the Functional oscillators in free-running conditions.

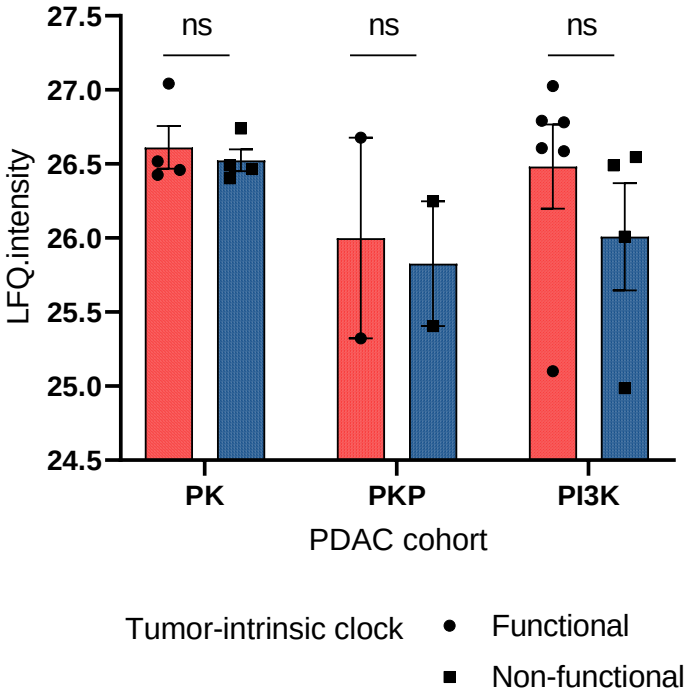

Figure 3.12: Glucocorticoid receptor (GR) protein levels expressed as LFQ intensity between Functional (red) and Non-functional (blue) oscillators in three *Bmal1::Luc* PDAC cell cohorts (two-sample *t*-test; ns: non-significant). PK: KRAS-driven; PI3K: PI3K-driven; PKP: KRAS;p53-driven; LFQ: label-free quantification.

3.1.2 Circadian functionality and core gene expression

As demonstrated in section 3.1.1, *Bmal1::Luc* PDAC cell lines show differential circadian rhythm properties within the same cohort indicating that the molecular mechanism of the circadian clock is probably impacted on a cell line-dependent manner by additional mutations and/or differential core clock gene expression.

Given the availability of transcriptomics data of the PK and PI3K cohorts from Prof. Saur's group, the expression of the core clock genes was extracted and was compared between cell lines harboring a Functional or Non-functional clock in both PDAC cohorts. Core clock genes are considered those comprising the positive and negative "arms" of the

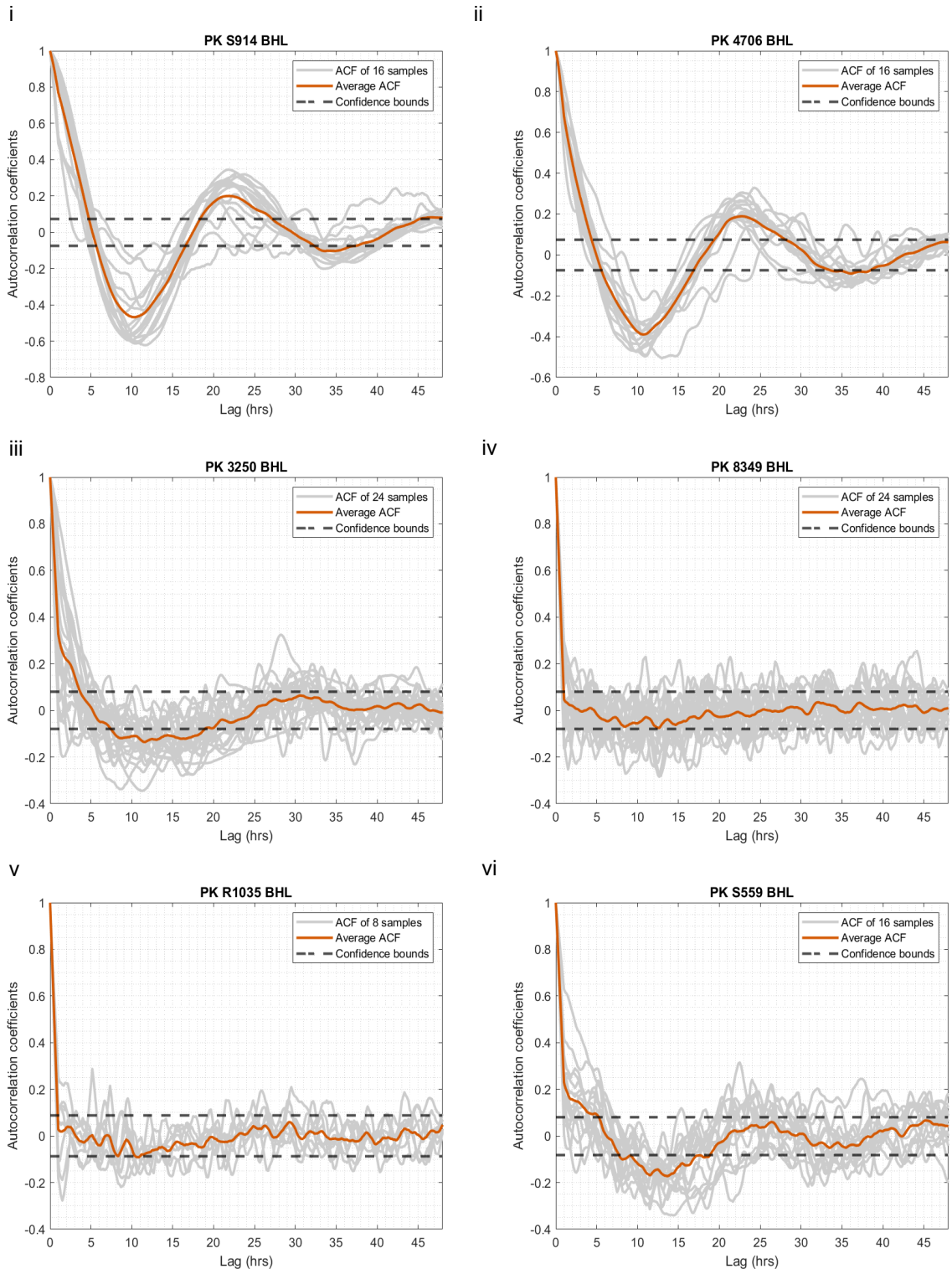

Figure 3.13: Assessment of circadian rhythmicity after releasing in free-running conditions following entrainment with temperatures cycles in PK cohort based on the autocorrelation function. In the inlet of each plot the number of replicates is given. BHL: *Bmal1::Luc*; PK: KRAS-driven PDAC.

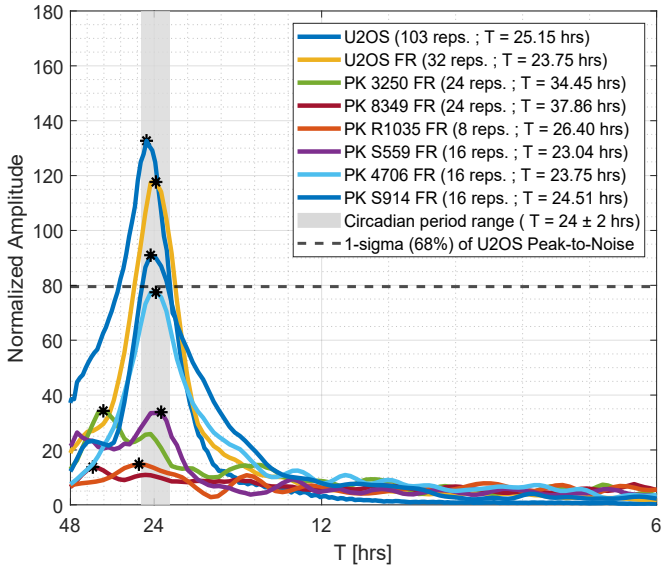

Figure 3.14: Period estimates (T; in hours) of *Bmal1::Luc* KRAS-driven PDAC (PK) cell lines after releasing in free-running (FR) conditions following entrainment with temperatures cycles. For details, see text.

molecular mechanism (for more details, see section 1.4.3). As depicted in Figures 3.15 and 3.16, for the PK and PI3K cohort, respectively, there are no statistically significant differences between the two groups in terms of core clock gene expression. Nevertheless, if considering both PDAC cohorts, it is worth noticing that *Bmal1* gene levels do not differ in Functional vs. Non-functional oscillators, while there is a trend for higher *Clock* gene levels in the Non-functional oscillators (Figs. 3.15 and 3.16).

Collectively, the expression levels of core clock genes between tumor-intrinsic Functional and Non-functional oscillators in PK and PI3K cohorts, which likely could explain the observed circadian rhythm differences, do not significantly differ in any of the two PDAC cohorts. However, core clock gene expression may account for subtype-specific differences in PDAC.

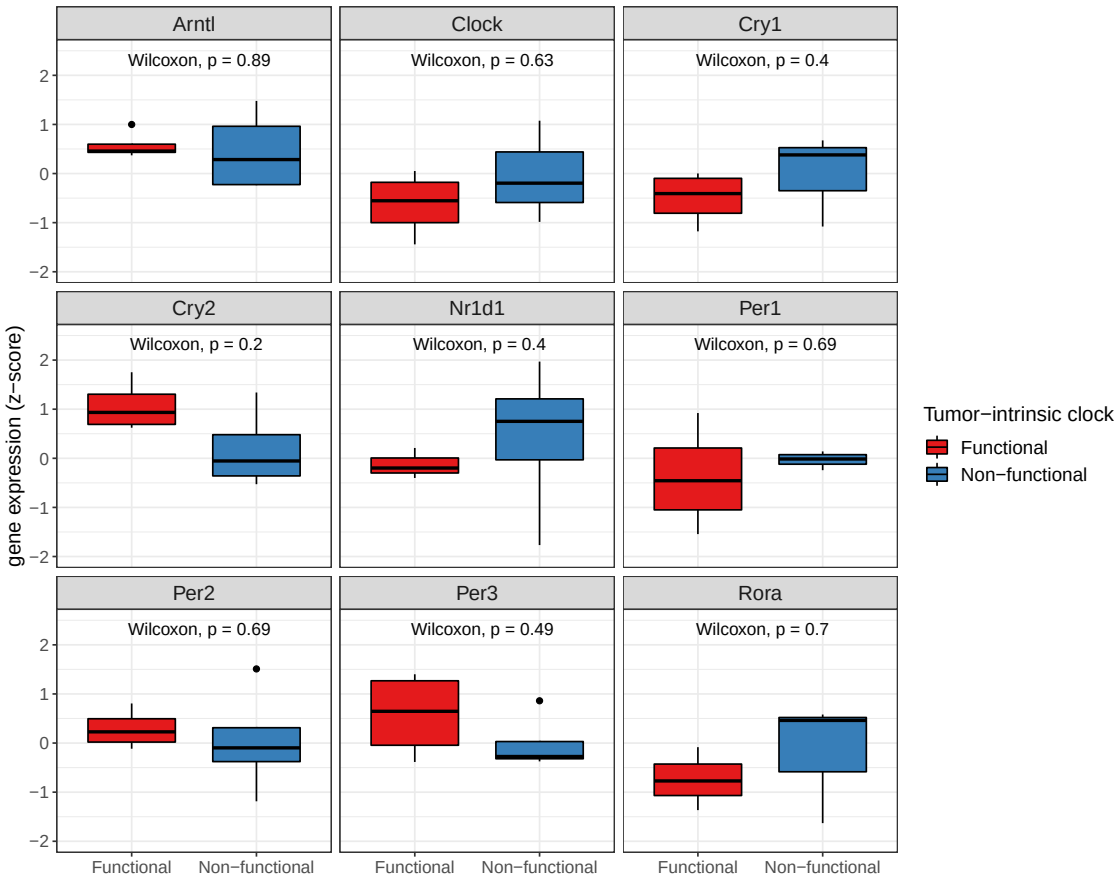

Figure 3.15: Core clock genes expression and tumor-intrinsic clock function in PK cohort. The non-parametric Mann-Whitney-Wilcoxon test was used for comparison between Functional (red) and Non-functional (blue) oscillators. On top of each individual plot, the p value is given. Significance level was set at $p < 0.05$.

3.1.3 Circadian functionality in KRAS-driven PDAC cell lines

The primary KRAS-driven PDAC cell lines that were included in the functional screening have been subjected to genomic analyses in Prof. Saur's group. To complement the exploratory analysis on circadian clock functionality, it was tested whether the available genomic and phenotypic characteristics of the PK cohort (molecular subtype, *Kras* gene dosage and *Cdkn2a* gene deletion) may correlate with circadian clock function. Importantly, as shown in section 3.1.2, the Functional oscillators consisted of four cell lines in

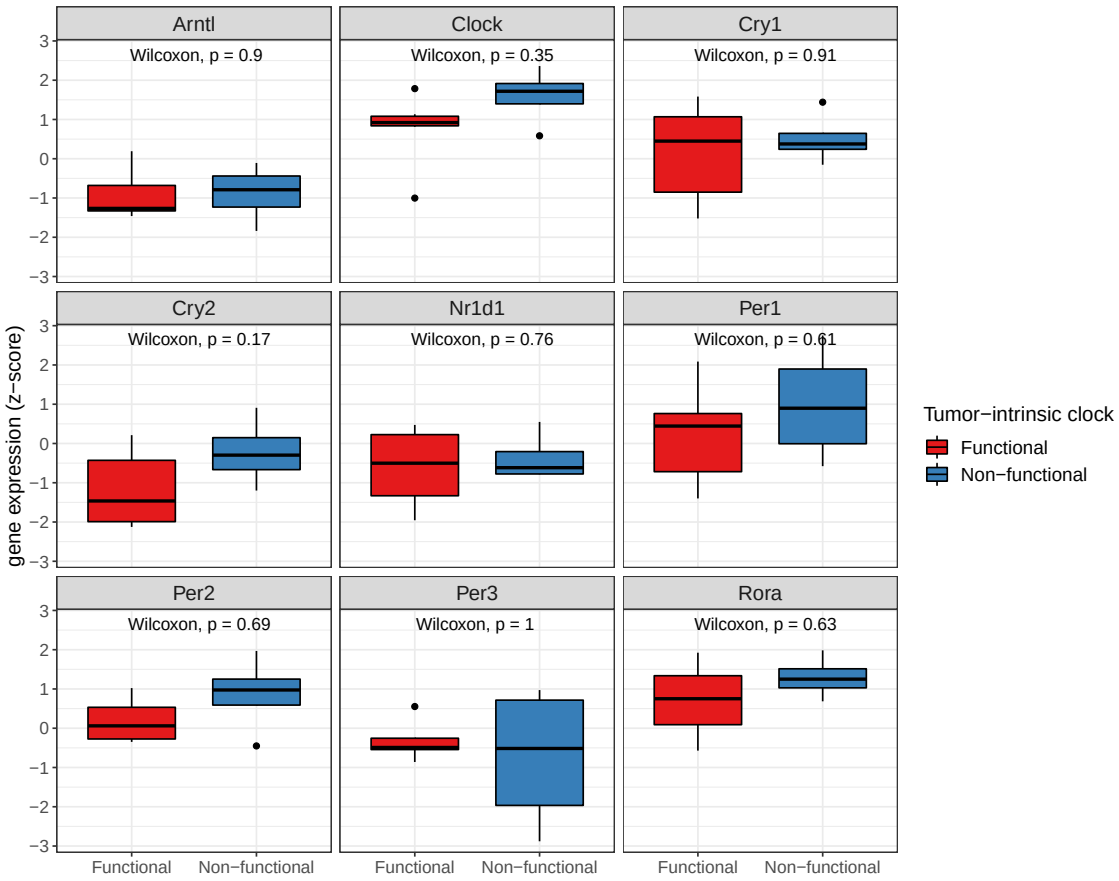

Figure 3.16: Core clock genes expression and tumor-intrinsic clock function in PI3K cohort. The non-parametric Mann-Whitney-Wilcoxon test was used for comparison between Functional (red) and Non-functional (blue) oscillators. On top of each individual plot, the p value is given. Significance level was set at $p < 0.05$.

which circadian rhythm was considered very robust (Fig. 3.4).

In Figure 3.17, the relative percentages of the PK cell lines harboring a Functional or Non-functional cell-intrinsic clock are presented depending on the molecular subtype (epithelial or mesenchymal; Fig. 3.17 A), the *Kras* gene dosage (heterozygous or increased; 3.17 B) and the *Cdkn2a* gene deletion (heterozygous or homozygous; 3.17 C). It is illustrated that neither the molecular subtype nor *Kras* gene dosage can be exclusively attributed to tumor-endogenous circadian clock function in KRAS-driven PDAC tumors

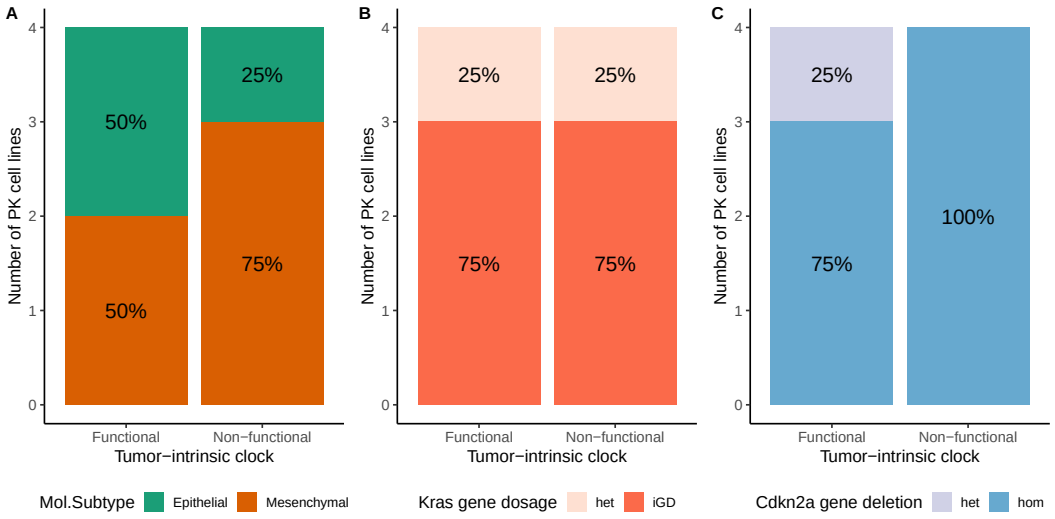

Figure 3.17: Genomic characteristics and tumor cell-intrinsic clock function in PK cohort.

(Fig. 3.17 A and B, respectively). Concerning the *Cdkn2a* gene, its homozygous deletion was found in all four Non-functional oscillators (Fig. 3.17 C).

Taken together, given the genomic characteristics of the PK cell lines, the tumor-endogenous circadian clock could be associated with homozygous *Cdkn2a* gene deletion in primary KRAS-driven PDAC tumors independently of the molecular subtype or the *Kras* gene dosage.

3.2 Proteomic profiling of primary PDAC cell lines

The PDAC cell lines provided by the large biological resource of Prof. Saur's research group, were cultured for protein collection and subsequent proteome analysis (see section 2.3), as well as for generating luciferase reporter (*Bmal1::Luc*) cell lines (see section 2.1.2). The genotype and the number of the PDAC cell lines corresponding to each of those two experimental purposes is given in Table 3.1. Importantly, all of the PDAC cell lines characterized for circadian clock functionality were included in those used for proteomic profiling.

3.2.1 Exploratory analysis based on genotype and molecular subtype

The mass spectromety (MS)-based quantitative proteomic analysis of the primary PDAC cell lines derived from distinct oncogenic driver mutations allowed their functional characterization on a systems-wide functional level. By employing single-shot MS-based proteomics for 52 different PDAC cell lines in quadruplicates from three oncogenic pools (Fig. 3.18 A), 7,683 proteins were identified in total resulting in 3,932 quantified proteins after filtering for at least 50 % of all the measurements (i.e., a given protein was quantified in at least 50 % of the total dataset). The corresponding numbers of identified and quantified proteins in each PDAC cell line are shown in Figure 3.18 (B-E).

The principal component analysis (PCA) plot depicted in Figure 3.19 shows the proteomic signatures of each PDAC cell line from the three oncogenic pools. The almost identical proteome profiles of the biological replicates in a given PDAC cell line indicates the reproducibility of the experimental design and MS measurement, and strongly supports the robustness of the large proteomics dataset. Importantly, a further division of the KRAS-driven (PK) cell lines based on the characterized molecular subtype (i.e., epithelial or mesenchymal) was included in the analysis (see below).

The PCA attributes the largest variance of the profiled proteomes to the difference between PK mesenchymal subtype (olive green triangles) and PK epithelial subtype (olive

Table 3.1: PDAC cell lines of the functional screening and proteomic profiling.

Oncogenic driver mutation	PDAC cohort	Characterized	
		Clock	Proteome
Pdx1-Cre;LSL-Kras$^{G12D/+}$	PK (Epithelial)	18	22
Pdx1-Cre;LSL-Kras$^{G12D/+}$	PK (Mesenchymal)	11	14
Pdx1-Cre;LSL-Kras$^{G12D/+}$*;p53*$^{R172H/+}$	PKP	5	4
Pdx1-Cre;LSL-Pi3kca$^{H1047R/+}$	PI3K	10	12

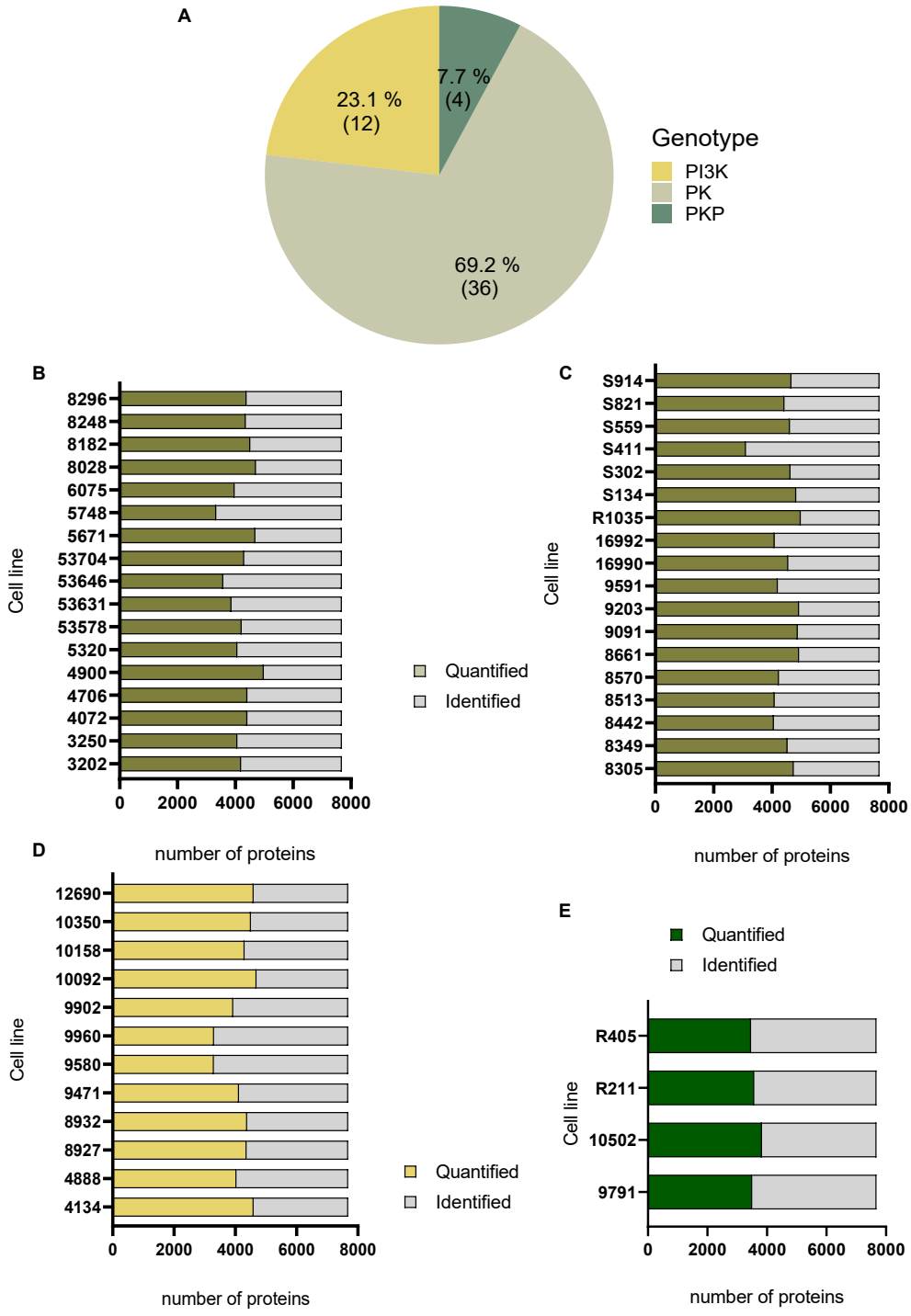

Figure 3.18: A) The relative proportions of the three PDAC oncogenic pools included in the mass spectrometry-based proteomic profiling. B)-E) Barplots representing the total number of identified and quantified proteins measured with shotgun label-free proteomics in each PDAC cell line of the PK (olive green), PI3K (yellow) and PKP (dark green) cohorts as the mean value of four biological replicates. PI3K: PI3K-driven; PK: KRAS-driven; PKP: KRAS;p53-driven.

green circles) (Component 1, 18.5 %), and the second largest variance (Component 2, 10.1 %) to the difference between the PK subtypes and both PI3K (yellow squares) and PKP (dark green squares) cohorts (Fig. 3.19). Interestingly, the PI3K cohort includes two cell lines that their proteome profile is more similar either to the PK epithelial subtype (cell line 9471), or to the PK mesenchymal subtype (cell line 4134). Regarding the PKP cell lines, their proteomic signatures are less clustered together, probably due to the small group size compared to the other two cohorts.

To gain functional insights into the data, I performed statistical analyses based on total protein abundances between four groups of the PDAC cell lines. Given the PCA analysis, it was determined that the PK cohort would be divided in two subgroups, therefore the four groups of the PDAC cell lines were: PK epithelial subtype (PK-E), PK mesenchymal subtype (PK-M), PI3K cohort and PKP cohort. Differential analysis using the Perseus software-integrated Analysis of Variance (ANOVA) statistical test with multiple hypothesis testing correction (permutation-based FDR) showed that 2,800 proteins were differentially expressed between the four groups (FDR < 0.05, $s0 = 0$). Based on subsequent post-hoc analysis, several clusters of protein groups are highlighted in the dendrogram demonstrating that there are proteins significantly upregulated between pairs of PDAC cohorts, whilst very few proteins can be characterized as unique signatures of a given cohort (Fig. 3.20 A). With this in mind, each node junction in the protein tree (Fig. 3.20 A) was inspected for potentially interesting protein clusters upregulated in distinct or groups of PDAC cohorts that could be potentially enriched in unique functional pathways. Based on this, three protein clusters were extracted (annotated in Fig. 3.20 A) and their corresponding profile plots are shown in Figure 3.20 B-D (for Clusters 1-3, respectively). Cluster 1 is strongly upregulated in PK-E (Fig. 3.20 B), Cluster 2 is strongly increased in PI3K and PKP (Fig. 3.20 C), and Cluster 3 is found upregulated in both PK-M and PKP cohorts (Fig. 3.20 D).

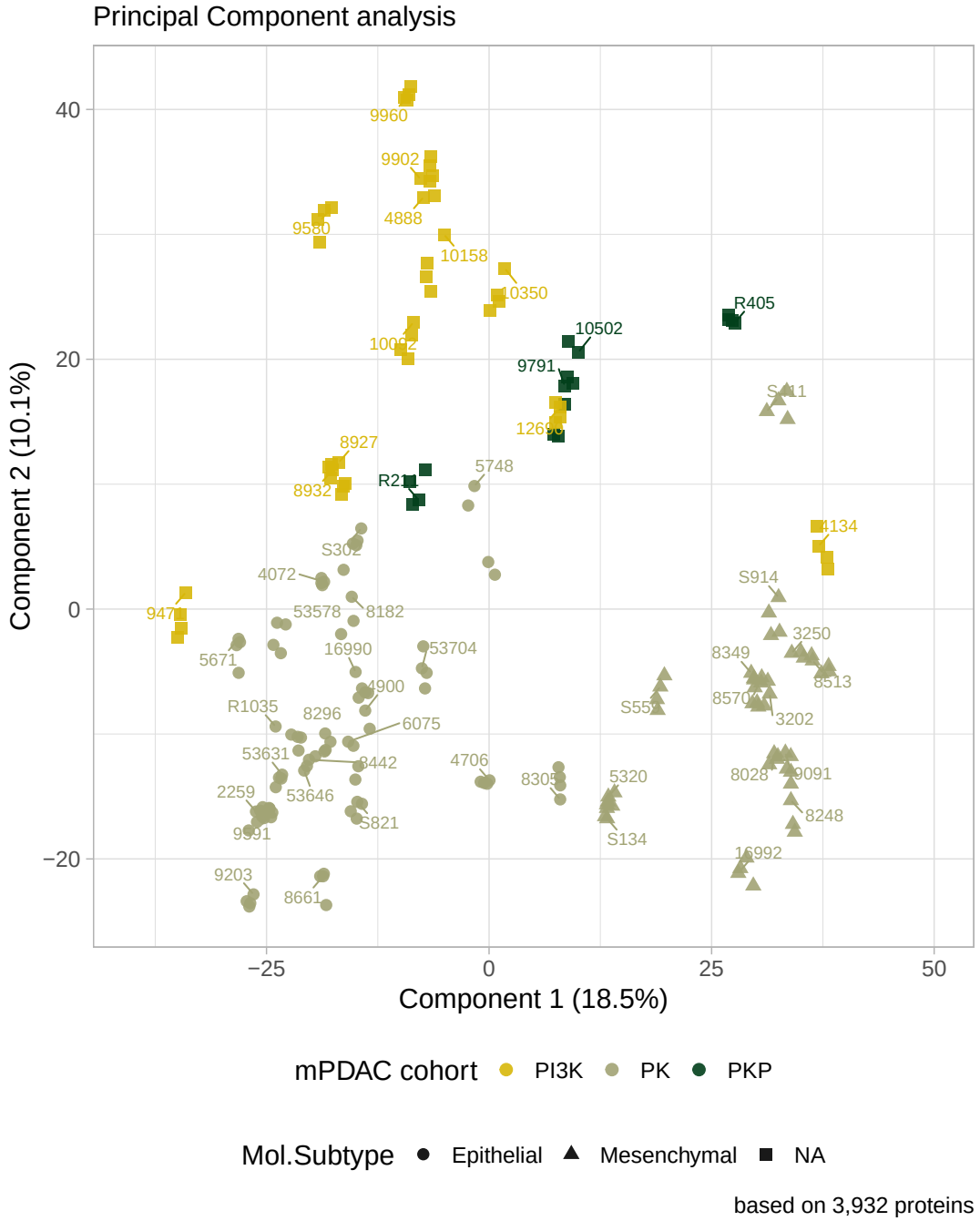

Figure 3.19: Principal Component Analysis (PCA) plot based on global protein abundances of PDAC cell lines from PI3K (yellow squares), PK (olive green) and PKP (dark green squares) cohorts. PK cell lines are further annotated based on the molecular subtype (epithelial in circles and mesenchymal in triangles). Each dot represents a biological replicate from each profiled PDAC cell line, and the cell line number is annotated next to the corresponding quadruplicates. PI3K: PI3K-driven; PK: KRAS-driven; PKP: KRAS;p53-driven; mPDAC: murine PDAC.

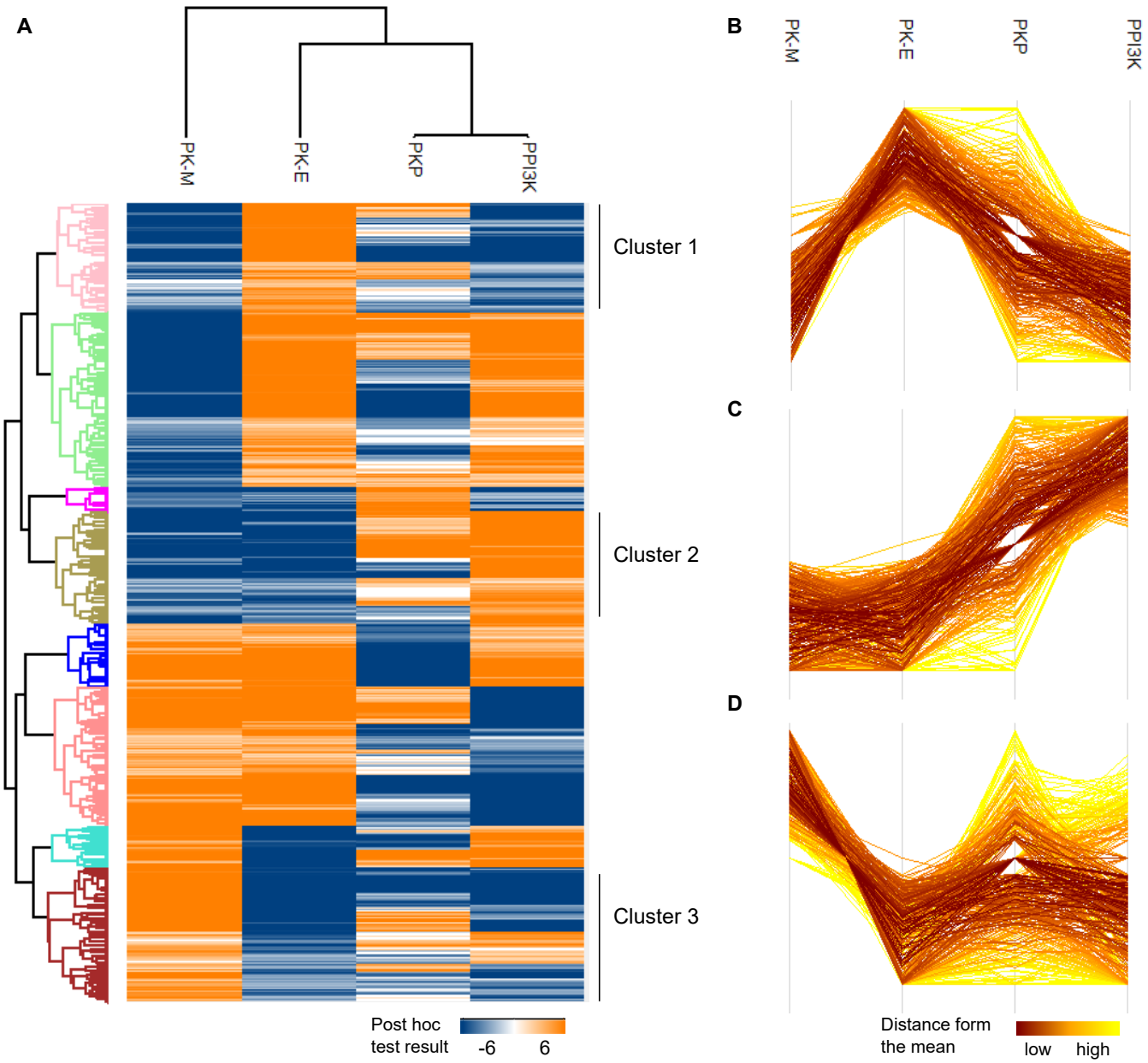

Figure 3.20: A) Hierarchical clustering of differentially expressed proteins (ANOVA; FDR < 0.05, *s0* = 0 and post-hoc; FDR < 0.05) between pairs of PDAC cohorts (PK-M, PK-E, PKP and PPI3K) represented in a heat map with high and low expression as orange and blue, respectively. Various protein clusters are highlighted in the dendrogram, and three main functional protein clusters with distinct protein signatures are annotated. B-D) The profile plots of the three Clusters (Cluster 1 in B, Cluster 2 in C and Cluster 3 in D). PK-M: KRAS-driven mesenchymal subtype; PK-E: KRAS-driven epithelial subtype; PKP: KRAS;p53-driven PDAC; PPI3K: PI3K-driven.

Subsequently, the three protein Clusters were used for functional enrichment analysis of protein terms annotated as Gene Ontology (GO) biological processes and cellular compartments or KEGG pathways (incorporated on the Perseus platform) by implementing the Fishers's exact test with multiple hypotheses correction (FDR < 0.02). Enriched categories in each Cluster and the corresponding p-values are shown in Figure 3.21. Interestingly, PK-E cell lines are enriched in metabolic-related processes, such as "Fatty acid metabolism", "PPAR signalling pathway" and "cellular amino acid metabolic process", as well as in pathways involved in transcriptional regulation, such as "mRNA processing", "RNA splicing" and "chromatin organization" (Fig. 3.21 Cluster 1). The PI3K and PKP cell lines show overpresentation of cellular pathways regarding protein synthesis, such "tRNA aminoacylation for protein translation", "translational initiation" and "ribonucleoprotein complex assembly" (Fig. 3.21 Cluster 2). The PK-M cell lines share upregulated proteins with the PKP cohort that found enriched in intracellular transport processes, such as "protein transport", "vacuole", "vesicle-mediated transport" and "cytoplasmic membrane-bounded vesicle", along with pathways related to "Phagosome", "endosome" and "protein folding" (Fig. 3.21 Cluster 3). Representative examples of upregulated proteins in each Cluster are shown in Figure 3.22.

Taken together, MS-based proteomic profiling of primary PDAC cell lines with distinct oncogenic mutations showed that the molecular subtype of PK cohort and the oncogenic mutation driver have the largest impact on proteome data variability. In addition, differential protein expression analysis and functional enrichment analysis demonstrated distinct metabolism-related pathways as protein signatures of either one or a combination of PDAC cohorts.

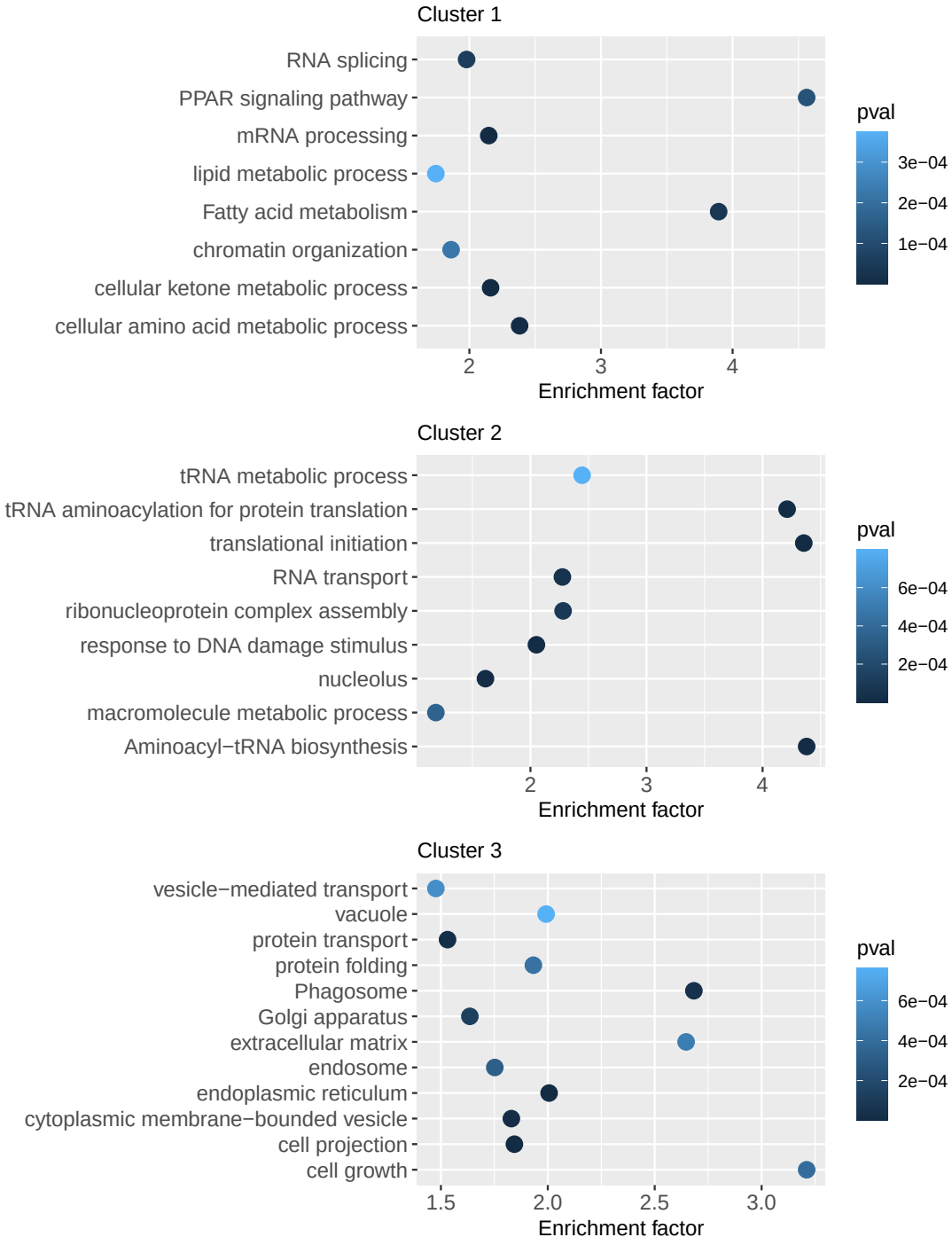

Figure 3.21: Pathway enrichment analysis (Fisher's exact test; FDR < 0.02) of the three functional protein Clusters in PDAC cohorts. In each individual plot the significantly enriched pathways (FDR < 0.02; enrichment factor > 1) in each Cluster with the corresponding enrichment factor and *p*-value (pval) are shown.

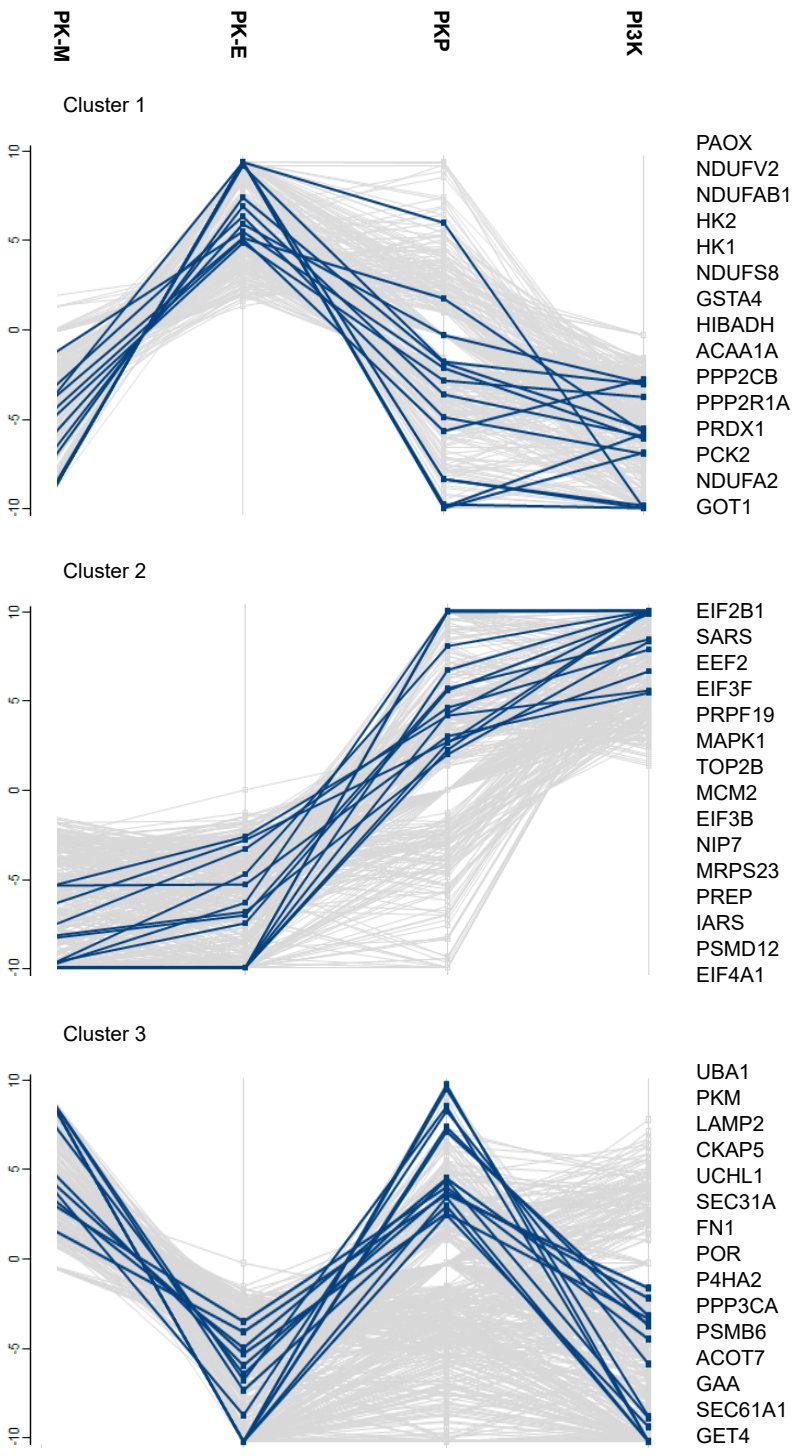

Figure 3.22: Extracted protein profiles from the three functional Clusters in PDAC. The quantitative expression profiles of 15 selected proteins (blue lines) annotated next to each Cluster were queried by similarity (based on pearson's correlation) to a reference protein profile following the mean protein abundance in each functional Cluster.

3.2.1.1 Exploratory analysis by integrating transcriptomic profiles

Based on the functional enrichment analysis of the four PDAC cohorts presented in section 3.2.1, it was found that PK-E tumors show significant upregulation of proteins related to glycolytic "switch" (HK1, HK2, PCK2) [142], reprogrammning of amino metabolism (GOT1) [142], or protein annotations (integrated on Perseus) related to fatty acid metabolism (ACAA1A, NDUFABLX, HIBADH), oxidative phosphorylation (NDUFV2, NDUFA2) and redox homeostasis (GSTA4, PRDX1, PAOX) as depicted in Figure 3.22 (Cluster 1).

I reasoned that it was intriguing that both lipogenic and glycolytic enzymes are significantly upregulated in the PK-E cohort. Considering that PK-E tumors are heterogeneous based on transcriptomics profiling with defined sub-clusters [143], it was further analyzed whether these clusters could be taken into consideration for proteomic profiling (given the available additional information about the trancriptomics cluster of each PK-E cell line). As shown in Figure 3.23, PK-E tumors depict distinct proteomic signatures, based on which they separate in three different Clusters. The C2b and C2c Transcriptomics clusters form a common cluster on the proteome level, while the Transcriptomics C2a and Outlier clusters show distinct proteomic profiles, well separated from each other and from the C2b-C2c cluster. Interestingly, two PDAC cell lines from C2b (cell line 8661) and C2c (cell line 4900) Transcripotmics clusters show similarity with the Outlier Cluster on the proteome level (Fig. 3.23). Based on this, three analysis-derived PK-E Proteomics Clusters were identified and annotated as C2A, OUTLIER (OUTL) and C2BC (Fig. 3.23).

Subsequent statistical analyses (ANOVA test with multiple hypothesis correction, FDR < 0.05 and post-hoc analysis) showed that there are 2,743 proteins with significant differences in abundance between the three Proteomic Clusters of PK-E tumors. Four clusters of protein groups are highlighted in the dendrogram (Fig. 3.24 A) demonstrating that

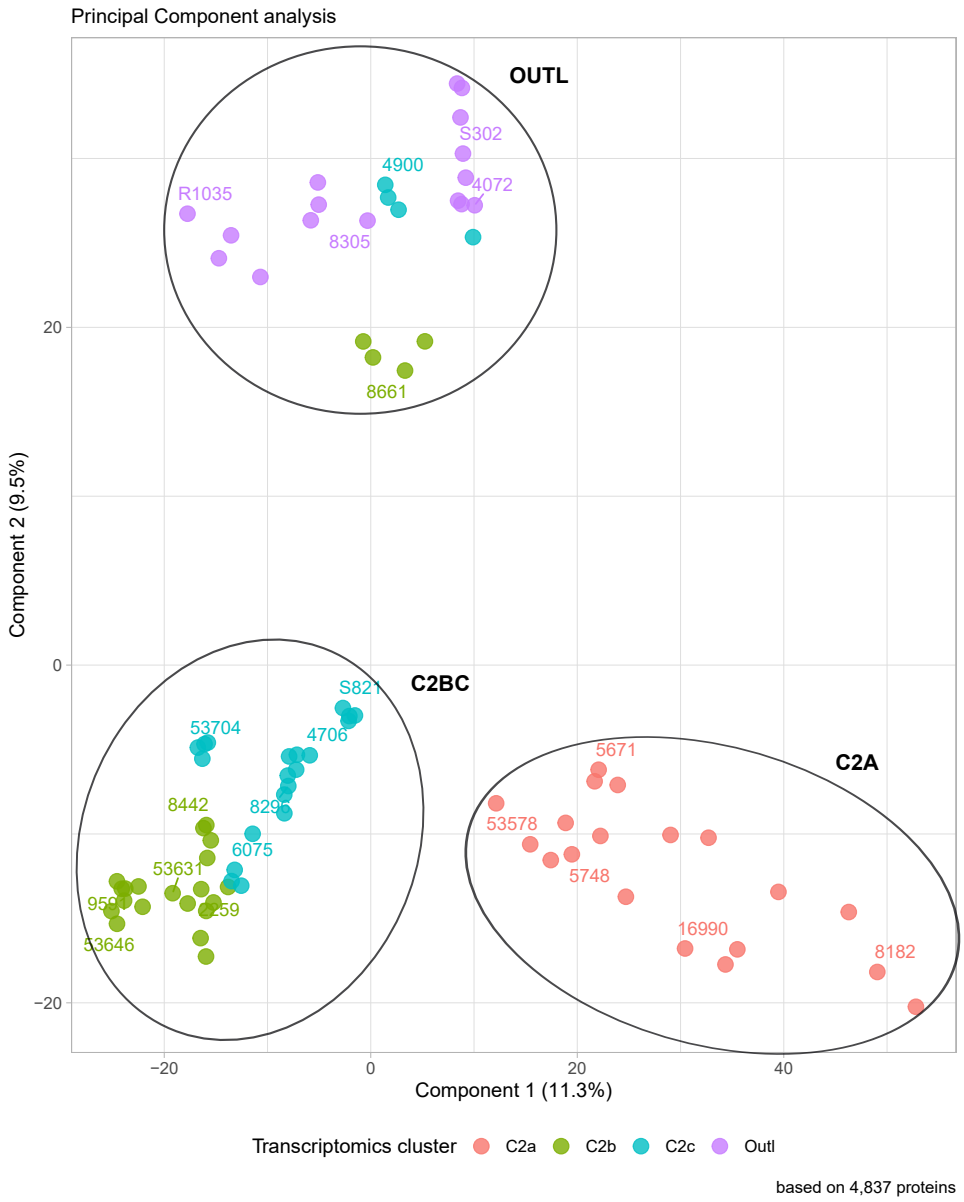

Figure 3.23: Principal Component Analysis (PCA) plot based on global protein abundances of C2a (red), C2b (green), C2c (light blue) and Outlier (purple) Transciptomics-based clusters in PK-E cell lines. Each dot represents a biological replicate from each profiled PDAC cell line, and the cell line number is annotated next to the corresponding quadruplicates. Three Proteomic Clusters in PK-E cell lines are annotated: C2A, C2BC and OUTL. PK-E: KRAS-driven epithelial PDAC.

there are proteins significantly upregulated between pairs of PK-E protein groups, whilst very few proteins can be characterized as unique signatures of a given protein group. Each node junction in the dendrogram was inspected for potentially interesting protein clusters upregulated in distinct or groups of PDAC cohorts that could be potentially enriched in unique functional pathways. Based on this, two protein Clusters were extracted (annotated in Fig. 3.24 A). Cluster 1 includes 157 proteins and shows upregulation in C2A and C2BC, while Cluster 2 consists of 213 proteins that found significantly upregulated in OUTL and C2BC groups. Functional annotation enrichment analysis (Fisher's exact test; FDR < 0.02) in each of the two Clusters identified that C2A and C2BC PK-E tumors are enriched in "Oxidative phosphorylation" and "protein complex" (Fig. 3.24 B - Cluster 1), whilst pathways such as "biosynthetic process", "translation" and "Ribosome" were found overrepresented in OUTL and C2BC PK-E tumors (Fig. 3.24 B - Cluster 2). Selected protein markers of the annotated pathways "Oxidative phosphorylation", "Fatty acid metabolism" and "cellular amino acid metabolic process" are shown in Figure 3.24 C).

Collectively, MS-based proteomic profiling of KRAS-driven PDAC epithelial tumors identified three Proteomic groups that form two enriched functional Clusters with regard to energy metabolism-related pathways, indicating that KRAS oncogenic signaling result in functional divergencies in a subset of KRAS-driven PDAC tumors.

3.2.2 Exploratory analysis based on circadian clock functionality

Given the characterization of circadian clock function and the proteomic profiling data of the different PDAC cohorts, I aimed to investigate whether there are global differences in protein abundances based on the functionality of the circadian clock in each PDAC cohort. The majority of the cell lines characterized at the proteome level were included in the functional screening (see section 3.1.1 and Table 3.1).

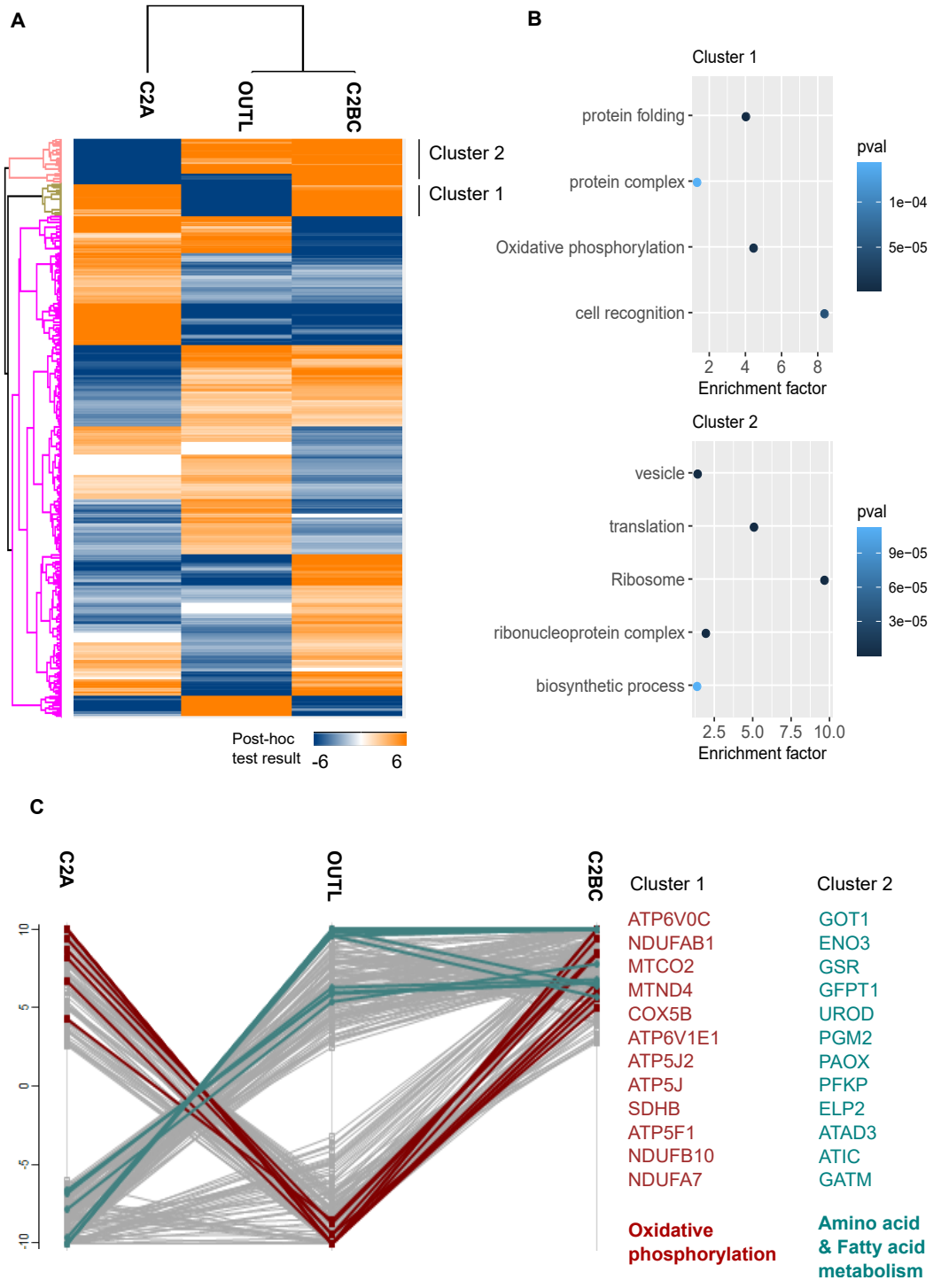

Figure 3.24: A) Hierarchical clustering of differentially expressed proteins (ANOVA; permutation-based FDR < 0.05 and post-hoc) between pairs of Proteomic groups of PK-E tumors represented in a heat map with high and low expression as orange and blue, respectively. B) Functional annotation enrichment analysis (Fisher's exact test, FDR < 0.02) of the annotated protein Clusters 1 and 2. C) Representative protein profiles related to Oxidative phosphorylation and Amino acid metabolism, are highlighted in red and green, respectively. The 12 selected proteins (highlighted lines) in each cluster were queried by similarity (based on pearson's correlation) to a reference protein profile following the mean protein abundance in each Cluster. PK-E: KRAS-driven epithelial PDAC.

As depicted in Figure 3.25, circadian clock functionality in the profiled PDAC cell lines does not constitute a robust driver for global protein differences when considering all three PDAC cohorts. Similar to the PCA plot in Figure 3.19, the largest variance that can explain differences on global protein abundance are the PK molecular subtype and the oncogenic mutation driver (Fig. 3.25). For this, subsequent statistical analysis (two-sample *t*-test, FDR < 0.05, *s0* = 0) separately in PK and PKP cohorts showed that there are significantly different proteins expressed between cell lines harboring a Functional or Non-functional tumor-intrinsic circadian clock (Figs. 3.26 A and 3.27 A).

Subsequently, functional enrichment analysis (Fisher's exact test, FDR < 0.02) of the protein signatures in each group showed that the PK Functional oscillators are enriched in proteins related to "Oxidative phosphorylation" and "NADH dehydrogenase complex" (Fig. 3.26 B), while the Non-functional oscillators in the PKP cohort showed significant upregulation in proteins related to "tRNA aminoacylation" and "Arginine and proline metabolism". The pathways "Oxidative phosphorylation" and "tRNA aminoacylation" were shown to be enriched in the identified protein Clusters when four PDAC cohorts were compared without taking into account circadian clock functionality (Fig. 3.21 Cluster 2 corresponding to PKP and PI3K tumors, and Cluster 1 corresponding to PK-E tumors, respectively).

Given that the results of the enrichment analysis of the differentially expressed proteins between the four PDAC cohorts are similar to those when considering circadian clock function, it is challenging to unravel which functional outputs on the proteome level may be exclusively attributed to the tumor-intrinsic clock functionality (Figs. 3.20, 3.21, 3.26 and 3.27).

Taken together, proteomic profiling of PDAC cell lines with distinct oncogenic mutations indicates that oncogenic driver mutation(s) and associated metabolic rewiring may determine marked functional divergences on the proteome level, which in turn may dif-

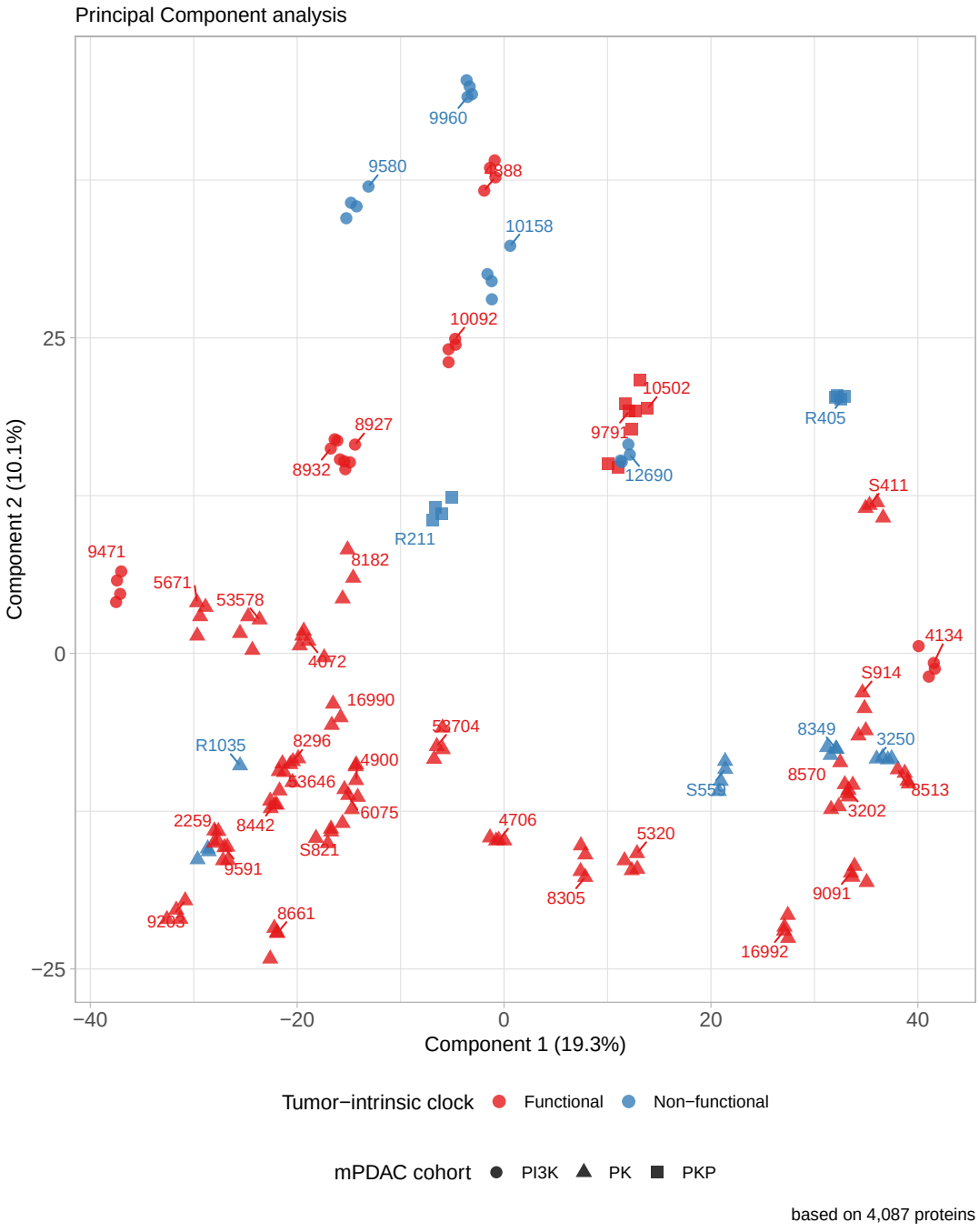

Figure 3.25: Principal Component Analysis (PCA) plot based on global protein abundances of PI3K (circles), PK (triangles) and PKP (squares) characterized for circadian clock functionality. Each dot represents a biological replicate from each profiled PDAC cell line, and the cell line number is annotated next to the corresponding quadruplicates. PDAC cell lines harbor either a Functional (red) or Non-functional (blue) cell-intrinsic clock. PI3K: PI3K-driven; PK: KRAS-driven; PKP: KRAS;p53-driven; mPDAC: murine PDAC.

ferentially modulate clock-associated proteome outputs in each PDAC cohort.

3.2.2.1 Exploratory analysis based on genetic disruption of the circadian clock

To elucidate whether functional annotation categories, and thereby protein markers, could be merely associated to circadian clock outputs at steady-state conditions, proteome profiles from one mesenchymal (S914) and one epithelial (4706) *Bmal1::Luc* KRAS-driven PDAC cell lines were analyzed after genetically disrupting the molecular mechanism of the circadian clock in each of them by gene editing of *Bmal1* -the main transcription factor of the clock (see sections 1.4.3, 2.1.3, 3.3.1 and Fig. 3.34 A-C).

In both PK cell line pairs, it was investigated whether there are significant differences on global protein abundances between Bmal1 non-edited (sglacZ) and Bmal1-edited (sg284) cells. Subsequent functional enrichment analysis (Fisher'S exact test; FDR < 0.02) identified that in the mesenchymal S914 control cells (sglacZ), the upregulated proteins are enriched for "Protein digestion and absorption", "extracellular matrix" and "response to stress" (Fig. 3.28 B). Following the same analysis steps, the epithelial 4706 Bmal1-edited cells (sg284) show higher levels of proteins related to pathways as "Fatty acid metabolism", "Ribosome" and "generation of precursor metabolites and energy" (Fig. 3.29 B).

These results indicate a probable association of a functional circadian clock with fatty acid metabolism in KRAS-driven epithelial tumors, while in KRAS-driven mesenchymal tumors the cell-intrinsic circadian oscillator is likely associated with protein digestion and transport. In combination with the functionally enriched categories presented in sections 3.2.1 and 3.2.1.1, it is suggested that in KRAS-driven tumors probable time-dependent functional vulnerabilities could be identified. Indeed, it has been shown that drug efficacy and toxicity are changed when the circadian clock is disrupted in mice injected with U2-0S cells [144], indicating that it is worth investigating such a concept in

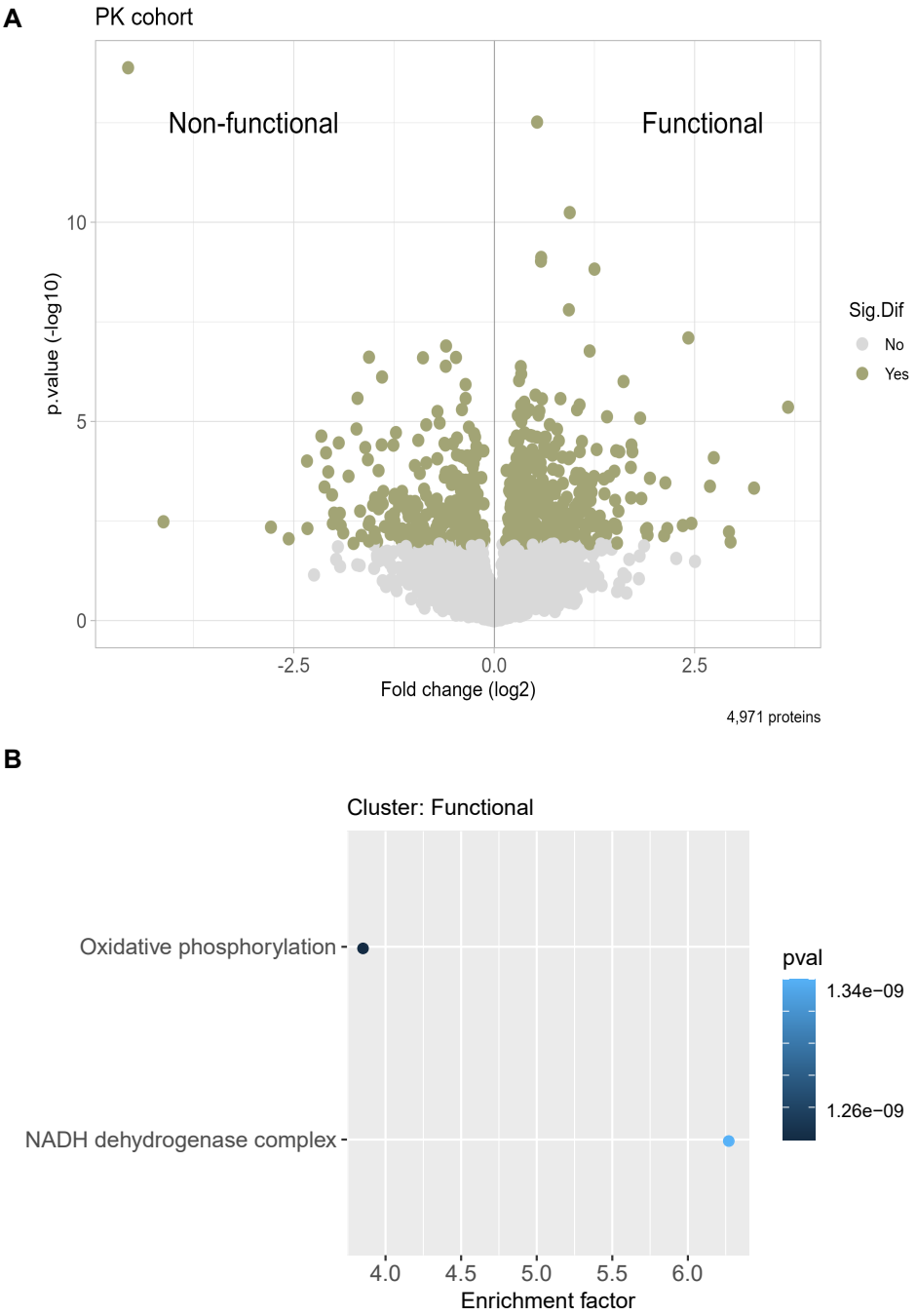

Figure 3.26: A) Protein abundance differences in PK cohort represented as two-sample *t*-test (log2) difference (fold change) between Functional and Non-functional oscillators with corresponding *p* value (-log*10*). Significantly upregulated proteins (FDR < 0.05, *s0* = 0) are highlighted (olive green dots) in each group. B) Enriched annotation categories (Fisher's exact test; FDR < 0.02) in upregulated proteins (olive green dots in A) of the Functional oscillators.

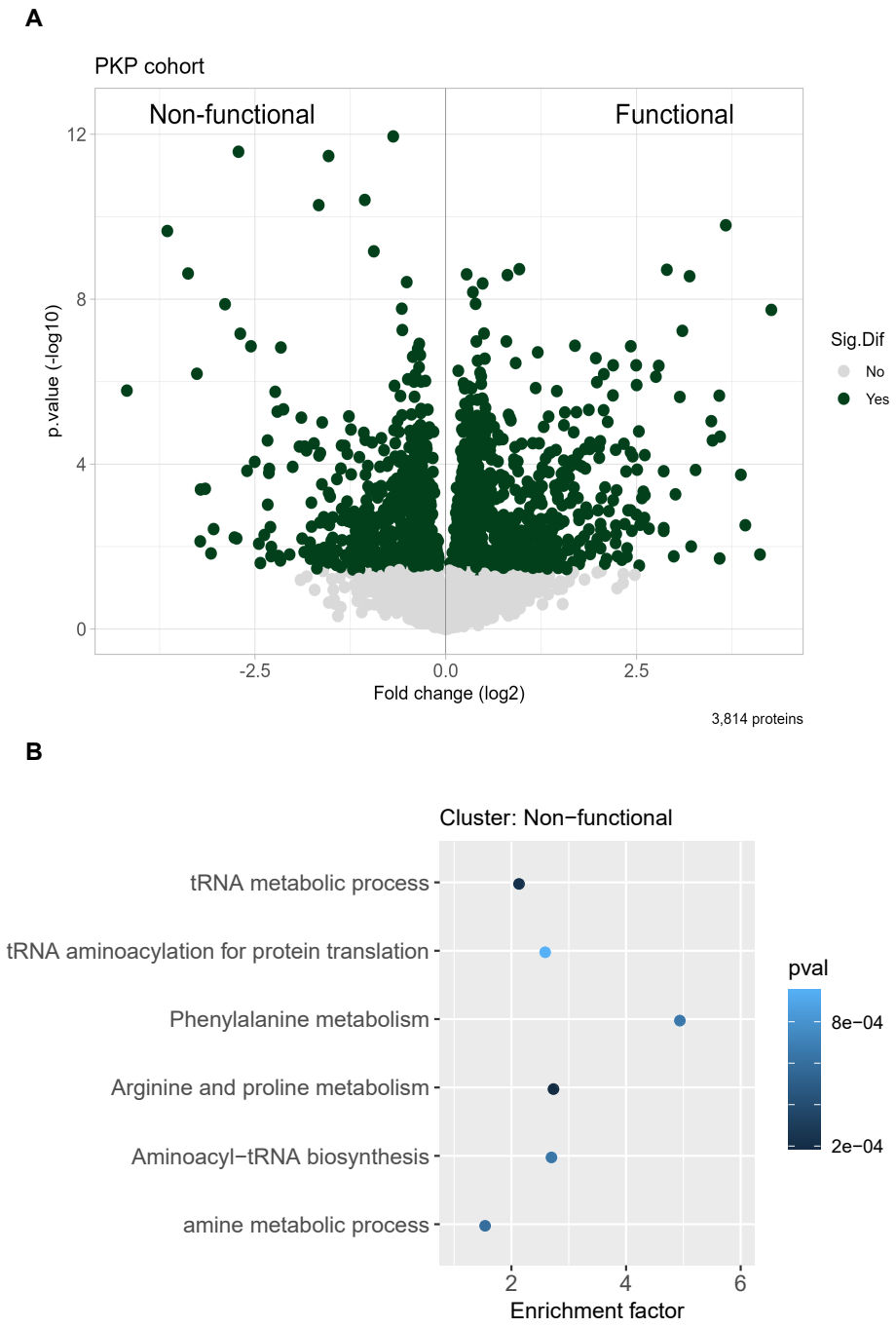

Figure 3.27: A) Protein abundance differences in PKP cohort represented as two-sample *t*-test (log2) difference (fold change) between Functional and Non-functional oscillators with corresponding *p* value (-log*10*). Significantly upregulated proteins (FDR < 0.05, *s0* = 0) are highlighted (dark green dots in A) in each group. B) Enriched annotation categories (Fisher's exact test; FDR < 0.02) in upregulated proteins (dark green dots) of the Non-functional oscillators.

PDAC.

Taken together, these data show that deregulated protein pathways in Bmal1-deficient KRAS-mutant PDAC cells could underlie clock-regulated processes that could be translated in potential time-dependent, therapeutically targeted, vulnerabilities.

3.3 The role of tumor-intrinsic circadian clock in PDAC development and progression

Given the heterogeneity on both the genomic and proteome level of the PDAC cell lines characterized for circadian clock functionality (see sections 3.1 and 3.2), and considering the clinical relevance of the *Kras* mutation in human PDAC (see sections 1.6.2 and 1.6.3), four different *Bmal1::Luc* KRAS-driven PDAC cell lines were selected for genetic disruption of the molecular clock mechanism with the aim to ultimately study the role of the tumor-endogenous circadian clock *in vivo*.

3.3.1 Genetic disruption of the tumor-intrinsic clock

The selection of the four KRAS-driven PDAC cell lines was based on the robustness of the circadian rhythm as exhibited in the normalized amplitude of the Lomb-Scargle periodogram (Fig. 3.9). The selected four KRAS-mutant PDAC (PK) cell lines were the S914 and 16992 from the mesenchymal subtype and the 4706 and 53704 from the epithelial subtype.

The genetic ablation of the molecular mechanism of the circadian clock in all four *Bmal1::Luc* PK cell lines was performed using the CRISPR-Cas9 editing system as described in section 2.1.3 and shown in Figure 2.1. Each parental *Bmal1::Luc* PK cell line was transduced with two different Bmal1-targeted sgRNAs (sgArntl26 and sgArntl284) and a non-targeted sgRNA (sglacZ), therefore 12 new *Bmal1::Luc* PK cell lines were generated in total. To verify the CRISPR edits after antibiotic selection, the *Bmal1* locus was

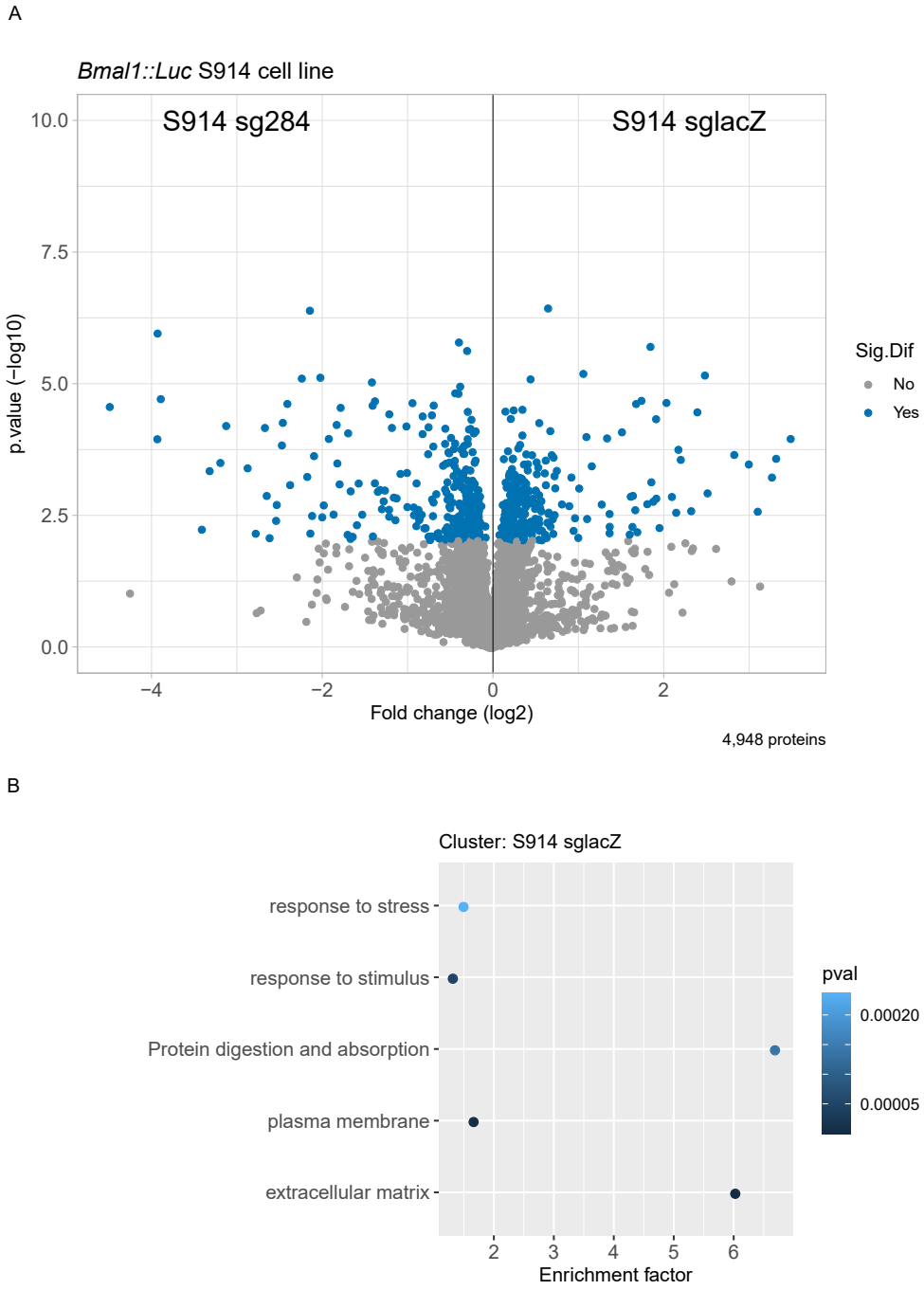

Figure 3.28: A) Protein abundance differences in *Bmal1::Luc* KRAS-driven mesenchymal cell line S914 represented as two-sample *t*-test (log2) difference (fold change) between Bmal1-proficient (sglacZ) and Bmal1-deficient (sg284) with corresponding *p* value (-log*10*). Significantly upregulated proteins (FDR < 0.05, *s0* = 0) are highlighted (blue dots) in each group. B) Enriched annotation categories (Fisher's exact test; FDR < 0.02) in upregulated proteins (blue dots in A) of the Bmal1-proficient (sglacZ) cells.

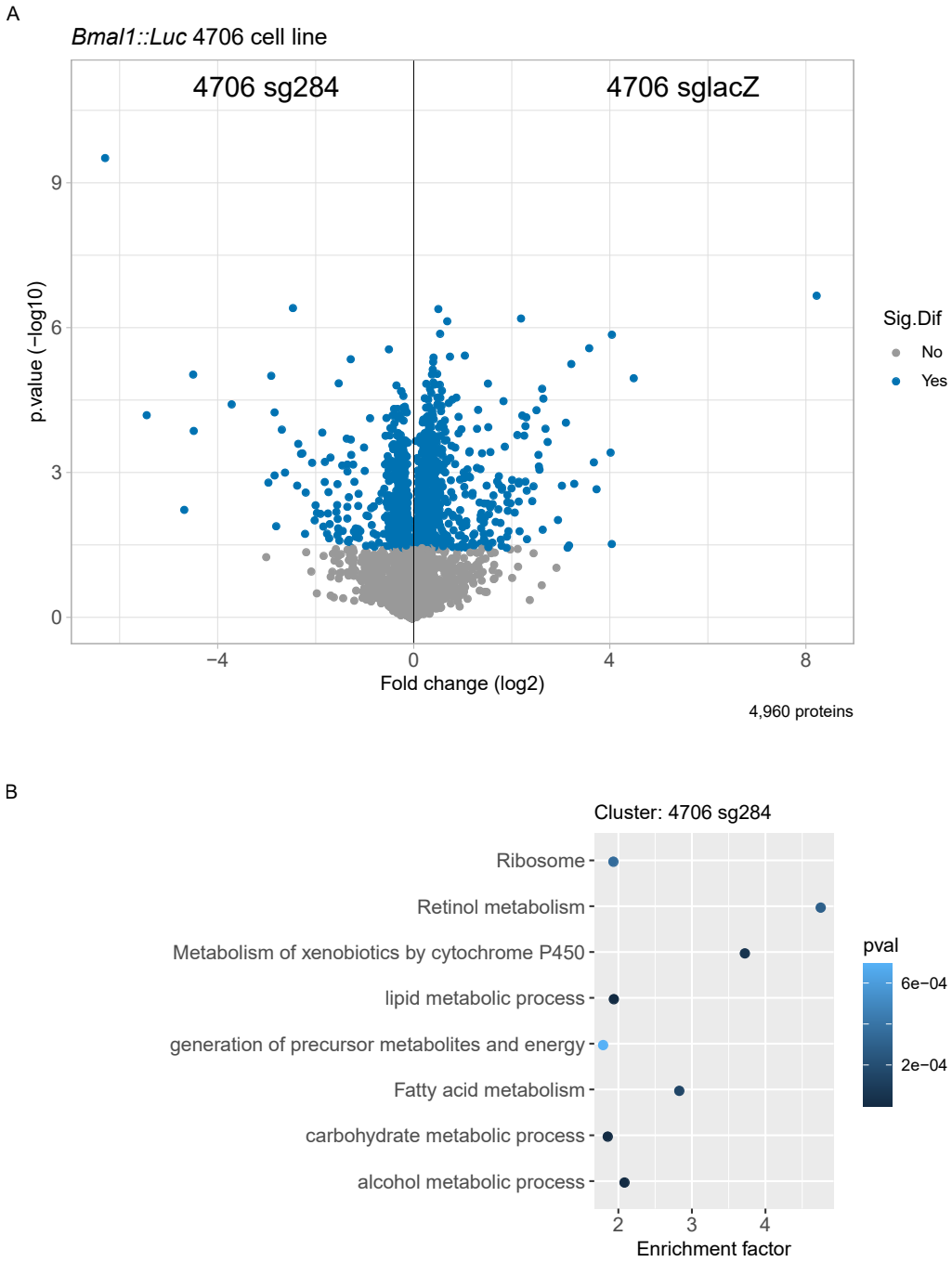

Figure 3.29: A) Protein abundance differences in *Bmal1::Luc* KRAS-driven epithelial cell line 4706 represented as two-sample *t*-test (log2) difference (fold change) between Bmal1-proficient (sglacZ) and Bmal1-deficient (sg284) with corresponding *p* value (-log*10*). Significantly upregulated proteins (FDR < 0.05, *s0* = 0) are highlighted (blue dots) in each group. B) Enriched annotation categories (Fisher's exact test; FDR < 0.02) in upregulated proteins (blue dots in A) of the Bmal1-deficient (sg284) cells.

sequenced via Sanger sequencing, and the assessment of editing efficiency was facilitated by the software tool ICE (for details, see 2.1.3 and Appendix C). The percentage of insertions and deletions (indels) in the Bmal1-targeted cell lines compared to the non-targeted cells is given in Figure 3.34 A. For all four *Bmal1::Luc* PK cell lines, the editing efficiency was overall high for both sgRNAs ranging from 68 % up to 95 %. The Bmal1-targeting guide RNA sgArntl26 resulted in higher percentage of indels compared to the sgArntl284 with the highest difference being in the 16992 cell line.

Subsequently, the validation for the *Bmal1* editing was performed by evaluating the circadian rhythm based on bioluminescence recordings, and by semi-quantification of the BMAL1 protein levels after Western blotting (section 2.1.5).

All *Bmal1::Luc* Bmal1-targeted and Bmal1 non-targeted *Bmal1::Luc* PK cell lines were assessed for circadian clock functionality following the initial experimental set-up of the functional screening (Fig. 2.2). The ACF results depicted in Figures 3.30, 3.31, 3.32 and 3.33 show that circadian rhythmicity was abolished only in two Bmal1-edited *Bmal1::Luc* PK cell lines, the 4706 sgAnrtl284 (sg284) and S914 sgAnrtl284 (sg284) (Figs 3.30 C and 3.32 C, respectively). Those two cell line pairs (4706 sglacZ and sg284, S914 sglacZ and sg284) were used for the rest of the experimental work.

Western blotting and semi-quantification of those two *Bmal1::Luc* PK cell line pairs showed that after CRISPR/Cas9-mediated *Bmal1* editing, BMAL1 protein was detected primarily in a truncated form (Fig. 3.34 B; lower band) resulting in statistically significant decreased full-length BMAL1 levels (3.34 C). Given the disruption of circadian rhythms in the Bmal1-edited cells (sg284) in both *Bmal1::Luc* PK cell lines, I reasoned to speculate that BMAL1 function was abolished.

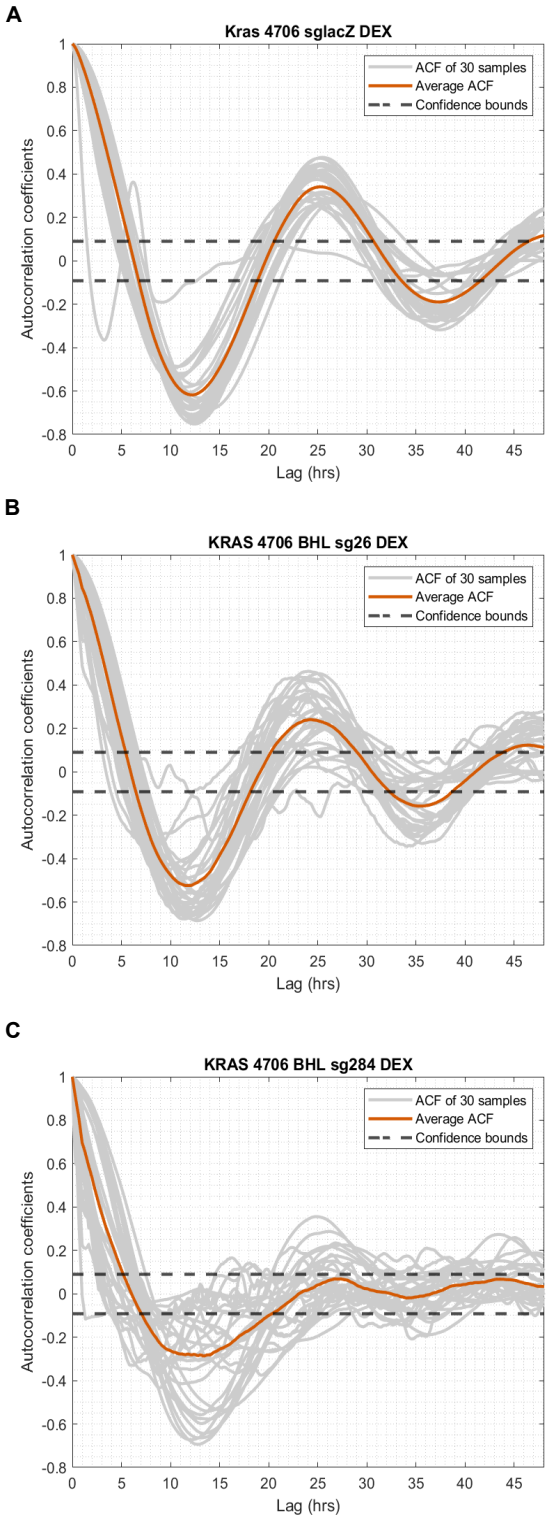

Figure 3.30: Functional assessment of Bmal1-editing in *Bmal1::Luc* (BHL) KRAS-driven epithelial 4706 cell lines via the autocorrelation function. In the inlet of each plot the number of replicates is given. DEX: dexamethasone.

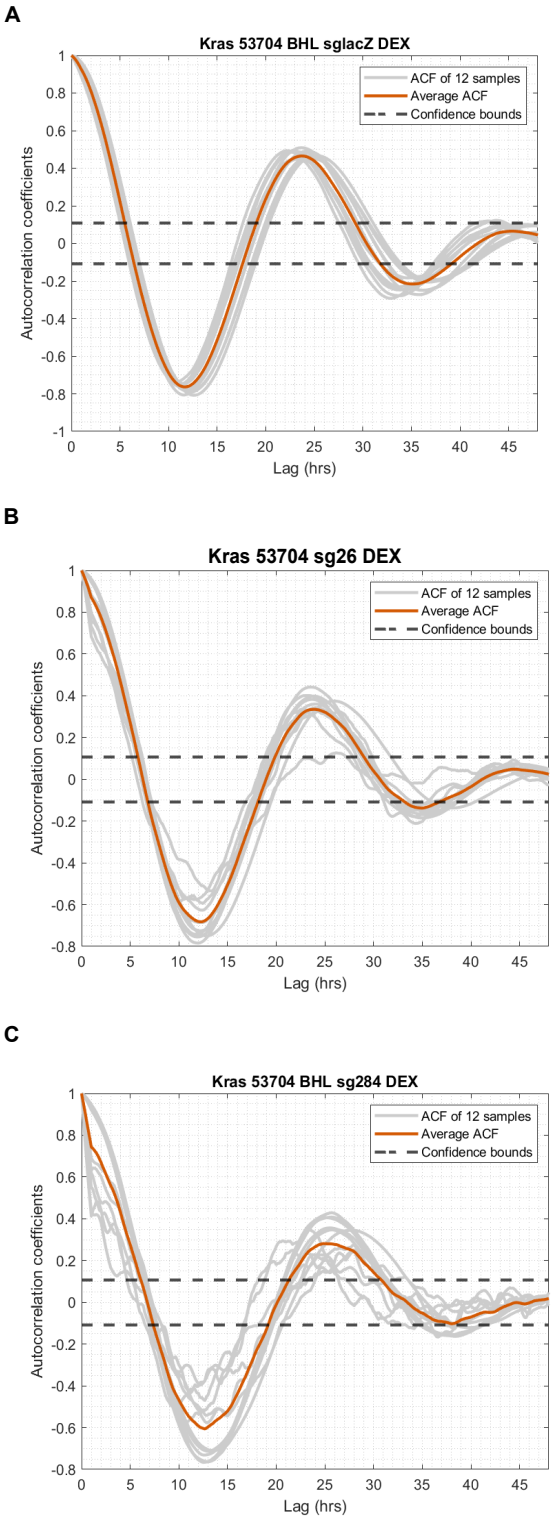

Figure 3.31: Functional assessment of Bmal1-editing in *Bmal1::Luc* (BHL) KRAS-driven epithelial 53704 cell lines via the autocorrelation function. In the inlet of each plot the number of replicates is given. DEX: dexamethasone.

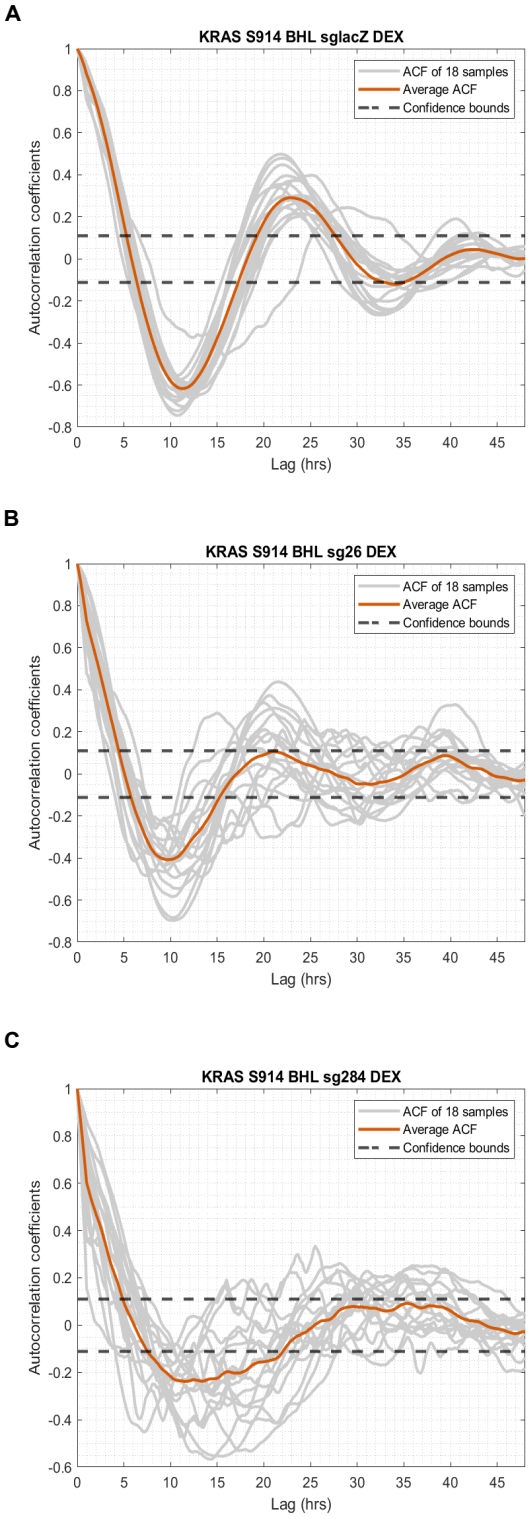

Figure 3.32: Functional assessment of Bmal1-editing in *Bmal1::Luc* (BHL) KRAS-driven mesenchymal S914 cell line via the autocorrelation function. In the inlet of each plot the number of replicates is given. DEX: dexamethasone.

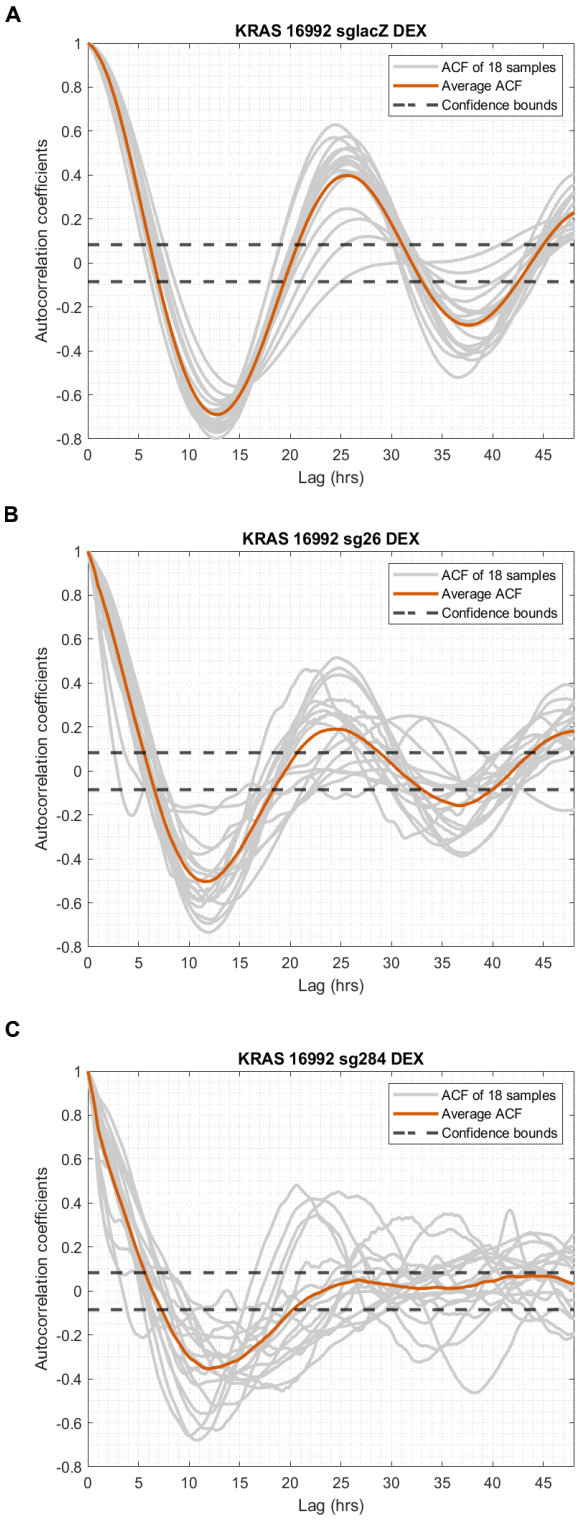

Figure 3.33: Functional assessment of Bmal1-editing in *Bmal1::Luc* (BHL) KRAS-driven mesenchymal 16992 cell line via the autocorrelation function. In the inlet of each plot the number of replicates is given. DEX: dexamethasone.

3.3.2 Genetic disruption of the tumor-intrinsic clock impacts cell proliferation

After validating the significant downregulation of BMAL1 protein levels (Fig. 3.34 B-C) and abolishment of circadian rhythm in the Bmal1-edited *Bmal1::Luc* PK cell lines (Figs. 3.32 and 3.30), the impact of the cell-intrinsic circadian clock on cell survival and proliferation was investigated by performing the MTT assay (see section 2.1.4.1) and the colony formation assay (see section 2.1.4.2), respectively.

First, using the MTT assay, it was tested whether *Bmal1* editing had an effect on cell viability. For this, the cellular metabolic activity was estimated by indirect measurement of the NADH dehydrogenase-mediated reduction of the MTT reagent over the course of five consecutive days. The absorbance values (normalized to the first day of measurement) for the *Bmal1::Luc* S914 and 4706 cell line pairs are depicted in Figures 3.34 D and 3.34 E, respectively. In the Bmal1-edited cells (sg284) of the S914 cell line, the absorbance values show no significant difference compared to the control (sglacZ) cells (Fig. 3.34 D). However, the Bmal1-deficient cells (sg284) of the 4706 cell line showed significantly higher absorbance values compared to the Bmal1 non-edited cells (sglacZ) the last day of measurement (Fig. 3.34 E). These results demonstrate that BMAL1 deficiency affected the metabolic activity of the KRAS-driven PDAC epithelial cells, as an indirect output of cell viability.

In the colony formation assay, the proliferative capacity of both Bmal1-targeting and Bmal1 non-targeting cells was assessed. At the end of the experiment, the number of colonies formed were directly linked to the absorbance values after dissolving the crystal violet stain (see 2.1.4.2). In Figure 3.34 F, it is shown that the absorbance in 4706 Bmal1-edited cells is 1.5 times higher than in the corresponding control cells (sglacZ). In the S914 cell line pair, *Bmal1*-editing significantly increased cell proliferation in the Bmal1-targeted cells, albeit at a lower degree as depicted by the absorbance values (Fig. 3.34

F).

These results indicate that in both *Bmal1::Luc* PDAC cell line pairs the ablation of the cell-intrinsic circadian clock leads to higher cell proliferation, and the respective impact on cell survival was found to be PK molecular subtype-specific.

3.3.3 The tumor-endogenous circadian rhythm is maintained *in vivo*

An important consideration about the fact that the Bmal1-edited cell lines did not constitute full *Bmal1* gene knockout was whether the circadian rhythm ablation as shown *in vitro* (Figs. 3.30 C, 3.32 C) could be recapitulated in the tumor *in vivo*. For this, an orthotopic implantation experiment was performed, where two groups of wild-type C57BL/6J;129S6/SvEv (F1 hybrid; F1) mice were injected in the pancreas with the *Bmal1::Luc* PK cell line 4706 with either Bmal1-proficiency (sglacZ) or Bmal1-deficiency (sg284).

At the terminal state, the mice were sacrificed and tissue sectioning was performed using fresh tumor samples from three animals of each group (see section 2.4.2). From each tumor three organotypic slices were used for *ex vivo* bioluminescence recording for eight consecutive days. Each slice was obtained consecutively from each tumor sample leaving 300 μM apart from the next one. Approximately 36 hours after the commencement of the biolumescence measurement, the tumor slices were treated with dexamethasone (DEX) to induce circadian rhythm phase synchronization and the recording continued after removing DEX from the assay medium.

As demonstrated in Figures 3.35 and 3.36, the DEX treatment -indicated with an arrow- resulted in significant increase in the amplitude of the circadian rhythm in the Bmal1-proficient tumor slices (Fig. 3.35 A-C) compared to the Bmal1-deficient tumors (Fig. 3.36 A-C). Importantly, in the Bmal1-deficient tumor slices the amplitude of the circadian rhythm was only slightly increased after DEX treatment (Fig. 3.36 A-C), which

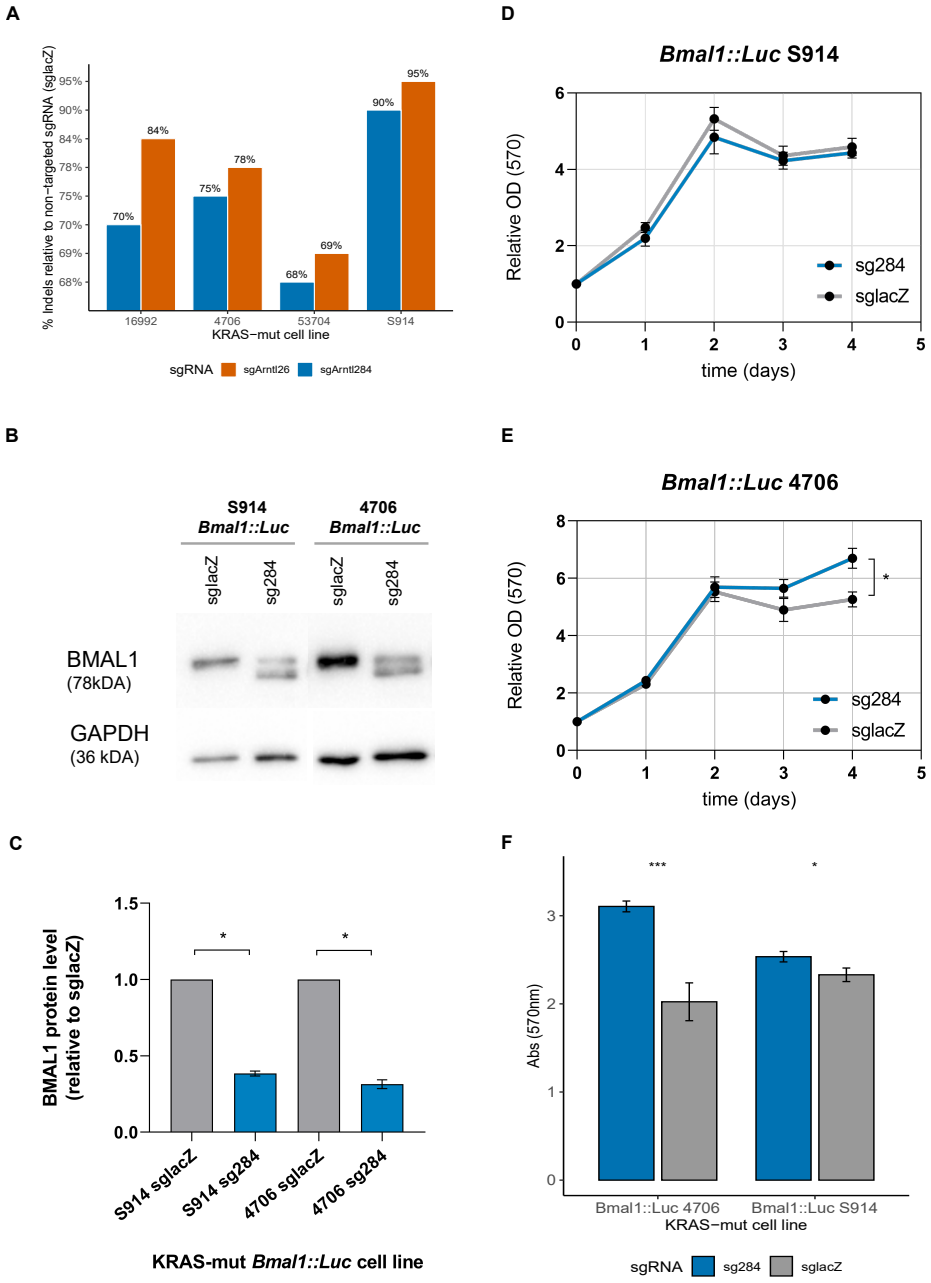

Figure 3.34: Genetic disruption of the tumor-intrinsic clock in *Kras*-mutant PDAC cell lines impacts cell proliferation. A) Indels (%) in *Bmal1* gene locus after gene editing using the CRISPR-Cas9 system. Western blotting (B) and semi-quantification (C) of BMAL1 levels in Bmal1-edited (blue) and Bmal1 non-edited (grey) cells of the *Bmal1::Luc* KRAS-driven PDAC cell lines normalized to house-keeping GAPDH protein levels. D)-E) Quantitative results of the MTT viability assay in both *Bmal1::Luc* KRAS-mutant PDAC cell line pairs. F) Quantitative result of the colony formation assay in both *Bmal1::Luc* KRAS-mutant PDAC cell line pairs. For C-F: Results are from at least three independent experiments (two-sample t-test; significance was at $p < 0.05$). $^{*}p < 0.05$, $^{***}p < 0.001$.

dampened substantially three cycles after DEX stimulation. In the Bmal1-deficient tumors, the bioluminescent signal recorded only from a single tumor slice showed relatively high amplitude after DEX (Fig. 3.36 A; slice B), indicating that the elicited rhythmicity was due to partially deleted cell-intrinsic circadian clock in the PDAC cells. In the control tumor samples, the amplitude of the circadian rhythm was also dampened, albeit in a lower degree four cycles after DEX treatment. Importantly, in the Bmal1-proficient tumor slices, a low-amplitude circadian rhythm was recorded before DEX stimulation (Fig. 3.35 A-C), indicating a residual circadian rhythmicity directly after fresh tumor processing.

Moreover, bioluminescence data analysis was performed using the LumiCycle software to determine rhythmicity (section 2.4.2), and to extract the cycling parameters, such as period, phase and amplitude (and normalized amplitude). Those parameters were compared between Bmal1-proficient (n = 8) and Bmal1-deficient (n = 6) tumor slices (Fig. 3.37 and Table 3.2). It was found that between the two groups the period in Bmal1-edited tumors was significantly shorter (22.62 ± 0.36 hours) compared to the control tumors (24.04 ± 0.36 hours; Fig. 3.37 a). The phase was not affected by the deficiency of BMAL1, albeit it showed larger variability within the Bmal1-deficient group (Fig. 3.37 b). The amplitude and normalized amplitude were both statistically significant higher in the Bmal1-proficient tumor slices (9.96 ± 1.46 and 0.11 ± 0.01, respectively) than in the Bmal1-deficient tumors (3.80 ± 0.75 and 0.04, respectively) as shown in Figure 3.37 c-d, respectively.

Taken together, the *ex vivo* bioluminescence time series assessed the circadian rhythm of tumor cells harboring a functional or non-functional circadian clock in PDAC tissue. The analysis revealed that the Bmal1-proficient tumor cells do maintain cell-intrinsic circadian rhythm *in vivo*, which was a crucial aspect of the overall experimental approach of the mouse studies. The low-amplitude circadian rhythm detected in the Bmal1-deficient tumor slices can be attributed to a small percentage of Bmal1 non-edited

cells (see also section 3.3.1 and Fig. 3.34 A-C). All phenotypic characteristics of each tumor mouse is given in Table A.2.

3.3.4 Genetic disruption of the tumor-endogenous circadian clock does not impact tumor growth nor survival

After elucidating that the tumor-intrinsic circadian rhythm is maintained *in vivo* (section 3.3.3), I further focused on investigating the role of the tumor-endogenous circadian clock on PDAC development and progression. For this, two different mouse experiments were designed as collectively depicted in Figure 2.5, both of which were based on PDAC implantation models. Furthermore, in both sets of experiments, two groups of wild-type C57BL/6J;129S6/SvEv (F1 hybrid; F1) female mice were orthotopically injected in the pancreas with a *Bmal1::Luc* KRAS-mutant PDAC (PK) cell line retaining either a functional (Bmal1 non-edited cells; sglacZ) or a disrupted (Bmal1-edited cells; sg284) circadian clock.

In the first, time point experiment, the *Bmal1::Luc* PK 4706 cell line pair was injected in both wild-type immunocompetent (F1) and immunodeficient (Rag2^{-}/$^{-}$) mice. For the former mouse cohort, the tumor growth was assessed after four weeks and for the latter cohort three weeks after the implantation. The time point was indicated by when an animal became moribund independent of the experimental group. The tumor samples from the F1 mice were additionally used for immunophenotyping by flow-assisted cell

Table 3.2: Cycling parameters after *ex vivo* bioluminescence recordings from Bmal1-proficient (4706 sglacZ) and Bmal1-deficient (4706 sg284) *Bmal1::Luc* PDAC tumors.

Bmal1::Luc tumors	Period (h)		Phase		Amplitude		Norm. amplitude	
	Mean	SEM	Mean	SEM	Mean	SEM	Mean	SEM
4706 sglacZ	24.04	0.36	6.43	0.58	9.96	1.46	0.11	0.01
4706 sg284	22.62	0.36	5.72	0.69	3.80	0.75	0.04	0.00

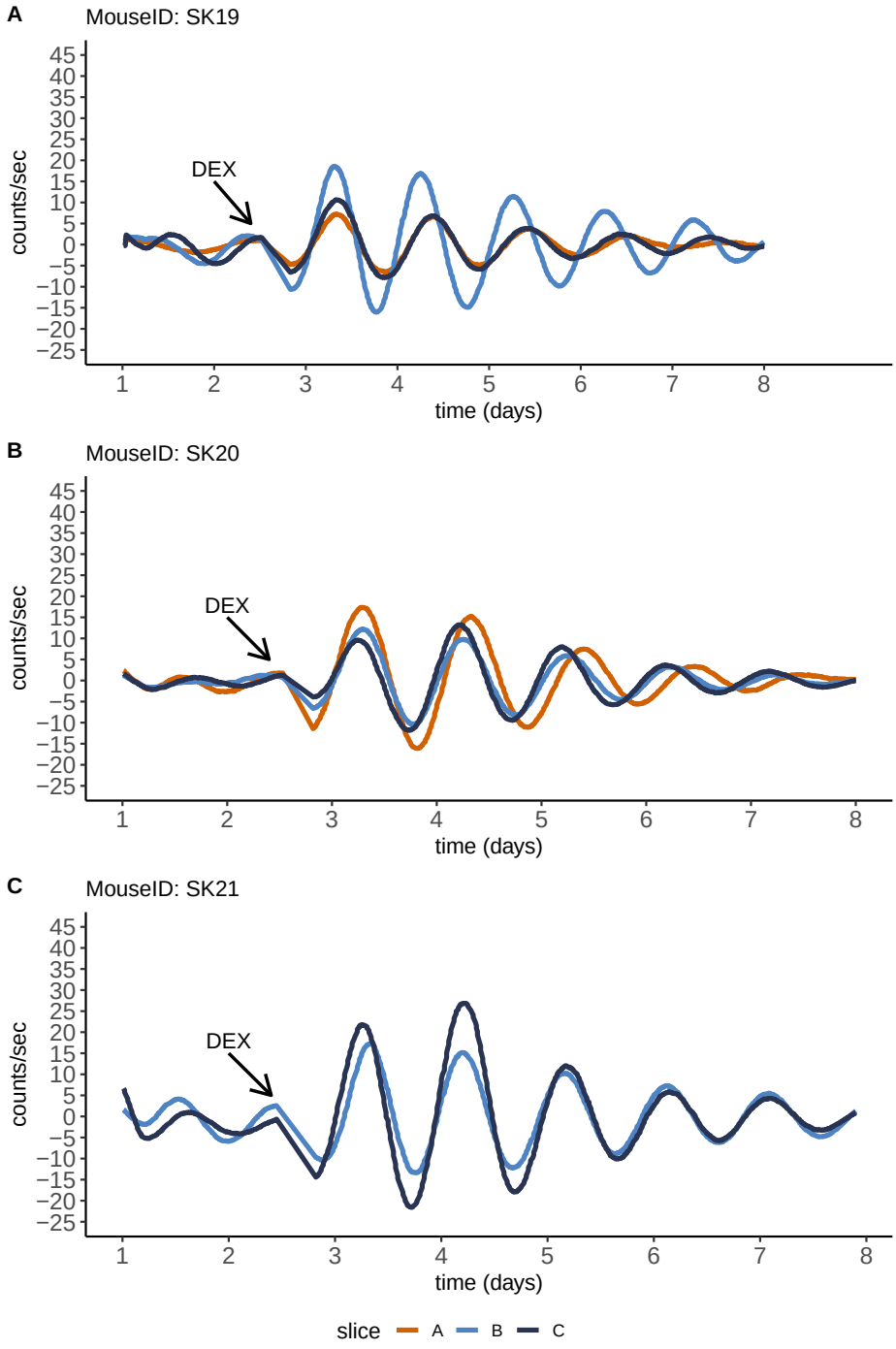

Figure 3.35: *Ex vivo* bioluminescence recordings from Bmal1-proficient (control) tumor slices. Each plot (A-C) corresponds to a tumor sample. The recorded bioluminescent signal expressed as (light) counts per second over the course of the measurement before and after DEX treatment (arrow). Three different slices were obtained from each tumor sample. Slices A (orange) were obtained closer to the surface, slices B (light blue) and C (dark blue) were closer to the middle and the bottom of the tumor tissue, respectively. DEX: dexamethasone.

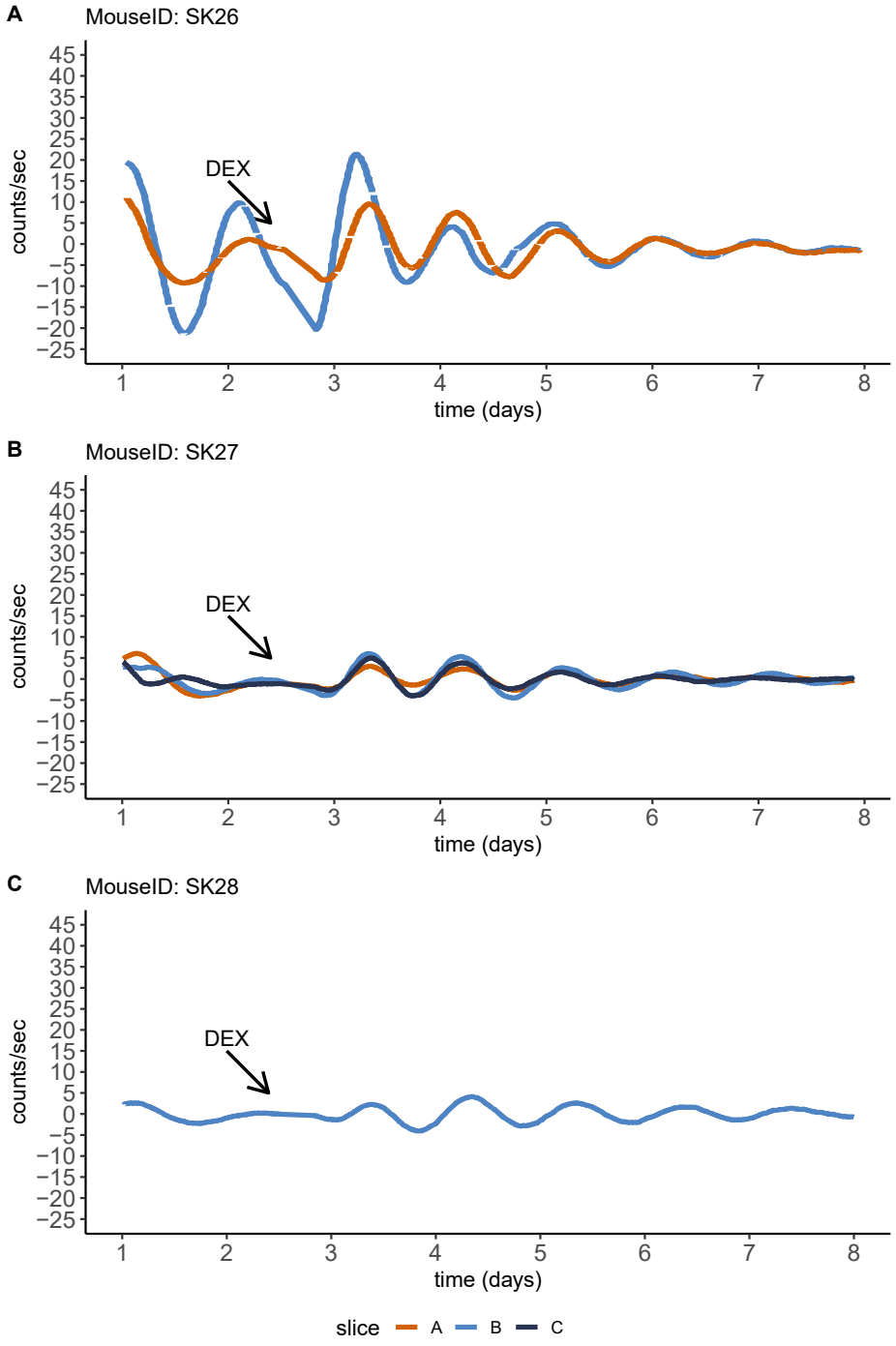

Figure 3.36: *Ex vivo* Bioluminescence recordings from Bmal1-deficient tumor slices. Each plot (A-C) corresponds to a tumor sample The recorded bioluminescent signal expressed as (light) counts per second over the course of the measurement before and after DEX treatment (arrow). Three different slices were obtained from each tumor sample. Slices A (orange) were obtained closer to the surface, slices B (light blue) and C (dark blue) were closer to the middle and the bottom of the tumor tissue, respectively. DEX: dexamethasone.

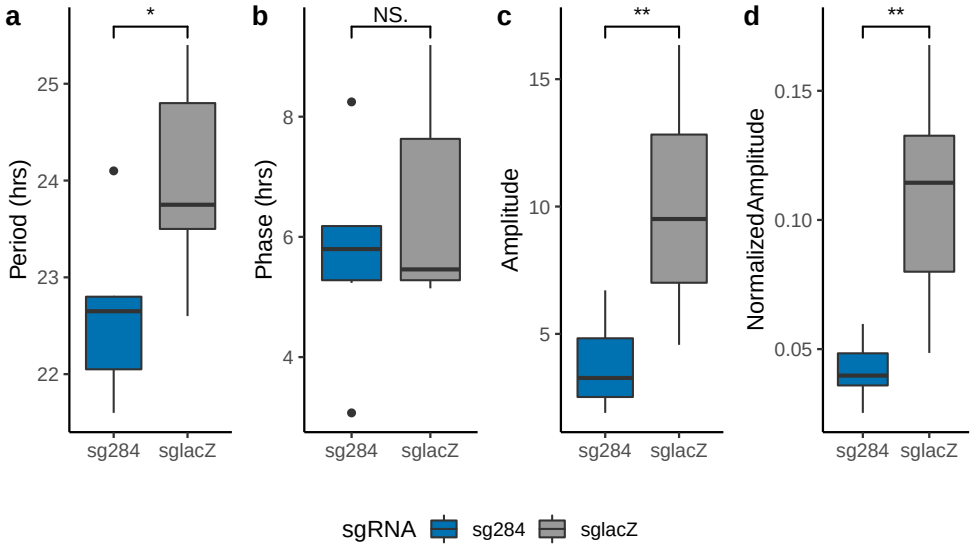

Figure 3.37: Cycle parameters from *ex vivo* bioluminescence recordings of organotypic slices from Bmal1-proficient (sglacZ; grey) and Bmal1-deficient (sg284; blue) tumors. Two-sample *t*-test; significance at $p < 0.05$. *$p < 0.05$; **$p < 0.01$; NS: non-significant.

sorting (FACS), which is described in section 3.3.5.

The results showed that at a given point in time after the transplatation, the growth of the Bmal1-deficient (sg284) tumors was overall comparable to the tumor growth of the Bmal1-proficient (sglacZ) group with no statistically significant differences as shown in Figure 3.38 and in Table 3.3 for both immunocompetent and immunodeficient animals. The tumor size as indicated by the tumor weight in the immunocompetent mice was heterogeneous within each group (Fig. 3.38) ranging from 0.10 g to 0.68 g suggesting that tumor development *in vivo* is affected by host-intrinsic factors likely associated with the tumor microenvironment (see section 3.3.5 and 4.3). Individual values for tumor and mouse weight at the end of the study is given in Table A.2.

Overall, this study demonstrated that the presence of a functional tumor-intrinsic circadian clock does not impact PDAC development *in vivo* after a defined time period post-implantation.

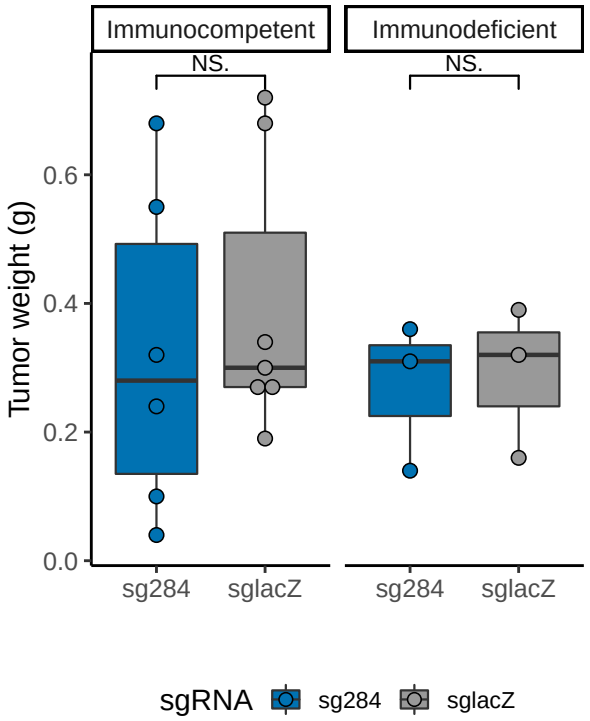

Figure 3.38: Tumor weight as porxy for tumor size at the end of the time point *in vivo* experiment was assessed in Bmal1-deficient (sg284; blue) and Bmal1-proficient (sglacZ; grey) tumors in both immunocompetent and immunodeficient mice. Two-sample t-test; significance at $p < 0.05$. NS: non-significant.

Regarding tumor progression in immunocompetent mice, metastatic lesions in the liver of both groups were observed. As summarised in Table 3.4, three out of seven (42.8 %) mice with Bmal1-proficient tumors developed hepatic metastatic lesions, while in three out of six (50 %) mice with Bmal1-deficient tumors liver metastases were developed. This suggests that in a defined period of time, the presence of a functional cell-intrinsic clock in the tumor does not impact tumor progression in PDAC.

Considering that tumor development in orthotopic models of PDAC is rapid and consistent, but also subject to host-tumor microenvironment interactions, an additional *in vivo* experiment was designed to elucidate whether the tumor-intrinsic circadian

Table 3.3: Tumor size of the mice at the time point experiment.

Immnune system	*Bmal1::Luc* Cell line	Tumor weight (g)	
		Mean	SEM
Competent	4706 sglacZ	0.40	0.08
Competent	4706 sg284	0.32	0.10
Deficient	4706 sglacZ	0.29	0.07
Deficient	4706 sg284	0.27	0.07

clock affects PDAC development. In the endpoint experiment, C57BL/6J;129S6/SvEv (F1 hybrid; F1) female mice were orthotopically injected with Bmal1-deficient or Bmal1-proficient tumor cells of *Bmal1::Luc* KRAS-mutant PDAC (PK) S914 and 4706 cell lines. All animals were sacrificed immediately after they became moribund. Importantly, two mice from the S914 sglacZ and one from the S914 sg284 group did not develop tumors or metastases at the end of the study -likely due to lack of engraftment of the tumor cells in the pancreas after the transplatation- and, therefore, they were excluded from the analysis.

The tumor weight from each mouse at the terminal state was used as a proxy for tumor size. As seen in Table 3.5, the 4706 Bmal1-deficient (sg284) tumors reached on average 0.82 ± 0.28 g compared to 0.68 ± 0.10 g of the corresponding control (sglacZ) group. The S914 Bmal1-edited (sg284) tumors weighed 1.05 ± 0.14 g, while the control (sglacZ) group reached on average 1.44 ± 0.45 g. The difference on tumor growth between the two mice groups in each *Bmal1::Luc* PK cell line pair was not found statistically significant as depicted in Figure 3.39 A.

Furthermore, Figure 3.39 B and Table 3.5 show that mice injected with Bmal1-proficient PDAC cells survived overall a shorter time compared to the group with Bmal1-deficient tumors, in both of the two cell line pairs. The mice implanted with 4706 sg284 cells survived 66.16 ± 5.87 days, while the mice injected with the corresponding control

Table 3.4: Phenotypic characteristics of PDAC progression in the time point experiment (Immunocompetent mice).

MouseID	*Bmal1::Luc* PDAC cell line	Metastasis	
		Liver	Macroscopic metastases
SK15	4706 sglacZ	no	na*
SK16	4706 sglacZ	yes	4
SK17	4706 sglacZ	yes	7
SK18	4706 sglacZ	no	na
SK19	4706 sglacZ	no	na
SK20	4706 sglacZ	yes	3
SK21	4706 sglacZ	no	na
SK22	4706 sg284	no	na
SK23	4706 sg284	no	na
SK25	4706 sg284	yes	2
SK26	4706 sg284	yes	5
SK27	4706 sg284	yes	1
SK28	4706 sg284	no	na

* not applied

cells (sglacZ) survived, albeit not statistically significant, shorter with 57.86 ± 2.61 days. For the S914 cell line pair, mice with Bmal1-deficient tumors survived 63.83 ± 7.07 days compared to the Bmal1-proficient group that survived 55.60 ± 3.79 days (Table 3.5). Individual values from each tumor mouse for both tumor weight and survival for the endpoint experiment is given in Table A.3.

A further aim of the endpoint study was to investigate whether there is a link between tumor progression and the presence of a functional tumor-intrinsic circadian clock. At the terminal state, primarily the liver and the lungs were inspected macroscopically for any tumor metastases present. The number of metastatic lesions was counted and is given in the Tables 3.6 and 3.7 for the *Bmal1::Luc* PK S914 and 4706 cell line pair, respectively. In the mesenchymal PDAC mice, the lesions were directly visible and distinguishable for the majority of the animals. However, in most of the mice injected with epithelial PK cells, the metastatic lesions in the liver were not distinct and rather covering a wide

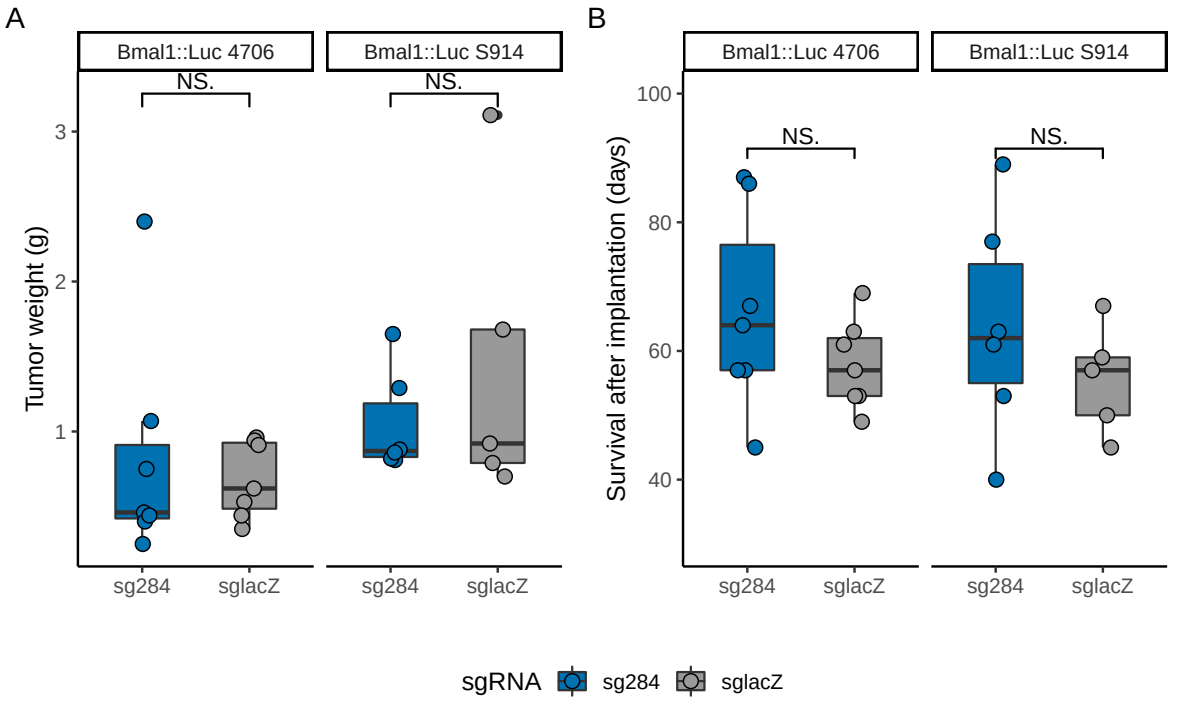

Figure 3.39: A) Tumor weight (g) and B) survival (days) of the F1 tumor mice at the endpoint experiment implanted with either Bmal1-proficient (sglacZ; grey) or Bmal1-deficient (sg284; blue) *Bmal1::Luc* KRAS-mutant PDAC cells. Tumor weight is given as a proxy for tumor size. Two-sample *t*-test; significance was at $p < 0.05$. NS : non-significant.

surface of the liver lobes, thereby an estimate of the corresponding number of metastases is given in Table 3.7).

As mentioned, in total three animals implanted with *Bmal1::Luc* PK S914 cells were excluded. In the remaining five animals of the control (sglacZ) group, four developed liver metastases with two animals having an extensively metastasized liver, while two developed additional metastases in the lungs (Table 3.6). In half of the animals injected with Bmal1-edited cells (sg284) liver metastases were observed and in one animal lung metastatic lesions were further developed (Table 3.6). Taken together, there were fewer metastases observed in the Bmal1-edited animals at the endpoint of this mesenchymal PK cohort, however a larger cohort size is likely necessary to increase statistical power

between the two groups.

In the *Bmal1::Luc* PK 4706 implanted mice, six out of seven mice from the control group (sglacZ) developed liver metastases and one mouse depicted two metastatic lesions in the lungs (Table 3.7). The liver metastases were seven and nine in two animals, while in the rest four animals the lesions were so extensive that they could not be separable, therefore the number is reported within a range of either 20 to 30 or ten to 20. In the group implanted with Bmal1-deficient cells (sg284), all seven animals showed established metastatic lesions in the liver, and four animals additionally in the lungs (Table 3.7). Regarding the number of the metastases in the liver, the same pattern of widespread non-distinguishable lesions was observed in the Bmal1-edited (sg284) group. In the lungs, the developed metastases were fewer compared to the liver, whilst for two animals they are reported within a range five to ten and ten to 20.

Overall, Bmal1-proficiency in the *Bmal1::Luc* PK cells from both KRAS-mutant molecular subtypes showed no direct correlation with tumor progression as resembled in the number of metastatic lesions developed in peripheral organs, such as the liver and the lungs.

Table 3.5: Survival and tumor size of the mice at the endpoint experiment.

Bmal1::Luc PK Cell line	Survival days		Tumor weight (g)	
	Mean	SEM	Mean	SEM
4706 sglacZ	57.86	2.61	0.68	0.10
4706 sg284	66.14	5.87	0.82	0.28
S914 sglacZ	55.60	3.79	1.44	0.45
S914 sg284	63.83	7.07	1.05	0.14

Table 3.6: Phenotypic characteristics of mesenchymal KRAS-mutant PDAC progression in the endpoint experiment.

MouseID	*Bmal1::Luc* PDAC cell line	Metastasis		Macroscopic metastases	
		Liver	Lung	Liver	Lung
SK35	S914 sglacZ	yes	no	5	na*
SK37	S914 sglacZ	no	no	na	na
SK38	S914 sglacZ	yes	yes	20-30	10-20
SK40	S914 sglacZ	yes	no	20-30	na
SK41	S914 sglacZ	yes	yes	2	2
SK43	S914 sg284	no	no	na	na
SK44	S914 sg284	no	no	na	na
SK45	S914 sg284	yes	no	20-30	na
SK46	S914 sg284	yes	yes	10	2
SK47	S914 sg284	no	no	na	na
SK48	S914 sg284	yes	no	4	na

* not applied

Table 3.7: Phenotypic characteristics of epithelial KRAS-mutant PDAC progression in the endpoint experiment.

MouseID	*Bmal1::Luc* PDAC cell line	Metastasis		Macroscopic metastases	
		Liver	Lung	Liver	Lung
SK49	4706 sglacZ	no	no	na	na*
SK50	4706 sglacZ	yes	no	20-30	na
SK51	4706 sglacZ	yes	no	20-30	na
SK52	4706 sglacZ	yes	no	10-20	na
SK53	4706 sglacZ	yes	no	20-30	na
SK54	4706 sglacZ	yes	no	7	na
SK55	4706 sglacZ	yes	yes	9	2
SK56	4706 sg284	yes	yes	30-40	5-10
SK57	4706 sg284	yes	no	20-30	na
SK58	4706 sg284	no	no	30-40	na
SK59	4706 sg284	yes	yes	30-40	2
SK60	4706 sg284	yes	yes	30-40	5
SK61	4706 sg284	yes	yes	30-40	10-20
SK62	4706 sg284	yes	no	10	na

* not applied

3.3.5 Genetic disruption of the tumor-endogenous circadian clock does not lead to immune-cell remodelling in PDAC

In both *in vivo* experiments with F1 mice, it was further investigated whether genetic disruption of the tumor-intrinsic clock is associated with immune cell remodelling in the tumor microenvironment (TME). The impact of the tumor-endogenous circadian clock on immune cell inflitrates in PDAC of the epithelial and mesenchymal subtype was assessed by FACS-assisted immunophenotyping directly after tumor dissection (see section 2.4.3).

First, in the time point experiment, the innate immune cell populations (neutrophils, macrophages and dendritic cells) showed no statistically significant differences between Bmal1-proficient and Bmal1-deficient tumors (Fig. 3.42). In addition, the observed T cell populations, consisting of T cytotoxic (Tc) and T helper (Th) cells, or B cell infiltration in the TME were not found to have statistically significant differences (Fig. 3.42).

Second, in the endpoint experiment, anti-tumor immunity in both KRAS-mutant PDAC subtypes (PK) was not affected between the two groups of mice (Figs. 3.41, 3.40). Immune infiltration in the TME by T cell subpopulations and B cells in both molecular PK subtypes of Bmal1-proficient (sglacZ) and Bmal1-deficient (sg284) tumors was at very low levels expressed as relative percentage of the total live cells (Figs. 3.41, 3.40). The innate immunity pool (i.e., neutrophils, macrophages and dendritic cells) neither showed statistically significant differences between Bmal1-edited (sg284) and control (sglacZ) tumors in both KRAS-driven PDAC subtypes (Figs. 3.40 and 3.41).

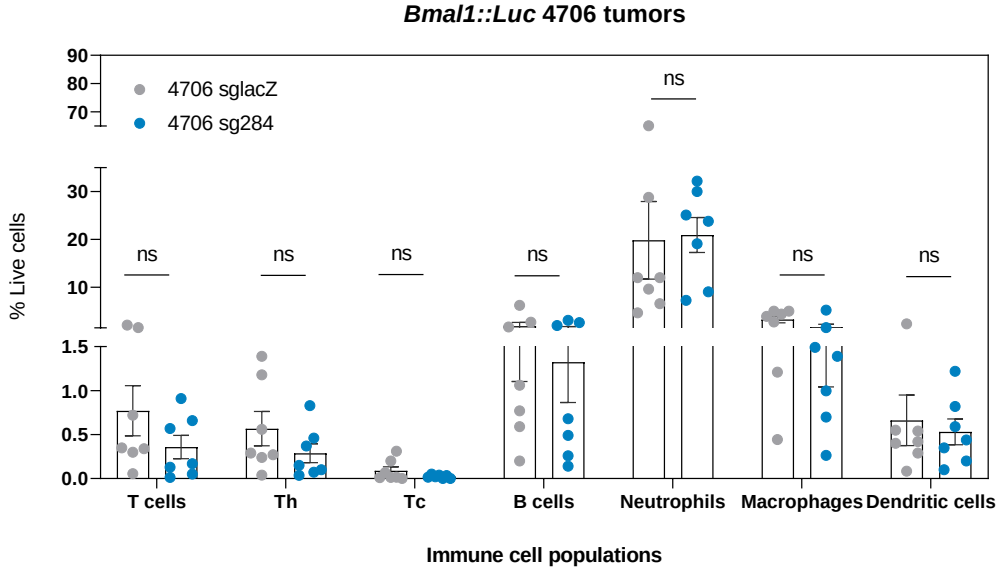

Figure 3.40: Tumor immune cell populations expressed as percentage (%) of live tumor cells based on immunophenotyping by FACS from *Bmal1::Luc* KRAS-mutant PDAC epithelial (4706) tumor samples from Bmal1-proficient (sglacZ; grey dots) and Bmal1-deficient (sg284; blue dots) at the endpoint point experiment. Two-sample t-test; significance at $p < 0.05$. ns: non-significant; T_h: helper T cells; T_c: cytotoxic T cells.

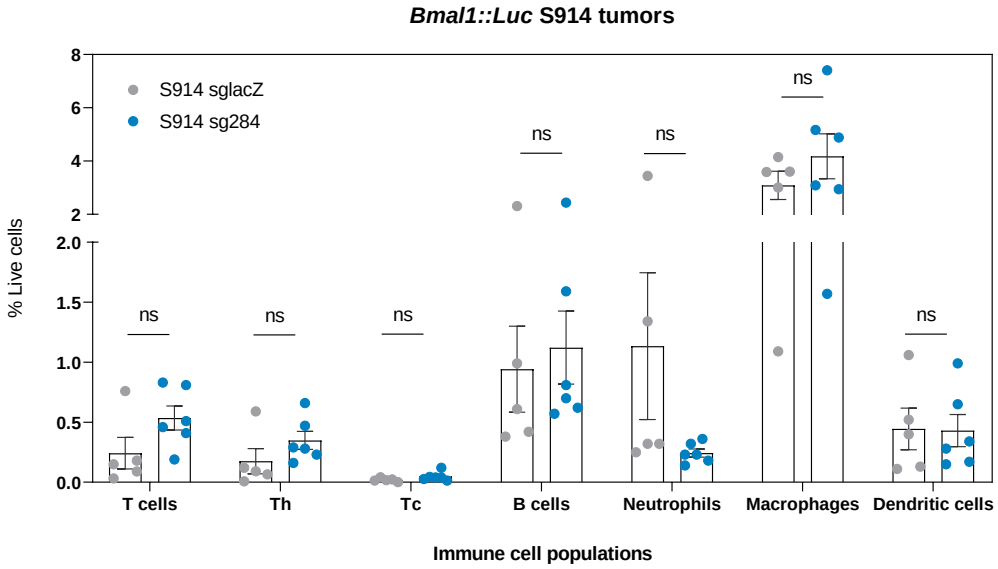

Figure 3.41: Tumor immune cell populations expressed as percentage (%) of live tumor cells based on immunophenotyping by FACS from *Bmal1::Luc* KRAS-mutant PDAC mesenchymal (S914) tumor samples from Bmal1-proficient (sglacZ; grey dots) and Bmal1-deficient (sg284; blue dots) at the endpoint point experiment. Two-sample *t*-test; significance at $p < 0.05$. ns: non-significant; T_h: helper T cells; T_c: cytotoxic T cells.

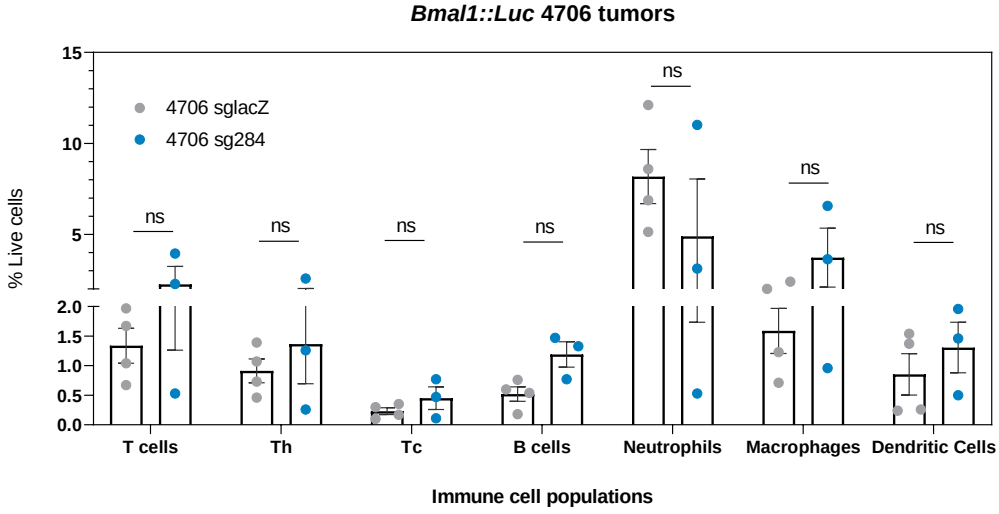

Figure 3.42: Tumor immune cell populations expressed as percentage (%) of live tumor cells based on immunophenotyping by FACS from *Bmal1::Luc* KRAS-mutant PDAC epithelial (4706) tumor samples from Bmal1-proficient (sglacZ; grey dots) and Bmal1-deficient (sg284; blue dots) at the time point point experiment. Two-sample *t*-test; significance at $p < 0.05$. ns: non-significant; T_h: helper T cells; T_c: cytotoxic T cells.

CHAPTER 4

Discussion

Abstract | In this chapter, the results of the thesis work presented in Chapter 3 are discussed.

Contents

4.1 Circadian clock function in primary PDAC cell lines

Unlike with other solid tumors, the circadian function in PDAC has been largely unexplored [145], [110]. For this, a large cohort of primary murine PDAC cell lines derived from distinct oncogenic pools were characterized for endogenous circadian clock function after generating the necessary circadian rhythm-reporter PDAC (*Bmal1::Luc*) cell lines (section 2.1.2). The luminometry-based functional screening included 44 different PDAC cell lines (Fig. 3.2 A) and was based on real-time bioluminescence recordings of *Bmal1::Luc* PDAC cells (sections 2.2.1, 2.2.2 and Fig. 2.2). The time series signal analysis (sections 2.2.2.1-2.2.2.3) revealed maintenance of circadian rhythms in the majority of the screened *Bmal1::Luc* PDAC cell lines independently of the oncogenic mutation driver (Fig. 3.2 B-C). This finding suggests that the circadian clock function is overall retained

in primary PDAC cells, which was unexpected given the established notion that transformed cells exhibit disrupted circadian rhythms [146], [122].

Combining the bioluminescent signal analysis with two different methods (sections 2.2.2.2 and 2.2.2.3), the screened luciferase reporter PDAC cell lines were characterized as Non-functional oscillators only if both methods converged (Figs. 3.4 and 3.9; 3.8 and 3.10; 3.6 and 3.11). In KRAS-driven PDAC tumor cells, high heterogeneity in the relative amplitude of the circadian rhythm was observed (Fig. 3.9), which may be accounted to cell-intrinsic rhythm characteristics.

An important aspect of the functional screening was the usage of DEX as phase synchronizing agent among individual cells. DEX is extensively used for re-setting oscillations in peripheral tissues and cells *in vitro* [42]. Cultured cells or tissue explants are desynchronized and circadian rhythm is seemingly absent in a population readout, since *in vitro* conditions lack the daily humoral and neuronal stimuli that are essential for entrainment *in vivo* [147]. Thus, mainly chemical factors are used for *in vitro* experiments that mimic the entrainment effects of different *Zeitgebers* and allow to synchronize, and therefore, to observe the endogenous circadian oscillations in cell populations in culture. As such, DEX treatment was important for "re-setting" the circadian rhythm within the cell population in each individual replicate in the 96-well plate, and, in practice, for setting a common starting point in time before the recording of the *Bmal1*-driven luciferase activity started.

For those *Bmal1::Luc* PDAC cell lines that were characterized as Non-functional oscillators, three additional synchronizing agents (forskolin, serum shock and temperatures cycles) were employed to ensure the validity of disrupted circadian rhythm as observed after DEX treatment (see sections 1.5.2 and 3.1.1.1). For all three PDAC cell cohorts, forskolin and serum shock did not elicit rhythmicity in the characterized Functional oscillators that were used as positive controls, indicating that these agents are not suitable

for phase synchronization in PDAC. Albeit temperature is considered a weak synchronizer for peripheral tissues and cells in culture [147], the elicited response in Functional oscillators of the PK cohort (Fig. 3.13 i-ii) compared to the Non-functional oscillators (Fig. 3.13 iii-vi) indicates the validity of the characterized circadian functionality in PK cohort after DEX treatment. Regarding the PI3K and PKP cohorts, temperature cycles did not result in elicited rhythmicity in the positive controls, thereby further excluding this method for phase synchronization in these two PDAC cell cohorts.

Furthermore, by comparing the normalized amplitude of the exerted circadian rhythm in the model cell line U2-OS between all aforementioned synchronizing agents, it confirms that cell stimulation with DEX results in the most robust circadian rhythm and period estimate with the highest statistical significance (Fig. 4.1), which is in agreement with previous reports [148].

Several studies have reported that core clock gene expression in tumors is altered compared to healthy tissue [113], [149], [150]. Given the availability of additional genomic features and gene expression data for KRAS-driven and PI3K-driven PDAC cell lines, it was explored whether differences in characterized genetic alterations or expression of the core clock genes may explain the disturbed circadian rhythm in the Non-functional oscillators. However, no significant differences were found (Figs. 3.15, 3.16 and 3.17). In alignment to this outcome, it has been suggested that there are other protein regulators essential for normal circadian clock function which are not components of the core clock molecular mechanism [151], [152]. In this context, post-transcriptional and post-translational modifications may account for changes in core clock protein function and abundance, which cannot be taken into account when solely measuring mRNA levels in steady-state conditions. Moreover, it has been shown that certain oncogenes, such as *c-Myc*, may impact the function of the circadian clock mechanism by directly binding to DNA sites preventing the BMAL1:CLOCK heterodimer complex to regulate the expres-

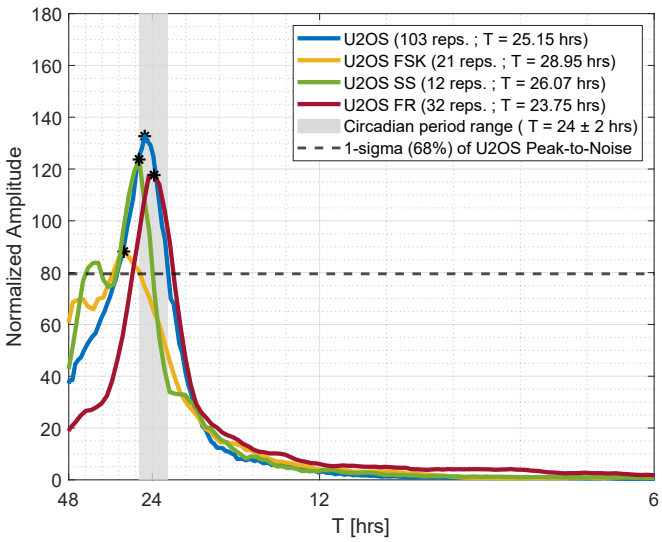

Figure 4.1: Circadian rhythmicity in U2-OS cells based on LSP period estimates (T; in hours) after phase synchronization with dexamethasone (blue) and other synchronization agents. FSK: forskolin 1 μ M (yellow) ; SS: serum shock with 50 % FCS (green); FR: free-rum period after entrainment with temperatures cycles (red); LSP: Lomb-Scargle periodogram; reps: replicates.

sion of downstream genes [129].

Taken together, the functionality of the cell-intrinsic circadian rhythm in KRAS- and PI3K-driven PDAC cell lines cannot be attributed to differences in steady-state levels of core clock gene expression levels or any known genomic alterations of those cell lines.

4.2 Proteomic profiling of primary PDAC cell lines

Over the last two decades, technological advances in next-generation sequencing platforms have paved the molecular characterization of pancreatic cancer at a high-throughput manner and new insights have been gained about PDAC biology and progression [100]. It is thereby well established that PDAC is governed by genomic alterations and gene expression modulations that support resistance to standard chemo- and radiotherapy regimens [81].

The valuable biological resource of primary murine PDAC cell lines in Prof. Saur's group at the Technische Universität München has recently been profiled at the transcriptome level, which resulted in the molecular identification of two distinct KRAS-driven PDAC molecular subtypes [143]. To gain further insights into PDAC biology and signaling pathways that may constitute important drivers for functional adaptations associated with resistance mechanisms, I investigated whether distinct oncogenic mutations in PDAC may diversify on the proteome level. For this, MS-based quantitative proteomics analysis was employed using primary murine PDAC cell lines originating from oncogenic pools with well characterized genetic mutation(s) (Table 3.1 and Fig. 3.18 A).

MS-based proteomics is a powerful technology that generates in an unbiased manner high-throughput quantitative data that can unravel discrepancies underpinning functional adaptation mechanisms (e.g., through metabolic rewiring) that often characterize cancer cells [153]. In addition, a systems biology approach on protein abundance is advantageous, because proteins constitute the functional players in the cell, thereby, in comparison to systems-wide gene expression analysis, proteomic signatures reflect biological function in a direct and quantitative manner. In the same context, several studies have shown a low correlation between copy number variations and relative change at the protein level, which implies that genomic alterations are not or only partially translated at differences on the protein level [154].

In this thesis work, the proteomic profiles of primary PDAC cell lines, with a defined mutational and gene expression landscape, were characterized by MS-based proteomics (see section 2.3). The data analysis revealed that PDAC cell lines with distinct oncogenic mutation(s) share functional characteristics based on their proteomic signatures (Figs. 3.19 and 3.20). Functional enrichment pathway analysis of differentially expressed proteins between four PDAC cohorts showed that KRAS-driven epithelial (PK-E) tumors are distinct in metabolic-related processes that involve fatty acid-dependent energy produc-

tion, PPAR signaling and redox homeostasis (Fig. 3.21 Cluster 1).

An important aspect of extensive cell proliferation is the increased lipid metabolism, since lipids are necessary components of all membrane structures in the cell. It has been shown that lipogenic enzymes, such as ATP-citrate lyase (ACLY), acetyl-CoA carboxylase (ACC) and fatty acid synthase (FASN), are upregulated in cancer cells, which lead to aberrant fatty acid synthesis, therefore supporting tumor development [155], [156]. In xenograft PDAC mouse models, ACLY inhibition reduced tumor growth [157], while in a lung cancer mouse model inhibition of ACC was shown to suppress tumor growth [158]. In this context, it can be hypothesized that PK-E tumors might be less sensitive to inhibitors of those enzymes considering their higher protein abundance.

Based on the enriched signaling pathways in KRAS-driven mesenchymal (PK-M) subtype together with PKP tumors (Fig. 3.21 Cluster 2), it can be derived that both types of PDAC tumors likely depend on scavenging of extracellular protein as a metabolic adaptation for energy production. It has been shown that scavenging and subsequent hydrolysis of extracellular protein via macropinocytosis supports cell proliferation [159]. Noteworthy, a number of studies have attributed such metabolic adaptation, along with autophagy and reprogrammed glutamine metabolism, to oncogenic KRAS signaling [160]. It has been shown that mutant KRAS signaling results in upregulation of the glucose transporter 1 (GLUT1) [86] and of rate-limiting enzymes in glycolysis cascade, such as phosphofructokinase 1 (PFK1), thus enhancing glucose uptake and metabolism [85], [86]. Importantly, in the hypoxic and nutrient-limited TME, constitutive KRAS activation in PDAC cells supports nutrient salvaging, greatly supported by autophagy and macropinocytosis [81]. Therefore, it can be speculated that targeted inhibition of those pathways in both PK-M and PKP PDAC tumors might decrease tumor cell growth.

PKP tumors share in addition functional characteristics with PI3K tumors, such as aminoacyl-transfer RNA (tRNA) biosynthesis, that play an important role in translation,

and response to DNA damage (Fig. 3.21 Cluster 3). Intriguingly, recent studies have shown that the enzymes required for aminoacylation of tRNAs, called aminoacyl-tRNA synthetases (ARSs), are associated with cancer development [161], [162]. What is more, it has been suggested that certain ARSs and ARS-interacting multifunctional proteins (AIMPs) may enhance tumor development by modulation of p53 expression [163]. Wang and colleagues showed that in mice under high-fat diet, a colon-specific ARS was associated with DNA damage via accumulation of lysine homo- cysteinylation and thereby indirectly inhibited p53 function, leading to increased cell proliferation in the colon [163]. It would be interesting to investigate whether inhibition of proteins related to aminoacyl-transfer RNA biosynthesis, such as ARSs, might elicit an inhibitory growth effect in PKP PDAC tumors.

The large number of available KRAS-epithelial tumor cell lines that were included in the proteomics analysis greatly contributed to the identification of proteome-based functional Clusters (Figs. 3.23 and 3.24) related to differential metabolic adaptations for energy production. This favors the understanding of how metabolic reprogramming even in the absence of any stimulus might highly impact the response of PDAC cells in chemo- and radiotherapeutic approaches, since it can be speculated that the ability to escape from such treatment strategies relies on the ability to sustain energy production and redox homeostasis.

It is noteworthy, that in a relatively recent study Daemen and colleagues showed that metabolite profiling in primary PDAC cell lines stratifies PDAC in three metabolic subtypes, glycolytic, lipogenic and slow proliferating [164]. The glycolytic subtype generates metabolites associated with glycolysis and decreased redox homeostasis, while in the lipogenic subtype lipid-related and TCA cycle metabolites are enriched. Slow proliferative metabolic subtype produces low levels of amino acids and carbohydrates [164]. This characterization is in agreement with the results of this thesis work, which

identified different metabolic rewiring strategies between epithelial and mesenchymal KRAS-driven subtypes as well as in PI3K and PKP tumors based on single-shot proteome analysis. The analysis of proteome profiles highlighted that functional characterization of PDAC tumors with a systems-wide and unbiased approach can unravel discrepancies that are either considered as joint on the genomic level or not possible to decipher on the transcriptome level.

The integration of circadian clock functionality and proteome characterization in PDAC aimed to identify at steady-state conditions whether there are functional outputs of the circadian clock independently of the oncogenic mutation driver or KRAS-driven molecular subtype. The analysis showed that it is challenging to disentangle functional discrepancies that lead to differential metabolic adaptations as an output of either cell-intrinsic circadian rhythms or oncogenic mutation drivers (Figs. 3.21, 3.26 B and 3.27 B).

Proteomic profiling of a rhythmic epithelial KRAS-driven PDAC cell line before and after deleting the cell-intrinsic clock showed a number of cellular biological pathways may could be under circadian control. It was identified that proteins involved in xenobiotics metabolism were significantly downregulated in rhythmic vs non-rhythmic cells (Fig. 3.29 B). It has been shown that in healthy tissues cytochrome P450 enzymes are encoded by clock-regulated genes [28], indicating that also in PDAC a functional cell-endogenous oscillator may be necessary for drug oxidation, which is the main function of the cytochrome P450 monooxygenase system. This greatly favors the notion that the dynamic relationship between circadian clock and cell metabolism can be exploited as functional therapeutic vulnerability in PDAC. As part of the circadian clock output, the temporal variability in expression, abundance and/or function of processes involved in drug absorption and metabolism may be used for optimal time-of-day drug administration, expanding the available therapeutic reservoir for ultimately increasing drug efficacy

and decreasing toxicity (chronopharmacology; see also chapter 5). Nevertheless, it is important to note that the functional discrepancy related to drug metabolism was not identified in the mesenchymal KRAS-driven PDAC cell line upon genetic disruption of the cell-intrinsic circadian mechanism (Fig. 3.28 B). Arguably, a common therapeutic vulnerability based on the presence of a functional endogenous oscillator would facilitate any aforementioned clinical applications. However, a recent study showed that KRAS-driven PDAC subtypes are governed by differential responses to chemo- and immunotherapy [165] indicating that the molecular reservoir of KRAS-driven PDAC tumors is highly dynamic and less likely to be impacted (or directed) solely by circadian clock outputs. Reciprocally, outputs of the circadian clock could be KRAS-driven PDAC subtype-specific that could explain different responses to therapy.

Cell transformation in a cancer state, resulted from accumulation of genetic alterations and epigenetic modifications, leads to metabolic plasticity that sustains energy production and redox homeostasis, both required for aberrant cell proliferation and growth. This metabolic plasticity per se depends on the cancer type and proliferation rate [166], [167], but it comprises an available functional reservoir to favor the cancer cell's response against chemo- and radiotherapeutic agents. Moreover, it has been shown in other studies [86] and also in this thesis work, that oncogenic signaling as a result of genomic alterations, greatly impacts metabolic adaptation mechanisms. Given the complex relationship between altered metabolism, drug response and genetic heterogeneity in PDAC, the utilization of circadian rhythms -and therefore time of day- as therapeutic vulnerability might prove to be highly beneficial as a customized treatment strategy for PDAC patients that do not respond favorably to chemotherapy (see also chapter 5).

4.3 The role of tumor-intrinsic circadian clock in PDAC development and progression

As described in section 1.6.2 PDAC is a heterogeneous malignancy that progresses to metastatic and chemoresistant phenotypes resulting in poor prognosis. *Kras* mutations characterize 90 % of PDAC tumors in human patients [168], therefore characterizing functional outputs in KRAS-driven PDAC tumors is considered of high clinical relevance.

I aimed to investigate the role of the tumor-intrinsic circadian clock in PDAC biology, development and progression. Given the characterized circadian clock functionality in the PDAC cohorts as a result of this thesis work, a selection of PDAC *Bmal1::Luc* PDAC cell lines that were included in the functional screening was required. The selection comprised the KRAS-mutant cohort and it was subsequently based on the robustness of the circadian rhythm as a reflection of a likely robust biological significance in the tumor cells.

One approach to elucidate the impact of the tumor-endogenous oscillator (TEO) in PDAC development and progression would be to orthotopically implant a PDAC cell line harboring a functional clock in one group of wild-type mice, and a PDAC cell line that does not retain circadian functionality in another group of mice. On one hand, this would favor the importance of TEO, albeit it would not answer whether -and at which degree- any differences on the genetic level (e.g., probable additional mutations), transcriptome or proteome levels between the two KRAS-mutant PDAC cell lines may account for a given outcome on tumor growth, tumor progression and/or survival of the experimental animals. In fact, proteomic signatures constitute an additional level of functional heterogeneity in PDAC (see section 3.2).

An alternative experimental approach, as implemented in this thesis work, considered the characterized and systems-wide discrepancies in KRAS-mutant PDAC tumors

[143] for the selection of robust KRAS-mutant oscillators to genetically disrupt their function. On this regard, a defined loss-of-function genetic alteration in a fraction of *Bmal1::Luc* PDAC cell lines resulted in disturbed circadian rhythms. Thus, a comparison between a control and a mutated TEO originating from the same parental KRAS-mutant PDAC cell line would strengthen any direct link between TEO and its potential role in PDAC development and progression. Conclusively, four different KRAS-mutant PDAC cell lines were chosen, two from the epithelial and two from the mesenchymal KRAS-driven PDAC molecular subtypes, in which the molecular mechanism of the clock was genetically ablated by CRISPR/Cas9-mediated *Bmal1* knockout (see section 2.1.3 and Figs. 3.30-3.33 and 3.34).

It is of high significance to note that in the Bmal1-deficient cells, the *Bmal1* gene was not fully knocked-out in the whole cellular population (Fig. 3.34 A) inherited by the editing efficiency of the CRISPR-Cas9 system. A global (i.e., 100 %) gene knockout could have been an alternative experimental route via clonal selection and expansion. However, there is evidence that different clonal PDAC cell lines originating from the very same parental cell line show differential proliferative capacity (Prof. Saur's group; data not shown). This would directly hassle and even bias the selection of the clonal cell line for any subsequent phenotypic characterization and *in vivo* work.

Given the degree of circadian disruption as depicted in Figures 3.30-3.33, the *Bmal1::Luc* KRAS-mutant PDAC cell lines 53704 and 16992 were excluded, and the rest of experimental work included the *Bmal1::Luc* cell lines S914 from the mesenchymal, and 4706 from the epithelial KRAS-driven PDAC molecular subtypes. Based on the *in vitro* phenotype of Bmal1-deficient cells from both cell line pairs, which exerted higher proliferative capacity compared to the Bmal1-proficient cells (Fig. 3.34 E), it was hypothesized that the TEO would impact tumor growth *in vivo* (see below).

In the first (time point) mouse study the aim was to resemble the design of the *in vitro* experiment, thereby the tumor growth was assessed between the two groups of mice after a predefined period of time starting from the same cell inoculation in the pancreas. In this first *in vivo* experiment, the *Bmal1::Luc* KRAS-mutant PDAC epithelial cell line pair was used based on the result of the colony formation assay. It was demonstrated that for this cell line the difference between Bmal1-deficient and Bmal1-proficient cells in proliferative capacity was larger compared to the S914 cell line pair (Fig. 3.34 E). It was, thereby, speculated that the tumor cells with a disrupted TEO would proliferate more *in vivo* as well, leading to increased tumor growth compared to the control group. The study showed that the tumor size did not differ between the two groups of mice (Fig. 3.38). Therefore, the higher proliferative effect *in vitro* of the Bmal1-deficient cells did not translate into larger or more aggressive PDAC tumors *in vivo*, indicating that host and/or TME-related factors likely play a role in tumor development and progression.

Furthermore, the time point experiment included both immunodeficient (Rag2-/-; Rag2-KO) and immunocompetent (F1) mice. The Rag2-KO mice were used as control host for CAS9 immunogenicity (Prof. Saur's group; data not shown). The Rag2-KO group was sacrificed three weeks and the F1 group four weeks after the transplantations, which were performed the same day with the same cell suspension of each *Bmal1::Luc* KRAS-mutant PDAC cell line (4706). Given that the tumor growth in the F1 mice, albeit evaluated one week later, was comparable to the Rag2-KO mice, confirmed that the presence of CAS9 in the PDAC cells did not elicit any vast immunogenic reaction that would not allow for any of the PDAC cell lines to grow in immunocompetent mice.

In the second mouse study (endpoint), the experimental design was similar to the first one. Bmal1-deficient and Bmal1-proficient PDAC cells originating from the same KRAS-mutant cell line were injected in the pancreas of F1 mice. This experiment included the same epithelial *Bmal::Luc* PDAC cell line pair (4706 sglacZ and 4706 sg284), and in addi-

tion the mesenchymal S914 *Bmal::Luc* KRAS-mutant PDAC cell line pair (S914 sglacZ and S914 sg284) in another animal cohort. However, the duration of the experiment was not predetermined, meaning that the mice were sacrificed when moribund, which presumed that fully developed PDAC tumors were established in the host.

Given the heterogeneity in the tumor growth within the groups in the first study, it was speculated that the course of PDAC development and progression is different in each mouse and affected by additional host-intrinsic factors. Therefore, in the second study, the tumor growth was evaluated at the terminal state. In addition, it was investigated whether the presence of a functional TEO may impact the survival of the mice. In both groups of KRAS-mutant PDAC cell line pairs, the tumor growth between Bmal1-deficient and Bmal1-proficient cells was not statistically significant different (Fig. 3.39 A) and the survival rate was neither correlated with tumor-intrinsic clock functionality (Fig. 3.39 B).

Taken together, the *in vivo* studies did not resemble the phenotype of Bmal1-deficient cells in cultured conditions either at a given time point or at a relatively final stage in tumor development. An important aspect of PDAC biological hallmarks constitutes the TME (see section 1.6.3), which may impact cancer cells' proliferation *in vivo* and may surpass the effect of a TEO. It has been shown that growth factors and cytokines secreted by pancreatic stellate cells (PSCs) play an active role in tumor cell proliferation and progression [84]. For example, Seux and colleagues showed that the secreted protein acidic and rich in cysteine (SPARC) is secreted by PSCs affecting cell migration and proliferation [169]. It has also been shown that PSCs secrete a protein called periostin that is involved in tumor cells invasion by activating AKT signaling [170], [171].

Another consideration regarding the tumor growth in both mouse studies is the fact that the intrinsic proliferative capacity *in vivo* differs from cell cultured conditions in terms of nutrient availability, growth factors and oxygen. These characteristics are limiting factors in the TME, while are constantly provided in the cells in culture. PDAC is

comparably more hypoxic than other solid tumors [172], yet PDAC cells can particularly adapt to hypoxic conditions by metabolically reprogramming pathways that allow them to utilize alternative sources of nutrients via routes of autophagy and macropinocytosis [90]. What is more, hypoxia-inducible factor-1 (HIF-1) has been shown to link metabolic adaptation, apoptosis and cell proliferation and invasion [173], [174]. One strategy that would facilitate to study any direct link between TEO and tumor growth *in vivo* would be to orthotopically or heterotopically transplant the KRAS-mutant PDAC cell line pairs of interest and follow the growth of the tumor over the course of time. This could limit the effect of biological heterogeneity between syngeneic mice as well as the effects of TME (in case of heterotopic injection). Certainly, TME is an indispensable part of tumor development and progression in PDAC, however an *in vivo* study of TEO's role in PDAC biology might require to bypass it.

The FACS-assisted immunophenotyping in the *in vivo* studies contributed to the understanding of whether a TEO might influence tumor-associated immune cell remodelling. It was recently shown in a melanoma mouse model that physiological circadian disruption alters the immune microenvironment, likely facilitating tumor growth and progression [175]. In both mouse studies of this thesis work the composition of immune cell populations remained unaffected by the presence of PDAC cells harboring a functional circadian clock or not (Figs. 3.42, 3.40 and 3.41). Arguably, considering the high within-group variability (Figs. 3.42, 3.40 and 3.41), additional experiments consisting of larger animal cohorts could potentially uncover statistically significant differences.

Regarding the effect of a TEO on PDAC progression, the mouse studies included a macroscopic assessment of metastasis formation in peripheral organs, such as the liver and the lungs. It was found that, unlike the initial hypothesis, no direct link between the presence of a functional TEO and tumor progression can be made as resulted by compar-

ing the presence and the number of metastatic lesions in mice implanted with Bmal1-deficient or Bmal1-proficient KRAS-mutant PDAC tumor cells (Tables 3.4, 3.6 and 3.7).

It is worth highlighting that the *in vivo* studies focused on the tumor-endogenous self-sustained circadian rhythm and its potential role on tumor development and progression. The experimental approach was different to a number of other studies that have shown a connection between systemic circadian disruption and tumor growth. For example, in a mouse model of lung adenocarcinoma both genetic and physiological disruption of the central clock decreased survival and promoted tumor growth and progression [107]. Additionally, physiological disruption in wild-type mice induced hepatocellular carcinoma along with global liver metabolic deregulation [132]. Also, in a murine melanoma model, jet-lag-induced tumor growth increased compared to animals that kept under normal light-dark cycles [175], and circadian disruption further ablated rhythmic clock gene expression in the liver [175]. What is more, in a mouse model of lung adenocarcinoma, it was found that hepatic metabolic reprogramming is exerted exclusively in tumor-bearing mice, in which the tumor may act as an circadian reorganizer of hepatic metabolism [135].

Collectively, these studies suggest that -either at a higher degree or in conjuction with the TEO- disruption of the central circadian clock impacts the alignment with peripheral oscillators, which in turn impact immune cell distribution and metabolic reprogramming in peripheral organs, such as the liver. As a result, tumor growth and/or progression of a pre-exisiting tumor could be enhanced.

Last but not least, an important aspect of the experimental work was the hypothesis that the cell-intrinsic circadian rhythms recorded *in vitro* from the *Bmal1::Luc* PDAC cells would be recapitulated *in vivo*. The hypothesis was tested by bioluminescence recordings of organotypic slices from both Bmal1-deficient and Bmal1-proficient KRAS-mutant

epithelial PDAC tumors. Given that several cell populations reside in the TME, the presence of *Bmal1::Luc* exclusively in PDAC cells excluded any interference from non-tumor cells in the recorded bioluminiscent signal. A residual circadian rhythm was detectable in the Bmal1-proficient tumor slices before the dexamethasone (DEX) treatment, which was not the case for Bmal1-deficient tumors (Figs. 3.35 and 3.36). After treating the organotypic slices with DEX the circadian rhythm was robustly elicited in the Bmal1-proficient tumors (Fig. 3.35), since DEX is required for phase synchronization between the PDAC cells in the tumor slice (Fig. 3.35; see also 1.5.2). To note, in the Bmal1-edited tumos slices, an oscillation pattern was observed after DEX treatment, yet the amplitude of the rhythm was comparable to the baseline, demonstrating that the circadian rhythm in the Bmal1-edited tumors was significantly disrupted (Fig. 3.36). It is important to highlight again that the Bmal1-deficient cells that were orthotopically implanted contained 25 % wild-type cells (with BMAL1 proficiency; Fig. 3.34 A), which likely were able to induce the observed circadian rhythm in the Bmal1-deficient tumor slices.

Recent studies have inferred *in vitro* rhythmicitiy of tumor cells based on gene expression time-course data [145], [110], and others have shown *in vivo* rhythmicity of non-tumor cells based on fluorescence-based imaging of core clock genes [176]. In this thesis work, it was demonstrated for the first time that circadian rhythm is maintained in a tumor *in vivo* by real-time recording of the bioluminescence-generating activity of the *Bmal1* promoter. It would be interesting to investigate the phase relationship between the tumor cells and the surrounding cell types, which presumably retain circadian functionality, within the PDAC tissue as well as with the central pacemaker. In a recent study it was shown that transforming growth factor-β (TGF-β) signaling is important for paracrine coupling between peripheral oscillators resulting in an appropriate phase relationship [177]. Therefore, it would be interesting to investigate the role of TGF-β in this context. Furthermore, it would be important to characterize circadian clock prop-

erties of cancer and non-cancerous cells within a malignant tissue, because the cancer-endogenous oscillator may greatly impact the metastastic potential of cancer stem cells, as recently was shown in glioblastoma [178].

Conclusively, the relationship between tumor-autonomous clocks and host circadian oscillators is considered dynamic [18]. Given the *in vivo* findings of the present thesis work, the biological significance of a TEO in the host may be masked by rhythmic systemic signals as well as by aberrant signaling in the TME. Certainly, more studies are required to further explore and disentangle this complex relationship.

CHAPTER 5

Conclusions and Outlook

Contents

Organismal and organ circadian rhythms are considered functional outputs of an endogenous circadian oscillator to ultimately maximize the potential of the organism to survive by regulating the timing of behavioral and physiological processes.

Over the last two decades, several epidemiological studies have supported the association between circadian misalignment and susceptibility to cancer pathogenesis. Although few animal studies have revealed that cancer cells maintain circadian rhythmicity, there has not been a more comprehensive characterization of tumor-intrinsic clock functionality in primary PDAC cell lines before this thesis work.

PDAC is an aggressive malignancy characterized by genetic heterogeneity, invasiveness and chemoresistance. Systems-wide studies have been performed to understand the biology of PDAC's aggressiveness and reveal potential vulnerabilities that could be targeted, and ultimately lead to discovery of novel therapeutic agents.

The utilization of circadian rhythms for timed chemotherapy in PDAC to increase drug efficacy and safety (termed as *chronotherapy* or *circadian medicine*) is an attractive idea to be considered in the spectrum of multimodal treatment strategies in PDAC given the low response of patients to current monotherapies. In addition, proteome profiling

of primary and metastasized PDAC tissue as well as clinical samples has the potential to identify novel protein targets (biomarkers) that may determine the disease stage or predict the response to a therapeutic agent, and thereby, prevent undesired side effects in non-responder patients.

5.1 Studying circadian rhythms in PDAC

The degree and nature of interrelationship between the circadian clock and cancer remains a topic of debate. Disturbances in circadian rhythms have been associated with increased susceptibility to cancer [5], whilst some established cancer cell lines have been found to retain circadian functionality that potentially drives cycles of gene expression with a 24-hour periodicity [110], [145]. However, experimental studies about the role of those rhythms in tumor growth and progression are scarce.

In this thesis work, a large cohort of murine primary PDAC cell lines derived from distinct oncogenic pools were assessed whether they retained circadian oscillations after generating the necessary circadian rhythm-reporter (*Bmal1::Luc*) cell lines (section 2.1.2). The medium-scale luminometry-screening revealed that the majority of the PDAC cell lines harbor a functional circadian clock independently of the oncogenic driver mutation(s).

Given that core clock gene expression and genomic features of KRAS-driven PDAC cell lines cannot explain the observed differences between the cell lines characterized as Functional and Non-functional oscillators, it would be important to investigate the role of other oncogenes that have been shown to disrupt the core clock mechanism, such as *c-Myc* [129]. For instance, an inducible genetic system for *c-Myc* overexpression in a subset of *Bmal1::Luc* PDAC Functional oscillators, and the subsequent analysis of the bioluminescent signal (see section 2.2.2), would elucidate whether the role of *c-Myc* in

PDAC were similar as in other types of cancer [129], regarding its impact on the core clock mechanism. In addition, it should be highlighted that a comparison of circadian rhythmicity between PDAC and healthy pancreatic tissue would be valuable to elucidate whether and to which degree endogenous oscillations are disturbed in the transformed state of exocrine pancreatic cells.

Furthermore, using a PDAC implantation model as part of this thesis work, it was shown that the partially deleted tumor-endogenous circadian clock does not directly impact tumor growth or metastasis formation independently of the KRAS-driven molecular subtype (Fig. 3.39 A) or the duration of tumor development (Figs. 3.38 and 3.39 A). This indicates that additional experiments are required with 100 % deletion of the tumor cell-intrinsic clock in order for the *in vivo* findings of this thesis to be further considered. As another future perspective, a probably more direct connection between tumor-intrinsic clock and tumor growth could be drawn by longitudinally measuring the tumor size following the same experimental procedure as in this thesis work (e.g., orthotopic implantation of KRAS-mutant PDAC cells with Bmal1-deficiency or Bmal1-efficiency). This could be performed by *in vivo* bioluminescence imaging of the tumor given the availability of luciferase-reporter PDAC cell lines assuring that the bioluminescent signal is a direct output of the tumor cells exclusively.

Importantly, although usually considered as granted notion, it was shown that the circadian rhythm is maintained *in vivo* in the tumor after phase synchronization with dexamethasone (section 3.3.3). A perspective would be to investigate the impact of systemic clock disruption on PDAC development, as it has been shown in other cancer types [107]. The circadian clock could be either physiologically disturbed under chronic jet-lag conditions compared to normal light-dark cycles (LD), or genetically by using whole-body *Cry1*/*Cry2* knockout mice.

Regarding the role of the tumor-intrinsic circadian clock in tumor progression *in vivo*

as was investigated in this thesis, it was neither found a direct correlation between clock functionality in the tumor and the potential to metastasize or the number of metastases in distal organs (Table 3.4). As aforementioned, a future *in vivo* approach would be not only a full (100 %) ablation of the tumor-endogenous circadian clock, but also to systemically disrupt the circadian clock -physiologically or genetically- and study the effect on metastasis formation in the periphery. In terms of systemic metabolic reprogramming due to the presence of a tumor, in a mouse model of lung adenocarcinoma it was found that the tumor could act as circadian reorganizer of hepatic metabolism [135]. In the same context, mass spectrometry-based proteomic profiling of PDAC cell lines derived from the primary and metastatic tumor sites might reveal in an unbiased manner metabolic rewiring pathways that could potentially be linked to establishment of metastasis. For example, a recent mechanistic study identified that loss of phosphoglycerate dehydrogenase (PHGDH) -a glycolytic enzyme- potentiates metastatic dissemination in mice [179]. The plasticity of tumor cells to adapt to a plethora of stressful conditions, such as hypoxia, lack of nutrients and oxidative stress, results in metabolic heterogeneity that enables them to metastasize and/or develop resistance to cytotoxic agents [81].

From the translational point of view, the study of circadian rhythms in cancer research has ultimately the goal to understand which genes are expressed and, perhaps more importantly, which proteins change in abundance and/or function in a cancer cell or tissue following a 24-hour periodicity. This is of high significance, because it could serve as foundation for circadian medicine. In essence, the possibility to optimize the timing of drug administration to a circadian window in which the drug target is likely to be less abundant or less stable (e.g., via post-translational modifications) would undoubtedly increase drug efficacy and decrease undesired side effects. The concept of circadian pharmacology aims, thereby, to utilize the output of circadian rhythms in physiology and try to optimize the dosing of medical interventions in order to make them more effective

and safer for the patients.

Primarily, circadian therapeutics aims the design of optimal time-modulated drug administration at specific schedules. On the cellular level, circadian therapeutics is based on the fact that clock-controlled genes are involved in xenobiotic metabolism and detoxification, cell proliferation -and related metabolic processes- DNA repair mechanisms and apoptosis [180], accounting for circadian modulation of pharmacokinetics and pharmacodynamics [181]. It has been hypothesized that in tumor cells the aforementioned processes are not in alignment with the surrounding healthy tissue, thereby there is likely a circadian time window in which a given drug is absorbed and metabolized by the tumor cells, and subsequently impacting the corresponding target (e.g., cell cycle, DNA repair or apoptosis regulator) at a different degree compared to the normal cells. This chronomodulated drug sensitivity in the tumor can, as a result, be exerted as reduced toxicity in the normal cells.

The last few years, several experimental data have supported the concept of circadian pharmacology in cancer based on animal and human studies. For example, Lee and colleagues showed that in a mouse model of melanoma the administration of an HSP90 inhibitor at two different times of day led to different tumor growth outcome, and importantly, drug efficacy decreased in clock-deficient tumors [182]. This study further provided mechanistic evidence for circadian modulation of the drug action, not only by lower levels of the target at specific times of day, but also by having a time-dependent effect on the cell cycle, highlighting the significance of a tumor-endogenous functional clock. In another recent study, the authors comprehensively analyzed protein-protein interaction and immunoprecipitation sequening data from 14 cancer types and suggested a strong interaction of core clock genes with clinically "actionable" genes [112]. It has been also experimentally shown that 40 anti-cancer drugs exert differential toxicity based on circadian timed delivery in rodents [181].

In this context, a perspective research objective for PDAC biology would be to identify clock-regulated genes and/or proteins on a time-of-day-dependent manner, and further analyze those targets against which sensitivity might change at different times of day. Importantly, it would be interesting to investigate whether and if so, at which degree, different oncogenic driver mutations impact the output of the clock, and which genes or proteins are commonly, rather than in a context-specific manner, regulated by the circadian clock. For this, time-course experiments are required, i.e., sampling cell or tissue extracts at distinct time points over the course of at least 24 hours. As resulted from this thesis work, the elucidation of circadian clock outputs on the proteome level in different PDAC cohorts at steady-state conditions can be challenging (see sections 3.2 and 4.2).

These aforementioned pre-clinical studies have gained the attention of clinical professionals. For instance, in several human studies, chronomodulated drug efficacy was based on monotherapy or combination therapy for a defined time period given either at standard or predefined circadian times. Time-of-day-dependent drug admininstration of oxaliplatin was performed in 114 metastatic patients with colorectal cancer (CRC) at two different time points (4 pm or 4 am) and the results showed that 16.7 % of the patients delivered with oxaliplatin at 4 pm exerted severe side effects compared to 80 % of the corresponding patients with adverse effects when the drug was delivered at 4 am [183]. However, a larger multinational cohort study with CRC patients showed that timed administration of chronoFLO4 (chronomodulated administration of fluorouracil, leucovorin, and oxaliplatin) did not increase prognosis, rather it was found that mortality risk in women treated with chronoFLO4 increased by 38 % and in men by 25 % compared to those that received conventional therapy [184]. These data suggest that there is still lack of consistent translational evidence for a routine clinical application of chronotherapeutics in cancer treatment [185].

Lastly, it is important to consider that the aforementioned studies, as well as stud-

ies that aim to implement circadian modulation of drug administration in human patients, often lack consideration of additional important information, such as chronotype, endogenous circadian period and sleep patterns. These parameters vary substantially between healthy individuals [186], indicating a further variability in patients because of their disease state. In addition, internal time is further impacted by factors, such as age, gender, exposure to light and season [187]. Therefore, for any circadian therapeutic intervention to be designed or optimized, a tool for measuring an individual's or patient's internal time might be necessary. In fact, a novel diagnostic method for such purposes utilizing blood samples has recently been developed [187].

5.2 Proteomic profiling in PDAC

In recent years, the profound technological advancements in mass spectrometry (MS) along with bioinformatics tools that allowed the automated identification and quantification of thousands of peptides (and therefore proteins) in a single shot have paved the way for the application of MS-based quantitative proteomics in cancer research [188]. Undoubtedly, genomic and transcriptomic profiling of tumors generates invaluable knowledge about genetic alterations, chromosomal rearrangements and modification of gene expression. However, the large-scale comprehensive study of the functionally relevant proteins of a tumor, the proteome, can dramatically increase the understanding of disease biology and direct further targeted studies [100].

In this thesis work, proteomic profiling of a large cohort of primary murine PDAC cell lines with distinct oncogenic mutations (Fig. 3.18 A) aimed to characterize putative functional strategies within the different PDAC cell cohorts. As shown in 3.2.1 and discussed in 4.2, the results demonstrated that proteomic signatures in PDAC resemble at a lower extent the well-defined genetic differences between the given groups, since it was

found that different PDAC cohorts share functional pathways related to energy production (Figs. 3.20 and 3.21). Moreover, in the KRAS-driven epithelial cohort, the analysis additionally showed that the recently characterized transcriptomic clusters [143] are not entirely maintained on the proteome level (Figs. 3.23 and 3.24), demonstrating that oncogenic KRAS signaling results in functional discrepancies on the proteome level in this subgroup of KRAS-driven PDAC tumors. Therefore, proteomic profiling of previously established transcriptomic subtypes is key to identify subtype-specific protein biomarkers [100]. Regarding the PDAC cohorts included in this thesis work, the identified functional differences could be translated as vulnerabilities that could lead to development of novel targets for therapeutic purposes. The integration of genomic, transcriptomic and proteomic data has led to the emerging field of proteogenomics that advocates a comprehensive understanding of cancer biology that would allow to target functional determinants which cannot derive alone from genomic analysis of tumors [100].

It is important to note that the proteomic characterization of PDAC cohorts was based on primary cell lines without including bulk tumor samples. Given the heterogeneous tumor microenvironment (TME) in PDAC (section 1.6.3), the generation of primary cancer cell lines is advantageous because it allows the study of direct outputs of cancer cells and excludes any probable masking from other cell types. Transcriptomic profiling of bulk tumor samples has been used to estimate the proportions of cell populations and their gene expression profiles (deconvolution) [189]. RNA sequencing (RNA-seq) data of primary cell lines from the correspoding tumors can be used as "pure" reference signals to better estimate tumor composition that could indicate different subtypes [189]. Intriguingly, the last few years, bioinformatics tools have been developed to extrapolate gene expression information from single-cell RNA-seq experiments in oncology [190]. As a future perspective, such an analytical approach could be applied in PDAC using proteomic profiling of bulk tumor samples, since the importance of proteomic analysis in

human disease studies has been shown to outperform transcriptomic profiling [99]. Even more exciting would be the possibility to perform single-cell proteomics with PDAC tissue, both primary and metastatic, which could unravel functional vulnerabilities within the TME, but also in relation to tumor progression.

Numerous studies have shown that desmoplastic reaction is an important feature in PDAC [83] (see also section 1.6.3) and has been correlated with chemoresistance [191] and poor prognosis in preclinical studies [192]. A recent proteomic study distinguished and characterized the extracellular matrix (ECM) proteins produced by tumor and stromal cells during PDAC progression [193]. The authors showed that the stromal-derived ECM proteins have both pro- and antitumorigenic effects, while tumor cell-derived ECM proteins strongly associated with poor patient survival [193]. Therefore, the work of my thesis together with this study highlights the importance of proteomic analyses for better understanding of PDAC biology and predicting translational outputs, since TME is an integral part of the PDAC tissue.

What is more, one of the most exciting areas in PDAC research is the identification of protein biomarkers for diagnostic purposes and prediction of treatment response. First, one of the major bottlenecks in PDAC treatment is the lack of symptoms at the early stage. MS-based proteomic studies using diverse quantification methods (iTRAQ [194], TMT-labelling [195] or label-free [196]), and a variety of validation methods (ELISA [194], [195], Immunohistochemistry [197] or Targeted proteomics [198]) in other tumors or healthy controls have intensified the potential for novel biomarker discovery that could be linked as reliably as possible to early disease onset. The original biofluid material in those studies was serum or plasma, since a non-invasive method for diagnostic purposes is preferable [199]. In addition, several recent studies have shown that MS-based proteomics can identify predictive and prognostic biomarkers. Those studies are inherently more analytically challenging, because they rely on fixed PDAC tissue [200], [201], which is at

the same time necessary for translational outcomes. Fewer studies have used pancreatic juice or urine as biofluid starting material [199]. Advanced technologies such as automated laser-assisted microdissection together with unbiased proteomic analyses have been employed in PDAC [201] and in other cancer types [202] for improving patient phenotyping and stratification that could enable prediction response to treatment. In this context, as aforementioned, it would be highly interesting to perform proteomic profiling of PDAC tissue and use the findings from the PDAC cell lines to draw plausible conclusions about functional vulnerabilities of tumor cells as well as of the surrounding cell populations.

Conclusively, the work presented in this thesis would aim to combine the knowledge acquired both from studying circadian rhythms and characterizing proteome outputs in PDAC. Ultimately, a translational perspective would be to perform a time-course administration of drug targets that were identified as functional vulnerabilities by integrating the circadian clock functionality in the proteomic analysis (Fig. 3.2.2). For example, a drug screening experiment including autophagy-related agents could be performed at different times-of-day (e.g., every four or six hours) after phase synchronization with dexamethasone using Bmal1-proficient and Bmal1-deficient PDAC cells. The drug response would be directly linked to cell survival which could be assessed at a certain time after drug administration (e.g., 72 hours) -adjusted to each time point- by performing a cytotoxicity assay (e.g., see 2.1.4.1). In addition, a complementary experiment for proteomic analysis after the drug treatment at the corresponding time points of highest and lowest cytotoxicity could identify clock-controlled pathways likely linked to the drug response at specific time of day. Thereby, the integrated clock-regulated proteome profiling would validate the effect of circadian timed drug administration on survival *it vitro* paving the way to employ circadian drug administration *in vivo*.

The importance of studying circadian rhythms in disease, and particularly in can-

cer, has augmented the last decade, and several lines of evidence support the idea of chronomodulation of drug delivery in patients. In the context of PDAC, current conventional therapies improve marginally patient survival, because resistance mechanisms are promoted by both the plasticity of tumor cell metabolism and the complex tumor microenvironment. As a future challenge in the field would be to integrate the invaluable information generated by the systems-wide studies, and also, to apply chronotherapy in the clinic given that novel multimodal treatment strategies are to be developed for the continuous fight against such an aggressive malignancy as PDAC.

References

[1] V. D. Gao, S. Morley-Fletcher, S. Maccari, M. H. Vitaterna, and F. W. Turek, "Resource competition shapes biological rhythms and promotes temporal niche differentiation in a community simulation," *Ecol. Evol.*, vol. 10, no. 20, pp. 11322–11334, 2020. (Cited on page 3.)

[2] M. Stolarz, "Circumnutation as a visible plant action and reaction," *Plant Signaling and Behavior*, vol. 4, no. 5, pp. 380–387, 2009. (Cited on page 3.)

[3] S. Gibo and H. Ito, "Discrete and ultradiscrete models for biological rhythms comprising a simple negative feedback loop," *Journal of Theoretical Biology*, vol. 378, pp. 89–95, 2015. (Cited on page 3.)

[4] B. Helm, R. Ben-Shlomo, M. J. Sheriff, R. A. Hut, R. Foster, B. M. Barnes, and D. Dominoni, "Annual rhythms that underlie phenology: Biological time-keeping meets environmental change," *Proc. R. Soc. B Biol. Sci.*, vol. 280, no. 1765, 2013. (Cited on page 3.)

[5] T. Roenneberg and M. Merrow, "The circadian clock and human health," *Curr. Biol.*, vol. 26, no. 10, pp. R432–R443, 2016. (Cited on pages 3, 10, 12, 33 and 144.)

[6] C. T. Hotta, M. J. Gardner, K. E. Hubbard, S. J. Baek, N. Dalchau, D. Suhita, A. N. Dodd, and A. A. Webb, "Modulation of environmental responses of plants by circadian clocks," *Plant, Cell Environ.*, vol. 30, no. 3, pp. 333–349, 2007. (Cited on page 3.)

[7] U. Schibler and P. Sassone-Corsi, "A Web of Circadian Pacemakers," *Cell*, vol. 111, no. 7, pp. 919–922, 2002. (Cited on page 4.)

[8] T. Roenneberg, "The complex circadian system of Gonyaulax polyedra," *Physiologia Plantarum*, vol. 96, no. 4, pp. 733–737, 1996. (Cited on page 4.)

[9] T. Roenneberg and M. Merrow, "Circadian clocks â€" the fall and rise of physiology," *Nat. Rev. Mol. Cell Biol.*, vol. 6, no. 12, pp. 965–971, 2005. (Cited on pages 4 and 7.)

[10] C. S. Pittendrigh, "Circadian Rhythms and the Circadian Organization of Living Systems," *Cold Spring Harbor Symposia on Quantitative Biology*, vol. 25, pp. 159–184, 1960. (Cited on page 5.)

[11] I. Edery, "Circadian rhythms in a nutshell," *Physiological Genomics*, vol. 3, no. 2, pp. 59–74, 2000. (Cited on page 5.)

[12] D. M. J., "Observation botanique," *Histoire de l Academie Royale des Sciences*, pp. 35–36, 1729. (Cited on page 5.)

[13] J. N. Mills, D. S. Minors, and J. M. Waterhouse, "The circadian rhythms of human subjects without timepieces or indication of the alternation of day and night," *The Journal of Physiology*, vol. 240, no. 3, pp. 567–594, 1974. (Cited on page 5.)

[14] C. P. Richter, "Inherent twenty-four hour and lunar clocks of a primate-the squirrel monkey," *mmun . Behav. Biol.*, vol. 1, pp. 305–332, 1968. (Cited on page 5.)

[15] J. Aschoff, E. Poeppel, and R. Wever, "Circadiane Periodik des Menschen unter dem Einfluss von Licht-Dunkel-Wechseln unterschiedlicher Periode," *Pfluegers Arch. Eur. J. Physiol.*, vol. 306, no. 1, pp. 58–70, 1969. (Cited on page 6.)

[16] M. Merrow, M. Brunner, and T. Roenneberg, "Assignment of circadian function for the Neurospora clock gene frequency," *Nature*, vol. 399, no. 6736, pp. 584–586, 1999. (Cited on page 7.)

[17] E. D. Buhr, S.-H. Yoo, and J. S. Takahashi, "Temperature as a Universal Resetting Cue for Mammalian Circadian Oscillators," *Science*, vol. 330, no. 6002, pp. 379–385, 2010. (Cited on pages 7 and 14.)

[18] K. Kinouchi and P. Sassone-Corsi, "Metabolic rivalry: circadian homeostasis and tumorigenesis," *Nat. Rev. Cancer*, vol. 20, no. 11, pp. 645–661, 2020. (Cited on pages 8, 38, 39 and 142.)

[19] U. Albrecht, "Timing to Perfection: The Biology of Central and Peripheral Circadian Clocks," *Neuron*, vol. 74, no. 2, pp. 246–260, 2012. (Cited on page 7.)

[20] J. A. Mohawk, C. B. Green, and J. S. Takahashi, "Central and Peripheral Circadian Clocks in Mammals," *Annual Review of Neuroscience*, vol. 35, no. 1, pp. 445–462, 2012. (Cited on page 7.)

[21] J. Bass and J. S. Takahashi, "Circadian Integration of Metabolism and Energetics," *Science*, vol. 330, no. 6009, pp. 1349–1354, 2010. (Cited on page 7.)

[22] F. Damiola, N. Le Minli, N. Preitner, B. Kornmann, F. Fleury-Olela, and U. Schibler, "Restricted feeding uncouples circadian oscillators in peripheral tissues from the central pacemaker in the suprachiasmatic nucleus," *Genes Dev.*, vol. 14, no. 23, pp. 2950–2961, 2000. (Cited on page 7.)

[23] S. Yamazaki, R. Numano, M. Abe, A. Hida, R. ichi Takahashi, M. Ueda, G. D. Block, Y. Sakaki, M. Menaker, and H. Tei, "Resetting Central and Peripheral Circadian Oscillators in Transgenic Rats," *Science*, vol. 288, no. 5466, pp. 682–685, 2000. (Cited on page 8.)

[24] D. K. Welsh, S.-H. Yoo, A. C. Liu, J. S. Takahashi, and S. A. Kay, "Bioluminescence Imaging of Individual Fibroblasts Reveals Persistent, Independently Phased Circa-

dian Rhythms of Clock Gene Expression," *Current Biology*, vol. 14, no. 24, pp. 2289–2295, 2004. (Cited on page 8.)

[25] M. Akashi, Y. Tsuchiya, T. Yoshino, and E. Nishida, "Control of Intracellular Dynamics of Mammalian Period Proteins by Casein Kinase I epsilon (CKIepsilon) and CKIdelta in cultured cells," *Molecular and Cellular Biology*, vol. 22, no. 6, pp. 1693–1703, 2002. (Cited on page 10.)

[26] L. Busino, F. Bassermann, A. Maiolica, C. Lee, P. M. Nolan, S. I. H. Godinho, G. F. Draetta, and M. Pagano, "SCFFbxl3 Controls the Oscillation of the Circadian Clock by Directing the Degradation of Cryptochrome Proteins," *Science*, vol. 316, no. 5826, pp. 900–904, 2007. (Cited on page 10.)

[27] E. D. Buhr and J. S. Takahashi, "Molecular Components of the Mammalian Circadian Clock," *Handbook of Experimental Pharmacology*, vol. 217, pp. 3–27, 2013. (Cited on page 10.)

[28] S. Panda, M. P. Antoch, B. H. Miller, A. I. Su, A. B. Schook, M. Straume, P. G. Schultz, S. A. Kay, J. S. Takahashi, and J. B. Hogenesch, "Coordinated Transcription of Key Pathways in the Mouse by the Circadian Clock," *Cell*, vol. 109, no. 3, pp. 307–320, 2002. (Cited on pages 10 and 133.)

[29] R. Zhang, N. F. Lahens, H. I. Ballance, M. E. Hughes, and J. B. Hogenesch, "A circadian gene expression atlas in mammals: Implications for biology and medicine," *Proceedings of the National Academy of Sciences*, vol. 111, no. 45, pp. 16219–16224, 2014. (Cited on page 10.)

[30] "Painting, fire-fighting, and shiftwork," *IARC monographs on the evaluation of carcinogenic risks to humans*, vol. 98, 2010. (Cited on page 10.)

[31] S. Sahar and P. Sassone-Corsi, "Metabolism and cancer: The circadian clock connection," *Nat. Rev. Cancer*, vol. 9, no. 12, pp. 886–896, 2009. (Cited on page 11.)

[32] J. D. Levine, P. Funes, H. B. Dowse, and J. C. Hall, "Signal analysis of behavioral and molecular cycles," *BMC Neurosci.*, vol. 3, pp. 1–25, 2002. (Cited on pages 11, 12, 15, 16, 18, 19 and 20.)

[33] E. D. Herzog, I. Z. Kiss, and C. Mazuski, "Measuring Synchrony in the Mammalian Central Circadian Circuit," *Methods in Enzymology*, vol. 552, pp. 3–22, 2015. (Cited on pages 12, 17, 20 and 21.)

[34] M. Merrow and M. Harrington, "A functional context for heterogeneity of the circadian clock in cells," *PLOS Biology*, vol. 18, pp. 1–7, 10 2020. (Cited on page 12.)

[35] R. Refinetti, G. CornÃ©lissen, and F. Halberg, "Procedures for numerical analysis of circadian rhythms," *Biological Rhythm Research*, vol. 38, no. 4, pp. 275–325, 2007. (Cited on pages 13, 19 and 20.)

[36] D. K. Welsh and S. A. Kay, "Bioluminescence imaging in living organisms," *Current Opinion in Biotechnology*, vol. 16, no. 1, pp. 73–78, 2005. (Cited on pages 13 and 14.)

[37] S. J. Kuhlman, J. E. Quintero, and D. G. McMahon, "GFP fluorescence reports Period 1 circadian gene regulation in the mammalian biological clock," *Neuroreport*, vol. 11, no. 7, 2000. (Cited on page 13.)

[38] J. S. O'Neill, E. S. Maywood, J. E. Chesham, J. S. Takahashi, and M. H. Hastings, "cAMP-Dependent Signaling as a Core Component of the Mammalian Circadian Pacemaker," *Science*, vol. 320, no. 5878, pp. 949–953, 2008. (Cited on page 13.)

[39] T. Kondo, C. A. Strayer, R. D. Kulkarni, W. Taylor, M. Ishiura, S. S. Golden, and C. H. Johnson, "Circadian rhythms in prokaryotes: luciferase as a reporter of circadian

gene expression in cyanobacteria.," *Proceedings of the National Academy of Sciences*, vol. 90, no. 12, pp. 5672–5676, 1993. (Cited on page 13.)

[40] K. A. Hicks, A. J. Millar, I. A. Carre, D. E. Somers, M. Straume, D. R. Meeks-Wagner, and S. A. Kay, "Conditional Circadian Dysfunction of the Arabidopsis early-flowering 3 Mutant," *Science*, vol. 274, no. 5288, pp. 790–792, 1996. (Cited on page 13.)

[41] S. Yamaguchi, M. Kobayashi, S. Mitsui, Y. Ishida, G. T. J. van der Horst, M. Suzuki, S. Shibata, and H. Okamura, "View of a mouse clock gene ticking," *Nature*, vol. 409, no. 6821, p. 684, 2001. (Cited on page 13.)

[42] A. Balsalobre, S. A. Brown, L. Marcacci, F. Tronche, C. Kellendonk, H. M. Reichardt, G. SchÃ¼tz, and U. Schibler, "Resetting of Circadian Time in Peripheral Tissues by Glucocorticoid Signaling," *Science*, vol. 289, no. 5488, pp. 2344–2347, 2000. (Cited on pages 14 and 127.)

[43] K. Yagita and H. Okamura, "Forskolin induces circadian gene expression of rPer1, rPer2 and dbp in mammalian rat-1 fibroblasts," *FEBS Letters*, vol. 465, no. 1, pp. 79–82, 2000. (Cited on page 14.)

[44] H. Jung, Y. Choe, H. Kim, N. Park, G. H. Son, I. Khang, and K. Kim, "Involvement of CLOCK:BMAL1 heterodimer in serum-responsive mPer1 induction," *Neuroreport*, vol. 14, no. 1, 2003. (Cited on page 14.)

[45] S. A. Brown, G. Zumbrunn, F. Fleury-Olela, N. Preitner, and U. Schibler, "Rhythms of Mammalian Body Temperature Can Sustain Peripheral Circadian Clocks," *Current Biology*, vol. 12, no. 18, pp. 1574–1583, 2002. (Cited on page 14.)

[46] J. H. Meijer and W. J. Schwartz, "In Search of the Pathways for Light-Induced Pacemaker Resetting in the Suprachiasmatic Nucleus," *Journal of Biological Rhythms*, vol. 18, no. 3, pp. 235–249, 2003. (Cited on page 14.)

[47] H. S. Shim, H. Kim, J. Lee, G. H. Son, S. Cho, T. H. Oh, S. H. Kang, D.-S. Seen, K. H. Lee, and K. Kim, "Rapid activation of CLOCK by Ca2+-dependent protein kinase C mediates resetting of the mammalian circadian clock," *EMBO reports*, vol. 8, no. 4, pp. 366–371, 2007. (Cited on page 14.)

[48] T. L. Leise, "Analysis of Nonstationary Time Series for Biological Rhythms Research," *J. Biol. Rhythms*, vol. 32, no. 3, pp. 187–194, 2017. (Cited on pages 15, 17 and 20.)

[49] M. Hamblen-coyle, R. J. Konopka, L. J. Zwiebel, H. V. Colot, H. B. Dowse, M. Rosbash, and J. C. Hall, "A New Mutation at the Period Locus of Drosophila Melanogaster With Some Novel Effects on Circadian Rhythms," *Journal of Neurogenetics*, vol. 5, no. 4, pp. 229–256, 1989. (Cited on page 15.)

[50] R. Cheong and A. Levchenko, "Oscillatory signaling processes: the how, the why and the where," *Current Opinion in Genetics and Development*, vol. 20, no. 6, pp. 665–669, 2010. (Cited on page 16.)

[51] T. L. Leise and M. E. Harrington, "Wavelet-based time series analysis of Circadian rhythms," *J. Biol. Rhythms*, vol. 26, no. 5, pp. 454–463, 2011. (Cited on page 16.)

[52] F. Halberg, Y. L. Tong, and E. A. Johnson, "Circadian System Phase - An Aspect of Temporal Morphology; Procedures and Illustrative Examples," pp. 20–48, 1967. (Cited on page 19.)

[53] J. B. J. Fourier, G. Darboux, *et al.*, "Théorie analytique de la chaleur," *Didot Paris*, vol. 504, 1822. (Cited on page 19.)

[54] T. Zielinski, A. M. Moore, E. Troup, K. J. Halliday, and A. J. Millar, "Strengths and limitations of period estimation methods for circadian data," *PLoS One*, vol. 9, no. 5, 2014. (Cited on page 20.)

[55] J. T. VanderPlas, "Understanding the Lombâ€"Scargle Periodogram," *Astrophys. J. Suppl. Ser.*, vol. 236, no. 1, p. 16, 2018. (Cited on page 20.)

[56] M. C. Tackenberg and J. J. Hughey, "The risks of using the chi-square periodogram to estimate the period of biological rhythms," *PLOS Computational Biology*, 2021. (Cited on page 20.)

[57] R. H. Hruban, N. V. Adsay, J. Albores-Saavedra, M. R. Anver, A. V. Biankin, G. P. Boivin, E. E. Furth, T. Furukawa, A. Klein, D. S. Klimstra, G. Kloppel, G. Y. Lauwers, D. S. Longnecker, J. Luttges, A. Maitra, G. J. A. Offerhaus, L. Perez-Gallego, M. Redston, and D. A. Tuveson, "Pathology of genetically engineered mouse models of pancreatic exocrine cancer: Consensus report and recommendations," *Cancer Res.*, vol. 66, no. 1, pp. 95–106, 2006. (Cited on pages 22, 23, 26 and 27.)

[58] M. H. Cleveland, J. M. Sawyer, S. Afelik, J. Jensen, and S. D. Leach, "Exocrine ontogenies: On the development of pancreatic acinar, ductal and centroacinar cells," *Seminars in Cell and Developmental Biology*, vol. 23, no. 6, pp. 711–719, 2012. (Cited on page 22.)

[59] Q. Zhou, J. Brown, A. Kanarek, J. Rajagopal, and D. A. Melton, "In vivo reprogramming of adult pancreatic exocrine cells to β-cells," *Nature*, vol. 455, no. 7213, pp. 627–632, 2008. (Cited on page 22.)

[60] J. Liu, N. Akanuma, C. Liu, A. Naji, G. A. Halff, W. K. Washburn, L. Sun, and P. Wang, "TGF-β1 promotes acinar to ductal metaplasia of human pancreatic acinar cells," *Sci. Rep.*, vol. 6, no. August, pp. 1–11, 2016. (Cited on page 23.)

[61] J. Kleeff, M. Korc, M. Apte, C. La Vecchia, C. D. Johnson, A. V. Biankin, R. E. Neale, M. Tempero, D. A. Tuveson, R. H. Hruban, and J. P. Neoptolemos, "Pancreatic cancer," *Nat. Rev. Dis. Prim.*, vol. 2, no. 1, p. 16022, 2016. (Cited on page 23.)

[62] J. L. Soto, V. M. Barbera, M. Saceda, and A. Carrato, "Molecular biology of exocrine pancreatic cancer," *Clin. Transl. Oncol.*, vol. 8, no. 5, pp. 306–312, 2006. (Cited on pages 24 and 27.)

[63] P. Ghaneh, E. Costello, and J. P. Neoptolemos, "Biology and management of pancreatic cancer," *Postgrad. Med. J.*, vol. 84, no. 995, pp. 478–497, 2008. (Cited on pages 24 and 25.)

[64] N. Bardeesy, K.-h. Cheng, J. H. Berger, G. C. Chu, J. Pahler, P. Olson, A. F. Hezel, J. Horner, G. Y. Lauwers, D. Hanahan, *et al.*, "Smad4 is dispensable for normal pancreas development yet critical in progression and tumor biology of pancreas cancer," *Genes & development*, vol. 20, no. 22, pp. 3130–3146, 2006. (Cited on page 24.)

[65] J. Guo, K. Xie, and S. Zheng, "Molecular Biomarkers of Pancreatic Intraepithelial Neoplasia and Their Implications in Early Diagnosis and Therapeutic Intervention of Pancreatic Cancer," *Int J Biol Sci*, vol. 12, pp. 292–301, 2016. (Cited on page 24.)

[66] H. Ying, P. Dey, W. Yao, A. C. Kimmelman, G. F. Draetta, A. Maitra, and R. A. Depinho, "Genetics and biology of pancreatic ductal adenocarcinoma," *Genes Dev.*, vol. 30, no. 4, pp. 355–385, 2016. (Cited on page 25.)

[67] J. Lee, K.-T. Jang, C.-S. Ki, T. Lim, Y. S. Park, H. Y. Lim, D.-W. Choi, W. K. Kang, K. Park, and J. O. Park, "Impact of epidermal growth factor receptor (EGFR) kinase mutations, EGFR gene amplifications, and KRAS mutations on survival of pancreatic adenocarcinoma," *Cancer*, vol. 109, no. 8, pp. 1561–1569, 2007. (Cited on page 25.)

[68] J. M. Stommel, A. C. Kimmelman, H. Ying, R. Nabioullin, A. H. Ponugoti, R. Wiedemeyer, A. H. Stegh, J. E. Bradner, K. L. Ligon, C. Brennan, L. Chin, and R. A. DePinho, "Coactivation of receptor tyrosine kinases affects the response of tumor cells to targeted therapies," *Science*, vol. 318, no. 5848, pp. 287–290, 2007. (Cited on page 25.)

[69] B. A. Ruggeri, L. Huang, M. Wood, J. Q. Cheng, and J. R. Testa, "Amplification and overexpression of the AKT2 oncogene in a subset of human pancreatic ductal adenocarcinomas," *Molecular Carcinogenesis*, vol. 21, no. 2, pp. 81–86, 1998. (Cited on page 25.)

[70] D. Mossmann, S. Park, and M. N. Hall, "mTOR signalling and cellular metabolism are mutual determinants in cancer," *Nat. Rev. Cancer*, vol. 18, no. 12, pp. 744–757, 2018. (Cited on page 26.)

[71] L. Buscail, B. Bournet, and P. Cordelier, "Role of oncogenic KRAS in the diagnosis, prognosis and treatment of pancreatic cancer," *Nat. Rev. Gastroenterol. Hepatol.*, vol. 17, no. 3, pp. 153–168, 2020. (Cited on page 26.)

[72] M. Ayres Pereira and I. I. C. Chio, "Metastasis in Pancreatic Ductal Adenocarcinoma: Current Standing and Methodologies," *Genes*, vol. 11, no. 1, p. 6, 2020. (Cited on pages 27 and 31.)

[73] W. W. Tseng, D. Winer, J. A. Kenkel, O. Choi, A. H. Shain, J. R. Pollack, R. French, A. M. Lowy, and E. G. Engleman, "Development of an orthotopic model of invasive

pancreatic cancer in an immunocompetent murine host," *Clin. Cancer Res.*, vol. 16, no. 14, pp. 3684–3695, 2010. (Cited on page 27.)

[74] M. K. Sung, Y. Park, B. J. Kwak, E. Jun, W. Lee, K. B. Song, J. H. Lee, D. W. Hwang, and S. C. Kim, "Comparison of Characteristics and Survival Rates of Resectable Pancreatic Ductal Adenocarcinoma according to Tumor Location," *Biomedicines*, vol. 9, no. 11, 2021. (Cited on page 27.)

[75] M. Orth, P. Metzger, S. Gerum, J. Mayerle, G. Schneider, C. Belka, M. Schnurr, and K. Lauber, "Pancreatic ductal adenocarcinoma: biological hallmarks, current status, and future perspectives of combined modality treatment approaches," *Radiat. Oncol.*, vol. 14, no. 1, p. 141, 2019. (Cited on pages 27 and 29.)

[76] P. Rawla, T. Sunkara, and V. Gaduputi, "Epidemiology of Pancreatic Cancer: Global Trends, Etiology and Risk Factors," *World Journal of Oncology*, vol. 10, no. 1, 2019. (Cited on page 28.)

[77] J. Font-Burgada, B. Sun, and M. Karin, "Obesity and Cancer: The Oil that Feeds the Flame," *Cell Metabolism*, vol. 23, no. 1, pp. 48–62, 2016. (Cited on page 28.)

[78] S. Rahn, V. Zimmermann, F. Viol, H. Knaack, K. Stemmer, L. Peters, L. Lenk, H. Ungefroren, D. Saur, H. SchÃ¤fer, O. Helm, and S. Sebens, "Diabetes as risk factor for pancreatic cancer: Hyperglycemia promotes epithelial-mesenchymal-transition and stem cell properties in pancreatic ductal epithelial cells," *Cancer Letters*, vol. 415, pp. 129–150, 2018. (Cited on page 28.)

[79] S. M. Gapstur, E. J. Jacobs, A. Deka, M. L. McCullough, A. V. Patel, and M. J. Thun, "Association of Alcohol Intake With Pancreatic Cancer Mortality in Never Smokers," *Arch. Intern. Med.*, vol. 171, no. 5, pp. 444–451, 2011. (Cited on page 28.)

[80] D. Hu, D. Ansari, K. Pawlowski, Q. Zhou, A. Sasor, C. Welinder, T. Kristl, M. Bauden, M. Rezeli, Y. Jiang, G. Marko-Varga, and R. Andersson, "Proteomic analyses identify prognostic biomarkers for pancreatic ductal adenocarcinoma," *Oncotarget*, vol. 9, no. 11, pp. 9789–9807, 2018. (Cited on page 28.)

[81] S. Wang, Y. Zheng, F. Yang, L. Zhu, X.-Q. Zhu, Z.-F. Wang, X.-L. Wu, C.-H. Zhou, J.-Y. Yan, B.-Y. Hu, B. Kong, D.-L. Fu, C. Bruns, Y. Zhao, L.-X. Qin, and Q.-Z. Dong, "The molecular biology of pancreatic adenocarcinoma: translational challenges and clinical perspectives," *Signal Transduct. Target. Ther.*, vol. 6, no. 1, p. 249, 2021. (Cited on pages 28, 129, 131 and 146.)

[82] N. A. Ottenhof, R. F. de Wilde, A. Maitra, R. H. Hruban, and G. J. A. Offerhaus, "Molecular Characteristics of Pancreatic Ductal Adenocarcinoma," *Patholog. Res. Int.*, vol. 2011, pp. 1–16, 2011. (Cited on page 28.)

[83] A. Bulle and K.-H. Lim, "Beyond just a tight fortress: contribution of stroma to epithelial-mesenchymal transition in pancreatic cancer," *Signal Transduct. Target. Ther.*, vol. 5, no. 1, p. 249, 2020. (Cited on pages 28, 29 and 151.)

[84] Z. A. Rasheed, W. Matsui, and A. Maitra, "Pathology of pancreatic stroma in PDAC," *Transworld Research Network, Trivandrum (India)*, 2012. (Cited on pages 29 and 138.)

[85] D. Gaglio, C. M. Metallo, P. A. Gameiro, K. Hiller, L. S. Danna, C. Balestrieri, L. Alberghina, G. Stephanopoulos, and F. Chiaradonna, "Oncogenic K-Ras decouples glucose and glutamine metabolism to support cancer cell growth," *Molecular Systems Biology*, vol. 7, no. 1, p. 523, 2011. (Cited on pages 29 and 131.)

[86] H. Ying, A. C. Kimmelman, C. A. Lyssiotis, S. Hua, G. C. Chu, E. Fletcher-Sananikone, J. W. Locasale, J. Son, H. Zhang, J. L. Coloff, H. Yan, W. Wang, S. Chen,

A. Viale, H. Zheng, J. H. Paik, C. Lim, A. R. Guimaraes, E. S. Martin, J. Chang, A. F. Hezel, S. R. Perry, J. Hu, B. Gan, Y. Xiao, J. M. Asara, R. Weissleder, Y. A. Wang, L. Chin, L. C. Cantley, and R. A. Depinho, "Oncogenic kras maintains pancreatic tumors through regulation of anabolic glucose metabolism," *Cell*, vol. 149, no. 3, pp. 656–670, 2012. (Cited on pages 29, 30, 131 and 134.)

[87] J. Son, C. A. Lyssiotis, H. Ying, X. Wang, S. Hua, M. Ligorio, R. M. Perera, C. R. Ferrone, E. Mullarky, N. Shyh-Chang, Y. Kang, J. B. Fleming, N. Bardeesy, J. M. Asara, M. C. Haigis, R. A. DePinho, L. C. Cantley, and A. C. Kimmelman, "Glutamine supports pancreatic cancer growth through a KRAS-regulated metabolic pathway," *Nature*, vol. 496, no. 7443, pp. 101–105, 2013. (Cited on page 30.)

[88] J.-T. Li, Y.-P. Wang, M. Yin, and Q.-Y. Lei, "Metabolism remodeling in pancreatic ductal adenocarcinoma," *Cell Stress*, vol. 3, no. 12, pp. 361–368, 2019. (Cited on page 30.)

[89] A. Kelekar, "Autophagy," *Annals of the New York Academy of Sciences*, vol. 1066, no. 1, pp. 259–271, 2006. (Cited on page 30.)

[90] E. Michalopoulou, V. Bulusu, and J. J. Kamphorst, "Metabolic scavenging by cancer cells: When the going gets tough, the tough keep eating," *Br. J. Cancer*, vol. 115, no. 6, pp. 635–640, 2016. (Cited on pages 30 and 139.)

[91] S. Y. Wong and R. O. Hynes, "Lymphatic or hematogenous dissemination: How does a metastatic tumor cell decide?," *Cell Cycle*, vol. 5, no. 8, pp. 812–817, 2006. (Cited on page 30.)

[92] P. J. Miettinen, R. Ebner, A. R. Lopez, and R. Derynck, "TGF-β induced transdifferentiation of mammary epithelial cells to mesenchymal cells: Involvement of type

I receptors," *J. Cell Biol.*, vol. 127, no. 6 II, pp. 2021–2036, 1994. (Cited on pages 30 and 31.)

[93] G. Greenburg and E. D. Hay, "Epithelia suspended in collagen gels can lose polarity and express characteristics of migrating mesenchymal cells," *J. Cell Biol.*, vol. 95, no. 1, pp. 333–339, 1982. (Cited on page 31.)

[94] P. Papageorgis, "TGF β signaling in tumor initiation, epithelial-to-mesenchymal transition, and metastasis," *J. Oncol.*, vol. 2015, 2015. (Cited on page 31.)

[95] A. P. Makohon-Moore, M. Zhang, J. G. Reiter, I. Bozic, B. Allen, D. Kundu, K. Chatterjee, F. Wong, Y. Jiao, Z. A. Kohutek, J. Hong, M. Attiyeh, B. Javier, L. D. Wood, R. H. Hruban, M. A. Nowak, N. Papadopoulos, K. W. Kinzler, B. Vogelstein, and C. A. Iacobuzio-Donahue, "Limited heterogeneity of known driver gene mutations among the metastases of individual patients with pancreatic cancer," *Nat. Genet.*, vol. 49, no. 3, pp. 358–366, 2017. (Cited on page 31.)

[96] E. A. Collisson, A. Sadanandam, P. Olson, W. J. Gibb, S. Gu, J. Cooc, J. Weinkle, G. E. Kim, L. Jakkula, H. S. Feiler, A. H. Ko, A. B. Olshen, K. L. Danenberg, A. Margaret, P. T. Spellman, D. Hanahan, and J. W. Gray, "Subtypes of Pancreatic Ductal Adenocarcinoma and Their Differing Responses to Therapy," *Nat med*, vol. 17, no. 4, pp. 500–503, 2011. (Cited on page 32.)

[97] R. A. Moffitt, R. Marayati, E. L. Flate, K. E. Volmar, S. G. H. Loeza, K. A. Hoadley, N. U. Rashid, L. A. Williams, S. C. Eaton, A. H. Chung, J. K. Smyla, J. M. Anderson, H. J. Kim, D. J. Bentrem, M. S. Talamonti, C. A. Iacobuzio-Donahue, M. A. Hollingsworth, and J. J. Yeh, "Virtual microdissection identifies distinct tumor- and stroma-specific subtypes of pancreatic ductal adenocarcinoma," *Nat. Genet.*, vol. 47, no. 10, pp. 1168–1178, 2015. (Cited on page 32.)

[98] P. Bailey, D. K. Chang, K. Nones, A. L. Johns, A. M. Patch, M. C. Gingras, D. K. Miller, A. N. Christ, T. J. Bruxner, M. C. Quinn, C. Nourse, L. C. Murtaugh, I. Harliwong, S. Idrisoglu, S. Manning, E. Nourbakhsh, S. Wani, L. Fink, O. Holmes, V. Chin, M. J. Anderson, S. Kazakoff, C. Leonard, F. Newell, N. Waddell, S. Wood, Q. Xu, P. J. Wilson, N. Cloonan, K. S. Kassahn, D. Taylor, K. Quek, A. Robertson, L. Pantano, L. Mincarelli, L. N. Sanchez, L. Evers, J. Wu, M. Pinese, M. J. Cowley, M. D. Jones, E. K. Colvin, A. M. Nagrial, E. S. Humphrey, L. A. Chantrill, A. Mawson, J. Humphris, A. Chou, M. Pajic, C. J. Scarlett, A. V. Pinho, M. Giry-Laterriere, I. Rooman, J. S. Samra, J. G. Kench, J. A. Lovell, N. D. Merrett, C. W. Toon, K. Epari, N. Q. Nguyen, A. Barbour, N. Zeps, K. Moran-Jones, N. B. Jamieson, J. S. Graham, F. Duthie, K. Oien, J. Hair, R. Grützmann, A. Maitra, C. A. Iacobuzio-Donahue, C. L. Wolfgang, R. A. Morgan, R. T. Lawlor, V. Corbo, C. Bassi, B. Rusev, P. Capelli, R. Salvia, G. Tortora, D. Mukhopadhyay, G. M. Petersen, D. M. Munzy, W. E. Fisher, S. A. Karim, J. R. Eshleman, R. H. Hruban, C. Pilarsky, J. P. Morton, O. J. Sansom, A. Scarpa, E. A. Musgrove, U. M. H. Bailey, O. Hofmann, R. L. Sutherland, D. A. Wheeler, A. J. Gill, R. A. Gibbs, J. V. Pearson, N. Waddell, A. V. Biankin, and S. M. Grimmond, "Genomic analyses identify molecular subtypes of pancreatic cancer," *Nature*, vol. 531, no. 7592, pp. 47–52, 2016. (Cited on page 32.)

[99] J. Wang, Z. Ma, S. A. Carr, P. Mertins, H. Zhang, Z. Zhang, D. W. Chan, M. J. Ellis, R. R. Townsend, R. D. Smith, J. E. McDermott, X. Chen, A. G. Paulovich, E. S. Boja, M. Mesri, C. R. Kinsinger, H. Rodriguez, K. D. Rodland, D. C. Liebler, and B. Zhang, "Proteome Profiling Outperforms Transcriptome Profiling for Coexpression Based Gene Function Prediction," *Molecular & Cellular Proteomics*, vol. 16, no. 1, pp. 121–134, 2017. (Cited on pages 32 and 151.)

[100] T. L. Large, M. Bijlsma, G. Kazemier, H. van Laarhoven, E. Giovannetti, and

C. Jimenez, "Key biological processes driving metastatic spread of pancreatic cancer as identified by multi-omics studies," *Seminars in Cancer Biology*, vol. 44, pp. 153–169, 2017. (Cited on pages 33, 129, 149 and 150.)

[101] M.-C. Mormont and F. Levi, "Cancer chronotherapy: Principles, applications, and perspectives," *Cancer*, vol. 97, no. 1, pp. 155–169, 2003. (Cited on page 33.)

[102] E. S. Schernhammer, F. Laden, F. E. Speizer, W. C. Willett, D. J. Hunter, I. Kawachi, C. S. Fuchs, and G. A. Colditz, "Night-shift work and risk of colorectal cancer in the nurses' health study," *Journal of the National Cancer Institute*, vol. 95, no. 11, pp. 825–828, 2003. (Cited on page 33.)

[103] E. S. Schernhammer, F. Laden, F. E. Speizer, W. C. Willett, D. J. Hunter, I. Kawachi, and G. A. Colditz, "Rotating Night Shifts and Risk of Breast Cancer in Women Participating in the Nurses' Health Study," *JNCI J. Natl. Cancer Inst.*, vol. 93, no. 20, pp. 1563–1568, 2001. (Cited on page 34.)

[104] E. Cordina-Duverger, F. Menegaux, A. Popa, S. Rabstein, V. Harth, B. Pesch, T. Bruening, L. Fritschi, D. C. Glass, J. S. Heyworth, T. C. Erren, G. Castano-Vinyals, K. Papantoniou, A. Espinosa, M. Kogevinas, A. Grundy, J. J. Spinelli, K. J. Aronson, and P. Guenel, "Night shift work and breast cancer: a pooled analysis of population-based caseâ€"control studies with complete work history," *Eur. J. Epidemiol.*, vol. 33, no. 4, pp. 369–379, 2018. (Cited on page 34.)

[105] T. Kubo, K. Ozasa, K. Mikami, K. Wakai, Y. Fujino, Y. Watanabe, T. Miki, M. Nakao, K. Hayashi, K. Suzuki, M. Mori, M. Washio, F. Sakauchi, Y. Ito, T. Yoshimura, and A. Tamakoshi, "Prospective Cohort Study of the Risk of Prostate Cancer among Rotating-Shift Workers: Findings from the Japan Collaborative Cohort Study," *Am. J. Epidemiol.*, vol. 164, no. 6, pp. 549–555, 2006. (Cited on page 34.)

[106] M. Kogevinas, A. Espinosa, A. Castello, I. Gomez-Acebo, M. Guevara, V. Martin, P. Amiano, J. Alguacil, R. Peiro, V. Moreno, L. Costas, G. Fernandez-Tardon, J. J. Jimenez, R. Marcos-Gragera, B. Perez-Gomez, J. Llorca, C. Moreno-Iribas, T. Fernandez-Villa, M. Oribe, N. Aragones, K. Papantoniou, M. Pollan, G. Castano-Vinyals, and D. Romaguera, "Effect of mistimed eating patterns on breast and prostate cancer risk (MCC-Spain Study)," *International Journal of Cancer*, vol. 143, no. 10, pp. 2380–2389, 2018. (Cited on page 34.)

[107] T. Papagiannakopoulos, M. R. Bauer, S. M. Davidson, M. Heimann, L. Subbaraj, A. Bhutkar, J. Bartlebaugh, M. G. Vander Heiden, and T. Jacks, "Circadian Rhythm Disruption Promotes Lung Tumorigenesis," *Cell Metab.*, vol. 24, no. 2, pp. 324–331, 2016. (Cited on pages 34, 140 and 145.)

[108] K. C. V. Dycke, W. Rodenburg, C. T. van Oostrom, L. W. van Kerkhof, J. L. Pennings, T. Roenneberg, H. van Steeg, and G. T. van der Horst, "Chronically Alternating Light Cycles Increase Breast Cancer Risk in Mice," *Current Biology*, vol. 25, no. 14, pp. 1932–1937, 2015. (Cited on page 34.)

[109] V. N. Anisimov, D. A. Baturin, I. G. Popovich, M. A. Zabezhinski, K. G. Manton, A. V. Semenchenko, and A. I. Yashin, "Effect of exposure to light-at-night on life span and spontaneous carcinogenesis in female CBA mice," *International Journal of Cancer*, vol. 111, no. 4, pp. 475–479, 2004. (Cited on page 34.)

[110] S. Kiessling, L. Beaulieu-Laroche, I. D. Blum, D. Landgraf, D. K. Welsh, K. F. Storch, N. Labrecque, and N. Cermakian, "Enhancing circadian clock function in cancer cells inhibits tumor growth," *BMC Biol.*, vol. 15, no. 1, pp. 1–18, 2017. (Cited on pages 34, 76, 126, 141 and 144.)

[111] E. Filipski, X. M. Li, and F. Lévi, "Disruption of circadian coordination and malig-

nant growth," *Cancer Causes Control*, vol. 17, no. 4, pp. 509–514, 2006. (Cited on page 35.)

[112] Y. Ye, Y. Xiang, F. M. Ozguc, Y. Kim, C.-J. Liu, P. K. Park, Q. Hu, L. Diao, Y. Lou, C. Lin, A.-Y. Guo, B. Zhou, L. Wang, Z. Chen, J. S. Takahashi, G. B. Mills, S.-H. Yoo, and L. Han, "The Genomic Landscape and Pharmacogenomic Interactions of Clock Genes in Cancer Chronotherapy," *Cell Systems*, vol. 6, no. 3, pp. 314–328, 2018. (Cited on pages 35 and 147.)

[113] S.-T. Chen, K.-B. Choo, M.-F. Hou, K.-T. Yeh, S.-J. Kuo, and J.-G. Chang, " Deregulated expression of the PER1 , PER2 and PER3 genes in breast cancers ," *Carcinogenesis*, vol. 26, no. 7, pp. 1241–1246, 2005. (Cited on pages 35 and 128.)

[114] S. L. Winter, L. Bosnoyan-Collins, D. Pinnaduwage, and I. L. Andrulis, "Expression of the Circadian Clock Genes Pert, Per2 in Sporadic, Familial Breast Tumors," *Neoplasia*, vol. 9, no. 10, pp. 797–800, 2007. (Cited on page 35.)

[115] W. Jiang, S. Zhao, J. Shen, L. Guo, Y. Sun, Y. Zhu, Z. Ma, X. Zhang, Y. Hu, W. Xiao, K. Li, S. Li, L. Zhou, L. Huang, Z. Lu, Y. Feng, J. Xiao, E. E. Zhang, L. Yang, and R. Wan, "The MiR-135bâ€"BMAL1â€"YY1 loop disturbs pancreatic clockwork to promote tumourigenesis and chemoresistance," *Cell Death Dis.*, vol. 9, no. 2, p. 149, 2018. (Cited on page 35.)

[116] H. Tokunaga, Y. Takebayahi, H. Utsunomiya, J.-I. Akahira, M. Higashimoto, M. Mashiko, K. Ito, H. Nikura, S.-I. Takenoshita, and N. Yaegashi, "Clinicopathological significance of circadian rhythm-related gene expression levels in patients with epithelial ovarian cancer," *Acta Obstetricia et Gynecologica Scandinavica*, vol. 87, no. 10, pp. 1060–1070, 2008. (Cited on page 35.)

[117] T. Oshima, S. Takenoshita, M. Akaike, C. Kunisaki, S. Fujii, A. Nozaki, K. Numata, M. Shiozawa, Y. Rino, K. Tanaka, M. Masuda, and T. Imada, "Expression of circadian genes correlates with liver metastasis and outcomes in colorectal cancer," *Oncol. Rep.*, vol. 25, no. 5, pp. 1439–1446, 2011. (Cited on page 35.)

[118] L. Fu, H. Pelicano, J. Liu, P. Huang, and C. C. Lee, "The Circadian Gene Period2 Plays an Important Role in Tumor Suppression and DNA Damage Response In Vivo," *Cell*, vol. 111, no. 1, pp. 41–50, 2002. (Cited on page 36.)

[119] E. A. Yu and D. R. Weaver, "Disrupting the circadian clock: Gene-specific effects on aging, cancer, and other phenotypes," *Aging*, vol. 3, no. 5, pp. 479–493, 2011. (Cited on page 36.)

[120] R. V. Khapre, A. A. Kondratova, S. Patel, Y. Dubrovsky, M. Wrobel, M. P. Antoch, and R. V. Kondratov, "BMAL1-dependent regulation of the mTOR signaling pathway delays aging," *Aging*, vol. 6, no. 1, pp. 48–57, 2014. (Cited on page 36.)

[121] A. Sancar, L. A. Lindsey-Boltz, T. H. Kang, J. T. Reardon, J. H. Lee, and N. Ozturk, "Circadian clock control of the cellular response to DNA damage," *FEBS Lett.*, vol. 584, no. 12, pp. 2618–2625, 2010. (Cited on page 36.)

[122] M. N. Morgan, S. Dvuchbabny, C.-A. Martinez, B. Kerr, P. A. Cistulli, and K. M. Cook, "The Cancer Clock Is (Not) Ticking: Links between Circadian Rhythms and Cancer," *Clocks and Sleep*, vol. 1, no. 4, pp. 435–458, 2019. (Cited on pages 36 and 127.)

[123] "Nuclear incorporation of P32 as demonstrated by autoradiographs," *Experimental Cell Research*. (Cited on page 37.)

[124] T. Pederson, "Historical review: An energy reservoir for mitosis, and its productive

wake," *Trends in Biochemical Sciences*, vol. 28, no. 3, pp. 125–129, 2003. (Cited on page 37.)

[125] Y. Arata and H. Takagi, "Quantitative Studies for Cell-Division Cycle Control," *Frontiers in Physiology*, vol. 10, 2019. (Cited on page 37.)

[126] D. Hanahan and R. A. Weinberg, "The Hallmarks of Cancer," *Cell*, vol. 100, no. 1, pp. 57–70, 2000. (Cited on pages 37 and 39.)

[127] S. L. Harvey, A. Charlet, W. Haas, S. P. Gygi, and D. R. Kellogg, "Cdk1-Dependent Regulation of the Mitotic Inhibitor Wee1," *Cell*, vol. 122, no. 3, pp. 407–420, 2005. (Cited on page 37.)

[128] L. Fu and N. M. Kettner, "The circadian clock in cancer development and therapy," *Progress in molecular biology and translational science*, vol. 119, pp. 221–282, 2013. (Cited on page 37.)

[129] B. J. Altman, A. L. Hsieh, A. Sengupta, S. Y. Krishnanaiah, Z. E. Stine, Z. E. Walton, A. M. Gouw, A. Venkataraman, B. Li, P. Goraksha-Hicks, S. J. Diskin, D. I. Bellovin, M. C. Simon, J. C. Rathmell, M. A. Lazar, J. M. Maris, D. W. Felsher, J. B. Hogenesch, A. M. Weljie, and C. V. Dang, "MYC Disrupts the Circadian Clock and Metabolism in Cancer Cells," *Cell Metab.*, vol. 22, no. 6, pp. 1009–1019, 2015. (Cited on pages 38, 129, 144 and 145.)

[130] A.-L. Huber, S. J. Papp, A. B. Chan, E. Henriksson, S. D. Jordan, A. Kriebs, M. Nguyen, M. Wallace, Z. Li, C. M. Metallo, and K. A. Lamia, "CRY2 and FBXL3 Cooperatively Degrade c-MYC," *Molecular Cell*, vol. 64, no. 4, pp. 774–789, 2016. (Cited on page 38.)

[131] C. Feillet, G. T. van der Horst, F. Levi, D. A. Rand, and F. Delaunay, "Coupling between the circadian clock and cell cycle oscillators: Implication for healthy cells and malignant growth," *Front. Neurol.*, vol. 6, no. MAY, pp. 1–7, 2015. (Cited on page 38.)

[132] N. M. Kettner, H. Voicu, M. J. Finegold, C. Coarfa, A. Sreekumar, N. Putluri, C. A. Katchy, C. Lee, D. D. Moore, and L. Fu, "Circadian Homeostasis of Liver Metabolism Suppresses Hepatocarcinogenesis," *Cancer Cell*, vol. 30, no. 6, pp. 909–924, 2016. (Cited on pages 39 and 140.)

[133] N. N. Guerrero-Vargas, R. Navarro-Espindola, M. A. Guzman-Ruiz, M. d. C. Basualdo, E. Espitia-Bautista, A. Lopez-Bago, R. Lascurain, C. Cordoba-Manilla, R. M. Buijs, and C. Escobar, "Circadian disruption promotes tumor growth by anabolic host metabolism; experimental evidence in a rat model," *BMC Cancer*, vol. 17, no. 1, pp. 1–13, 2017. (Cited on page 39.)

[134] F. W. Turek, C. Joshu, A. Kohsaka, E. Lin, G. Ivanova, E. McDearmon, A. Laposky, S. Losee-Olson, A. Easton, D. R. Jensen, R. H. Eckel, J. S. Takahashi, and J. Bass, "Obesity and Metabolic Syndrome in Circadian Clock Mutant Mice," *Science*, vol. 308, no. 5724, pp. 1043–1045, 2005. (Cited on page 39.)

[135] S. Masri, T. Papagiannakopoulos, K. Kinouchi, Y. Liu, M. Cervantes, P. Baldi, T. Jacks, and P. Sassone-Corsi, "Lung Adenocarcinoma Distally Rewires Hepatic Circadian Homeostasis," *Cell*, vol. 165, no. 4, pp. 896–909, 2016. (Cited on pages 39, 140 and 146.)

[136] Y. Nakahata, M. Kaluzova, B. Grimaldi, S. Sahar, J. Hirayama, D. Chen, L. P. Guarente, and P. Sassone-Corsi, "The NAD+-Dependent Deacetylase SIRT1 Modulates

CLOCK-Mediated Chromatin Remodeling and Circadian Control," *Cell*, vol. 134, no. 2, pp. 329–340, 2008. (Cited on pages 39 and 40.)

[137] J. T. Rodgers, C. Lerin, W. Haas, S. P. Gygi, B. M. Spiegelman, and P. Puigserver, "Nutrient control of glucose homeostasis through a complex of PGC-1α and SIRT1," *Nature*, vol. 434, no. 7029, pp. 113–118, 2005. (Cited on page 40.)

[138] F. Picard, M. Kurtev, N. Chung, A. Topark-Ngarm, T. Senawong, R. M. De Oliveira, M. Leid, M. W. McBurney, and L. Guarente, "Sirt1 promotes fat mobilization in white adipocytes by repressing PPAR-γ," *Nature*, vol. 429, no. 6993, pp. 771–776, 2004. (Cited on page 40.)

[139] M. C. Motta, N. Divecha, M. Lemieux, C. Kamel, D. Chen, W. Gu, Y. Bultsma, M. McBurney, and L. Guarente, "Mammalian SIRT1 Represses Forkhead Transcription Factors," *Cell*, vol. 116, no. 4, pp. 551–563, 2004. (Cited on page 40.)

[140] J. Cox and M. Mann, "MaxQuant enables high peptide identification rates, individualized p.p.b.-range mass accuracies and proteome-wide protein quantification," *Nat. Biotechnol.*, vol. 26, no. 12, pp. 1367–1372, 2008. (Cited on page 56.)

[141] S. Tyanova, T. Temu, P. Sinitcyn, A. Carlson, M. Y. Hein, T. Geiger, M. Mann, and J. Cox, "The Perseus computational platform for comprehensive analysis of (prote)omics data," *Nat. Methods*, vol. 13, no. 9, pp. 731–740, 2016. (Cited on page 57.)

[142] C. M. Sousa and A. C. Kimmelman, "The complex landscape of pancreatic cancer metabolism," *Carcinogenesis*, vol. 35, no. 7, pp. 1441–1450, 2014. (Cited on page 92.)

[143] S. Mueller, T. Engleitner, R. Maresch, M. Zukowska, S. Lange, T. Kaltenbacher, B. Konukiewitz, R. Oellinger, M. Zwiebel, A. Strong, H. Y. Yen, R. Banerjee, S. Louzada, B. Fu, B. Seidler, J. Goetzfried, K. Schuck, Z. Hassan, A. Arbeiter, N. Schoenhuber, S. Klein, C. Veltkamp, M. Friedrich, L. Rad, M. Barenboim, C. Ziegenhain, J. Hess, O. M. Dovey, S. Eser, S. Parekh, F. Constantino-Casas, J. De La Rosa, M. I. Sierra, M. Fraga, J. Mayerle, G. Kloeppel, J. Cadinanos, P. Liu, G. Vassiliou, W. Weichert, K. Steiger, W. Enard, R. M. Schmid, F. Yang, K. Unger, G. Schneider, I. Varela, A. Bradley, D. Saur, and R. Rad, "Evolutionary routes and KRAS dosage define pancreatic cancer phenotypes," *Nature*, vol. 554, no. 7690, pp. 62–68, 2018. (Cited on pages 92, 130, 136 and 150.)

[144] G. K. Paschos, J. E. Baggs, J. B. Hogenesch, and G. A. Fitzgerald, "The role of clock genes in pharmacology," *Annu. Rev. Pharmacol. Toxicol.*, vol. 50, pp. 187–214, 2010. (Cited on page 98.)

[145] A. Relogio, P. Thomas, P. Medina-Perez, S. Reischl, S. Bervoets, E. Gloc, P. Riemer, S. Mang-Fatehi, B. Maier, R. Schaefer, U. Leser, H. Herzel, A. Kramer, and C. Sers, "Ras-Mediated Deregulation of the Circadian Clock in Cancer," *PLoS Genet.*, vol. 10, no. 5, 2014. (Cited on pages 126, 141 and 144.)

[146] J. Gaucher, E. Montellier, and P. Sassone-Corsi, "Molecular Cogs: Interplay between Circadian Clock and Cell Cycle," *Trends Cell Biol.*, vol. 28, no. 5, pp. 368–379, 2018. (Cited on page 127.)

[147] Y. Xie, Q. Tang, G. Chen, M. Xie, S. Yu, J. Zhao, and L. Chen, "New insights into the circadian rhythm and its related diseases," *Front. Physiol.*, vol. 10, no. JUN, pp. 1–19, 2019. (Cited on pages 127 and 128.)

[148] M. Izumo, C. H. Johnson, and S. Yamazaki, "Circadian gene expression in mam-

malian fibroblasts revealed by real-time luminescence reporting: Temperature compensation and damping," *Proceedings of the National Academy of Sciences*, vol. 100, no. 26, pp. 16089–16094, 2003. (Cited on page 128.)

[149] W. Krugluger, A. Brandstaetter, E. Kallay, J. Schueller, E. Krexner, S. Kriwanek, E. Bonner, and H. S. Cross, "Regulation of genes of the circadian clock in human colon cancer: reduced period-1 and dihydropyrimidine dehydrogenase transcription correlates in high-grade tumors," *Cancer research*, vol. 67, no. 16, pp. 7917–7922, 2007. (Cited on page 128.)

[150] H.-c. Xia, Z.-f. Niu, H. Ma, S.-z. Cao, S.-c. Hao, Z.-t. Liu, and F. Wang, "Deregulated expression of the Per1 and Per2 in human gliomas," *Canadian journal of neurological sciences*, vol. 37, no. 3, pp. 365–370, 2010. (Cited on page 128.)

[151] N. Cermakian and P. Sassone-Corsi, "Multilevel regulation of the circadian clock," *Nat. Rev. Mol. Cell Biol.*, vol. 1, no. 1, pp. 59–67, 2000. (Cited on page 128.)

[152] M. Gallego and D. M. Virshup, "Post-translational modifications regulate the ticking of the circadian clock," *Nat. Rev. Mol. Cell Biol.*, vol. 8, no. 2, pp. 139–148, 2007. (Cited on page 128.)

[153] W. Zhou, L. A. Liotta, and E. F. Petricoin, "Cancer metabolism and mass spectrometry-based proteomics," *Cancer Letters*, vol. 356, no. 2, pp. 176–183, 2015. (Cited on page 130.)

[154] T. Geiger, J. Cox, and M. Mann, "Proteomic changes resulting from gene copy number variations in cancer cells," *PLoS Genet.*, vol. 6, no. 9, 2010. (Cited on page 130.)

[155] F. Baenke, B. Peck, H. Miess, and A. Schulze, "Hooked on fat: the role of lipid syn-

thesis in cancer metabolism and tumour development," *Dis. Model. Mech.*, vol. 6, no. 6, pp. 1353–1363, 2013. (Cited on page 131.)

[156] Y. Sunami, A. Rebelo, and J. Kleeff, "Lipid metabolism and lipid droplets in pancreatic cancer and stellate cells," *Cancers*, vol. 10, no. 1, pp. 1–20, 2018. (Cited on page 131.)

[157] G. Hatzivassiliou, F. Zhao, D. E. Bauer, C. Andreadis, A. N. Shaw, D. Dhanak, S. R. Hingorani, D. A. Tuveson, and C. B. Thompson, "ATP citrate lyase inhibition can suppress tumor cell growth," *Cancer Cell*, vol. 8, no. 4, pp. 311–321, 2005. (Cited on page 131.)

[158] R. U. Svensson, S. J. Parker, L. J. Eichner, M. J. Kolar, M. Wallace, S. N. Brun, P. S. Lombardo, J. L. Van Nostrand, A. Hutchins, L. Vera, L. Gerken, J. Greenwood, S. Bhat, G. Harriman, W. F. Westlin, H. J. Harwood, A. Saghatelian, R. Kapeller, C. M. Metallo, and R. J. Shaw, "Inhibition of acetyl-CoA carboxylase suppresses fatty acid synthesis and tumor growth of non-small-cell lung cancer in preclinical models," *Nat. Med.*, vol. 22, no. 10, pp. 1108–1119, 2016. (Cited on page 131.)

[159] J. J. Kamphorst, M. Nofal, C. Commisso, S. R. Hackett, W. Lu, E. Grabocka, M. G. Vander Heiden, G. Miller, J. A. Drebin, D. Bar-Sagi, C. B. Thompson, and J. D. Rabinowitz, "Human Pancreatic Cancer Tumors Are Nutrient Poor and Tumor Cells Actively Scavenge Extracellular Protein," *Cancer Res.*, vol. 75, no. 3, pp. 544–553, 2015. (Cited on page 131.)

[160] K. L. Bryant, J. D. Mancias, A. C. Kimmelman, and C. J. Der, "KRAS: Feeding pancreatic cancer proliferation," *Trends Biochem. Sci.*, vol. 39, no. 2, pp. 91–100, 2014. (Cited on page 131.)

[161] Z. Fang, X. Wang, Q. Yan, S. Zhang, and Y. Li, "Knockdown of IARS2 suppressed growth of gastric cancer cells by regulating the phosphorylation of cell cycle-related proteins," *Mol. Cell. Biochem.*, vol. 443, no. 1, pp. 93–100, 2018. (Cited on page 132.)

[162] E. Yeom, D.-W. Kwon, J. Lee, S.-H. Kim, J.-H. Lee, K.-J. Min, K.-S. Lee, and K. Yu, "Asparaginyl-tRNA Synthetase, a Novel Component of Hippo Signaling, Binds to Salvador and Enhances Yorkie-Mediated Tumorigenesis," *Frontiers in Cell and Developmental Biology*, vol. 8, 2020. (Cited on page 132.)

[163] D. Wang, R. Zhao, Y.-Y. Qu, X.-Y. Mei, X. Zhang, Q. Zhou, Y. Li, S.-B. Yang, Z.-G. Zuo, Y.-M. Chen, Y. Lin, W. Xu, C. Chen, S.-M. Zhao, and J.-Y. Zhao, "Colonic Lysine Homocysteinylation Induced by High-Fat Diet Suppresses DNA Damage Repair," *Cell Reports*, vol. 25, no. 2, pp. 398–412, 2018. (Cited on page 132.)

[164] A. Daemen, D. Peterson, N. Sahu, R. McCord, X. Du, B. Liu, K. Kowanetz, R. Hong, J. Moffat, M. Gao, A. Boudreau, R. Mroue, L. Corson, T. OBrien, J. Qing, D. Sampath, M. Merchant, R. Yauch, G. Manning, J. Settleman, G. Hatzivassiliou, and M. Evangelista, "Metabolite profiling stratifies pancreatic ductal adenocarcinomas into subtypes with distinct sensitivities to metabolic inhibitors," *Proceedings of the National Academy of Sciences*, vol. 112, no. 32, pp. E4410–E4417, 2015. (Cited on page 132.)

[165] C. Falcomata, S. Baerthel, S. A. Widholz, C. Schneeweis, J. J. Montero, A. Toska, J. Mir, T. Kaltenbacher, J. Heetmeyer, J. J. Swietlik, J.-Y. Cheng, B. Teodorescu, O. Reichert, C. Schmitt, K. Grabichler, A. Coluccio, F. Boniolo, C. Veltkamp, M. Zukowska, A. A. Vargas, W. H. Paik, M. Jesinghaus, K. Steiger, R. Maresch, R. Oellinger, T. Ammon, O. Baranov, M. S. Robles, J. Rechenberger, B. Kuster, F. Meissner, M. Reichert,

M. Flossdorf, R. Rad, M. Schmidt-Supprian, G. Schneider, and D. Saur, "Selective multi-kinase inhibition sensitizes mesenchymal pancreatic cancer to immune checkpoint blockade by remodeling the tumor microenvironment," *Nat. Cancer*, vol. 3, no. 3, pp. 318–336, 2022. (Cited on page 134.)

[166] M. Jain, R. Nilsson, S. Sharma, N. Madhusudhan, T. Kitami, A. L. Souza, R. Kafri, M. W. Kirschner, C. B. Clish, and V. K. Mootha, "Metabolite Profiling Identifies a Key Role for Glycine in Rapid Cancer Cell Proliferation," *Science*, vol. 336, no. 6084, pp. 1040–1044, 2012. (Cited on page 134.)

[167] J. Hu, J. W. Locasale, J. H. Bielas, J. O'Sullivan, K. Sheahan, L. C. Cantley, M. G. V. Heiden, and D. Vitkup, "Heterogeneity of tumor-induced gene expression changes in the human metabolic network," *Nat. Biotechnol.*, vol. 31, no. 6, pp. 522–529, 2013. (Cited on page 134.)

[168] A. M. Waters and C. J. Der, "KRAS: The Critical Driver and Therapeutic Target for Pancreatic Cancer," *Cold Spring Harbor Perspectives in Medicine*, no. 9, pp. 1–17, 2018. (Cited on page 135.)

[169] M. Seux, S. Peuget, M. P. Montero, C. Siret, V. Rigot, P. Clerc, V. Gigoux, E. Pellegrino, L. Pouyet, P. N'Guessan, S. Garcia, M. Dufresne, J. L. Iovanna, A. Carrier, F. André, and N. J. Dusetti, "TP53INP1 decreases pancreatic cancer cell migration by regulating SPARC expression," *Oncogene*, vol. 30, no. 27, pp. 3049–3061, 2011. (Cited on page 138.)

[170] M. Erkan, J. Kleeff, A. Gorbachevski, C. Reiser, T. Mitkus, I. Esposito, T. Giese, M. W. BÃ¼chler, N. A. Giese, and H. Friess, "Periostin Creates a Tumor-Supportive Microenvironment in the Pancreas by Sustaining Fibrogenic Stellate Cell Activity," *Gastroenterology*, vol. 132, no. 4, pp. 1447–1464, 2007. (Cited on page 138.)

[171] A. Kanno, K. Satoh, A. Masamune, M. Hirota, K. Kimura, J. Umino, S. Hamada, A. Satoh, S. Egawa, F. Motoi, M. Unno, and T. Shimosegawa, "Periostin, secreted from stromal cells, has biphasic effect on cell migration and correlates with the epithelial to mesenchymal transition of human pancreatic cancer cells," *International Journal of Cancer*, vol. 122, no. 12, pp. 2707–2718, 2008. (Cited on page 138.)

[172] M. Erkan, M. Kurtoglu, and J. Kleeff, "The role of hypoxia in pancreatic cancer: a potential therapeutic target?," *Expert Review of Gastroenterology & Hepatology*, vol. 10, no. 3, pp. 301–316, 2016. (Cited on page 139.)

[173] H. Zhu, D. Wang, Y. Liu, Z. Su, L. Zhang, F. Chen, Y. Zhou, Y. Wu, M. Yu, Z. Zhang, and G. Shao, "Role of the Hypoxia-inducible factor-1 alpha induced autophagy in the conversion of non-stem pancreatic cancer cells into CD133+ pancreatic cancer stem-like cells," *Cancer Cell Int.*, vol. 13, no. 1, p. 119, 2013. (Cited on page 139.)

[174] X. Jin, L. Dai, Y. Ma, J. Wang, and Z. Liu, "Implications of HIF-1α in the tumorigenesis and progression of pancreatic cancer," *Cancer Cell Int.*, vol. 20, no. 1, p. 273, 2020. (Cited on page 139.)

[175] I. Aiello, M. L. M. Fedele, F. RomÃ¡n, L. Marpegan, C. Caldart, J. J. Chiesa, D. A. Golombek, C. V. Finkielstein, and N. Paladino, "Circadian disruption promotes tumor-immune microenvironment remodeling favoring tumor cell proliferation," *Science Advances*, vol. 6, no. 42, p. eaaz4530, 2020. (Cited on pages 139 and 140.)

[176] L. Mei, Y. Fan, X. Lv, D. K. Welsh, C. Zhan, and E. E. Zhang, "Long-term in vivo recording of circadian rhythms in brains of freely moving mice," *Proc. Natl. Acad. Sci. U. S. A.*, vol. 115, no. 16, pp. 4276–4281, 2018. (Cited on page 141.)

[177] A. M. Finger, S. Jäschke, M. del Olmo, R. Hurwitz, A. E. Granada, H. Herzel, and

A. Kramer, "Intercellular coupling between peripheral circadian oscillators by TGF-β signaling," *Sci. Adv.*, vol. 7, no. 30, pp. 1–19, 2021. (Cited on page 141.)

[178] A. Malik, S. Nalluri, A. De, D. Beligala, and M. E. Geusz, "The Relevance of Circadian Clocks to Stem Cell Differentiation and Cancer Progression," *NeuroSci*, vol. 3, no. 2, pp. 146–165, 2022. (Cited on page 142.)

[179] M. Rossi, P. Altea-Manzano, M. Demicco, G. Doglioni, L. Bornes, M. Fukano, A. Vandekeere, A. M. Cuadros, J. Fernández-García, C. Riera-Domingo, C. Jauset, M. Planque, H. F. Alkan, D. Nittner, D. Zuo, L. A. Broadfield, S. Parik, A. A. Pane, F. Rizzollo, G. Rinaldi, T. Zhang, S. T. Teoh, A. B. Aurora, P. Karras, I. Vermeire, D. Broekaert, J. V. Elsen, M. M. L. Knott, M. F. Orth, S. Demeyer, G. Eelen, L. E. Dobrolecki, A. Bassez, T. V. Brussel, K. Sotlar, M. T. Lewis, H. Bartsch, M. Wuhrer, P. van Veelen, P. Carmeliet, J. Cools, S. J. Morrison, J.-C. Marine, D. Lambrechts, M. Mazzone, G. J. Hannon, S. Y. Lunt, T. G. P. Grünewald, M. Park, J. van Rheenen, and S.-M. Fendt, "PHGDH heterogeneity potentiates cancer cell dissemination and metastasis," *Nature*, 2022. (Cited on page 146.)

[180] F. Lévi and U. Schibler, "Circadian Rhythms: Mechanisms and Therapeutic Implications," *Annu. Rev. Pharmacol. Toxicol.*, vol. 47, no. 1, pp. 593–628, 2007. (Cited on page 147.)

[181] F. Levi, A. Okyar, S. Dulong, P. F. Innominato, and J. Clairambault, "Circadian timing in cancer treatments," *Annu. Rev. Pharmacol. Toxicol.*, vol. 50, pp. 377–421, 2010. (Cited on page 147.)

[182] Y. Lee, S. Y. Fong, J. Shon, S. L. Zhang, R. Brooks, N. F. Lahens, D. Chen, C. van Dang, J. M. Field, and A. Sehgal, "Time-of-day specificity of anticancer drugs may

be mediated by circadian regulation of the cell cycle," *Sci. Adv.*, vol. 7, no. 7, pp. 1–16, 2021. (Cited on page 147.)

[183] F. Levi, C. Focan, A. KarabouÃ©, V. de la Valette, D. Focan-Henrard, B. Baron, F. Kreutz, and S. Giacchetti, "Implications of circadian clocks for the rhythmic delivery of cancer therapeutics," *Advanced Drug Delivery Reviews*, vol. 59, no. 9, pp. 1015–1035, 2007. (Cited on page 148.)

[184] S. Giacchetti, G. Bjarnason, C. Garufi, D. Genet, S. Iacobelli, M. Tampellini, R. Smaaland, C. Focan, B. Coudert, Y. Humblet, J. L. Canon, A. Adenis, G. L. Re, C. Carvalho, J. Schueller, N. Anciaux, M. A. Lentz, B. Baron, T. Gorlia, and F. Lévi, "Phase III trial comparing 4-day chronomodulated therapy versus 2-day conventional delivery of fluorouracil, leucovorin, and oxaliplatin as first-line chemotherapy of metastatic colorectal cancer: The European Organisation for Research and Treatment of Cancer Chronotherapy Group," *J. Clin. Oncol.*, vol. 24, no. 22, pp. 3562–3569, 2006. (Cited on page 148.)

[185] A. Sancar and R. N. Van Gelder, "Clocks, cancer, and chronochemotherapy," *Science*, vol. 371, no. 6524, 2021. (Cited on page 148.)

[186] R. M. Kelly, U. Healy, S. Sreenan, J. H. McDermott, and A. N. Coogan, "Clocks in the clinic: Circadian rhythms in health and disease," *Postgrad. Med. J.*, vol. 94, no. 1117, pp. 653–658, 2018. (Cited on page 149.)

[187] N. Wittenbrink, B. Ananthasubramaniam, M. Münch, B. Koller, B. Maier, C. Weschke, F. Bes, J. De Zeeuw, C. Nowozin, A. Wahnschaffe, S. Wisniewski, M. Zaleska, O. Bartok, R. Ashwal-Fluss, H. Lammert, H. Herzel, M. Hummel, S. Kadener, D. Kunz, and A. Kramer, "High-accuracy determination of internal circadian time

from a single blood sample," *J. Clin. Invest.*, vol. 128, no. 9, pp. 3826–3839, 2018. (Cited on page 149.)

[188] A. Macklin, S. Khan, and T. Kislinger, "Recent advances in mass spectrometry based clinical proteomics: Applications to cancer research," *Clin. Proteomics*, vol. 17, no. 1, pp. 1–25, 2020. (Cited on page 149.)

[189] Y. Qin, W. Zhang, X. Sun, S. Nan, N. Wei, H. J. Wu, and X. Zheng, "Deconvolution of heterogeneous tumor samples using partial reference signals," *PLoS Comput. Biol.*, vol. 16, no. 11, pp. 1–18, 2020. (Cited on page 150.)

[190] T. Chu, Z. Wang, D. Pe'er, and C. G. Danko, "Cell type and gene expression deconvolution with BayesPrism enables Bayesian integrative analysis across bulk and single-cell RNA sequencing in oncology," *Nat. Cancer*, vol. 3, no. 4, pp. 505–517, 2022. (Cited on page 150.)

[191] A. N. Hosein, R. A. Brekken, and A. Maitra, "Pancreatic cancer stroma: an update on therapeutic targeting strategies," *Nat. Rev. Gastroenterol. Hepatol.*, vol. 17, no. 8, pp. 487–505, 2020. (Cited on page 151.)

[192] D. Amakye, Z. Jagani, and M. Dorsch, "Unraveling the therapeutic potential of the Hedgehog pathway in cancer," *Nat. Med.*, vol. 19, no. 11, pp. 1410–1422, 2013. (Cited on page 151.)

[193] C. Tian, K. R. Clauser, D. Öhlund, S. Rickelt, Y. Huang, M. Gupta, D. R. Mani, S. A. Carr, D. A. Tuveson, and R. O. Hynes, "Proteomic analyses of ECM during pancreatic ductal adenocarcinoma progression reveal different contributions by tumor and stromal cells," *Proc. Natl. Acad. Sci. U. S. A.*, vol. 116, no. 39, pp. 19609–19618, 2019. (Cited on page 151.)

[194] C. Lin, W. C. Wu, G. C. Zhao, D. S. Wang, W. H. Lou, and D. Y. Jin, "ITRAQ-based quantitative proteomics reveals apolipoprotein A-I and transferrin as potential serum markers in CA19-9 negative pancreatic ductal adenocarcinoma," *Med. (United States)*, vol. 95, no. 31, pp. 1–5, 2016. (Cited on page 151.)

[195] K. Sogawa, S. Takano, F. Iida, M. Satoh, S. Tsuchida, Y. Kawashima, H. Yoshitomi, A. Sanda, Y. Kodera, H. Takizawa, R. Mikata, M. Ohtsuka, H. Shimizu, M. Miyazaki, O. Yokosuka, and F. Nomura, "Identification of a novel serum biomarker for pancreatic cancer, C4b-binding protein α-chain (C4BPA) by quantitative proteomic analysis using tandem mass tags," *Br. J. Cancer*, vol. 115, no. 8, pp. 949–956, 2016. (Cited on page 151.)

[196] S. Nie, A. Lo, J. Wu, J. Zhu, Z. Tan, D. M. Simeone, M. A. Anderson, K. A. Shedden, M. T. Ruffin, and D. M. Lubman, "Glycoprotein biomarker panel for pancreatic cancer discovered by quantitative proteomics analysis," *J. Proteome Res.*, vol. 13, no. 4, pp. 1873–1884, 2014. (Cited on page 151.)

[197] L. Kuhlmann, W. M. Nadler, A. Kerner, S. A. Hanke, E. M. Noll, C. Eisen, E. Espinet, V. Vogel, A. Trumpp, M. R. Sprick, and C. P. Roesli, "Identification and Validation of Novel Subtype-Specific Protein Biomarkers in Pancreatic Ductal Adenocarcinoma," *Pancreas*, vol. 46, no. 3, 2017. (Cited on page 151.)

[198] T. Yoneyama, S. Ohtsuki, K. Honda, M. Kobayashi, M. Iwasaki, Y. Uchida, T. Okusaka, S. Nakamori, M. Shimahara, T. Ueno, A. Tsuchida, N. Sata, T. Ioka, Y. Yasunami, T. Kosuge, T. Kaneda, T. Kato, K. Yagihara, S. Fujita, W. Huang, T. Yamada, M. Tachikawa, and T. Terasaki, "Identification of IGFBP2 and IGFBP3 as compensatory biomarkers for CA19-9 in early-stage pancreatic cancer using a combina-

tion of antibody-based and LC-MS/MS-based proteomics," *PLoS One*, vol. 11, no. 8, pp. 1–23, 2016. (Cited on page 151.)

[199] A. Bulle, J. Dekervel, S. Van Der Merwe, E. V. Cutsem, C. Verslype, and J. Van Pelt, "Relevance of the stroma in pancreatic ductal adenocarcinoma and its challenges for translational research Introduction: pancreatic cancer stands out from most other major forms of cancer," *J Cancer Treat. Diagn*, vol. 2, no. 1, pp. 1–15, 2017. (Cited on pages 151 and 152.)

[200] H. Kosanam, I. Prassas, C. C. Chrystoja, I. Soleas, A. Chan, A. Dimitromanolakis, I. M. Blasutig, F. Rueckert, R. Gruetzmann, C. Pilarsky, M. Maekawa, R. Brand, and E. P. Diamandis, "Laminin, gamma 2 (LAMC2): A promising new putative pancreatic cancer biomarker identified by proteomic analysis of pancreatic adenocarcinoma tissues," *Mol. Cell. Proteomics*, vol. 12, no. 10, pp. 2820–2832, 2013. (Cited on page 151.)

[201] J. Leca, S. Martinez, S. Lac, J. Nigri, V. Secq, M. Rubis, C. Bressy, A. Sergé, M. N. Lavaut, N. Dusetti, C. Loncle, J. Roques, D. Pietrasz, C. Bousquet, S. Garcia, S. Granjeaud, M. Ouaissi, J. B. Bachet, C. Brun, J. L. Iovanna, P. Zimmermann, S. Vasseur, and R. Tomasini, "Cancer-associated fibroblast-derived annexin A6+ extracellular vesicles support pancreatic cancer aggressiveness," *J. Clin. Invest.*, vol. 126, no. 11, pp. 4140–4156, 2016. (Cited on pages 151 and 152.)

[202] F. Coscia, S. Doll, J. M. Bech, L. Schweizer, A. Mund, E. Lengyel, J. Lindebjerg, G. I. Madsen, J. M. Moreira, and M. Mann, "A streamlined mass spectrometry based proteomics workflow for large-scale FFPE tissue analysis," *The Journal of pathology*, vol. 251, no. 1, pp. 100–112, 2020. (Cited on page 152.)

[203] F. Jiang and J. A. Doudna, "CRISPR/Cas9 Structures and Mechanisms," *Annu. Rev. Biophys.*, vol. 46, pp. 505–531, 2017. (Cited on page 201.)

APPENDIX A

Supplementary data

Table A.1: The *Bmal1::Luc* PDAC cell lines included in the functional screening and the corresponding replicates.

PDAC Cell line	Genotype	Number of replicates
10092	PI3K	14
10158	PI3K	15
10502	PKP	18
11628	PKP	20
12690	PI3K	20
16990	PK	27
16992	PK	30
2259	PK	24
3202	PK	10
3250	PK	36
4072	PK	41
4134	PI3K	10
4706	PK	24
4888	PI3K	10
4900	PK	27
5320	PK	35
53578	PK	46
53646	PK	28
53704	PK	28
6075	PK	22
8182	PK	30
8296	PK	41

Continued on next page

Table A.1 – *Continued from previous page*

PDAC Cell line	Genotype	Number of replicates
8305	PK	37
8349	PK	12
8442	PK	22
8513	PK	11
8570	PK	24
8661	PK	64
8927	PI3K	20
8932	PI3K	15
9091	PK	18
9203	PK	35
9471	PI3K	10
9580	PI3K	19
9591	PK	11
9791	PKP	18
9960	PI3K	10
R1035	PK	24
R211	PKP	20
R405	PKP	18
S411	PK	17
S559	PK	13
S821	PK	18
S914	PK	35

Table A.2: Phenotypic characteristics of each mouse from the time point experiment.

MouseID	Genotype	Immune system	sgRNA	Age at implantation (week)	Mouse weight (g)	Tumor weight (g)
SK15	F1*	Competent	sglacZ	10	23.8	0.34
SK16	F1	Competent	sglacZ	10	26.5	0.27
SK17	F1	Competent	sglacZ	10	23.2	0.68
SK18	F1	Competent	sglacZ	10	20.4	0.19
SK19	F1	Competent	sglacZ	10	23.3	0.27
SK20	F1	Competent	sglacZ	8	24.3	0.72
SK21	F1	Competent	sglacZ	9	28.4	0.30
SK22	F1	Competent	sg284	9	22.8	0.10
SK23	F1	Competent	sg284	9	24.6	0.04
SK24	F1	Competent	sg284	9	23.2	na+
SK25	F1	Competent	sg284	9	22.9	0.55
SK26	F1	Competent	sg284	9	22.1	0.68
SK27	F1	Competent	sg284	8	27.1	0.24
SK28	F1	Competent	sg284	9	22.2	0.32
SK29	Rag2 KO**	Deficient	sg284	28	23.2	0.14
SK30	Rag2 KO	Deficient	sg284	28	24.9	0.31
SK31	Rag2 KO	Deficient	sg284	28	24.2	0.36
SK32	Rag2 KO	Deficient	sglacZ	25	22.6	0.39
SK33	Rag2 KO	Deficient	sglacZ	25	23.5	0.16
SK34	Rag2 KO	Deficient	sglacZ	25	21.8	0.32

* C57BL/6J;129S6/SvEv

** $Rag2^{-}/^{-}$

+ not applied

Table A.3: Phenotypic characteristics of each mouse from the endpoint experiment.

MouseID	*Bmal1::Luc* PK Cell line	sgRNA	Survival days	Tumor weight (g)	Mouse weight (g)
SK35	S914	sglacZ	50	3.11	28.6
SK36	S914	sglacZ	89	na*	37.2
SK37	S914	sglacZ	45	0.70	21.9
SK38	S914	sglacZ	67	1.68	29.7
SK39	S914	sglacZ	84	na	35.4
SK40	S914	sglacZ	59	0.79	31.0
SK41	S914	sglacZ	57	0.92	29.0
SK42	S914	sg284	89	na	39.5
SK43	S914	sg284	89	0.88	36.3
SK44	S914	sg284	40	0.81	28.8
SK45	S914	sg284	63	1.65	27.9
SK46	S914	sg284	61	1.29	30.3
SK47	S914	sg284	53	0.82	27.8
SK48	S914	sg284	77	0.86	31.5
SK49	4706	sglacZ	53	0.35	25.7
SK50	4706	sglacZ	69	0.96	31.9
SK51	4706	sglacZ	57	0.94	26.9
SK52	4706	sglacZ	63	0.53	28.7
SK53	4706	sglacZ	61	0.44	37.4
SK54	4706	sglacZ	49	0.91	27.0
SK55	4706	sglacZ	53	0.62	28.1
SK56	4706	sg284	67	2.40	31.6
SK57	4706	sg284	57	1.07	26.8
SK58	4706	sg284	45	0.25	22.1
SK59	4706	sg284	87	0.75	29.1
SK60	4706	sg284	64	0.46	28.8
SK61	4706	sg284	86	0.40	28.9
SK62	4706	sg284	57	0.44	24.9

* not applied

APPENDIX B

The ChronoTool

For the analysis of the medium-scale bioluminescence-based functional screening of the *Bmal1::Luc* PDAC cell lines, the pipeline shown in Figure 2.3 was used for the inference of circadian clock's functionality in each of the cell lines.

The analysis was implemented in Matlab (R2019a) and the scripts were integrated in in-house made tool, the ChronoTool, using Matalab's base functions for applications' design with a graphical user interface (GUI). The overall programming was performed by the electrical engineer Ms. Graciela González Peytaví, MSc. after mutual discussions about the necessary functions. The Tool can be downloaded freely from the repository: https://bitbucket.org/gpeytavi/biolumi_tool/src/master/, and a Matlab license is required for it to be used.

In the following Figures, the ChronoTool's functions are presented and may be used as guidelines for further use by future lab members. The Tool includes additional preliminary functions, but they were not developed further. In addition, the tabs "Import CTG" and "CTG Staticstics" will not be explained, because they were later developed for other purposes than the bioluminescence pipeline. Here, the steps for the time series data analysis as part of this thesis work are shown.

In the first tab of the ChronoTool (Fig. B.1), the import of the time series data (by selecting the first "Browse" button; blue square 1.) derived from the luminometry MicroWin software after the end of the bioluminescence measurement. The time series data should be in .csv format and include in the first row "FORMAT_HHMMSS". This is a function that can be adjusted, so that the .csv files can be read without any modification

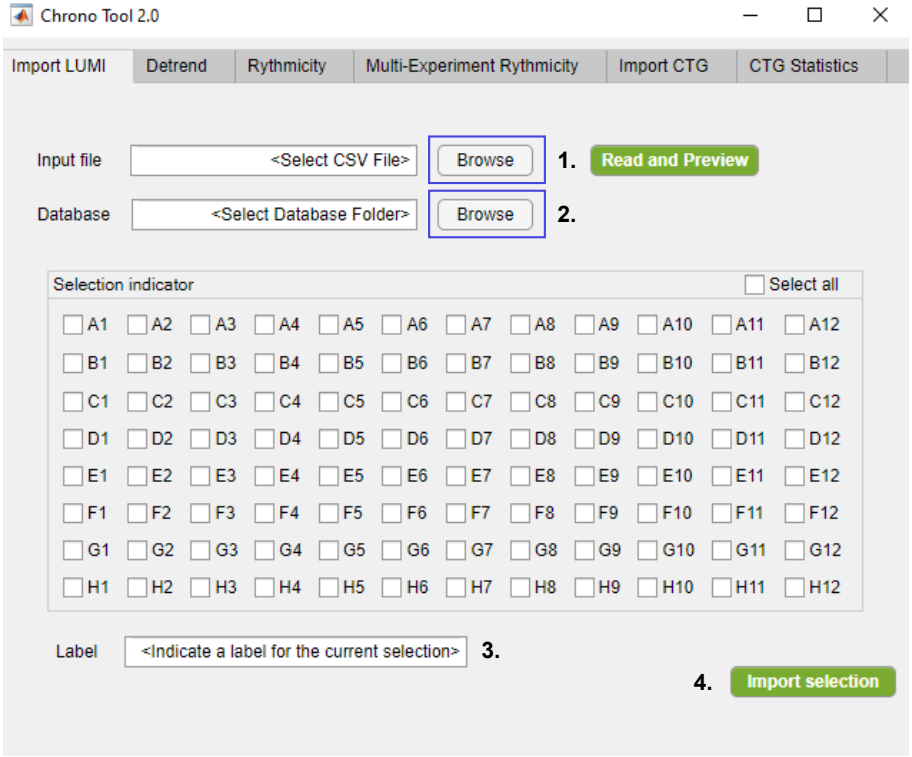

Figure B.1: Import settings of the ChronoTool.

by the user. By clicking the "Read and Preview" green button, the overall luminescence signal from each measured well is given as the average of the time series sequence, and it serves as a confirmation that the data are in the correct format have been imported.

One of the most important functionality of the ChronoTool design is that it "stores" the data assignment and any subsequent analysis in a form of a "Database", which is represented as a "structure" data type in the Matlab programming environment. This allows for the overall control of each experiment and gives the possibility to combine results for the same cell line that was included in more than one experimental plate. Therefore, it is highly recommended that for each experiment a new "Database" folder is created by selecting the second "Browse" button (blue square 2.).

Another advantage of the ChronoTool import function is that it is designed based on

the 96-well plate format that is used for the bioluminescence experiments. By selecting as many replicates of the same that were included in the experiment, one common Label (in the empty bar in the bottom of the tab) can be given and the correct assignment of the data is, thereby, highly controlled. In case of a mistake, it can easily be corrected by deleting the imported (.mat) data in the corresponding Database folder. To import the data in the Database, the "Import selection" is required.

In the second tab of the ChronoTool (Fig. B.2), settings for the detrending of the bioluminescence signal are given (blue square). First, the Database folder is selected by clicking the "Browse" button (blue square 1.). The green button "Update Label List" is by default red, and turns into green when a Database folder that contains assigned data is selected. Important settings for the detrending can be adjusted here: i) how many hours should be excluded (set at 24 for this thesis work), ii) the amplitude threshold above which potential "spikes" in the signal should automatically be removed from the analysis (the default value was used), iii) "smoothing" for the signal available, i.e., a certain number of sequential time points can be selected to average their RLU values (the default value was used) and iv) the method for trend removal (piecewise-linear of a 24-hour window was used).

Options for plotting, saving and adding the detrended data to the Database (blue arrows) are available. For saving, a Plot folder can be selected via the "Browse" button at the right bottom of the tab (blue square 3.). The time series of a given Database can be detrended individually -by selecting the "Detrend Cell Line" green button at the bottom right of the tab- or altogether -by selecting the "Detrend All" green button.

In the third tab (Fig. B.3), the presence of rhythmicity in the signal is tested. First, the Database folder is selected by the "Beowse" button (blue square 1.), and by clicking "Update Label List" the default red button turns green and the corresponding cell lines appear under "Process Label" (blue square 2.).

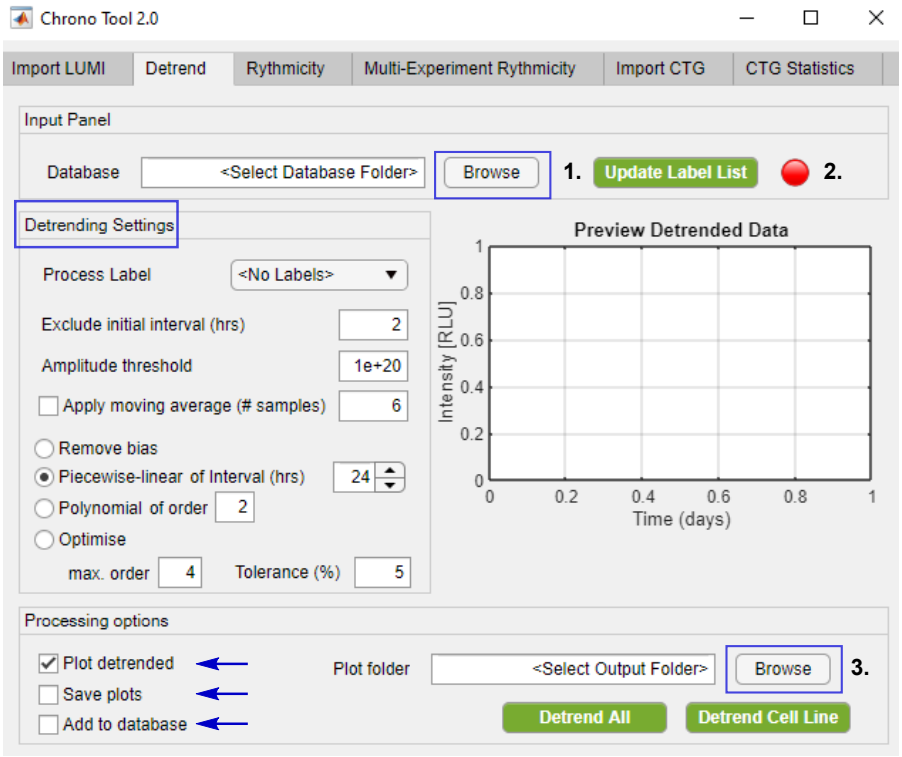

Figure B.2: Detrending settings of the ChronoTool.

Importantly, for the rhythmicity analysis only detrended data can be used. For this, it is required that the option "Add to database" in B.2 tab is enabled before proceeding and the option "Use detrended data" under "ACF Settings" is also enabled. The default values were use both for the number of lags and the confidence statistical bounds. The former option means that the detrended data should contain at least two full cycles (i.e., 48 hours).

Next, for an additional test for rhythmicity and for period estimation, the "Lomb-Scargle Periodogram" (LSP) option on the left, and "Periodogram Settings" tab on the right are selected. For the former, the default settings were used, which include i) the threshold for the false-alarm probabilities, ii) the range in hours for the estimated period, iii) the minimum period to be considered in the signal and iv) the oversampling factor

(OF). OF is used to interpolate the tested frequencies, which depend on the sampling interval and the length of the time series, therefore improving the resolution for the estimated period. For both ACF (B.3) and LSP functions (B.4), options for plotting, saving and adding the results to the database (blue arrows) are given. The output plotting folder can be selected by the "Browse" button (blue square 4.).

In both cases, the ACF and LSP for each replicate can be either calculates individually (green button "Estimate") or altogether (blue button "Estimate for all labels"). Lastly, for the LSP, the blue button "Generate Summary" creates in the output folder a .txt. file with the estimated period in each sample, the corresponding false-alarm probabilities, along with the averaged period and the associated statistics (standard deviation, standard error of the mean) among the replicates of a given cell line in the experimental plate. Importantly, for the averaged period only those replicates with a peak above of the 0.01 % false-alarm probability threshold are included.

In the "Estimation Method", two more options ("Welch's Periodogram" and "NLLS-FFT") are given, which were not further developed. However, the scripts are included in the ChronoTool src folder, and could be expanded by future users if desired.

Lastly, in the tab "Multi-Experiment Rhythmicity" (Figs. B.5 and B.6), the period estimation and ACF for a given cell line over multiple experiments can be performed. For both cases, the upper-level folder that contains all the database sub-folders can be selected using the "Browse" button (blue square 1.). By clicking the "Update" green button on the left of the tab (2.) the available database folders are then visible and the red dot turns green. The desired databases can be drawn to the blank box on the left using the double arrow (black square). Then, by clicking on the "Update" green button (3.), which also turns from red to green, all the individual cell lines (with the exact same name that were originally assigned during the import in the database) appear as a list by selecting the "Label" and can be drawn in the blank box on the right of the tab. This is important,

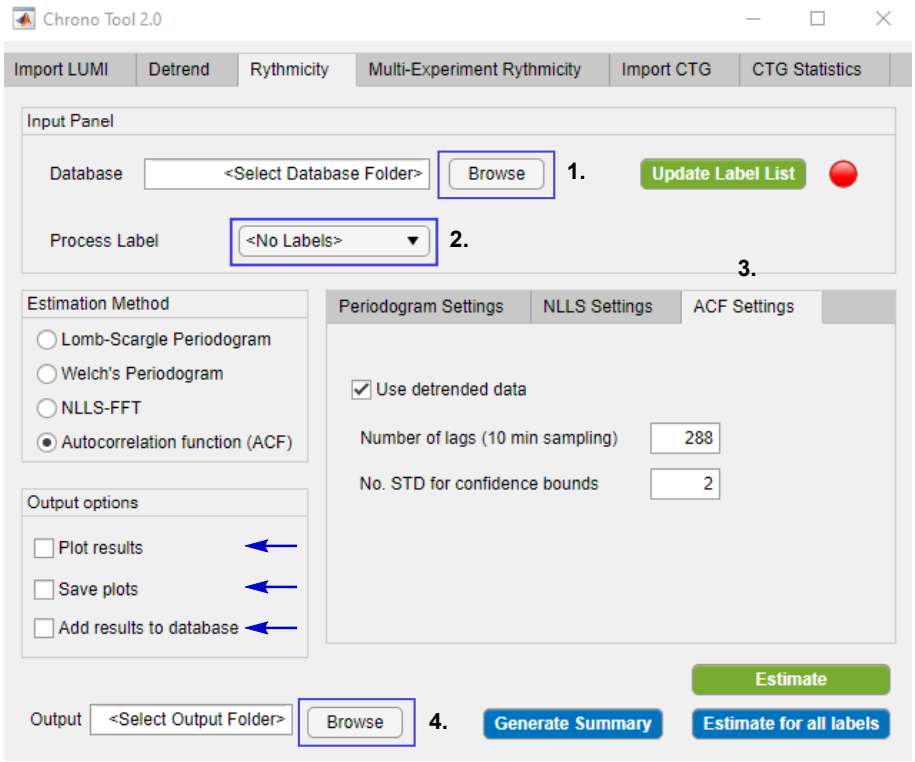

Figure B.3: Rhythmicity settings for autocorrelation function in the ChronoTool.

because a cell line may have been labelled slightly differently in different experimental plates, therefore all names can be selected simultaneously.

Next, for the period estimation, the Lomb-Scargle Periodogram option is selected (Fig. B.5 blue arrow) and the "Compute Average" green button on the upper right of the tab enables the averaged LSP of a given cell line. The output can be saved (blue arrow) with a new combined label (4.) in a desired folder by the "Browse" button (blue square 5.). Subsequently, selecting the "Update" green button on the bottom right shows the available combined cell line labels that have been generated in the output folder and can be drawn by the double arrow (square) into the blank square on the bottom right. Then, the "Combine" green button creates an average LSP of several period estimates for the selected cell line. In this thesis work, this function was developed so that the robustness

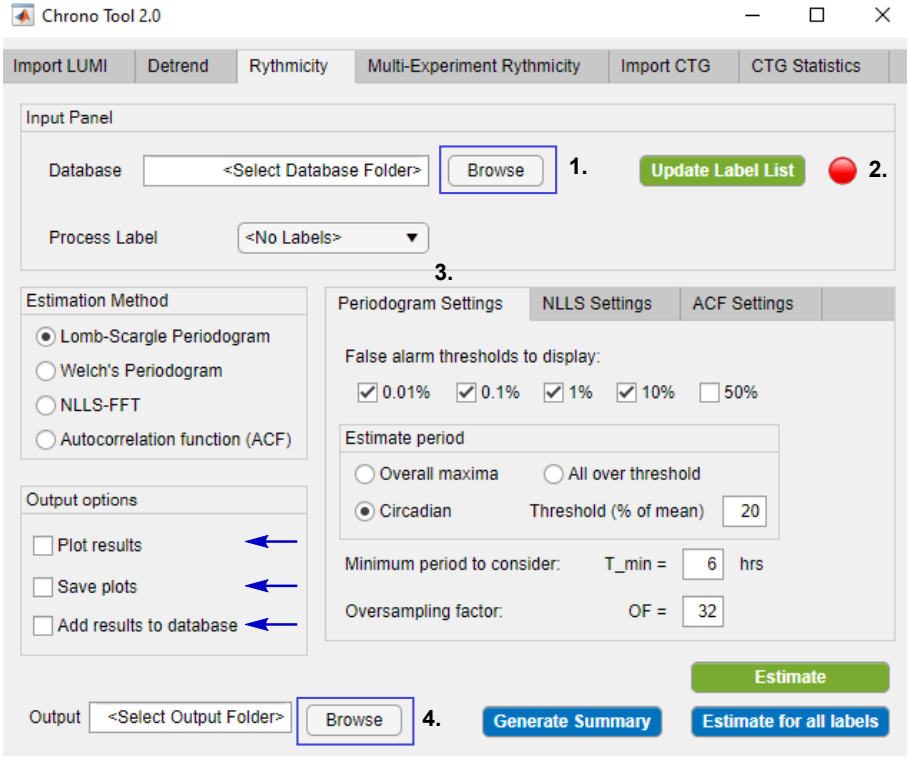

Figure B.4: Rhythmicity settings for Lomb-Scargle periodogram in the ChronoTool.

of the circadian rhythm given as power in the LSP can be compared between different cell lines. Importantly, a reference for such comparison was set the corresponding power in U2-OS model cell line. Therefore, in the blank space, the U2-OS is also selected -along with the desired cell lines to be compared- and a certain threshold is drawn with a dotted horizontal line on the generated LSP plot (e.g., Fig. 3.14). This line corresponds to a statistical threshold (68 % of U2-OS peak to noise level) above which the calculated averaged period estimate for a given cell line is considered significant and with robust amplitude. In addition, a selected range of periodicities is drawn in grey color including 22 to 26 hours and considered as "circadian".

A similar approach for the averaged autocorrelation coefficients can be performed in the same Mutli-Experiment rhythmicity tab by selecting the "Autocorrelation (ACF)"

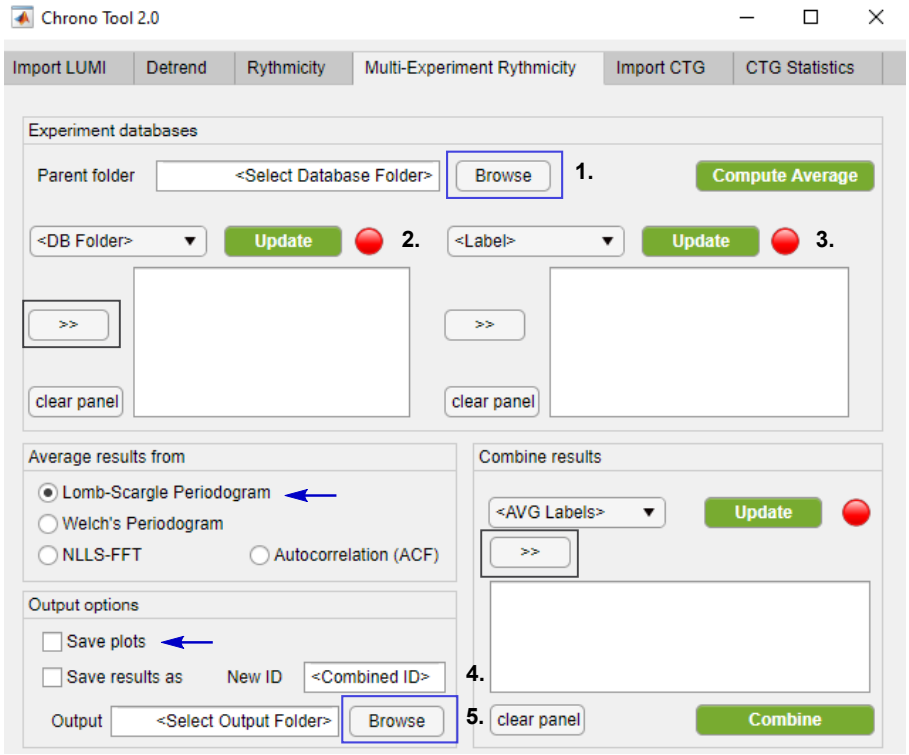

Figure B.5: Mutli-Rhythmicity settings for combining period estimates over several experiments.

option on the left (Fig. B.6 blue arrow) following the initial steps described above. Options for saving the plot with a combined new label in an output folder (blue square 4.) are also available. Here, the "Combine results" tab on the right of the tab is not applicable.

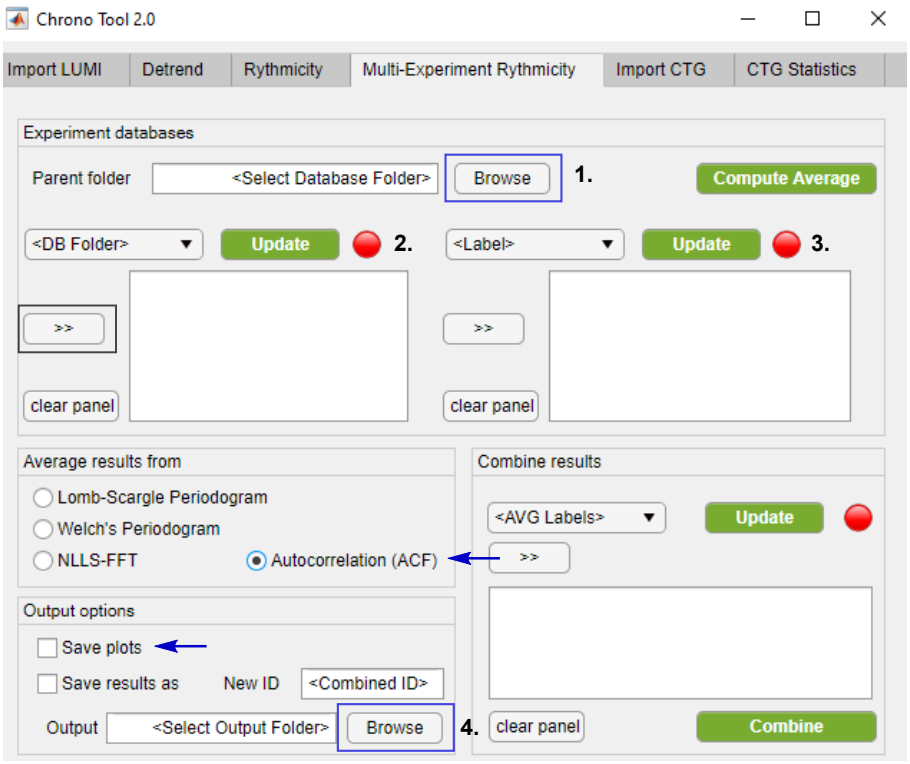

Figure B.6: Mutli-Rhythmicity settings for combining autocorrelation coefficients for a given cell line over several experiments.

APPENDIX C

ICE WebTool results

Using the freely available web tool for Inference CRISPR Editing (ICE; https://www.synthego.com/products/bioinformatics/crispr-analysis), the percentage of CRISPR-resulted insertions and deletions (indels) from Sanger sequencing was calculated.

In the each of the following Figures for each *Bmal1::Luc* KRAS-mutant PDAC cell line, the edited traces (sg26 or sg284) and control, non-edited (sglacZ) Sanger traces are depicted as they were derived from the ICE tool.

The single-guide RNA (sgRNA) sequence is represented by the black horizontal underlined region, and the red horizontal region underlines the Photospacer Adjacent Motif (PAM) site, which serves as binding signal for the CAS9 [203]. The vertical black dotted line shows the site where the cut on the DNA was introduced. Error-prone DNA repair mechanisms are activated resulting in mixed sequencing bases downstream of the DNA cut.

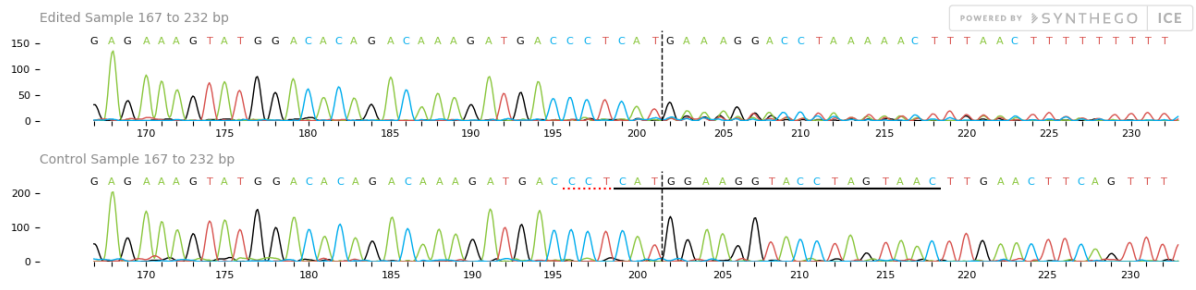

Figure C.1: Sanger sequencing traces of *Bmal1::Luc* 4706 sg26 compared to non-edited sglacZ traces.

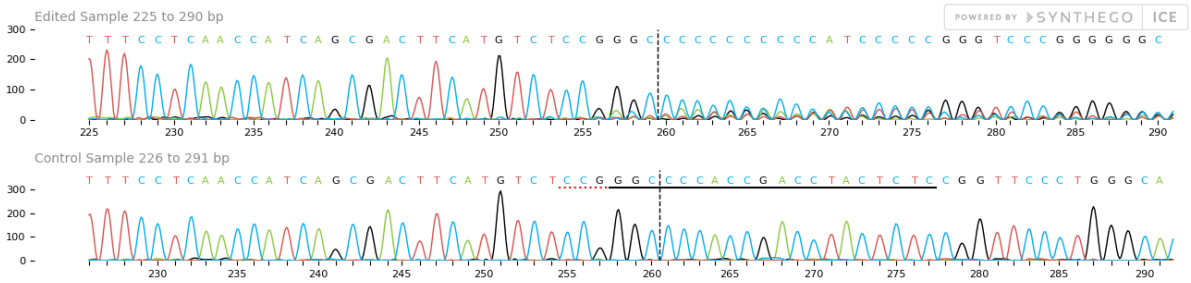

Figure C.2: Sanger sequencing traces of *Bmal1::Luc* 4706 sg284 compared to non-edited sglacZ traces.

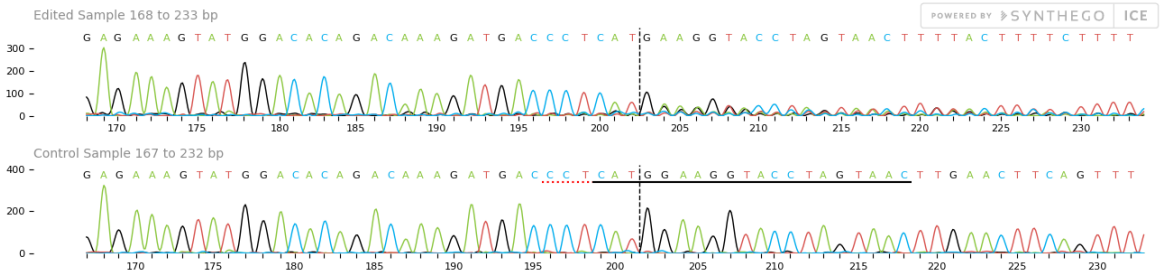

Figure C.3: Sanger sequencing traces of *Bmal1::Luc* 53704 sg26 compared to non-edited sglacZ traces.

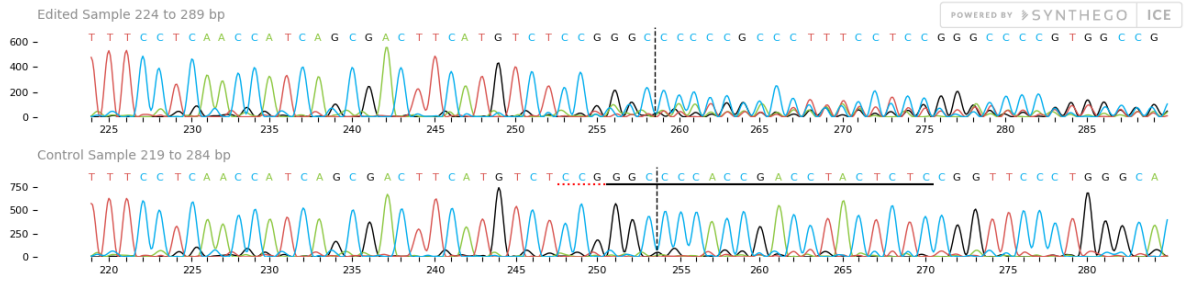

Figure C.4: Sanger sequencing traces of *Bmal1::Luc* 53704 sg284 compared to non-edited sglacZ traces.

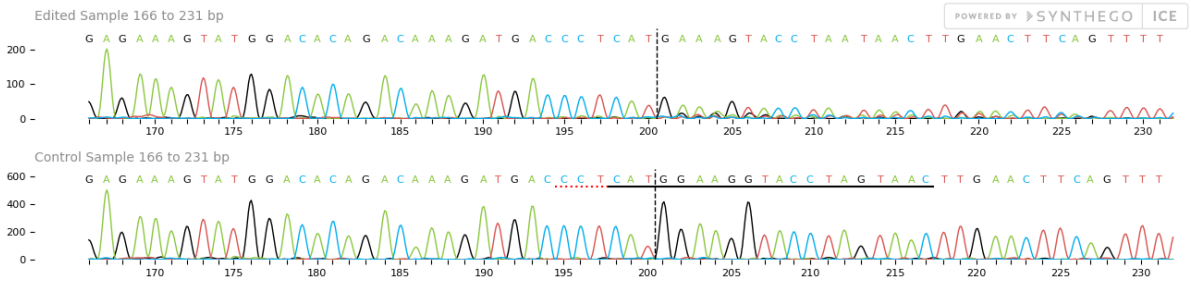

Figure C.5: Sanger sequencing traces of *Bmal1::Luc* 16992 sg26 compared to non-edited sglacZ traces.

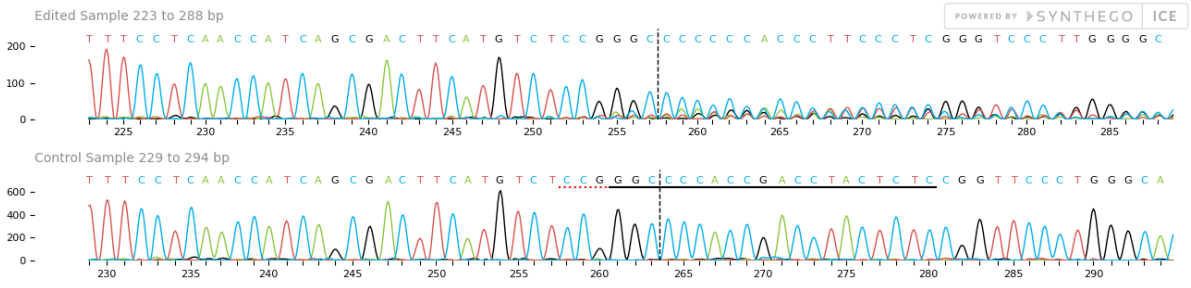

Figure C.6: Sanger sequencing traces of *Bmal1::Luc* 16992 sg284 compared to non-edited sglacZ traces.

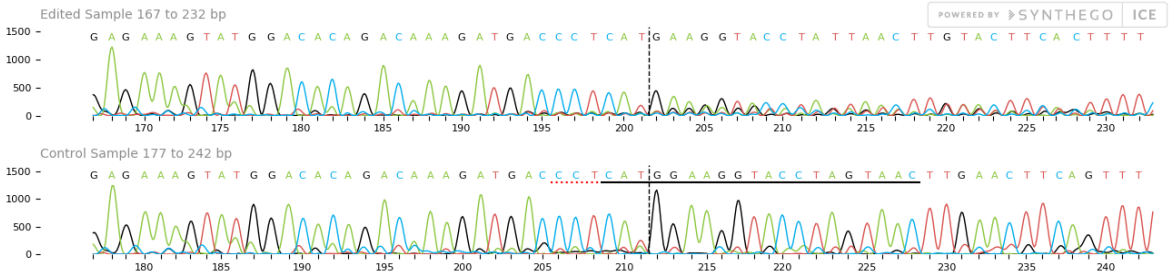

Figure C.7: Sanger sequencing traces of *Bmal1::Luc* S914 sg26 compared to non-edited sglacZ traces.

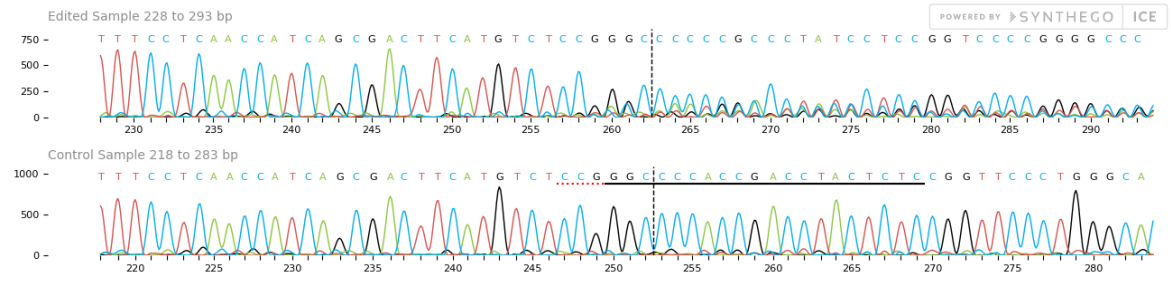

Figure C.8: Sanger sequencing traces of *Bmal1::Luc* S914 sg284 compared to non-edited sglacZ traces.

Afterword

First and foremost, I would like to thank Charo. She gave me the opportunity to join her young team and incorporated me in everything as soon as I started. From organizing the lab, learning about basic chronobiology, showing me the basics on Perseus and large dataset analysis to giving me credit during the revision experiments. Soon she gave me the freedom to organize my time and work between hers and Dieter's lab and she supported me to develop the necessary tools needed to answer scientific questions. In her lab, there has been -despite the realistic difficulties during the pandemic situation- a collaborative community of mutual support and scientific exchange.

Second, I want to thank the members of my Thesis Advisory Committee. They supported me during my PhD by giving constructive feedback and guidance. I want to especially thank Dieter for providing all the required biological resources for my PhD project to be completed. His expertise in PDAC biology and mouse genetics have been very inspiring during the years.

Most certainly, I would like to deeply thank my colleague and friend Tanja Bange, who taught me everything about mass-spectrometry, both for "hands-on" handling the equipment and providing valuable theoretical knowledge. Her unconditional availability of time, work, support and intellect were at difficult times the most supportive. I wish her good luck and all the best from my heart for the new steps in her scientific career as Independent Researcher. I want to also thank Franzi, who welcomed me when I started and showed me phospho- and proteome preps. She was so cool that she made it look really easy. I will always remember her talking about her bunny, the fast-talking with Tanja and, of course, the endless cups of coffee the two of them were drinking.

Many other people and friends in both labs have contributed and accompanied me throughout my PhD life. I want to thank Sebastian for his guidance in molecular biology, Stefanie and Chiara for welcoming me in Dieter's lab and their technical support with the mouse work. I also thank all the current and former lab members in both labs for doing their best to support me when possible. A special thank you to Fatih who tolerated my cleaning obsession as office and lab mate all these years, and was always ready to help.

Finally, I want to thank my family who always supported me throughout the years since I was an undergraduate student in the University of Athens. I would like also to thank Graciela for her support and patience during my PhD journey.

LMU LUDWIG-MAXIMILIANS-UNIVERSITÄT MÜNCHEN

Promotionsbüro
Medizinische Fakultät

MMRS

Eidesstattliche Versicherung

Koutsouli, Styliani

Name, Vorname

Ich erkläre hiermit an Eides statt,

dass ich die vorliegende Dissertation mit dem Titel

Proteomic profiling and circadian dynamics in pancreatic ductal adenocarcinoma

selbständig verfasst, mich außer der angegebenen keiner weiteren Hilfsmittel bedient und alle Erkenntnisse, die aus dem Schrifttum ganz oder annähernd übernommen sind, als solche kenntlich gemacht und nach ihrer Herkunft unter Bezeichnung der Fundstelle einzeln nachgewiesen habe.

Ich erkläre des Weiteren, dass die hier vorgelegte Dissertation nicht in gleicher oder in ähnlicher Form bei einer anderen Stelle zur Erlangung eines akademischen Grades eingereicht wurde.

München, den 14. März 2023

Ort, Datum

Styliani Koutsouli

Unterschrift Doktorandin bzw. Doktorand